Late Quaternary climate and environmental reconstruction of Lake Urmia sediments (Iran) inferred from mineralogical and geochemical records

Ting Kong

THESE DE DOCTORAT

NNT : 2022UPASJ024

université PARIS-SACLAY

Late Quaternary climate and environmental reconstruction of Lake Urmia sediments (Iran) inferred from mineralogical and geochemical records

Reconstruction paléoclimatique et paléoenvironnementale au Quaternaire supérieur des sédiments du lac Urmia (Iran) à partir des enregistrements minéralogiques et géochimiques

Thèse de doctorat de l'université Paris-Saclay

École doctorale n°579 : sciences mécaniques et énergétiques, matériaux et géosciences (SMEMAG)
Spécialité de doctorat : terre solide : géodynamique des enveloppes supérieures, paléobiosphère
Graduate School: Géosciences, climat, environnement et planètes
Référent: Faculté des sciences d'Orsay

Thèse préparée dans les unités de recherche **GEOPS (Université Paris-Saclay, CNRS)** et le **Laboratoire des sciences du climat et de l'environnement (Université Paris-Saclay, CNRS, CEA, UVSQ)** sous la direction d'**Elisabeth GIBERT-BRUNET**, directrice de recherche, la co-direction d'**Alina TUDRYN**, maîtresse de conférences

Thèse soutenue à Paris-Saclay, le 8 décembre 2022, par

Ting KONG

Composition du Jury

Membres du jury avec voix délibérative

Pascal SAILHAC Professeur, Université Paris-Saclay, UMR8148-GEOPS	Président
David WILLIAMSON Directeur de Recherche, IRD Montpellier	Rapporteur & Examinateur
Morteza DJAMALI Chargé de Recherche, HDR, CNRS, Université Aix Marseille, UMR7263-IMBE	Rapporteur & Examinateur
Françoise CHALIE Chargée de Recherche CNRS, UMR6635-CEREGE	Examinatrice
Seyed-Hani MOTAVALLI-ANBARAN Professeur, Université de Tehran (Iran), Institut de géophysique	Examinateur
Piotr TUCHOLKA Professeur Émérite, Université de Varsovie, Pologne	Examinateur

université PARIS-SACLAY

ÉCOLE DOCTORALE
Sciences mécaniques et énergétiques, matériaux et géosciences (SMEMAG)

Titre : Reconstruction paléoclimatique et paléoenvironnementale au Quaternaire supérieur des sédiments du lac Urmia (Iran) à partir des enregistrements minéralogiques et géochimiques

Mots clés : Lacs salés; Minéralogie; Sédimentologie; Isotopes stables; Paléoenvironnement; Quaternaire supérieur

Résumé : Au cours des dernières décennies, les lacs salés ont connu et connaissent encore des diminutions spectaculaires, principalement dans les zones arides. Situé dans le nord-ouest de l'Iran, le lac Urmia a subi le même sort avec une baisse significative de 8 m au cours des 20 dernières années. Afin d'étudier les causes de cette baisse et de développer une gestion durable des ressources hydro-écologiques, des enregistrements détaillés des environnements modernes et passés sont nécessaires pour comprendre les processus qui déterminent l'état actuel et l'évolution future du bassin du lac Urmia. Les objectifs sont (i) de déchiffrer les sources de matériaux détritiques et la dynamique de transport vers le lac en relation avec l'altération physique et chimique dans le bassin versant, la diagenèse précoce dans les sédiments du fond du lac et la sédimentation authigène dans le lac lui-même, et (ii) de comprendre la réponse des fluctuations du niveau d'eau et de la salinité aux forçages externes tels que les masses d'air précipitantes et le rapport P/E dans le bassin.

Dans le cadre du programme Gundishapur en 2016-2017, plusieurs carottes, des eaux de surface et souterraines ainsi que des échantillons géologiques de captage ont été échantillonnés sur la rive sud-ouest du lac dans le bassin de la rivière Shahr Chay. Sur la base de paramètres multidisciplinaires (susceptibilité magnétique, minéralogie, sédimentologie, éléments XRF, isotopes stables sur fractions authigènes), une carotte composite de 12.5 m de long a été définie et datée par AMS-^{14}C.

Les dépôts du lac Urmia, qui s'étendent sur une période allant de 30 à environ 2 cal kBP, peuvent être divisés en 8 phases environnementales. À environ 30 cal kBP, un bas niveau du lac associé à un paléosol sur le site de carottage, a été suivi par l'établissement de conditions lacustres pendant l'intervalle 29.9-20.2 cal kBP. Cette phase humide du Pléistocène tardif est en bon accord avec l'évolution des autres lacs à l'échelle régionale. Une régression lacustre caractérise la phase 20.2-15.3 cal kBP et est suivie par des conditions de haut niveau du lac entre 15.3 et 13.3 cal kBP qui correspondent au réchauffement du Bölling/Alleröd. Des conditions lacustres régressives sont mises en évidence pendant la période 13.3-11.8 cal kBP en accord avec le refroidissement du Dryas Récent. Pendant l'Holocène (11.8-2.3 cal kBP), un environnement lacustre clair est reconnu, seulement interrompu par une période sèche de 5.6 à 4.1 cal kBP, probablement en phase avec l'événement de sécheresse reconnu dans beaucoup de sites sur la Méditerranée orientale et l'Asie.

université PARIS-SACLAY

ÉCOLE DOCTORALE
Sciences mécaniques et énergétiques, matériaux et géosciences (SMEMAG)

Title: Late Quaternary climate and environmental reconstruction of Lake Urmia sediments (Iran) inferred from mineralogical and geochemical records

Keywords: Salt lakes; Mineralogy; Sedimentology; Stable isotopes; Paleoenvironment; Late Quaternary

Abstract: In recent decades, saline lakes have faced and are still facing dramatic shrinkages, mainly in arid area. Located in northwestern Iran, Lake Urmia has suffered the same fate with a significant drop of 8 m over the past 20 years. In order to investigate the causes of this drop and develop a sustainable management of hydro- and ecological resources, detailed records of modern and past environments are required to understand the processes that determine both the current state and the future evolution of Lake Urmia basin. The objectives are to decipher detrital material sources and transport dynamic to the lake in relation with physical versus chemical weathering in the catchment and with early diagenesis at the lake bottom sediment, and thus to understand the response of water level and salinity fluctuations to external forcing such as precipitating air masses and Precipitation/Evaporation balances over the basin.

Within the Gundishapur program in 2016-2017, several cores, surface and groundwater as well as catchment geological samples were sampled on the northwestern shore of the lake in the Sahar Chay River.

Based on multidisciplinary parameters (magnetic susceptibility, mineralogy, sedimentology, XRF elements, stables isotopes on authigenic fractions), a 12.5-m long composite core was defined and dated by AMS- ^{14}C ages.

Lake Urmia deposits, which spans a period from 30 to about 2 cal kBP, can be divided into 8 environmental phases. At about 30 cal kBP, a low lake level associated with a paleo-soil at the coring site, was followed by the establishment of lacustrine conditions during the 29.9-20.2 cal kBP interval. This Late Pleistocene humid phase is in good agreement with the evolution of surrounding waterbodies at a regional scale. Regressive lake conditions reappear during the 20.2-15.3 cal kBP phase. Lacustrine conditions were restored between 15.3 and 13.3 cal kBP, corresponding to the Bölling/Alleröd warming, and were followed by regressive limnological conditions during the 13.3-11.8 cal kBP in agreement with the Younger Dryas period. During the Holocene (11.8-2.3 cal kBP), a clear lacustrine environment is recognized, only interrupted by a dry spell from 5.6 to 4.1 cal kBP, likely in phase with the drought event in many sites over the eastern Mediterranean and Asia.

université PARIS-SACLAY

ÉCOLE DOCTORALE
Sciences mécaniques et énergétiques, matériaux et géosciences (SMEMAG)

论文标题:伊朗乌尔米亚湖盆地沉积物矿物学和地球化学记录：晚第四纪古气候与古环境重建

关键词: 盐湖; 矿物学; 沉积学; 稳定同位素; 古环境; 晚第四纪

摘 要: 近几十年，干旱地区的咸湖经历了急剧的萎缩。位于伊朗西北部的乌尔米亚湖也面临了同样的遭遇，过去二十年下降了 8 米。为了调查湖水下降的原因并且制定水利和生态资源的可持续管理，需要湖泊过去环境的详细记录来了解乌尔米亚湖盆地的演化过程，来破译其碎屑物质来源，湖盆输送动力和相关流域物理与化学风化过程以及湖泊自生矿物沉积和早期成岩作用，从而了解湖泊水位波动和盐度变化对外部因素(如降水水汽来源和降雨量-蒸发量的平衡)的响应过程。

2016-2017 年在法国-伊朗贡迪沙普尔项目资助下，乌尔米亚湖西南方向岩芯柱，地表水和地下水以及岩芯取样处附近的萨哈尔河流样品被采集。基于多学科参数（磁化率、矿物学、沉积学、XRF 元素、自生组分的稳定同位素），通过 AMS-^{14}C 确定了年代的 12.5 米长复合岩心被高分辨的阐释。

乌尔米亚湖沉积物的时间跨度为 30 至约 2 cal kBP，可分为 8 个环境阶段。在约 30 cal kBP 时，取芯地点与低湖水位的古土壤相关，随后在 29.9-20.2 cal kBP 期间建立了湖泊环境。这个晚更新世湿润阶段与区域范围内周围水体的演变十分吻合。在 20.2-15.3 cal kBP 阶段，湖泊再次收缩。在对应于 Bölling/Alleröd 暖期的 15.3-13.3 cal kBP 期间湖泊环境恢复。随后在与新仙女木冷期一致的 13.3-11.8 cal kBP 期间出现湖泊再次收缩。整个全新世（11.8-2.3 cal kBP）期间，岩芯取样处为较湿润的湖泊环境，但被 5.6-4.1 cal kBP 的旱季事件打断，这与地中海东部和亚洲许多地点的干旱事件同步。

Résumé en français

Au cours des dernières décennies, de nombreux lacs salés dans le monde ont été et sont encore confrontés à des baisses dramatiques de leur niveau. Les lacs étant des enregistreurs des conditions climatiques sur le long terme, ces variations de niveau peuvent être déchiffrées dans les sédiments lacustres et reliées aux différentes conditions environnementales de diminution et d'augmentation du niveau des lacs.

Le bassin du lac Urmia, situé au nord-ouest de l'Iran, est situé dans la zone méditerranéenne orientale, à la confluence de mécanismes atmosphériques majeurs : (i) les vents d'ouest de l'Atlantique Nord, (i) les hautes pressions subtropicales des latitudes moyennes, et (iii) les systèmes de haute pression sibériens. Toutefois, au cours des 20 dernières années, le lac Urmia a subi une baisse significative de plus de 8 m de son niveau d'eau, mettant en péril les éco-hydro-systèmes uniques de ce bassin ainsi que les sociétés humaines de la région.

Afin d'étudier les causes de cette réduction et ainsi développer une gestion durable des ressources hydrologiques et écologiques de la région, des enregistrements détaillés des environnements modernes et passés sont nécessaires pour comprendre les processus qui déterminent l'état actuel du bassin du lac Urmia. Les principaux objectifs de cette recherche étaient donc, en lien avec ce système de référence actuel, de reconstituer les paléoenvironnements du lac Urmia au cours des 30 derniers kyr, afin de comprendre l'évolution du climat à l'échelle régionale en termes d'identification de ses mécanismes au cours du Pléistocène supérieur et de l'Holocène, et de pouvoir potentiellement prédire son évolution future.

Nous présentons ici les analyses systématiques des enregistrements sédimentologiques, magnétiques, minéralogiques, géochimiques et chronologiques d'une carotte composite de 12.5 m de longueur provenant de la partie sud-ouest du lac Urmia.

Ce travail de recherche est structuré autour de cinq chapitres :

– Le chapitre 1 présente les informations de base sur la zone d'étude du lac Urmia. Le cadre de base du bassin d'Urmia, tel que les paramètres géologiques, tectoniques, hydrologiques et climatiques sont décrits. En outre, une brève revue des études publiées sur les études géochimiques et paléohydrologiques du lac Urmia est fournie.

– Le chapitre 2 présente (i) les matériaux collectés et les différentes méthodes sédimentologiques et géochimiques mises en œuvre (susceptibilité magnétique, granulométrie, minéraux argileux, teneur en carbonate, minéralogie totale, éléments XRF, isotopes stables sur la matière organique et les carbonates inorganiques, âges AMS-^{14}C), avec des informations détaillées sur la stratégie d'échantillonnage et les échantillons de sédiments collectés, (ii) les deux carottes provenant de la partie SO du lac qui permettent la reconstruction de la carotte composite de 12.5 m de long, et (iii) les échantillons recueillis dans le bassin versant de la rivière Shahr Chay, principal fournisseur de matériel détritique sur le site de carottage.

– Le chapitre 3 traite des caractères minéralogiques et granulométriques des séquences sédimentaires carottées et des échantillons géologiques, ainsi que de la méthodologie utilisée pour l'identification et la semi-quantification des silicates, carbonates, évaporites et minéraux argileux. Elle permet de clarifier ces phases environnementales et de mieux relier la sédimentation à l'embouchure de la rivière Shahr Chay avec les dépôts carottés. Les résultats montrent des changements importants dans le niveau d'eau du lac pour les derniers ~30 kyr, probablement attribués à l'humidité disponible.

– Le chapitre 4 s'est concentré sur l'analyse par fluorescence X à haute résolution de la carotte composite en combinaison avec les enregistrements minéralogiques. Les données élémentaires XRF montrent les variations des différents groupes d'éléments et reconnaissent les processus sédimentaires associés tels que l'altération physique et chimique et les flux de dépôt, les processus de cristallisation des carbonates dans l'eau du lac et la diagenèse précoce dans les sédiments de fond anoxiques. L'arsenic est rarement signalé dans les études marines et lacustres et peut être le résultat d'une activité anthropique. Dans le lac Urmia, il est présent naturellement et identifie facilement les sections anoxiques des sédiments et du fond du lac.

– Le chapitre 5 interprète les variations des teneurs en isotopes stables sur les carbonates inorganiques et la matière organique. Un modèle de correction en deux étapes pour les isotopes stables sur les carbonates est présenté, ce qui permet d'obtenir la composition isotopique réelle de la fraction authigène dans des environnements salins comme l'est le lac Urmia.

– L'annexe 1 (Tudryn et al., 2021) présente les détails de l'échantillonnage des sédiments et de l'eau au-delà du matériel utilisé dans cette thèse, les données acquises lors des missions de terrain et les premiers résultats des analyses de laboratoire obtenues.

– L'annexe 2 (Gibert-Brunet et al., soumis) traite de la compréhension de l'hydrologie et de l'hydrogéologie du lac Urmia, déduite des isotopes stables sur les eaux de surface et souterraines. L'établissement des relations entre les eaux souterraines et les sédiments du lac permet d'interpréter les impacts géochimiques et de valider le cadre chronologique AMS-^{14}C.

Nos résultats ont mis en lumière que la semi-quantification des composés détritiques et authigènes qui comprend des analyses détaillées des assemblages de carbonates et d'argiles sur la séquence composite, indique des fluctuations importantes du niveau d'eau du lac pour les derniers ~30 kyr. L'établissement du bilan hydrogéochimique actuel du lac ainsi que la comparaison des données obtenues sur marqueurs authigènes de la séquence composite ont permis de définir un effet « réservoir » d'environ 2000 ans pour le passé. Appliqué aux datations AMS ^{14}C, ceci nous a permis de valider la chronologie radiocarbone entre 22 et 2 cal kBP, en accord avec la lithostratigraphie et en correspondance avec les phases majeures de l'environnement régional.

La reconstitution paléoenvironnementale suggère un Pléistocène tardif humide pendant la période 29.2-20.2 cal kBP, suivi d'un épisode plus sec avant la période chaude et humide de Bølling-Allerød, la période sèche suivante du Younger Dryas, la période humide de l'Holocène précoce et des conditions d'évaporation pendant la transition de l'Holocène moyen à tardif. Les 30 derniers cal kBP ont été divisés en deux périodes environnementales principales : des conditions plus sèches pour les périodes 30-29.9, 20.2-15.3, 13.3-11.8, 5.6-4.1 cal kBP et des conditions humides pour les intervalles 29.9-20.2, 15.3-13.3, 11.8-5.6 et 4.1-2.3 cal kBP.

D'autres analyses élémentaires et d'isotopes stables, dans un cadre chronologique certifié, vérifient ce schéma et les tendances des changements environnementaux dans le bassin du lac Urmia au cours des 30 derniers kyr. Au-delà de la reconstruction de l'évolution paléoenvironnementale du lac, ce travail fournit un nouvel éclairage sur l'interprétation et la validité des contenus isotopiques définis sur des échantillons en vrac, rassemblant en même temps des informations sur l'origine et la nature des carbonates (autochtone/détritique,

mélange de différentes espèces de carbonates). En combinaison avec les résultats de la minéralogie, les données de l'analyse des carottes par XRF sur les dépôts du lac Urmia ont indiqué que la présence d'arsenic est systématiquement associée aux sulfures de fer comme origine naturelle. L'arsenic et les sulfures de fer étant d'origine diagénétique précoce, ils indiquent des conditions anoxiques (i) dans les sédiments du fond du lac pendant les hauts niveaux d'eau du lac en phase de 29.9-22 et environ 12-5.5 cal kBP et (ii) dans les niveaux riches en matières organiques pendant les bas niveaux du lac à 29.9 et 5.5 cal kBP.

Nos résultats ont été comparés à l'évolution d'autres lacs et bassins intracontinentaux au Moyen-Orient et confirment que les phases environnementales déterminées au lac Urmia s'inscrivent bien dans l'évolution de la Méditerranée orientale et de la sous-région anatolienne, en particulier pendant la période humide du Pléistocène supérieur, ainsi que pendant l'Optimum holocène précoce. Cela suggère qu'une télé-connection atmosphérique a dominé entre l'Atlantique Nord et l'Iran occidental au cours des 30 derniers kyr.

Au-delà des changements majeurs décrits, le lac Urmia a fourni un enregistrement unique pour la région, permettant de se concentrer sur des aspects nouveaux, à la fois :

– à l'échelle locale, en liaison avec l'ensemble des enregistrements minéralogiques, (i) l'identification de changements environnementaux à court terme autour de deux-trois cents ans comme en témoignent les éléments XRF, et (ii) la spécification du système carbonaté et la validation de la chronologie via les corrections en deux étapes,

– à l'échelle régionale et mondiale, avec une bonne corrélation avec l'évolution du climat de l'hémisphère nord, et l'apport des preuves de l’existence d’une télé-connection atmosphérique dominante entre l'Atlantique Nord et l'Iran occidental au cours des 30 derniers kyr.

En conclusion et selon la tendance récente du changement climatique et les nombreuses études sur le bassin du lac Urmia, nous pensons que l'avenir du lac Urmia est toujours en jeu. En combinaison avec les études précédentes, c'est la pertinence et l'interaction des facteurs mondiaux et régionaux, y compris le changement climatique et la gestion locale de l'eau, qui détermineront le sort du lac Urmia.

Acknowledgements

Until now, my doctoral research in Laboratoire de Geosciences Paris-Saclay (GEOPS) has come to an end. Looking back, my thesis can’t be completed without kind helps from my supervisors, friends, colleagues and family. During this period, I was able to study under the earnest inculcation of teachers who are very knowledgeable, to gain the care from my friends and colleagues, and to pursue my dream with the support of my family, which is the greatest luck in my life. Therefore, I would like to express my sincerely thanks to them all and I am so grateful to have them for their participation in my life in France and my PhD research work.

First of all, to my supervisors: borrowed from the river thousand Dendrobium water, research for calligraphy praise teacher's kindness. I even don’t know how to express my appreciation to my supervisors Prof. Elisabeth Gibert-Brunet and Alina Tudryn. They not only help me too much in scientific research using their abundant knowledge, patient guidance and helpful advices, but also give me many kindnesses in daily life such as cooking French and Polish food for me, inviting me to have a summer vacation near the sea with their family, giving me festival gifts and souvenirs. They are just like my mother to give me boundless love and tolerance. Thanks a lot for their support to make me overcome difficulties in my scientific research and inspire me to pursue professional improvement to be a better oneself.

I am also sincerely grateful to Piotr Tucholka, Seyed-Hani Motavalli-Anbaran, Hesam Ahmadi-Birgani and Mohammad Lankarani for their hardworking in the field missions for sampling. Particular thanks also go to Serge Miska, for his instructions in grain size analysis, total mineralogy identification and semi-quantification by XRD analysis, to Aurélie Noret for organizing and guiding my stable isotope analysis work, to Olivier Dufaure his kindly help in grain size analysis. Thanks to Aline Govin for her invaluable assistance with the elemental analysis using XRF core scanning at the Laboratoire des Sciences du Climat et de l'Environnement (LSCE).

Many people have helped me all the way in essential laboratory work and give me constructive comments during the preparation of this thesis. It is my great pleasure to work with them. I really appreciate the members of jury for their willingness to review my thesis and give me good advices to improve it.

To my friends, my sincere thanks go to Yutian Ke, Ruifang Ma, Xinquan Zhou, Jinjin Zhao, Yi Huang, Mengjun Li, Guohui Gao, Ansart Claire and Djak Aimé Djongon for their help and concern. Thanks to Chinese-French language study group Yali Wang and Pierre Vidal for me to better knowing France.

I also show our great appreciation for the China Scholarship Council for their full scholarship support of my four-year stay in Paris. Thanks a lot to my country for providing me this good opportunity to study in France.

Last but not least, I particularly thanks to my family: my loving mother Lianxiang Cai, my kind father Wangsheng Cheng, my brother Yong Kong, my sisters Jun Kong and Lixia Bi, my nieces Ziyu Kong and Yuhan Guo for their supports, companies and encouragements.

Hemingway wrote “If you are lucky enough to have lived in Paris as a young man, then wherever you go for the rest of your life, it stays with you, for Paris is a moveable feast” in book entitled “A Moveable Feast”. Thanks to this study journey in Paris, I am so happy to meet so many kind and nice persons in this feast and it will make me remember forever.

致　谢

韶华易逝，流水浮年，我在巴黎萨克雷大学地球科学实验室的博士研究生生活已经拉下帷幕。蓦然回首，我论文的完成离不开我的导师，同事，朋友和家人们的帮助。在此期间，我能够在学识渊博的导师谆谆教诲下学习，能够获得朋友和同事的关心，能够在家人的支持下追求梦想，这是我人生中最大的幸运。因此，我想向他们表达我最真诚的谢意，感谢他们参与我在法国的生活和支持我的博士研究工作。

首先，要感谢我的导师们——借得大江千斛水，研为翰墨颂师恩。我甚至不知道该如何表达对我的导师 Elisabeth Gibert-Brunet 和 Alina Tudryn 教授的感谢。他们不仅在科学研究中用他们丰富的知识、耐心的指导和有益的建议给了我很多帮助，而且在日常生活中也给了我很多关怀，包括为我做法国菜和波兰菜，邀请我和他们的家人在海边度假，送给我节日礼物和纪念品。她们就像我的母亲一样，给予我无限的爱和宽容。非常感谢她们的支持，使我在科学研究中克服困难，激励我在专业上追求进步，成为更好的自己。

我也衷心感谢 Piotr Tucholka、Seyed-Hani Motavalli-Anbaran、Hesam Ahmadi-Birgani 和 Mohammad Lankarani，感谢他们在野外取样任务中的辛勤工作。还要特别感谢 Serge Miska，感谢他在粒度分析、总矿物学鉴定和 XRD 分析半定量方面的指导，感谢 Aurélie Noret 组织和指导我的稳定同位素分析工作，感谢 Olivier Dufaure 在粒度分析方面的帮助。感谢 Aline Govin 在气候与环境科学实验室（LSCE）使用 XRF 核心扫描进行元素分析时提供的帮助。

在本论文的准备过程中，许多人在重要的实验工作中一直帮助我，并给予我建设性的意见。能与他们一起工作是我的荣幸。我非常感谢评委会成员愿意审查我的论文并给我提出改进意见。

对我的朋友们：我真诚地感谢柯雨田、马瑞芳、周辛全、赵金锦、黄怡、李梦君、高国辉、Ansart Claire 和 Djak Aimé Djongon 的帮助和关心。感谢中法语言小组的汪亚丽和 Pierre 的帮助让我更好的了解法国。

我也对中国国家留学基金管理委员会为我在法国四年的学习提供的全额奖学金支持表示感谢。非常感谢我的国家为我提供了在法国学习的好机会。

最后，我特别感谢我的家人：我亲爱的母亲蔡莲香，我慈祥的父亲程旺生，我的哥哥孔勇，我的姐姐孔俊和毕丽霞，我的侄女孔子遇和郭语菡，感谢他们的支持、陪伴和鼓励。

海明威在《流动的盛宴》一书中写道：“如果你有幸年轻时曾在巴黎生活过，那么你的余生无论走到哪里，它都会与你同在，因为巴黎是一场流动的盛宴”。 感谢这次巴黎的求学之旅，让我在这场盛宴中遇到如此多善良且美好的人，我将永远铭记。

Contents

List of Figures

General introduction

Chapter 1

Chapter 2

Chapter 3

Chapter 4

Chapter 5

General conclusions and perspectives

List of Tables

Chapter 1

Chapter 2

Chapter 3

Chapter 4

Chapter 5

General Introduction

Since the beginning of the Anthropocene, we have entered a time in which Earth's climates are influenced by human activity. Via modifications in the atmospheric dynamics, this climatic evolution deeply affects the global hydrological cycle and, consequently, the continental water bodies that are of the utmost importance for both ecosystems, human societies and water resources, whether surface or groundwater (Cohen et al., 2014; Wurtsbaugh et al., 2017; Wang et al., 2018). The combined effects of global environmental changes in the Anthropocene and human-centered water management have altered the natural hydrologic cycle by changing the quantity and quality of water, as well as the timescale of water resource recharge processes (Mehran et al., 2017). In order to find out the effect of natural and anthropic influences, part of the answer will be obtained by deciphering the paleoclimate changes, and meanwhile, understanding of the climate change in the past can provide us the information about changes appearing in the future.

Generally, the key to deciphering climate history is preserved in major archives such as ice, corals, trees or sediments, the last of which, deposited through water, are the primary climate archives for more than 99% of geological time on Earth (Ruddiman, 2008). Among terrestrial settings, lake deposits are one of the best archives for paleoenvironmental information. Indeed, when complete and continuous lake sequences are preserved, high temporal resolution studies are possible. Furthermore, closed lakes are very sensitive recorders of paleoclimate and paleoenvironment changes. Saline lakes are the most common closed lakes and are mostly formed either by tectonic movement, volcanism or glacial action (Hammer, 1986). They are mainly situated in arid and semi-arid regions and record the progressive salt accumulation of evaporative concentration process. Their water loss only through evaporation exceeds inflows including precipitation, surface runoff and groundwater discharge, resulting in a negative hydrological balance for extended intervals and thus giving rise to saline lakes (Schagerl and Renaut, 2016; Schagerl, 2021). Salt lakes, whose development is controlled by factors such as temperature and net evaporation relative to precipitation, respond to climate changes through the variations of water level, salinity and hydrogeochemistry (Yechieli and Wood, 2002). Therefore, these variations are preserved in sediments by stratigraphic records of the interaction between (i)

detrital input that reflects changes in the surrounding catchment and (ii) autochthonous fractions being of chemical and/or biogenic origin.

Nowadays, the majority of the world's saline lakes that represent 23% and 44% in surface and volume of the total waterbodies (Messager et al., 2016), are shrinking at alarming rates (Wurtsbaugh et al., 2017; Wang et al., 2018). Due to increasing water stress, it is evident that more and more inland water bodies are facing ecological degradation, especially in irrigated agricultural areas (Wurtsbaugh et al., 2017).

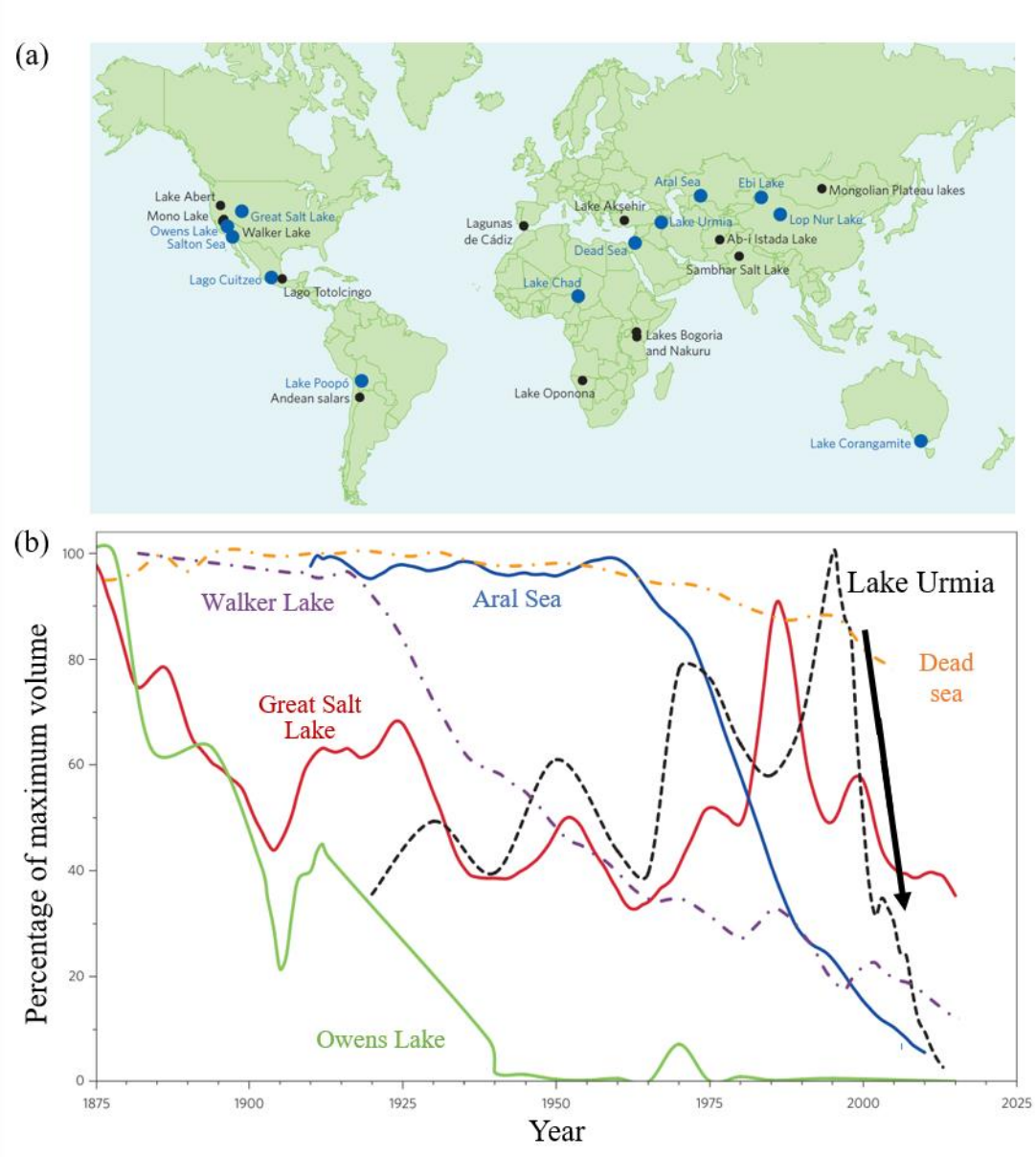

Fig. 1. *(a) Some world's declining saline lakes resulted from water diversions and/ or climate change. Blue symbols show lakes formerly larger than 250 km^2; (b) Decrease of the water volume from some important saline lakes during 1875-2015 according to Wurtsbaugh et al. (2017).*

Taking the Aral Sea watershed located in Central Asia as example, its agricultural water use results in the 74% decreases in lake surface area and 90% decrease in lake volume (Micklin, 2007). Other examples of drying terminal lakes in endorheic basins, including the Great Salt Lake in the United States (Wurtsbaugh et al., 2017), and Lake Urmia in northwestern Iran (AghaKouchak et al., 2015), have suffered a similar fate, as have many saline lakes on all continents (Fig. 1). These alarming cases of lake level decline have been major topics in climate change scenarios worldwide.

All these global evolutions of saline lakes can be represented by the on-going evolution of Lake Urmia, a very large lake in Iran that has experienced a drastic drop of about 8 m over the past 20 years. The Lake Urmia basin is the main groundwater resources for more than six million people, and the rapid expansion of irrigation-dependent agriculture led to huge and rapidly increasing demand for the very limited and inadequate fresh water sources in the basin area. This demand has resulted in the construction of an extremely large number of dams on the rivers feeding the lake, sometimes even drying up these rivers. In addition, periodic dry periods and droughts should be seriously considered for the shrinking of Lake Urmia, especially in the current climatic changes that predicts an increase in the recurrence of these extreme events. Thus, understanding the current evolution of Lake Urmia, as well as that which may be deciphered in the past sedimentary record, will provide essential information for understanding the future evolution of the basin.

As a National Park in NW Iran, Lake Urmia, one of the largest saline lakes in the world, displays a unique, highly valuable biodiversity (Asem et al., 2014). The lake plays a major role in creating a mild climate favoring a highly productive agriculture and brine shrimp farming and making the region, one of the most important economic poles of Iran. However, since the mid-1990, Lake Urmia has faced environmental disorders resulting in a deep environmental and socio-political crisis. The lake drop causes groundwater salinization, desertification and dust storms threatening health conditions of millions of people at a regional scale (Alipour, 2006; Pengra, 2012). In 2014, the Iranian government ranked the Urmia's environmental issue in first fighting priority and tackled this ecological disaster by supporting farmers in modifying crop types and irrigation techniques, limiting water retention in dams and planning other more or less realistic strategies as water transfer from neighboring

watersheds, and even from the Caspian Sea. Nevertheless, despite evident water overexploitation, the role of natural *versus* anthropogenic factors influencing the lake budget is not yet quantified and the ecosystem dynamics is almost omitted in proposed restoration efforts. Indeed, the lack of detailed record of modern and past environments limits the understanding of processes that determine current status and future evolution of the lake hydrosystem, thereby hindering the development of an integrated resource management and ecological restoration program.

Fig. 2. *Lake Urmia in 2017 (Credit photo: Alina Tudryn).*

Although Iranian institutions recurrently monitor Lake Urmia water chemistry and since several works have been published on modeling the water functioning of Lake Urmia, a comprehensive geochemical dataset including stable isotopes and radiometric analyses on both surface and groundwater is still lacking to model the entire lake hydrosystems considering both surface and groundwater. Moreover, Late Quaternary sediments of the Lake Urmia have not been extensively explored with a high temporal resolution for palaeoenvironmental reconstructions. The presented thesis is a part of the bilateral Gundishapur Franco-Iranian project aiming to the paleoclimate reconstructions in Lake Urmia basin (Iran).

The objectives of this research are to reconstruct the environmental evolution of Lake Urmia basin based on multidisciplinary parameters in order to:

(i) well recognize/identify these changes with time and complete the dataset for the region;

(ii) compare these changes with other regional data that allow the discussion on the possible

driving mechanisms of the observed changes;

(iii) produce accurate data to modelers, to allow reliable models of the climate change at both regional and global scales;

(iv) understand and anticipate the future lake evolution and in this way, to allow a better management of natural resources for people living around the lake.

Although my research program was interrupted by the Covid-19 pandemic (total confinement of Wuhan where I was for 15 days of vacations in February 2020) more than 6 months and the international situation didn't allow me to go on the filed for the last 2 years, I had the opportunity to analyze the coring sediments sampled during the 2016-2017 Urmia Project.

This manuscript therefore presents original and accurate results on the Lake Urmia environmental evolution during the Late Quaternary that are detailed in five chapters.

In the first chapter, I introduce the background information of Lake Urmia study area. I present the basic setting of Urmia basin, such as the geology, tectonic, hydrology and climate parameters. In addition, I also provide a brief review of previous geochemical and paleohydrological studies in Lake Urmia.

Chapter 2 presents the materials collected and the different sedimentological and geochemical methods implemented, with detailed information on the sampling strategy and the collected sediment samples. In order to decipher patterns and trends in the environmental evolution in Lake Urmia (Iran) during the Late Quaternary, we collected two cores from the SW part of the lake that represent a 12.5 m-long composite core, and eight samples from watershed of River Shahr Chay, the major supplier of detrital material into the coring location. The multi-proxy approaches (magnetic susceptibility, grain size, clay minerals, carbonate content, total mineralogy, XRF elements, stable isotopes on organic matter and inorganic carbonates, AMS-^{14}C ages) were conducted to decipher and then interpret the paleoclimatic record of Lake Urmia.

Chapter 3 discusses mineralogical and grain-size characters from both sedimentary cored sequences and from geological samples taken from the watershed of the Shahr Chay River, and clarify these environmental phases and to better link the sedimentation at the Shahr Chay River mouth with

the cored deposits.

In chapter 4, high resolution X-Ray fluorescence analysis of the composite core is investigated in combination with mineralogical records. XRF elemental data show the variations of different elemental groups and recognize associated sedimentary processes such as physical *versus* chemical weathering and depositional fluxes, processes of carbonate crystallization in the lake water and early diagenesis in anoxic bottom sediments.

Chapter 5 interprets the variations of stable isotope contents on inorganic carbonates and organic matter, with the details of the two-step correction methodology applied on the carbonate fraction.

Subsequently, general conclusion summarizes all the results of high temporal resolution records of environmental and climate changes in the SW Lake Urmia area during the Late Pleistocene and Holocene. These results integrating mineralogy, elemental geochemistry, and hydrogeochemistry are indispensable for identifying natural and human impacts on the hydro-environments of the lake and its catchment area, and allow us to compare Lake Urmia evolution with those of surrounding waterbodies at the scale of Inner Anatolia and Middle East.

Finally, after the references section, two appendices allow to deepen the complementary questions to the thesis.

Appendix 1 (Tudryn et al., 2021) presents the details of sediment and water sampling beyond the material used in this thesis, data acquired during the field missions and the first results of laboratory analyses obtained.

Appendix 2 (Gibert-Brunet et al., submitted) deals with the understanding of Lake Urmia hydrology and hydrogeology, inferred from stable isotope on surface and groundwater. Establishing the relationships between groundwater and the lake sediments allow to interpret the geochemical impacts and validate the AMS-^{14}C chronological framework.

Chapter 1: Geological and hydrological settings

1.1. Lake description

Lake Urmia is a shallow perennial saline lake in the lowest part of an endorheic depression located in the northwest of Iran, between West Azerbaijan and East Azerbaijan provinces, close to the borders of Turkey and Iraq (Fig. 1). It lies approximately between 45°00' and 46°00' east longitude and 37°00' and 38°16' north latitude, at an altitude of 1,270 m a.s.l., and is located on the Turkish-Iranian plateau that has a mean altitude of around 2000 m a.s.l. The lake is surrounded by the Zagros and Alborz Mountains ranges rising to a maximum elevation of 3155 m a.s.l. in the north, 3608 m a.s.l. in the west, 3332 m a.s.l. in the south, 3850 m a.s.l. in the east (Jalili et al., 2012).

Prior to the recent lake level fall that started at mid-1990s, Lake Urmia had a water level of 1278.4 m and a surface area of 5700 km^2 (140 km long and 15-50 km wide) and was considered as the second largest salty lake on earth after the Caspian Sea (Shahrabi, 1981; Tudryn et al., 2021). Before this drop, Lake Urmia salinity varied between 140 and to 220 $g.L^{-1}$ on an annual basis (Bottema, 1986; Eimanifar and Mohebbi, 2007; Sharifi et al., 2018). According to Alipour (2006), the major cations composition of the lake water includes Na^+, K^+, Ca^{2+}, Li^+ and Mg^{2+} while major anions are represented by Cl^-, SO_4^{2-}, and HCO_3^-. Meanwhile, the concentrations of Na^+ and Cl^- is about four times higher than that in natural seawater (Golabian, 2010).

Lake Urmia is naturally divided into two parts: the deeper northern part and the shallower southern part with a mean depth of 10 and 2 m, respectively, and a maximum depth of 13 m before the last drop. The separation into the two sub-basins became effective in the 1980s–1990s, when an east-west dike-type highway, the so-called Kalantari causeway, was constructed along 15 km of the center of the lake including a ~1.5 km gap over which a bridge was built (1998–2008).

The catchment area of the lake basin is of 52,000 km^2 (Fig. 2). The thirteen primary inflows from the surrounding mountains, correspond to the rivers Zarineh Rud, Gader Chay, Baranduz Chay, Nazlu Chay, Mahabad Chay, Simineh Rud, Aji Chay, Shahar Chay, Zola Chay, Rozeh Chay, Leylan Chay, Ghaleh Chay, Almalu Chay, all of which bring fresh water to the lake except the Aji Chay River that flows through saline sediments east of the lake (Alipour, 2006). As proposed by Sharifi et al. (2018), the water chemistry of all tributaries is of Ca-Mg type for major cations while the Aji Chay River is

predominantly of Na-K type. The position and mean annual river discharge of the nine major rivers are presented in Fig. 2a and Table 1. The majority of the lake's water supply comes from the Zarrineh Rud River in the south of Lake Urmia.

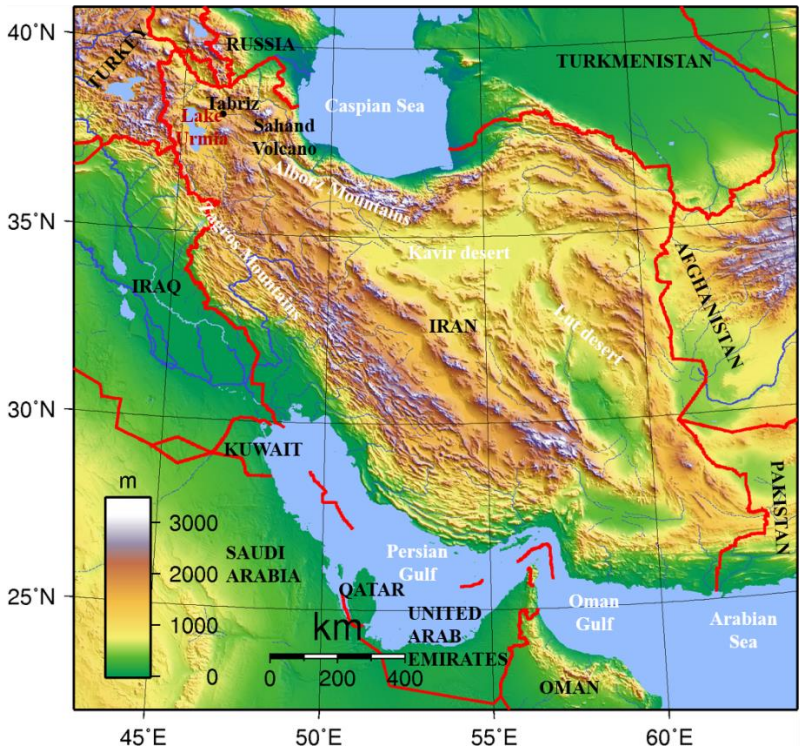

Fig. 1. *Map of Iran and the location of Lake Urmia in its NW part according to Iran Topography by Sadalmelik (2007).*

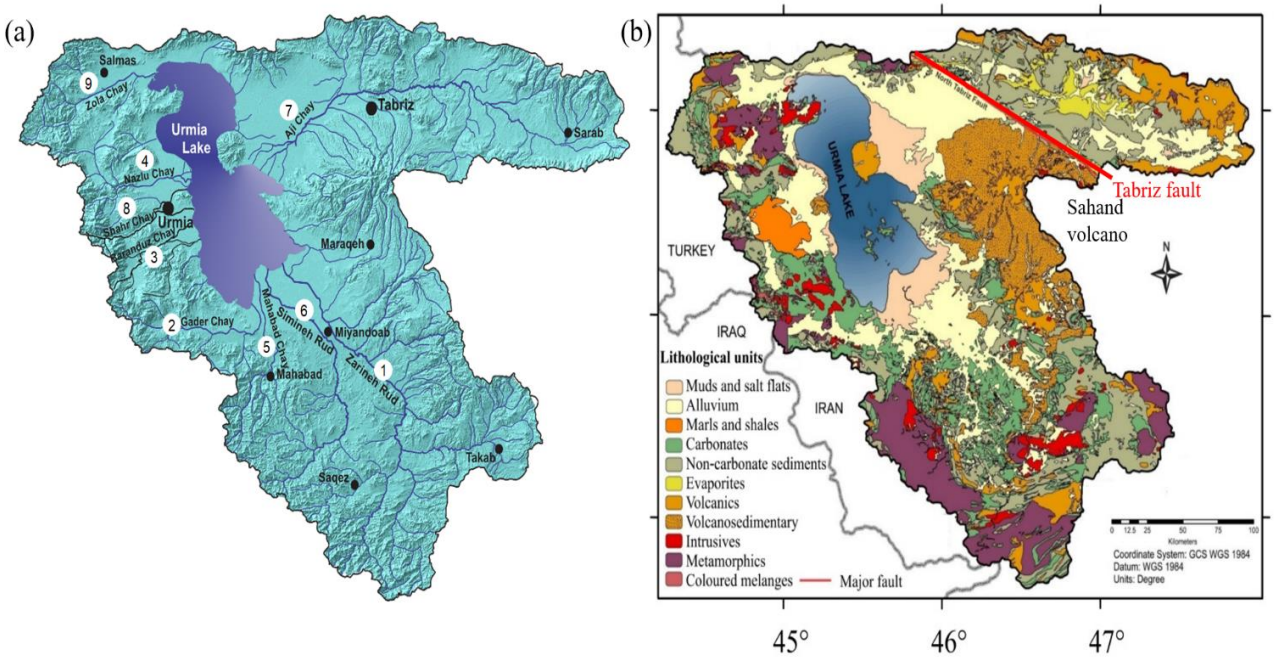

Fig. 2. *Catchment area of Lake Urmia and (a) location of the major nine rivers: 1. Zarineh Rud; 2. Gader Chay; 3. Baranduz Chay; 4. Nazlu Chay; 5. Mahabad Chay; 6. Simineh Rud; 7. Aji Chay; 8. Shahr Chay; 9. Zola Chay (Sharifi et al., 2018); (b) simplified geological map (after Sharifi et al., 2018, completed by Tudryn et al., 2021 with information from Geological Map of Iran, Sheet No 1 North-West Iran).*

Table 1 *Annual mean river discharge (in million cubic meter) of nine main rivers in Lake Urmia watershed up to 2001(Sharifi et al., 2018).*

Number	River's name	Mean discharge (million m^3)
1	Zarineh Rud	1433.22
2	Gader Chay	381.33
3	Baranduz Chay	260.15
4	Nazlu Chay	250.11
5	Mahabad Chay	193.2
6	Simineh Rud	183.54
7	Aji Chay	168.01
8	Shahr Chay	107.24
9	Zola Chay	64.51

1.2. Geological setting

The northwestern part of Iran, which belongs to the Turkish-Iranian plateau, is located in the center of the Arabian-Eurasian collision zone within the Alpine-Himalayan orogenic belt as presented in Fig. 3, where crustal deformation since the Late Miocene is dominated by a N-S shortening, associated with an E-W extension (Berberian and Arshadi, 1976; Solaymani Azad, 2009). This results in faults, earthquakes and the specific distribution of volcanoes that form the highest mountains on the plateau. Like other lakes in the region, Lake Urmia corresponds to a tectonic depression associated to the movement of large fault zones. The Tabriz Fault System lies to the N-E of Lake Urmia, and to the east of the lake, the Sahand volcano (3695 m a.s.l.), the 3rd highest volcano on the plateau, dominates (Fig. 2b). In addition, west of the lake (~100 km) passes the active Zagros thrust zone. Since 600 BC more than 450 large recorded earthquakes were caused by the Zagros thrust and since

858 AD, historical seismic data record a very high seismic activity in the Lake Urmia region, particularly associated with the Tabriz Fault System; during this period, at least 12 destructive earthquakes affecting the city of Tabriz have been recorded (Solaymani Azad, 2009). To date, no work has been done to search for earthquakes in the lake sediments.

The catchment area of Lake Urmia basin is composed of rocks ranging from Precambrian-Paleozoic metamorphic rocks, Cretaceous limestones, Tertiary volcanic and volcanoclastic formations to Quaternary mud deposits, reflecting the complex geological history of this region (Kelts and Shahrabi, 1986; Geological Map of Iran, Sheet No 1 North-West Iran). Metamorphic rocks are mainly distributed in the southern and in the northwestern parts of the basin cropping out in the Zagros mountains. Volcanic and volcano-sedimentary formations dominate the eastern and northeast parts of the catchment, as evidenced by the presence of Sahand volcanic complex in the east, and several small domes near the shores. Intrusive rocks are mainly present in the northwest, west and south. In addition, evaporative sedimentary units prevail in the northeastern part where several salt-domes of Miocene age pierce the surface. Carbonate sedimentary units are most dominant in the western and southern regions.

The relatively recent lake sediments all around the lake are principally composed of detrital particles of variable grain size (clays-silts-sand) (Sharifi et al., 2018) and chemical sediments precipitated in the lake like aragonite, shrimp fecal pellet sands, thin aragonite crusts, ooids, and evaporates (Kelts and Shahrabi, 1986). Alipour (2006) indicated the beginning of the lacustrine basin around 800 kyr or 400 kyr.

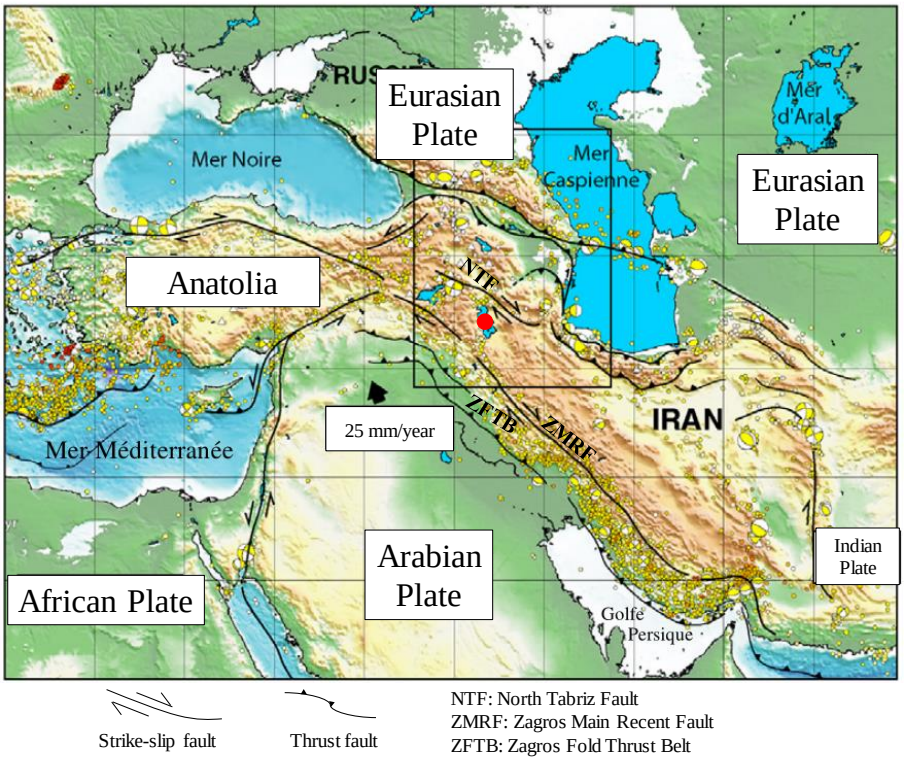

Fig. 3. *General geodynamic background of Iran in the Middle East territory, the location of Lake Urmia in the NW Iran domain (red point) and the distribution of the seismic deformation (the yellow circles) (after Solaymani Azad, 2009).*

1.3. Water level fluctuations over the past 100 years

The historical trend of the mean lake level over the last 86 years, from 1931 to 2017, is summarized in Fig. 4. According to Golabian (2010), the data, including those recorded by the Road Ministry of Iran, indicate that the level of Lake Urmia (i) stayed around 1274 m a.s.l. during the 1913–1954 period, (ii) fluctuated between 1273 and 1275 m a.s.l. during the 1954 – 1968 period, (iii) remained broadly stable at 1276 m a.s.l. during the 1968 – 1993 period, (iv) peaked in the mid-1990s at 1278.4 m a.s.l., and then (v) declined drastically to 1270 m in 2017, well below the long-term average of minimum ecological level at 1274.1 m. This minimum ecological level was defined based on the water quality index concentration of 240 $g.L^{-1}$, which is the maximum threshold tolerated by *Artemia* (Abbaspour and Nazaridoust, 2007). Since a peak in the mid-1990s, the surface area and water volume of the lake have decreased until today, except for some small regular seasonal variations with two brief expansions during the wetter periods of 2004-2006 and 2015.

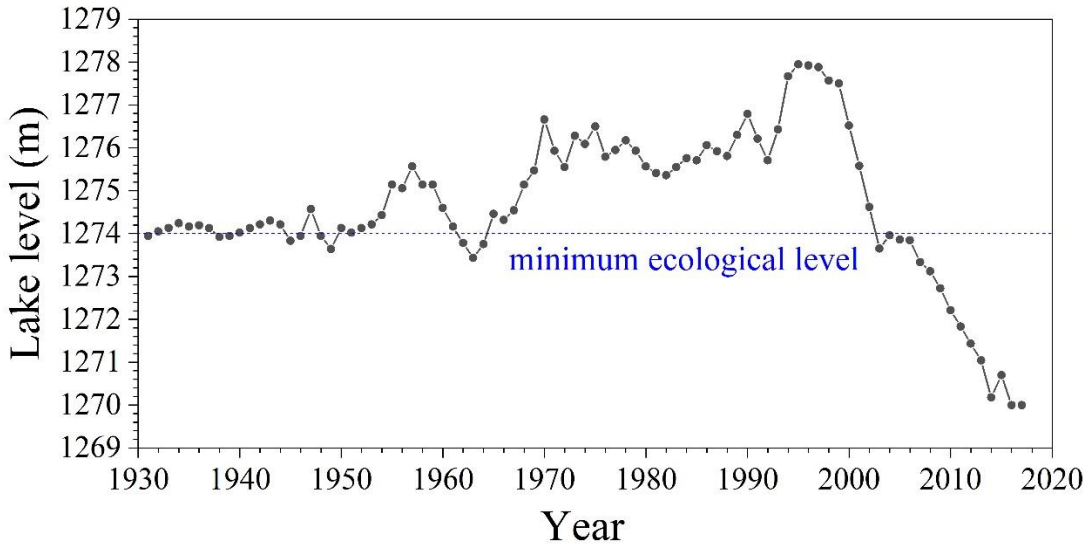

Fig. 4. *Water level of Lake Urmia during 1931-2017 (Golabian, 2010; Manaffar et al., 2011; Jalili et al., 2012; Pengra, 2012; Asem et al., 2019; Habibi et al., 2021).*

As shown in Fig. 5, the level of Lake Urmia decreased between 1999 and 2019 from 1277.5 m to 1270.85 m. Over this period, the lake lost about 20 bm^3 of its water volume and its surface area shrank from ~5000 km^2 to 2400 km^2, resulting in an increase in salinity to more than 300 g. L^{-1} and dramatic ecologic consequences for the lake catchment area (Ahmady-Birgani et al., 2020). When our cores were collected in 2017, Lake Urmia was close to the lake condition in 2019 (Fig. 5).

Due to the limited aquatic biodiversity caused by the water salinity, Lake Urmia support no fish or mollusk species and no plants other than phytoplankton (Alipour, 2006). The most important aquatic biota in the defined high salinity range of the lake is a species of brine shrimp, *Artemia urmiana*. This shrimp plays a key role in the lake's food chain, by feeding algae and in turn, being consumed by several bird species including the lake's migratory flamingo population (Djamali et al., 2010). Until now, Lake Urmia is one of the largest permanent hypersaline lakes in the world and resembles the Great Salt Lake of USA in many ways such as morphology, chemistry and sediments. As highlighted by Kelt and Shahrabi (1986), these two lakes are like twin sisters and even have a similar shape and size.

Fig. 5. *Lake Urmia in 1999 on the left and in 2019 on the right (after Ahmady-Birgani et al., 2020).*

1.4. Climate

Iran whose geographical position extends from 25° N to nearly 40° N, is dominated by an arid and semi-arid climate in 85 % of its territory and the remaining 15 % represents three types of climate: Mediterranean, wet Caspian and cold mountainous in Fig. 6 (Amiri and Eslamian, 2010). Almost all precipitation in Iran comes from the Mediterranean Sea and Atlantic Ocean, while the Black and Caspian Seas and Persian Gulf only support minor contributions (Alijani and Harman, 1985; Stevens et al., 2012).

Located in northwestern Iran, Lake Urmia is mainly influenced by the Mediterranean climate. This climate pattern is characterized by hot and dry summers and cold and wet winters in the Eastern Mediterranean and Anatolia regions (Finné et al., 2011). It is mainly controlled by the features of the general circulation (Fig. 7) including westerlies and the Siberian anticyclone in winter and subtropical high pressure in summer. In winter, the humid air mass from the North Atlantic and the Mediterranean is directed eastward by the westerlies towards the continental interior of the Middle East and its intensity is controlled by the intensity of north-east, cold and dry air from the Siberian high (Alijani and Harman, 1985; Stevens et al., 2001; Kehl, 2009). In summer, subsidence associated with the subtropical high pressure belt overspreads nearly all of Iran resulting in north-easterly wind and hot, dry conditions. Today, the Indian monsoon has no impact on this region. Additionally, orographical

barriers, namely the Alborz Mountains, limit the arrival of humid air from the Caspian Sea to Lake Urmia area. Finally, the climate of Lake Urmia is influenced by the surrounding mountains. Moreover, due to its higher altitude, Iran as a whole is considered colder than neighboring countries such as Iraq and Turkmenistan. Winters in Lake Urmia area are cold even with heavy snowfall and subfreezing temperatures. Indeed, the penetration of the most intense Atlantic and Mediterranean lows triggers winter snow (Alijani and Harman, 1985), and the Black Sea lows produce spring precipitation (Stevens et al., 2001).

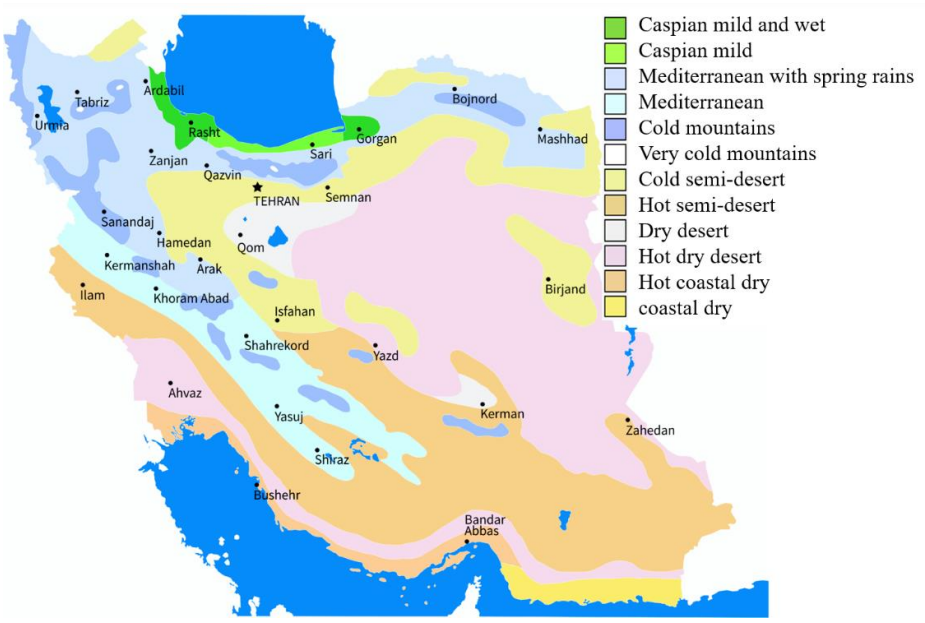

Fig. 6. *Climate distribution in Iran*
(from https://upload.wikimedia.org/wikipedia/commons/b/b3/Iran-climate.png).

The effects of local topography on the climate of the Urmia basin result in quite large temperature variations (Shahrabi, 1981), with extreme values ranging between -20 ℃ in winter and up to about 40 ℃ in summer (Ghaheri et al., 1999). The average maximum and minimum temperatures of the hottest (July) and coldest (January) months are 23.9 °C and -2.5 °C, respectively, and the mean annual temperature is of 11.2 °C (Djamali et al., 2008a). According to data for the period between 1986 and 2017, the mean annual temperature fluctuates around 11.4 °C with the minimum value of 9.3 C° recorded in 1992 and the maximum value of 12.7 ˚C recorded in 2001 (Fig. 8a; Nhu et al., 2020).

Fig. 7. *Schematic position of major synoptic systems over west Asia and the location of lake Urmia*

The average precipitation value in the Urmia basin is reported in the literature as 341 or 339 mm/yr (*e.g.*, Emdadi et al., 2016; Islamic, Republic of Iran Meteorological Organisation; Djamali et al., 2008a, b). This value is higher than the mean annual rainfall in Iran which is about 250 mm.yr-1. Precipitation data for the period 1986-2017 presented by Nhu et al. (2020) show values ranging from a minimum of 167 mm recorded in 2005 to the maximum of 543 mm recorded in 1993, and the average precipitation is of 300 $mm.yr^{-1}$ for the 31 years (Fig. 8b). This value is lower than the 341 or 339 $mm.yr^{-1}$ ones usually considered for the lake basin. This difference suggests a decrease in precipitation amounts over the past 30 years.

Combining the trends in temperature and precipitation changes with those in lake level (Fig. 8c), we can observe that the increase in precipitation was followed by the increase of the lake level around the mid-1990s. The level of the lake then declined, while temperature and precipitation remained nearly stable, suggesting that the climate is not the main reason for the recent lake level drop.

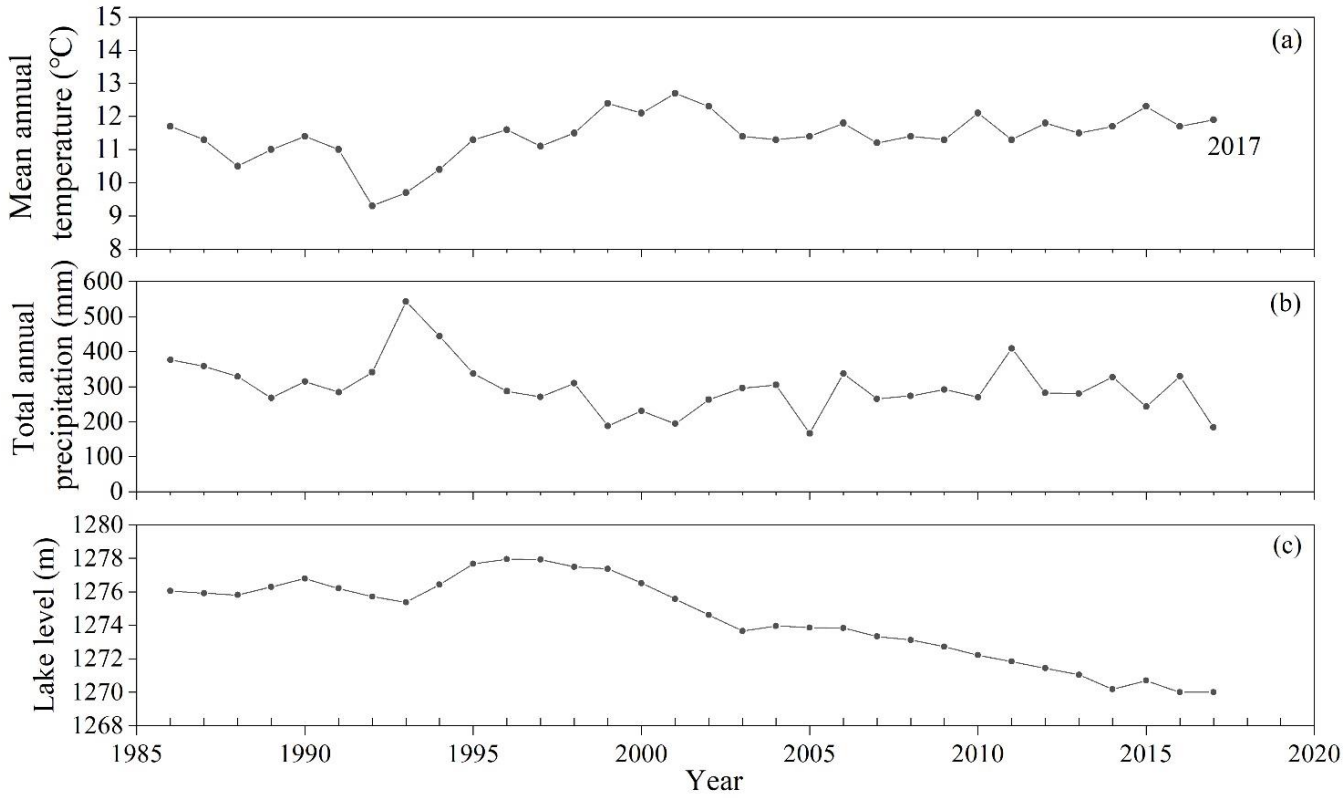

Fig. 8. *Lake Urmia during 1986-2017 (a) mean annual temperature values (°C); (b) mean annual precipitation (mm); (c) lake level (m a.s.l.). Figs (a) and (b) after (Nhu et al., 2020), (c) after (Golabian, 2010; Manaffar et al., 2011; Jalili et al., 2012; Pengra, 2012; Asem et al., 2019; Habibi et al., 2021).*

1.5. Previous studies on Lake Urmia

Lake Urmia has been the subject of a large number of studies concerning its present state in terms of hydrology, chemistry, biology and anthropogenic factors influencing its present evolution and, to a lesser extent, concerning its past evolution during the Late Quaternary.

(1) *Past lake evolution*

Studies on the Late Quaternary evolution of the lake are based on sedimentary archives and sedimentological/mineralogical, geochemical and biological proxies (pollen, brine shrimp *Artemia*). However, the published data do not yet provide a clear picture of the lake environment and of its exact chronological setting. Indeed, they (i) cover a large time scale (200 kyr) but with low temporal resolution and even with poor or missing information on the Late Pleistocene and Holocene (Djamali et al., 2008a; Djamali et al., 2008b; Stevens et al., 2012); (ii) focus on the whole Holocene

but still with a low temporal resolution (Bottema, 1986; Kelts and Shahrabi, 1986), or on Late Pleistocene and the Holocene without precise chronology (Mirzapour et al., 2021a; Mirzapour et al., 2021b), and/or (iii) concern only the most recent Holocene period, approximately the last 2550 years (Talebi et al., 2016), or surface sediments ((Erfan et al., 2017; Sharifi et al., 2018).

The existing studies show the greatest variations in lake level between glacial and interglacial periods and second-degree fluctuations during the Holocene. According to Djamali et al. (2008a), the high levels recorded by sedimentary and biological indicators occurred in the middle of the last glaciation. Stable isotopic data from Stevens et al. (2012) indicate dry conditions during the Late Pleistocene with a short-lived lacustrine episode at ~14 kyr, followed by a drying out likely in phase with the Younger Dryas and no recovery of lacustrine conditions before ~10 kyr. Mainly based on sedimentological studies, Kelts and Shahrabi (1986) indicate (i) a playa stage with saline lacustrine deposition in a cool arid climate prior to 9000 yr BP, (ii) a shallow saline lake with higher-energy facies from 9000 to 7500 yr BP, and (iii) a saline environment with numerous second-order water level fluctuations up to the present day. Mirzapour et al. (2021a; 2021b) suggest two dry periods with low lake stands, at ca. 13 cal kBP and ca. 4 cal kBP. Finally, Talebi et al. (2015) address the late Holocene by indicating a probable short rise in lake level between 2.0-1.9 cal kBP, a low state between 1.1 and 0.8 cal kBP corresponding to the time of the Medieval Climate Anomaly (MCA climate optimum) in Europe and again a high level at 0.45-0.15 cal kBP corresponding to the Little Ice Age (LIA) in Europe.

According to Djamali et al. (2008b), a dry climate and steppe dominated during glacial periods, and steppe-forest during interglacial periods. The early Holocene appears cold and dry, drier than in neighboring Anatolia and Europe. By 7 cal kBP, vegetation similar to that of today was established, but changed as a result of increasing anthropogenic pressure. At the beginning of the Late Holocene, between 2.5-1.5 cal kBP, steppe and a relatively dry climate dominated (Talebi et al., 2016). After this period, between 1.5 and 0.55 cal kBP, an expansion of the forest in the humid climate or a decrease in pastoral activities was recorded. During the MCA between 1.1 and 0.8 cal kBP, the climate of the Urmia region appeared to be warmer than today.

(2) Present day changes

Many papers on today's Lake Urmia discuss the ongoing change of its water level and the role of natural *versus* anthropogenic factors influencing this process (Pengra, 2012; Alizadeh-Choobari et al., 2016; Jalili et al., 2016; Alizade Govarchin Ghale et al., 2017; Chaudhari et al., 2018; Asem et al., 2019; Khazaei et al., 2019; Schulz et al., 2020).

Several articles report the degree of decline in water level and increase in water salinity and highlight the consequences. These consequences include reduced biodiversity, desertification, dust storms that threaten the health of local people, and difficulties in developing conventional land-based agriculture and shrimp farming (Alipour, 2006; Pengra, 2012; Asem et al., 2019). An example clearly illustrating these problems is given by Asem et al. (2019), who state that more than 90% of *Artemia urmiana* shrimps had been lost during the 1994-2004 decade due to salinity increase to levels at about 300 $g.L^{-1}$

The decline in water level over the last three decades is attributed to anthropogenic impacts and climatic change, but the predominant reason remains controversial.

Several authors have investigated the role of natural factors influencing the lake hydrology and they concluded on the increasing temperature and decreasing precipitation over the last decades (Zoljoodi and Didevarasl, 2014; Alizadeh-Choobari et al., 2016), resulting in severe droughts, as indicated by Delju et al. (2012). Schulz et al. (2020) reported that Lake Urmia lost about 60% of its surface and even more than 90% of its volume between 1995 and 2013. They quantified the components of the water balance, analyzed their temporal evolution over the last five decades and concluded that the water level variations of Lake Urmia were mainly triggered by climate changes.

However, other authors have highlighted the mismanagement of water resources by human activities with uncontrolled growth of irrigated area, groundwater pumping, extensive reservoir construction, and poor agricultural water use efficiency (Alizade Govarchin Ghale et al., 2017; Chaudhari et al., 2018; Nhu et al., 2020). Khazaei et al. (2019) proposed that the agricultural increase in vegetation cover in the catchment is well correlated with the variation in lake water level, indicating this human-induced vegetation cover and associated irrigation as the dominant human factor in the drying of Lake Urmia. Furthermore, Sharifi et al. (2018) considered that the catastrophic loss of Lake

Urmia's surface area over the past two decades is anthropogenic, leading to the increase in salinity from 140-220 $g.L^{-1}$ to over 380 $g.L^{-1}$.

Finally, Nhu et al. (2020), who analyzed the precipitation and temperature data from 1986 to 2017 in Lake Urmia, indicated that the temperature increase by about 19%, the decrease in precipitation amounts by about 62%, and the excessive construction of dams in the Urmia Basin as well as the mismanagement of water resources are the main factors for the decrease in the water level of Lake Urmia. Thus, they considered that Lake Urmia drying is caused by both, natural and anthropic origins.

Chapter 2: Material and methods

As presented before, the objectives of this PhD work are to:

- **decipher patterns and trends of modern and past lake environmental evolutions** in relation with natural vs anthropogenic changes, and
- **integrate the results into sustainable management strategies** for the development of an ecological and hydrological restoration program.

The aim of this research focuses on paleoenvironmental reconstruction and it is part of a French-Iranian multidisciplinary project (Fig. 1).

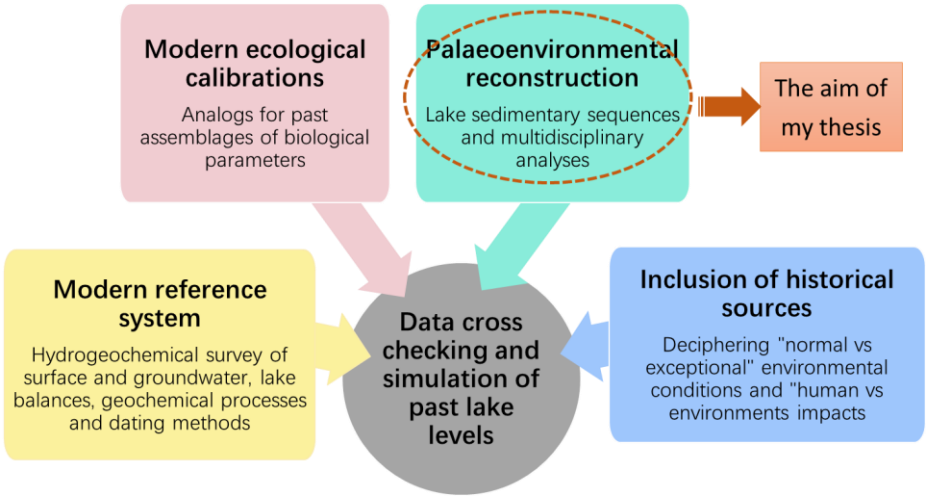

Fig. 1. The *French-Iranian multidisciplinary project for Lake Urmia*

Within the framework of paleoenvironmental reconstruction and in order to accurately reconstruct the Late Quaternary environmental changes, I conducted mineralogical analysis (both on clays and on bulk sedimentary samples), elemental (XRF core scanning) and stable isotope geochemistry ($^{18}O/^{13}C$ both on inorganic and organic fractions) analyses (Fig. 2).

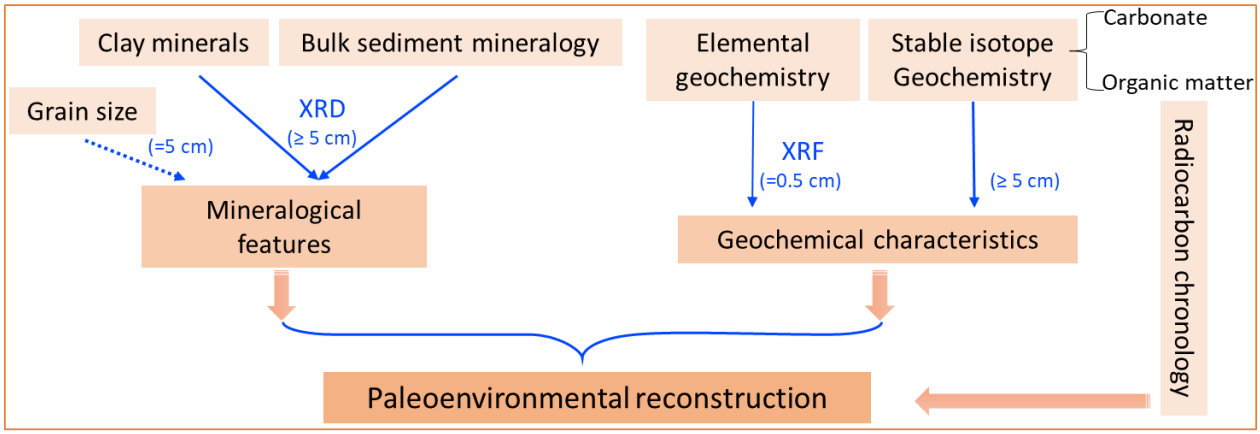

Fig. 2. *The framework of paleoenvironmental reconstruction in Lake Urmia*

All these results were interpreted in AMS-^{14}C reliable timescale.

2.1. Material

During the 2016 and 2017 fieldwork campaigns, seven sediment cores (0.6 m–14.2 m long), namely Golman 1 to Golman 7, have been drilled out from the recently dried out part of the lake near Urmia City. Additionally, in-situ parameters such as temperature, pH and conductivity were measured on all waters sampled: (i) on the surface water of Lake Urmia (at the coring site on the southern sub-basin and near the causeway in the northern sub-basin, Fig. 3) and the Shahr Chay River at several locations, and (ii) on groundwater, both on the muddy water rising up from the coring wells and on the 6 surrounding wells distributed according to a potential flow line. Samples from all water points have been taken for chemical (major anions and cations) and stable isotope analyses ($^{18}O_{water}$, $^{2}H_{water}$). Details of sampling and coring conditions are given in Table 1 and *Annexe 1* (Tudryn et al., 2021). In June 2021, the sample collection was completed by our Iranian colleagues. They sampled the various geological formations of the catchment area of the Shahr Chay River (Table 1), which is major supplier of detrital material into the lake at the coring location.

In the overall project of Lake Urmia, my PhD work has focused on the lake sediments obtained from two most complete cores, Golman 6 and Golman 7, as well as samples from the river's catchment area (marked as red in Table 1).

Between the two years of fieldworks, an important lake water level change both in seasonal and annual scale has been observed. In May 2016, the lake water level decreased by ~1 m just due to the end of the winter/spring intense rainfall period and the increased evaporation rate (Fig. 3a). By September 2017, the water level had dropped such that the 2016 lake water sampling sites had become dry (Fig. 3b, *Annexe 1*).

Table 1 *Location of sampling sites, both water and sediment in the vicinity of Urmia City, and the results of in situ measurements of pH, temperature and electric conductivity. Measurements of surface water, groundwater from wells and groundwater rising-up from coring wells Golman, have been done in May 2016 and in September 2017.*

Site name	**Comments on sampling**	**Latitude** **N**	**Longitude** **E**	**Altitude** m a.s.l. ±1 m	**pH**	**Temp.** °C	**Conductivity** $mS.cm^{-1}$
River Shahr Chay							
BARDESOOR	above dam, near Silvana city, 09/2017	37°26'14.592	44°49'26.92"	1606	8.38	13.8	0.299
SHAH 1	Urmia city, 05/2016	37°31'35.24"	45°02'50.53"	1354	8.41	14.2	0.249
SHAH 2	close to river outlet, 05/2016	37°33'16.93"	45°16'12.26"	1276	7.83	16.9	3.4
Well							
SALEH ABAD	in "Amir's garden", 09/2017	37°31'16.626	45°10'52.812"	1294	7.28	14.2	0.884
KESH 1	Kesh Tiban, 09/2017	37°32'28.788	45°14'07.224"	1281	8.13	19.9	0.575
GOLMAN 0	close to GOLMAN coring site, 09/2016	37°35'15.44"	45°15'19.70"	1278	7.35	15.3	1.178
HAJILAR 1	1st after sampling SHAH 2, 05/2016	37°33'22.00"	45°16'17.51"	1277	6.29	15.4	3.12
HAJILAR 2a	Double well - large well, 05/2016	37°33'09.07"	45°16'08.95"	1276	6.12	15.1	12.22
HAJILAR 2b	Double well - small well, 05/2016	37°33'09.07"	45°16'08.95"	1276	6.63	16.2	12.39
Coring well							
GOLMAN 1	9 m deep, 05/2016	37°35'35.86"	45°16'26.77"	1270	6.84	29.6	222
GOLMAN 1	9 m deep, 09/2017	37°35'35.86"	45°16'26.77"	1270	6.05	30.1	227
GOLMAN 2	14 m deep, 05/2016	37°35'35.09"	45°16'28.60"	1270	5.8	29.2	219
GOLMAN 2	14 m deep, 09/2017	37°35'35.09"	45°16'28.60"	1270	5.8	31.8	217
GOLMAN 3	14.2 m deep, presurized water, 05/2016	37°35'33,09"	45°16'31.20"	1270	6.48	25	141.1
GOLMAN 3	14.2 m deep, inside coring tubing, 05/2016	37°35'33,09"	45°16'31.20"	1270	6.35	20.2	147.1
GOLMAN 3	14.2 m deep, inside coring tubing, 09/2017	37°35'33,09"	45°16'31.20"	1270	6.24	18.9	142
GOLMAN 3	14.2 m deep, outside tubing, 05/2016	37°35'33,09"	45°16'31.20"	1270	6.61	27.5	158.8
GOLMAN 3	14.2 m deep, outside tubing, 09/2017	37°35'33,09"	45°16'31.20"	1270	6.29	19.1	140
GOLMAN 4	0.6 m deep, 05/2016	37°35'37.31"	45°16'38.38"	1270			
GOLMAN 5	5.25 m deep, 09/2017	37°35'33.4"	45°16'27.6"	1270	6.04	26.6	222
GOLMAN 6	8 m deep, 09/2017	37°35'28.85"	45°16'33.83"	1270			
GOLMAN 7	12.5 m deep, presurized water, 09/2017	37°35'28.75"	45°16'33.75"	1270			
Lake water							
GOLMAN	near coring GOLMAN 4, 09/2016	37°35'37.31"	45°16'38.38"	1270	8.02	21.3	207
Dam-bridge1	N side of the causeway, 09/2016	37°46'31.62"	45°19'47.04"	1270	7.53	27.9	190.2
Catchment samples	06/2021						
Sample 1	pyroclastic and claystone with vertebrate fauna remains, andesitic to basaltic volcanics	37°34'48"	45°12'00"	1370			
Sample 2	High level piedmont fan and valley terraces deposits	37°32'24"	45°07'12"	1311			
Sample 3	Red Beds composed of red conglomerate, sandstone, marl, gypsiferous marl (mostly limestones)	37°28'48"	44°57'36"	1484			
Sample 4	Red Beds composed of red conglomerate, sandstone, marl, gypsiferous marl (pure marl)	37°23'24"	44°55'12"	1720			
Sample 5	Red Beds composed of red conglomerate, sandstone, marl, gypsiferous marl	37°24'36"	44°52'48"	1614			
Sample 6	Phyllite, slate and meta-sandstone (Hamadan Phyllites)	37°22'12"	44°48'00"	2820			
Sample 7	High level piedmont fan and valley terraces deposits	37°28'48"	44°47'24"	1788			
Sample 8	Dark gray medium- bedded to massive limestone (limestone)	37°27'00"	44°45'00"	2246			

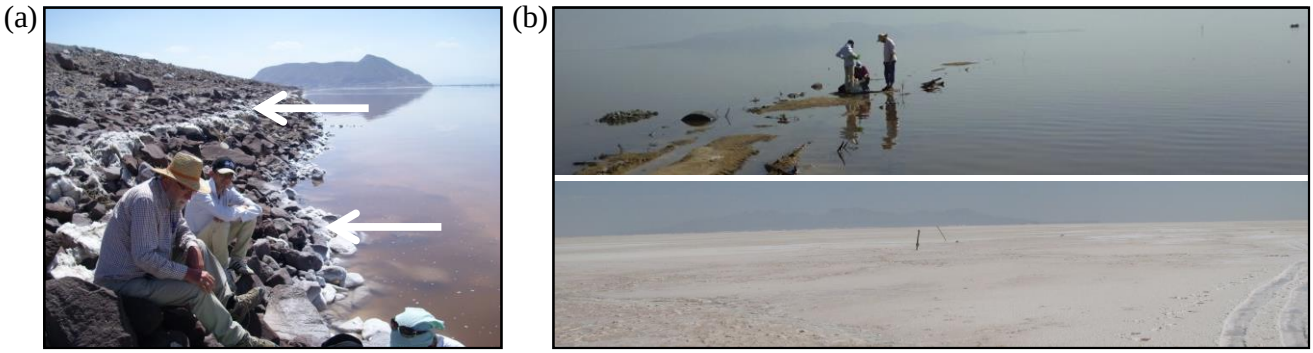

Fig. 3. *(a) Lake water sampling site at the foot of the east-west dike-type causeway in May 2016; arrows indicate two salty lines that highlight water level change in spring 2016; (b) Lake water sampling site close to the coring Golman 4: above - May 2016, below - September 2017.*

2.1.1. Catchment sediment sampling

Eight geological samples have been collected from the catchment area on the way of the Shahr Chay River, according to the main geological formations of the river catchment (Table 1, Fig. 4a). They represent the following formations: 1- pyroclastic and claystone with vertebrate fauna remains, andesitic to basaltic volcanics; 2 and 7- high level piedmont fan and valley terraces deposits; 3, 4 and 5-red beds composed of red conglomerate, sandstone, marl, gypsiferous marl; 6 - phyllite, slate and meta-sandstone (Hamadan phyllites); 8 - dark gray medium- bedded to massive limestone.

2.1.2. Lake sediment sampling

Sediment cores, Golman 6 (8.0 m long) and Golman 7 (12.5 m long), have been collected in close proximity to each other as shown in Fig. 4b. Both cores have been taken using a mechanical corer with a borehole casing at a distance from today's shoreline, where the safe use of the corer is allowed (Fig. 5a). Coring was stopped when pressurized water containing mud and gas with an intense H_2S odor rose up to the lake surface from the Golman 7 borehole (Fig. 5b) and when gas with the same odor rose up from the Golman 6 borehole.

Below the surface crust, the uppermost sediments were soft, sand-rich, and were collected either as an incomplete sequence (Golman 7) or as a compacted 0.85 m section of first 4 m thick (Golman

6). Due to the presence of interbedded captured water (either residual water from the sediment or ancient brines trapped within the deposits), the 4.2-8.65 m section of Golman 7 core was too humid to be retrieved by the corer, leading to an empty section for this depth interval.

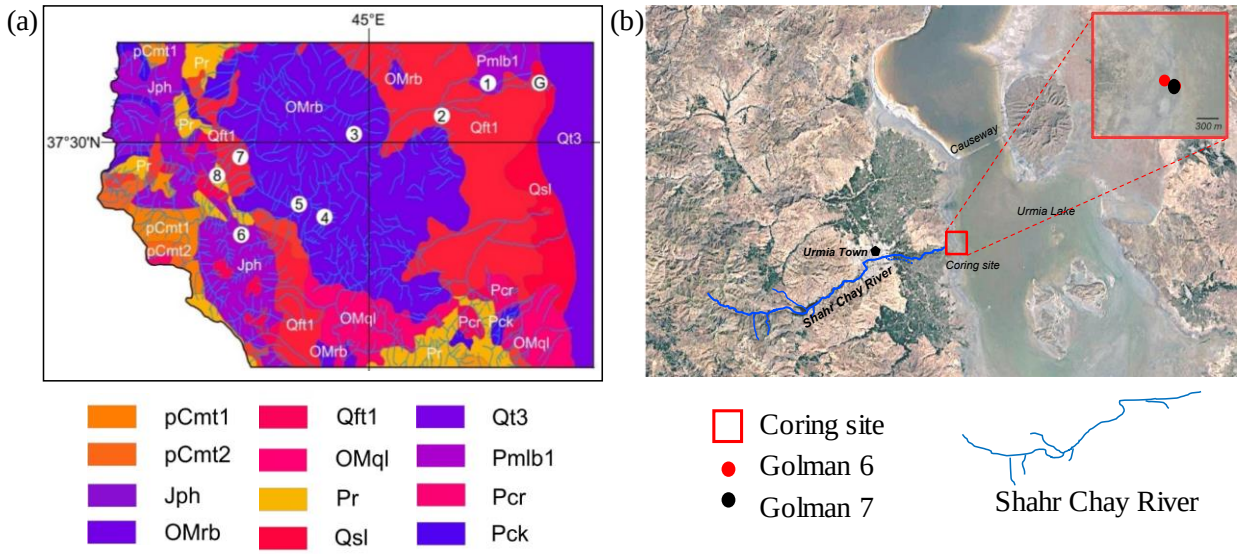

Fig. 4. *Sediment sampling site: (a) catchment sampling on the way of* Shahr Chay River, *Lithological units: pCmt1 - Medium grade (Amphibolite Facies) Precambrian metamorphic; pCmt2 – Low grade , regional metamorphic rocks (Green Schist Facies); Jph - Phyllite, slate and meta-sandstone (Hamadan Phyllites); Omrb - Red Beds composed of red conglomerate, sandstone, marl; Qft1 - High level piedmont fan and valley terraces deposits; Omql – Massive to thick - bedded reefal limestone; Pr - Dark grey medium - bedded to massive limestone (RUTEH); Qsl - Clay flate; Qt3 - no description – lake; Pmlb1 - Pyroclastics and claystone with vertebrate fauna remains; Pcr - Dolomite , sandstone and volcanic rocks (Rizu Series); Pck :Dull green grey slaty shales. (b) lake core sampling of Golman 6 and Golman 7.*

After fieldwork sampling, cores were stored in refrigerator of GEOPS laboratory, Paris-Saclay University (Orsay, France). In September 2018, five sections of the Golman 6 core and seven sections of the Golman 7 core were sampled by using u-channels to obtain continuous sequences and discrete samples were collected at every 1 cm. Although Golman 6 and Golman 7 cores present these inconsistencies, they allowed a continuous sequence to be established by crossing various recorded parameters such as magnetic susceptibility (Tudryn et al. 2021), which defined the composite core that will be primarily reported in this thesis.

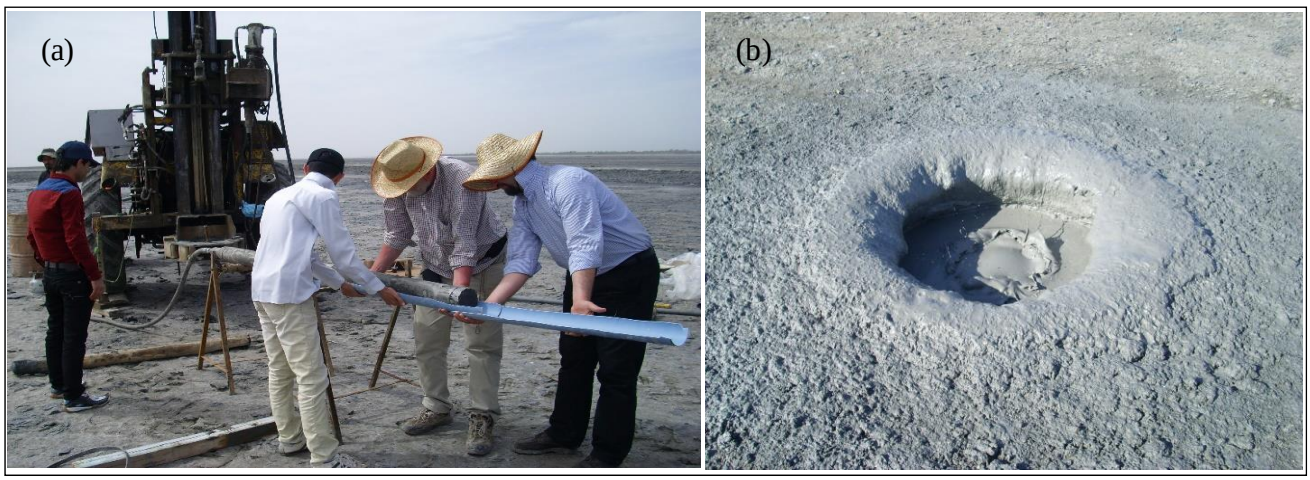

Fig. 5. *Sediment sampling: (a) taking out cores during field work in 2017; (b) underpressure mud rising up along the borehole Golman 7.*

2.2. Methods

Sediment characteristics have been obtained through laboratory analyses including mineralogical and geochemical investigations such as magnetic parameters, grain size, mineralogy by X-ray diffraction (XRD), elemental analyses through X-ray fluorescence (XRF), carbonate contents, stable isotopes on inorganic authigenic carbonates and organic matter, and ^{14}C dating.

2.2.1. Magnetic susceptibility

After opening the sealed cores, a MS-2 Bartington magnetic susceptibility meter was used to measure magnetic susceptibility (χ) directly on the sediment surface of the half-core at each 1 cm increments. Measurements were performed at the GEOPS laboratory, Paris-Saclay University (Orsay, France).

2.2.2. Grain size

Grain size analyses were carried out on 84 and 116 samples taken from Golman 6 and Golman 7 cores respectively at every 5 cm depth intervals and on 8 samples from the catchment area. About 5 g of air-dried, disaggregated sediment was pre-treated with 33% hydrogen peroxide (H_2O_2) bath to

remove organic matter and then with 20 % acetic acid (CH_3COOH) to remove carbonates. Subsequently, samples were rinsed with deionized water up to obtain neutral pH. These organic-free, non-calcareous sediment samples were then used for grain size analyses. The grain-size distribution was performed on samples dispersed by ultrasonic bath for 3 min before being analyzed using a Malvern Mastersizer 2000 laser device.

The Mastersizer 2000 works on the principle of the Mie's theory, which predicts how light is scattered by spherical particles and deals with the way light passes through, or is absorbed by, the particle. Meanwhile the Mie's theory assumes that the measured particles are perfect spheres, and the Mastersizer uses the volume of a particle to measure its size and calculate the diameter of an imaginary sphere that is equivalent in volume to 'equivalent spheres' technique. The Mastersizer 2000 has a measurement range of 0.02 to 2000 µm in diameter and a particle size resolution of 0.166 Ø in interval, resulting in 100 grain-size fractions [$Ø = \log_2(D)$, where D is the grain diameter in millimeters]. Grain-size statistical parameters and graphic representations are given in a logarithmic transformation of millimeters to integers. The Mastersizer dashboard provides the percentage by volume of each grain-size fraction in a sample. The relative error is <1% on the 50th percentile and 2% on the outlying percentiles. The mode is the most frequently-occurring particle diameter. The median corresponds to the 50 percentile on a cumulative curve, where half of the particles by weight are larger and half are smaller than the median. The mean is the average grain-size. All these analyses were performed at the GEOPS laboratory.

2.2.3. Clay mineralogy

Clay mineral analyses have undergone the same pretreatment as grain size analysis. 84 samples and 116 samples from cores Golman 6 and Golman 7 respectively at every 5 cm depth intervals and eight samples from the catchment area, were cleaned using 33% hydrogen peroxide (H_2O_2) bath and 20 % acetic acid (CH_3COOH) to obtain organic-free, non-calcareous sediment samples. Afterward, clay particles (≤ 2 µm) were separated by the sedimentation method according to Stokes' law and each sample was transferred to a glass slide by wet smearing. Samples were then air-dried under

natural conditions before clay analyses.

Clay minerals were identified by XRD on oriented flat mounts of clay sized (≤ 2 µm) particles with a PANalytical diffractometer. As shown in Fig. 6, three XRD runs were made, after air-drying (Ch), ethylene glycol solute treatment (EG) for 12 h, and heating at 500 °C for 2 h and returning back to normal temperature (N) (Holtzapffel, 1985). Peak identification of clay minerals was done primarily according to the position of the (001) series of basal reflections. Semi-quantitative estimates of basal reflection peak areas for four major clay mineral groups of smectite (16.9 Å), illite (10.0 Å), kaolinite (3.57 Å), chlorite (3.54 Å) and chlorite + kaolinite (7.16 Å) were carried out on the glycolated curve using the MacDiff software (Petschick, 2000). Relative proportions of kaolinite and chlorite in peak areas at 7.16 Å (kaolinite + chlorite) were determined based on the the peak area ratio of kaolinite (3.57 Å)/chlorite (3.54 Å). The evaluation of each clay mineral has an accuracy of about 5%. Furthermore, the chemistry index of illite was estimated using the ratio of the integrated 5 Å and 10 Å illite peak areas on the XRD diffractograms (Esquevin, 1969). The crystallinities of illite and smectite were separately obtained from the 10 Å and 16.9 Å peak full width at half maximum (FWHM) respectively. All analyses were performed at the GEOPS laboratory following the laboratory protocol.

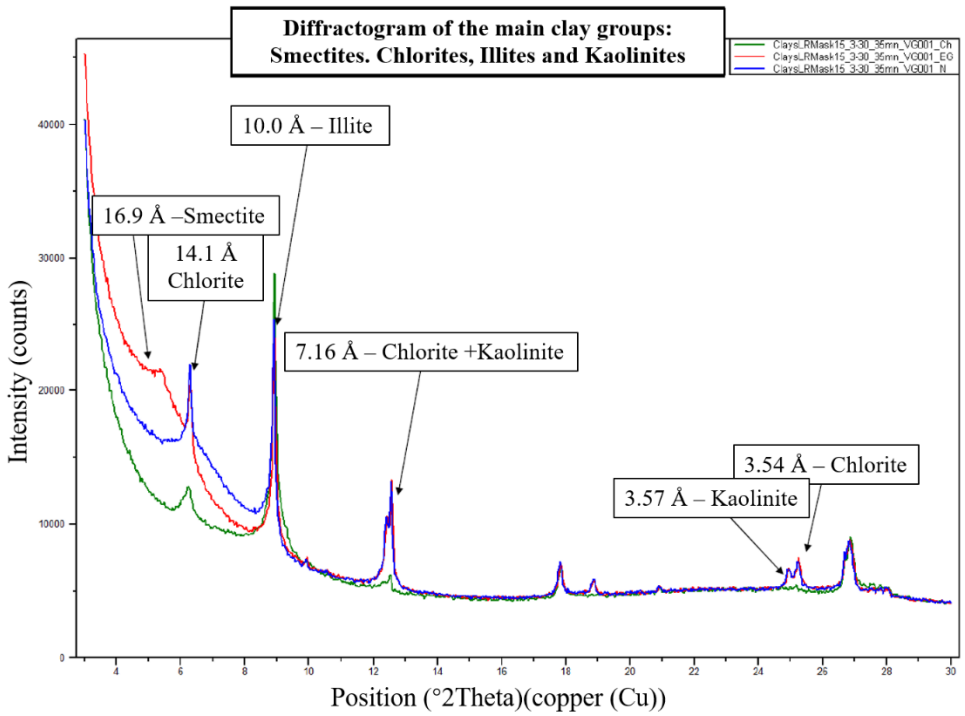

Fig. 6*. Diffractogram allowing an identification of the main groups of clays: smectites, chlorites, illites and kaolinites*

2.2.4. Bulk sediment mineralogy

Identification of total mineralogical components of the whole sediment was performed by XRD at the GEOPS laboratory. The XRD patterns of 54 samples from lake cores and 8 samples from the catchment area were analyzed with an X'Pert Pro PANalytical diffractometer, Cu-Kα1 source, 2Θ range 5°-80°, during 4 h runs. The identification of the mineralogical assemblages was performed using the PANalytical HighScore software with the open crystallography database and the ICDD PDF-4/Minerals database following the laboratory routine. The semi-quantification of all minerals including feldspars, mica, clay minerals, evaporates and carbonates was determined according to the area of the quartz main peak (3.34 Å).

In addition, specific carbonates could be identified by analyzing the 2Θ peaks in range of 24°-33° and the semi-quantification of the carbonate group was obtained by normalizing the areas of the main diffraction peaks of identified minerals (aragonite 3.39 Å; calcite 3.03 Å; Mg-calcite 2.99 Å; dolomite 2.88 Å). Since these four carbonates have similar structure and could overlap at the same 2Theta (2Θ) position, establishing the ratio of the normalized area of each carbonate to the sum of the standardized areas is complex. In order to obtain the real percentage of carbonate in our samples, we used carbonate standard samples (25% aragonite + 25% calcite + 25% Mg-calcite + 25% dolomite) to calculate the correlation coefficient of the main peaks of aragonite, calcite, Mg-calcite and dolomite in Fig. 7 (following GEOPS laboratory protocol established by S. Miska). Based on five repeatable experiments, the correlation coefficient of aragonite, calcite, Mg-calcite and dolomite are 0.0309, 0.3542, 0.2530, 0.3618 respectively. The calculated main peak areas of these four carbonate species in our samples are divided by the correlation coefficient to obtain their restored areas. The certain carbonate percentage is therefore equal to 100%*Restored Area $_{\text{certain carbonate}}$ /Restored Area $_{\text{(aragonite + calcite + Mg-calcite + dolomite)}}$. Taking aragonite as example, the equation is 100%*(Area $_{\text{aragonite}}$/0.0309)/ (Area $_{\text{aragonite}}$/0.0309+ Area $_{\text{calcite}}$/0.3542+ Area $_{\text{Mg-calcite}}$/0.2530+ Area $_{\text{dolomite}}$/0. 3618). In addition, the carbonate crystallinities of aragonite, calcite, Mg-calcite and dolomite were determined by the full width half maximum (FWHM) on the main peaks. This crystallinity index likely reflects the

authigenic or detrital origins of the crystal. As proposed by Fontes et al. (1993, 1996), detrital, well crystallized carbonates display thin shape of the peak and thus low values of crystallinity index while for authigenic carbonates that are less well crystallized, this index is high.

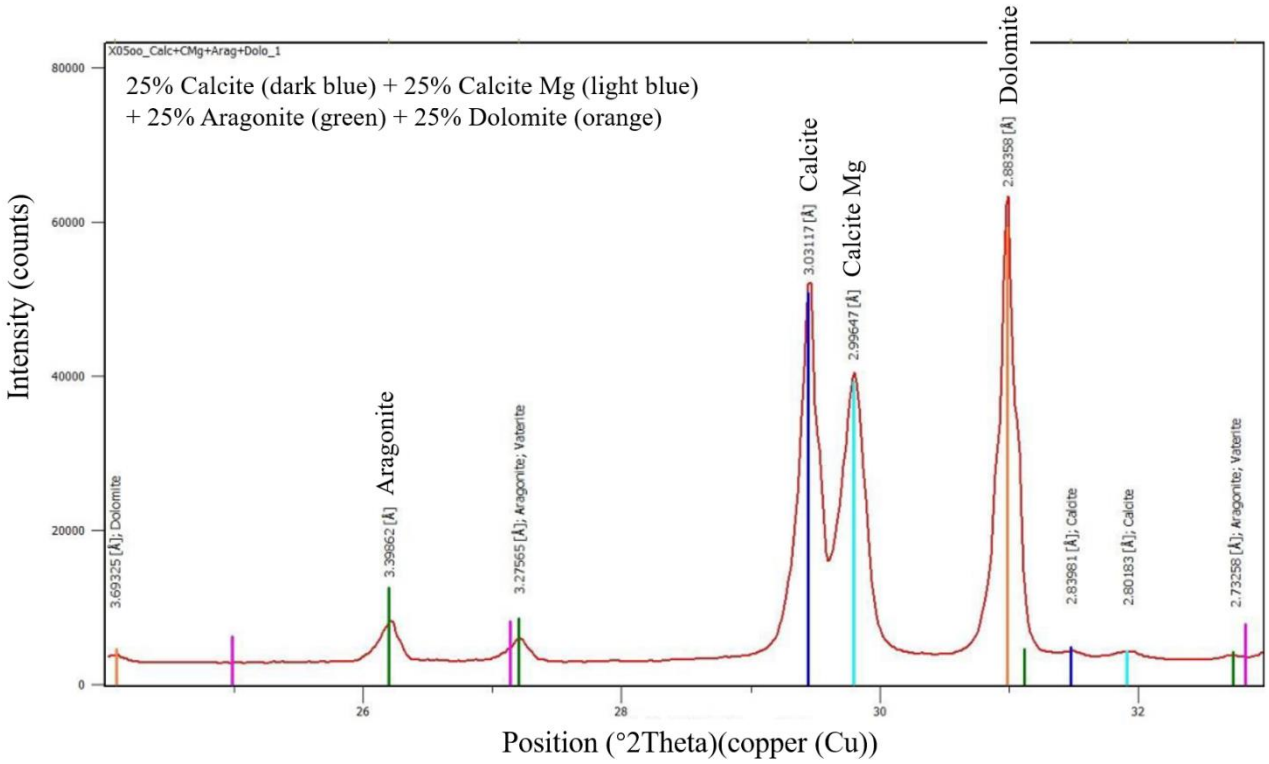

Fig. 7. *Diffractogram allowing identification of carbonates: calcite, Mg-rich calcite, aragonite and dolomite.*

2.2.5. XRF elementary Analysis

The elemental composition of the bulk sediments was non-destructively analyzed every 5 mm on the u-channel core using the 4th generation Avaatech XRF core scanner available at the Laboratoire des Sciences du Climat et de l'Environnement (LSCE, Gif sur Yvette, France).

Prior to the measurement, the sediment surface of each section was carefully smoothed, and covered with a 4-µm thick Ultralene foil to protect the measurement triangle and prevent sediment desiccation of the sediment. A molybdenum X-ray source set at 10 kV and 30 kV was used to generate a rectangular X-ray beam. Elemental intensities were obtained at 10 kV (current of 200 µA, no filter, under helium flow) for the light elements (Mg, Al, Si, K, Ca, Fe, Ti), and at 30 kV (current of 150

µA, thin Palladium filter, under air) for heavier elements (Fe, Ti, As, Zr, Rb, Sr). The measuring window is 5 mm (downcore) by 10 mm (crosscore), and the counting time is 10 s for both runs. The SARM4 certified standard (called "Monitor scan") was measured at 10 kV between each core section to ensure the scanner has no technical problems (e.g. absence of helium leak affecting the counts of light elements).

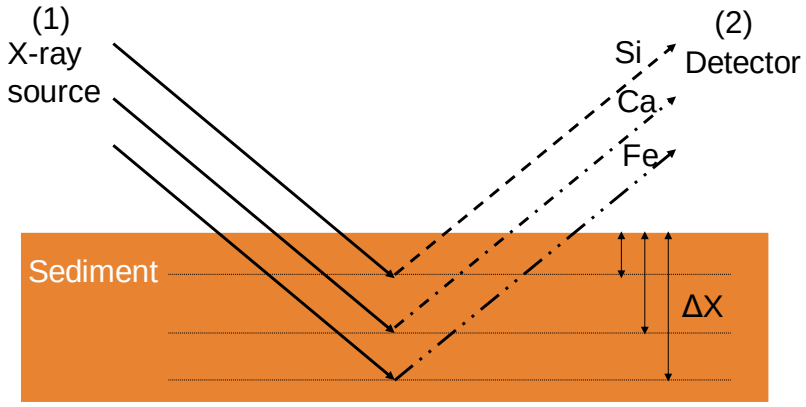

Fig. 8. *Simplified diagram representing principle of the X-ray fluorescence analysis of the elements Si, Ca, and Fe on sediment core and response depth (not to scale) (after Richter et al., 2016). Primary X rays (1) was used to ionize elements in the core sediment and each element emits an element-specific fluorescence radiation, which is registered by the detector; (2) Heavier elements emit stronger fluorescence energy, resulting in a larger depth (ΔX).*

As shown in Fig. 8, the primary X rays are emitted into the sediment and then the elements in the core sediment are ionized to emit an element-specific fluorescence radiation recorded by the detector (Richter et al., 2016). Generally, heavier elements emit stronger fluorescence energy and the detector records could display the presences of all elements occurring in core sediments. The fluorescent radiation emitted from the sample was recorded by an energy dispersive Si (Li) detector and transformed into element information for each measuring point. The chemical composition of the sediment is measured by the XRF scanner as element intensities in total counts (cnts), which are proportional to the chemical concentrations.

2.2.6. Carbonate content analysis

The percentage of carbonates including calcium carbonate ($CaCO_3$) and magnesium carbonates

($MgCO_3$) in samples was obtained by using a Mélières mono-calcimeter. The principle of this device is to measure the pressure of CO_2 released by a known mass of $CaCO_3$ after adding hydrochloric acid (HCl) in a closed glass tube of a volume normalized to one mole of gas.

In this study, 100 mg of pure calcium carbonate as a standard is reacted with 3 mL of 1 N HCl, obtaining a 1 atm pressure read on the manometer with the manometer reading error of about 0.5%. Therefore, 100 mg of dried and homogenized bulk sample reacting with 3 mL of 1 N HCl in a closed vessel, releases a pressure of 0.6 atm, which means that the percentage of $CaCO_3$ in the sample is 60%. All these measurements were done at the GEOPS laboratory.

2.2.7. Stable isotope analysis

2.2.7.1. Organic carbon analysis

In order to analyze the isotopic composition of organic carbon, mostly all original samples are pretreated using the classical acid (HCl)-alkali (NaOH)-acid (HCl) method adapted to the fragility and the available amount of the sample. The first step of the sample pretreatment is to remove the inorganic carbon (carbonates) in the samples by adding a volume of diluted 10% hydrochloric acid (HCl) solution into the glassware to about 10 g of sample until no reaction occurs. After removing all the inorganic carbon, deionized water is used to wash the sample until neutral pH. A second washing of the remaining sample with a 10% sodium hydroxide (NaOH) solution helps to remove humic acids during one hour, and then sample is rinsed until neutral pH. Finally, a second acid (HCl) attack is used to dissolve a potential carbonate secondary fraction due to atmospheric CO_2 absorption during the alkali step.

All sediment samples are then dried at 60 °C in an oven, mechanically crushed into homogenized powders using an agate mortar with a pestle, and finally weighted into a tin capsule. Meanwhile, three standards, including international standards USGS-40 and IAEA-600, and a working standard GG-IPG, are used to calibrate the elemental and isotopic values by linear regression equations for both carbon and nitrogen (Table 2). For each sediment and standard sample, three aliquots are prepared.

Carbon and Nitrogen percentage and the stable isotope analyses are conducted on an Elemental

Analyser (EA, Thermo Scientific Flash HT plus) coupled with a Thermo Scientific Delta V Advantage IRMS (Isotope Ratio Mass Spectrometry) under continuous flow mode at the GEOPS laboratory.

At the beginning of this experiment, the tin capsule containing the sample (or standard) is placed in a quartz combustion reactor with a stable temperature of 950 °C. The reactor delivers enough oxygen required for an optimal combustion of the sample at a precise time and then the oxygen reacts with the tin capsule at a temperature up to 1800 °C for a few seconds (flash combustion). Under this high temperature conditions, all substances containing C and N in the tin capsule are converted into oxidized gases CO_2 and NO_x (unstable). After further reduction of the nitrogen oxides on elemental copper, the CO_2 and N_2 gases are separated in a chromatographic column and could be detected by a highly sensitive thermal conductivity detector, delivering weight percentages of Carbon and Nitrogen. Subsequently, the IRMS detect elemental gases passing through the continuous flow interface, and the stable isotope ratios are acquired. Stable isotope of carbon ($\delta^{13}C$) and nitrogen ($\delta^{15}N$) respectively are expressed in ‰ relatively to the Vienna Pee Dee Belemnite (VPDB; form the PeeDee Formation, South Carolina, USA) and air (AIR) respectively (Coplen, 1995).

Table 2 *International and laboratory standards used for carbon and nitrogen isotope analyses on organic matter.*

Name	TOC(%)	TN (%)	C/N	δ^{13}C (‰)	δ^{15}N (‰)
USGS-40	40.8	9.5	4.3	-26.4	-4.5
IAEA-600	49.5	28.9	1.7	-27.8	1.0
GG-IPG	59.9	7.9	7.6	-23.2	10.0

2.2.7.2. Stable isotopes on carbonates

Carbon and oxygen isotope contents were determined through an automated carbonate preparation system, which is connected on-line to an isotope ratio mass spectrometer. The preparation line measured the isotope ratios of CO_2 released from the reactions of 100 µg carbonate with 100% orthophosphoric acid (H_3PO_4). The reaction was performed at 25 °C in a water bath for 24 hours, calcite ($CaCO_3$) could be fully reacted while dolomite ($CaMg(CO_3)_2$) would be only partially reacted as dolomite reacts much slower than calcite for a given grain size and crystallinity (Epstein et al.,

1964; Al-Aasm et al., 1990). The evolved CO_2 gas was subsequently analyzed for carbon and Oxygen stable isotopes at the Laboratoire des Sciences du Climat et de l'Environnement (LSCE, Gif sur Yvette, France). Stable isotopes of Carbon ($\delta^{13}C$) and Oxygen ($\delta^{18}O$) are calibrated according to two international standards (IAEA-CO8 and NBS-19) and an internal standard (IS-GEOPS) in Table 3 after the background was removed from an internal standard of LSCE.

The stable isotope ratio of oxygen marked as $\delta^{18}O$ is expressed in ‰ relatively to the Vienna Standard Mean Ocean Water (VSMOW), and then were converted to compared with the VPBD (Coplen, 1995).

Table 3 *International and laboratory standards used for stable isotope analyses on carbonates.*

Name	$\delta^{13}C$ (‰)	SD	$\delta^{18}O$ (‰)	SD
IAEA-CO8	-5.764	0.032	-22.7	0.2
NBS-19	1.95		-2.20	
IS-GEOPS	2.60		-2.40	

2.2.8. Radiocarbon chronology

An initial age model for the composite core (12.5 m long) of Lake Urmia was constructed based on AMS ^{14}C dating. Generally, ^{14}C analysis could be performed either on pure CO_2 gas or on graphite targets. The ^{14}C time-scale has been defined through 13 AMS dating both on (i) organic fractions including diffused organic matter and hand-picked charcoal, and (ii) carbonates on inorganic fractions or on hand-picked shrimp's fecal pellets when existing.

Each organic fraction was submitted to the standard chemical protocol for AMS analyses: 3 successive hydrochloric acid/sodium hydroxide/hydrochloric acid baths, followed by several rinses with deionized water up to neutral pH, and gently drying-up at 60 °C overnight.

The CO_2 gas was obtained (i) for organic fraction after the chemical pretreatment, burning at 860 °C for 30 min, under vacuum, in presence of a mixing of copper(II)- oxide/copper(III)-oxide and silver thread, and (ii) for carbonates, by an H_3PO_4 acid attack under vacuum during one night in a thermostatic bath according to an automated carbonate preparation system.

Then, AMS-^{14}C targets were obtained by graphitization of the CO_2 gas on powdered iron with

hydrogen at 650 °C for 100 min, and graphite compression under analytical plots. Aliquot of the CO_2 gas was then used for associated ^{13}C measurement. Graphite sources were pre- pared in GEOPS laboratory, and counted by the accelerator mass spectrometer at LSCE laboratory (Fig. 9, ECHoMICADAS facility, France).

Fig. 9. *The ECHoMICADAS Equipment (LSCE, Gif-sur-Yvette, France; Photo: F. Rhodes for the PANOPLY Platform, GEOPS/LSCE, University Paris-Saclay, Orsay, France).*

Analytical uncertainties, including laboratory errors, are between 0.5 and 0.8 pMC for ^{14}C activity. All the dates are converted to calendar ages according to the revised calibration program CALIB 8.2 (Execute Version 8.2 html 2020; Stuiver and Reimer, 1993; Stuiver et al., 2021).

Chapter 3: 30,000 years of the southwestern Lake Urmia (Iran) paleoenvironmental evolution inferred from mineralogical indicators from lake and watershed sediments

In this chapter, I present the results of research on the grain size and total mineralogy of lake sediments deposited in the south-western part of Lake Urmia over the last 30 kyr, and of the corresponding watershed rocks.

X-ray diffraction analyses were used to identify and semi-quantify the major silicates, carbonates, evaporates and clay minerals. Detrital and authigenic carbonates in lake sediment were also studied and semi-quantified. The timescale established is related to ^{14}C-AMS dates published in Tudryn and co-authors (2021; Annexe 1), but it is supplemented by 6 new reliable ^{14}C dates on organic matter and authigenic carbonates. The results show important changes in the lake water level for the past ~30 kyr, likely attributed to the available moisture. This unique palaeoenvironmental reconstruction complements the existing regional record and will contribute to a better understanding of past climate change on a supra-regional and global scales.

Journal of Asian Earth Sciences 239 (2022) 105387

Contents lists available at ScienceDirect

Journal of Asian Earth Sciences

journal homepage: www.elsevier.com/locate/jseaes

30,000 Years of the southwestern Lake Urmia (Iran) paleoenvironmental evolution inferred from mineralogical indicators from lake and watershed sediments

Ting Kong [a,*], Alina Tudryn [a], Elisabeth Gibert-Brunet [a], Piotr Tucholka [a], Seyed-Hani Motavalli-Anbaran [b], Hesam Ahmady-Birgani [c], Mohammad Lankarani [d], Serge Miska [a], Aurélie Noret [a], Olivier Dufaure [a]

[a] University Paris-Saclay, CNRS, UMR 8148-GEOPS, 91405 Orsay, France
[b] Institute of Geophysics, University of Tehran, Tehran, Iran
[c] Faculty of Natural Resources, Urmia University, Urmia, Iran
[d] School of Geology, University-College of Science, University of Tehran, Tehran, Iran

ARTICLE INFO

Keywords:
Lake Urmia
Late Quaternary palaeoenvironments
Water level change
Carbonates
Clay minerals,^{14}C dating

ABSTRACT

In order to understand the pattern and trends of the environmental evolution of Lake Urmia (Iran), one of the largest terminal lakes in Western Asia before its level drop over the past two decades, two sediment cores (Golman 6, 8.0 m; Golman 7, 12.5 m) were collected from the recently dried-out southwestern part of the lake. These sediment cores represent a continuous sedimentary sequence, composite core, that was extensively studied for grain size, total mineralogy including clay minerals, carbonates and their crystallinities, in comparison with the basin geological formations and within a reliable AMS-^{14}C timescale. Lake Urmia deposits cover the time-span from 30 to ca 2 cal kyr BP. Grain-size of the siliclastic fractions from the lower part of the composite core consists of fine-silt and clay particles likely representing lacustrine deposits while the top sediments are characterized by variable composition of sand and silt. At about 30 cal kyr BP, our proxies indicate a low lake stand and even drying out at the coring site, which was followed by water level rise and the establishment of lacustrine conditions between 29.9 and 20.2 cal kyr BP. Since then, all our data suggest lake's highly unstable conditions. Subsequently, clearly low lake levels to sometimes the drying out was recorded during the 20.2–15.3 cal kyr BP, 13.3–11.8 cal kyr BP and 5.6–4.1 cal kyr BP intervals. In contrast, lacustrine conditions were re-established between 15.3 and 13.3 cal kyr BP, between 11.8 and 5.6 cal kyr BP and between 4 0.1 and 2.3 cal kyr BP. High water level recorded between 15.3 and 13.3 cal kyr BP can be attributed to the Bölling/Alleröd warming, and the following regressive phase during the 13.3–11.8 cal kyr BP period corresponds to the Younger Dryas period. In the Early-Mid Holocene, the lacustrine environment from 11.8 to 5.6 cal kyr BP was characterized by high aragonite and salt contents, highlighting evaporative environment as like during the 29.9–20.2 cal kyr BP period. Our results allowed the Late Quaternary climate reconstruction at Lake Urmia basin scale and record the past climate change at a larger Western Asia scale.

1. Introduction

Located in Northwestern Iran, Lake Urmia is a natural habitat of brine shrimp *Artemia urmiana* and the salinity of lake water commonly ranges from 120 to 280 g.L^{-1}, regarded as a UNESCO biosphere reserve and a Ramsar wetland (Asem et al., 2012). However, since increased anthropic activities inside the lake basin (brine shrimp farming) and its watershed area (agriculture) in the mid-1990s, Lake Urmia dropped by 7 m, that led to drastic reduction in lake surface area, ground- and lake water salinization, desertification and dust storms threatening health conditions of millions of people at a regional scale (Alipour, 2006; Pengra, 2012; Ghalibaf and Moussavi, 2014; AghaKouchak et al., 2015; Ahmady-Birgani et al., 2015; Ahmady-Birgani et al., 2020). The decline of the lake water volume has already concentrated the original salinity

* Corresponding author.
E-mail address: ting.kong@universite-paris-saclay.fr (T. Kong).

https://doi.org/10.1016/j.jseaes.2022.105387
Received 8 April 2022; Received in revised form 25 August 2022; Accepted 31 August 2022
Available online 21 September 2022

even up to 380 $g.L^{-1}$ in many locations (Sharifi et al., 2018). The water-level drop has been attributed to anthropogenic causes such as the construction of many dams on rivers feeding the lake, abusive groundwater abstraction, and to rainfall declining (Alipour, 2006; Jalali et al., 2016), although the exact impact of both factors is still not clearly identified. Even if anthropogenic causes can be estimated and modified, the past evolution of the lake basin that may help to better understand the ongoing and future lakes evolutions is not well known although some data already existed. Asem et al. (2012) mentioned historical documents indicating that Lake Urmia experienced a severe drought in the beginning of the 1800's with a maximum lake depth of 75 cm and an east–west road created across the lakebed.

Existing studies of Late Quaternary sediments from Lake Urmia including sedimentology, geochemistry and pollen, are various but (i) concern only the most recent Holocene period about the last 2550 years (Talebi et al., 2016) or surface sediments (Erfan et al., 2017; Sharifi et al., 2018), (ii) focus on the whole Holocene but with a low temporal resolution (Bottema, 1986; Kelts and Shahrabi, 1986), or on Late Pleistocene and the Holocene without precise chronology (Mirzapour et al., 2021a; Mirzapour et al., 2021b), and/or (iii) cover large time scale (200 kyr) but again with poor or missing information on Late Pleistocene and the Holocene (Djamali et al., 2008a; Djamali et al., 2008b; Stevens et al., 2012). Whatever their chronological resolution, these studies indicate the highest amplitude of lake-level variations at a glacial-interglacial time scale with a dry open mountain steppe dominating during the glacial periods and a steppe-forest environment during interglacials. Over the Holocene, saline deposition seems almost continuous with clear water level changes but no visible total desiccation of the lake. The Artemisia steppe dominated the area, associated with saline lake deposition in a cool and arid climate up to ~ 9 kyr BP. A forest-steppe developed between 9 and 8 kyr BP and lasted until 7.5 kyr BP, at which time higher energy facies prevailed in a shallow saline saline lake. Finally, from 7 kyr BP onward, the vegetation became similar to that of today and present-day saline environments have persisted with many second-order water-level fluctuations (Bottema, 1986). In addition, the vegetation reached its maximum destruction due to increasing human impact during the last centuries. At a wider scale, a huge data set is available from the Anatolia region for Late Pleistocene and Holocene climate evolution (Kuzucuoğlu et al., 1999; Roberts et al., 2001; Jones et al., 2007; Roberts et al., 2008; Turner et al., 2008; Galicki and Doerner, 2010). For example, Lake Van displays high and changing water level between ca. 28 and 20 kyr (Kuzucuoğlu et al., 2010). Lakes as Gölhisar, Eski Acigöl and Van indicate a wetter early Holocene climate with deeper lakes that were less subject to evaporation. In contrast, during the mid-to-late Holocene, previous studies indicate that lake levels have declined to the point of drying up (Eastwood et al., 1999; Roberts et al., 2001; Jones et al., 2006; Eastwood et al., 2007; Jones and Roberts, 2008; Roberts et al., 2008).

As a consequence, most of the records are discontinuous during these dry-out periods. For Western Iran, detailed and complete climatic records from lacustrine sediments are rare. South of Lake Urmia, studies of Lakes Zeribar and Mirabad pointed out that Lake Zeribar displays a high stand during 25.7–21.1 and 15.4–12.6 cal kyr BP intervals, the most pronounced increase of salinity for the periods 17.7–15.4 and 12.6.–12.0 cal kyr BP, both associated with distinct drops in lake levels, a stable water level between 12.0 and 10.0 cal kyr BP, and from 6.0 cal kyr BP onwards, a periodically decreasing lake level with pronounced shallowing at about 7.8–7.5 and 4.5–3.8 cal kyr BP, and later on, less significant fluctuations (Wasylikowa et al., 2006). On the opposite, Lake Mirabad area, the early Holocene (10–6.5 cal kyr BP) was drier than the late Holocene, and a severe 600-yr drought occurred at ca. 5.5 cal kyr BP (Stevens et al., 2006).

Located at the eastern limit of the Mediterranean zone, Western Iran and Inner Anatolia link Southern Europe, North Africa and Asia. The climate there is governed by interactions between the mid-latitude westerlies, the Siberian Anticyclones and the Indian Ocean Summer Monsoon (Sharifi et al., 2015). However, most of the moisture is transported by westerlies from the North Atlantic, the Mediterranean and the Black Sea depression (Djamali et al., 2010).

However, other factors could have played an important role in bringing humid air masses into Western Iran and Inner Anatolia in the past. Indeed, as pointed by Jones and co-authors (2008), existing studies from Anatolia, suggest for example, that during the Early Holocene, phases of relatively high humidity rate are connected with an intensification of rainfall originating from the Indian monsoon while during Late Holocene, the effects is the opposite with increased monsoonal precipitation leading to increased evaporation in the study area (Eastwood et al., 1999; Roberts et al., 2001; Jones et al., 2006; Eastwood et al., 2007; Jones et al., 2007; Jones and Roberts, 2008; Roberts et al., 2008; Turner et al., 2008; Galicki and Doerner, 2010; Tudryn et al., 2013). Because of its geographical position, Lake Urmia, is a truly privileged place to compare its climate records with other sites in Anatolia. This composition is crucial to better identify moisture sources and thus better understand the processes driving climate change across the region.

The present study aims to accurately decipher the pattern and trends of environmental change in the southwestern part of the Lake Urmia basin over the last 30 kyr through accurate mineralogical and grain-size indicators from both sedimentary cored sequences and geological samples taken from the watershed of the Shahr Chay River, which is the main supplier of detrital inputs to our coring site. Preliminary results on Lake Urmia sedimentary cores were published by our team (Tudryn et al., 2021), proposing the lake level fluctuations mainly through magnetic records with however a ^{14}C timescale based on sparse but fairly reliable data. In order to clarify these environmental phases and to better link the sedimentation at the Shahr Chay River mouth with the cored deposits, we therefore performed X-ray diffraction analyses, separations and analyses of clay phases as well as a series of particle size distributions.

These data will allow us to decipher the major processes taking place on the Shahr Chay River watershed by deconvoluting the predominant chemical or physical erosional processes as precisely as possible, in order to understand the climatic conditions prevailing in the basin.

We thus present here the results of the identification and semi-quantification of the principal silicates, carbonates, evaporates, and clay minerals on the clayish fraction. We also distinguished and semi-quantified detrital and authigenic carbonates in the lake sediment. The timescale of this paleoenvironmental reconstruction is linked to ^{14}C-AMS dates published in Tudryn and co-authors (2021) but added by 6 new reliable ^{14}C dates of organic matter and authigenic carbonates.

Studies of environmental changes in the past 30,000 years as recorded in sediments of Lake Urmia provide new insights about climate change at the regional scale, identifying its causal mechanisms and better predicting its possible future evolution. This newly defined, robust and reliable dataset will help modelers to construct accurate models of climate evolution at both regional and global scales, and finally, to understand and anticipate the future lake evolution.

2. Study area

Lake Urmia (35.5–38.5° N and 44–48° E) is a basin lake tectonically in the converged zone between the colliding Arabian and Eurasian plates, in the Alps-Himalayan orogenic belt (McKenzie, 1976) (Fig. 1a). It corresponds to the tectonic depression associated to the functioning of both the major Tabriz fault system in the northeastern Lake Urmia and the western Zagros active overlapping zone (Solaymani Azad, 2009). Based on Sharifi et al. (2018), the lake has two sub-basins: the deep northern basin and the shallow southern basin with average water depths of 10 and 2 m respectively. Between two basins, an east–west dike-type highway that stretches 15 km across the center of the lake has been constructed. The whole lake has 13 perennial and seasonal tributaries, but the main water inflow to the southwestern lake area close to

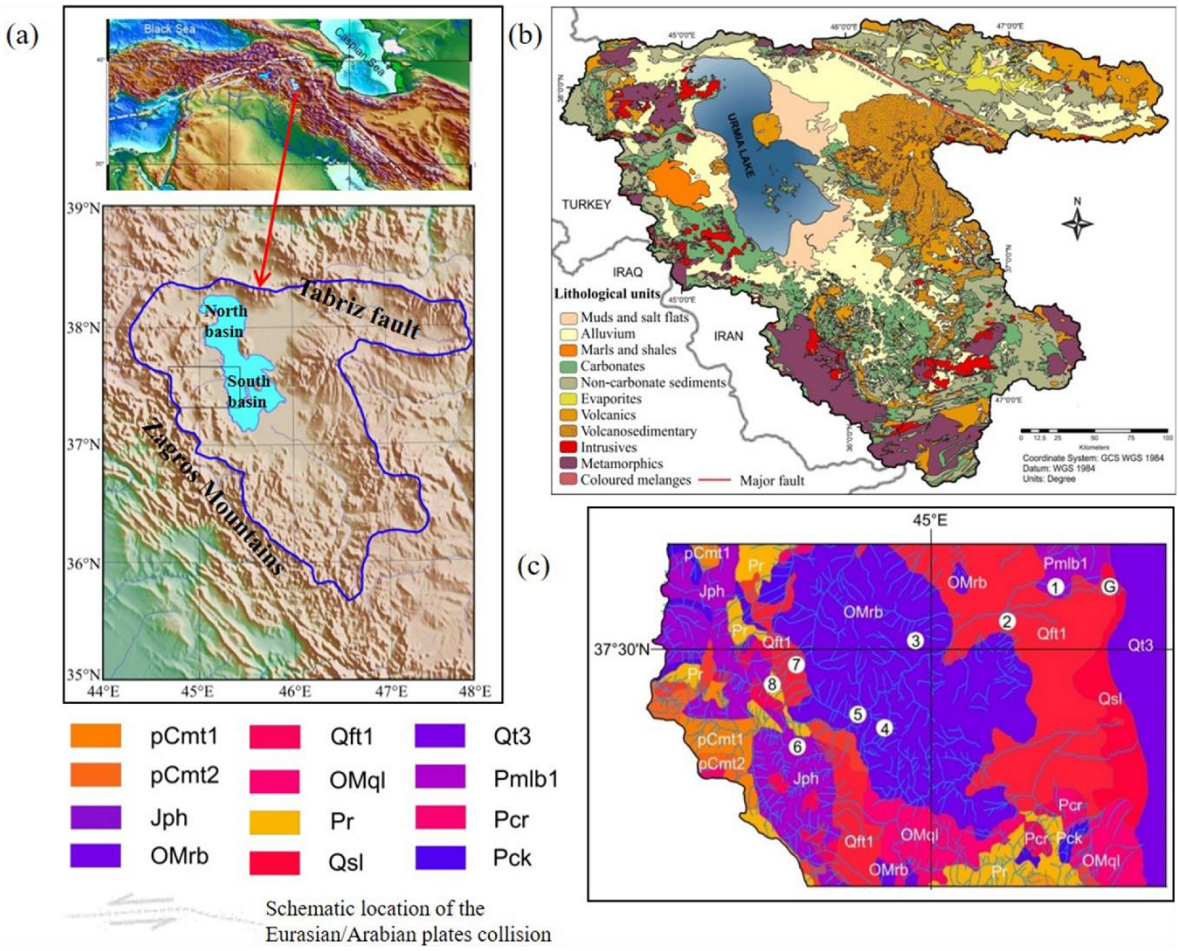

Fig. 1. Lake Urmia: (a) location of the lake and lake's catchment area, black rectangle indicates study area; (b) simplified geological map of Lake Urmia catchment area (after Sharifi et al., 2018, completed with information from Geological Map of Iran, Sheet No 1 North-West Iran); (c) detailed geological map of the study area with location of samples from the catchment area (1 to 8) and of coring site (G). Lithological units: pCmt1 - Medium grade (Amphibolite Facies) Precambrian metamorphic; pCmt2 – Low grade, regional metamorphic rocks (Green Schist Facies); Jph - Phyllite, slate and *meta*-sandstone (Hamadan Phyllites); Omrb - Red Beds composed of red conglomerate, sandstone, marl; Qft1 - High level piedmont fan and valley terraces deposits; Omql – Massive to thick - bedded reefal limestone; Pr - Dark grey medium - bedded to massive limestone (RUTEH); Qsl - Clay flate; Qt3 - no description – lake; Pmlb1 - Pyroclastics and claystone with vertebrate fauna remains; Pcr - Dolomite, sandstone and volcanic rocks (Rizu Series); Pck:Dull green grey slaty shales.

the coring site originates from Shahr Chay River that is also named Shahi Chay River (Sharifi et al., 2018). Sharifi and co-authors (2018) also report the annual mean river discharge and the mean catchment area of the major tributaries. Lake Urmia displays a unique, highly valuable biodiversity that favors a highly productive agriculture and brine shrimp farming, and makes the region as one of the most important economic poles of Iran.

The geology of Lake Urmia catchment is quite diverse, ranging from Precambrian metamorphic complexes to Quaternary mud deposits (Fig. 1b). In the east and northeast parts of the catchment, volcanic and volcano-sedimentary formations dominate while intrusive rocks prevail over the rest of the catchment, with mainly metamorphic rocky outcrops in the Zagros to the west, complemented in the south by dolomites, sandstones, quartz and volcanic rocks from the Infracambrian. Carbonate rocks are found in south and western parts of the basin while evaporative sedimentary units are only found northeast of the watershed.

Owing to the effects of local topography, the Urmia basin climate is mainly controlled by the surrounding mountains, and thus the semi-arid continental climate is characterized by rather large variations in temperature and precipitation. According to the Urmia meteorological station (west of Urmia Lake at 1,313 m a.s.L.), the temperature was below 10 °C in winter and up to 40 °C in summer, and the mean annual precipitation was recorded as about 300 mm (Kelts and Shahrabi, 1986; Sharifi et al., 2018). Westerlies are prevailing winds in winter, southwesterlies in spring and northeasterlies in summer (Djamali et al., 2008b).

Whereas a steady decline is registered since several years, the most recent satellite altimeter data indicating a drop of approximately 7 m over the last 20 years, with a lake level ranging from 1277.5 m in 1999 to 1270.85 m in 2019 (Ahmady-Birgani et al., 2020). Because the southern part of the lake (south of the dike-type highway) is relatively shallow, the water level decline exacerbates the dramatic decline of the lake surface area. According to Ahmady-Birgani et al.(2020), the lake surface decreases all the time and from 1999 to 2019, the lake even lost half of its surface area (5000 km^2 in 1999 vs 2400 km^2 in 2019) and had less of almost 20 bm^3 of its water volume.

3. Materials and methods

3.1. Material collection

3.1.1. Lake sediment sampling

In September 2017, two sediment cores, i.e. Golman 6 (8.0 m long) and Golman 7 (12.5 m long), have been collected from the SW part of recently dried out part of the lake, near the city of Urmia (Fig. 1c, Table 1). The cores have been taken in close proximity to each other, with the mechanic corer and a borehole casing at a distance from today's shoreline allowing safe use of the corer. Details of sampling and coring conditions are given in Tudryn et al. (2021). The coring was stopped when pressurized water with mud and gas with an intense H_2S odor rose up from the Golman 7 borehole to the lake surface and when gas with the same odor rose up from the Golman 6 borehole.

Due to the presence of interbedded captured water (either residual water from the sediment or ancient lake water trapped within the deposits), the 4.2 to 8.65 m section of Golman 7 core was too humid to be retrieved by the corer, leading to an empty section for this depth interval. Moreover, consequently to the soft and humid lacustrine ground at the core site, the first section of Golman 6 core taken from 0 m to 4.0 m depth, was compacted and only collected as 3.15–4.0 m depth. Although the two cores Golman 6 and Golman 7 present these inconsistencies, they represent together a continuous sequence as a composite core (Fig. 2a, b, c).

3.1.2. Catchment sediment sampling

In June 2021, eight geological samples have been collected from the catchment area of the Shahr Chay River that is the major supplier of detrital material into the lake at the coring location. These 8 samples have been selected according to the main geological formations of the river catchment (Table 1, Fig. 1c). Accordingly, samples represent the following formations: 1- pyroclastic and claystone with vertebrate fauna remains, andesitic to basaltic volcanics; 2 and 7- high level piedmont fan and valley terraces deposits; 3, 4 and 5-red beds composed of red conglomerate, sandstone, marl, gypsiferous marl; 6 - phyllite, slate and *meta*-sandstone (Hamadan phyllites); 8 - dark gray medium- bedded to massive limestone.

3.2. Methods

3.2.1. Grain size and clay mineralogy

Grain size and clay mineral analyses have been performed at the GEOPS laboratory, Paris-Saclay University (Orsay, France) on 116 and 84 samples taken at every 5 cm depth intervals from cores Golman 7 and Golman 6 respectively. For each sample, about 5 g of air-dried, disaggregated sediment was pre-treated in a 33 % hydrogen peroxide (H_2O_2) bath to remove organic matter and then with a 20 % acetic acid solution (CH_3COOH) to remove carbonates. After that, the samples were rinsed with deionized water in order to obtain neutral pH. These organic-free and carbonate-free samples have then been used for grain size distribution and for clay mineral analyses. The grain-size distribution was carried out on samples dispersed by ultrasonic vibrator for 3 min before analysis using a Malvern Mastersizer 2000 laser device.

Clay minerals have been identified by X-ray diffraction (XRD) on oriented mounts of clay sized (less than2 μm) particles with a PANalytical diffractometer, following the laboratory routine of the GEOPS laboratory. Three XRD runs were made, after a specific chemical treatment of air-drying, ethylene glycol solute leaching for 12 h, and heating at 500 °C for 2 h and return back to normal temperature (Holtzapffel, 1985). The identification of clay minerals peaks was made mainly according to the position of the (0 0 1) series of basal reflections. Semi-quantitative estimates of peak areas of the basal reflections for the main clay mineral groups of smectite (including mixed-layers) (16.9 Å), illite (10 Å), kaolinite (3.57 Å), chlorite (3.54 Å) and kaolinite + chlorite (7.16 Å) were carried out on the glycolated curve using the MacDiff software (Petschick, 2000). Relative proportions of kaolinite and chlorite were determined based on the ratio 3.57/3.54 Å of the peak areas. Evaluation of each clay mineral has an accuracy of ca 5 %. Furthermore, the illite chemistry index was estimated using the ratio of the integrated 5 Å and 10 Å illite peak areas on the XRD diffractograms (Esquevin, 1969). The illite chemistry index value greater than 0.4 represents the Al-rich illites, while a value less than 0.4 represents Fe- and Mg- rich illites (Diekmann et al., 1996; Ehrmann et al., 2005). Additionally, the illite and smectite crystallinities were separately obtained from the full width half maximum (FWHM) of the 10 Å and 16.9 Å peak respectively. According to Ehrmann et al. (2005), this parameter indicates the state of illite crystallization as (i) very well crystallized (less than0.4), well crystallized (0.4–0.6), moderately crystallized (0.6–0.8), poorly crystallized (greater than0.8), and of (ii) smectite as well crystallized (less than1.5), moderately crystallized (1.5–2.0), and poorly crystallized (greater than2.0) (Ehrmann et al., 2005).

3.2.2. Bulk sediment mineralogy

Identification of total mineralogical components of the whole sediment has been performed by XRD at GEOPS laboratory by XRD analyses of 52 samples with an X'Pert Pro PANalytical diffractometer, Cu-K source, 2Θ range 5°-80°, 4 h runs. The identification of mineralogical phases was conducted using the PANalytical HighScore software with crystallography open database and ICDD PDF-4/Minerals database following the laboratory routine at GEOPS laboratory. The semi quantification of minerals was determined according to the area of main peak on quartz (3.34 Å). In addition, specific carbonates have been identified through analyzes during 45 min with 2Θ range 24°–33°. Then the semi-quantification of the carbonates was obtained by normalizing the areas of the diffraction peaks of identified minerals (aragonite 3.39 Å; calcite 3.03 Å; dolomite 2.88 Å) with respect to the percentage of areas coming from an equi-mass mixture of carbonates, then setting the ratio of the

Table 1
Location and description of Lake Urmia cored sequences and of geological samples from the Shahr Chay River catchment. Numbering of cores and samples in the text and figures refers to this table.

	Site name	Comment on sampling	Latitude N	Longitude E	Altitude m asl ± 1 *m*
Coring well	Golman 6	8 m deep	37°35′28.854″	45°16′33.834″	1270
	Golman 7	12.5 m deep	37°35′28.746″	45°16′33.75″	1270
Catchment area samples	1	Pyroclastic and claystone with vertebrate fauna remains, andesitic to basaltic volcanics	37°34′48″	45°12′00″	1370
	2	High level piedmont fan and valley terraces deposits	37°32′24″	45°07′12″	1311
	3	Red Beds composed of red conglomerate, sandstone, marl, gypsiferous marl (mostly limestones)	37°28′48″	44°57′36″	1484
	4	Red Beds composed of red conglomerate, sandstone, marl, gypsiferous marl (pure marl)	37°23′24″	44°55′12″	1720
	5	Red Beds composed of red conglomerate, sandstone, marl, gypsiferous marl	37°24′36″	44°52′48″	1614
	6	Phyllite, slate and *meta*-sandstone (Hamadan Phyllites)	37°22′12″	44°48′00″	2820
	7	High level piedmont fan and valley terraces deposits	37°28′48″	44°47′24″	1788
	8	Dark gray medium- bedded to massive limestone (limestone)	37°27′00″	44°45′00″	2246

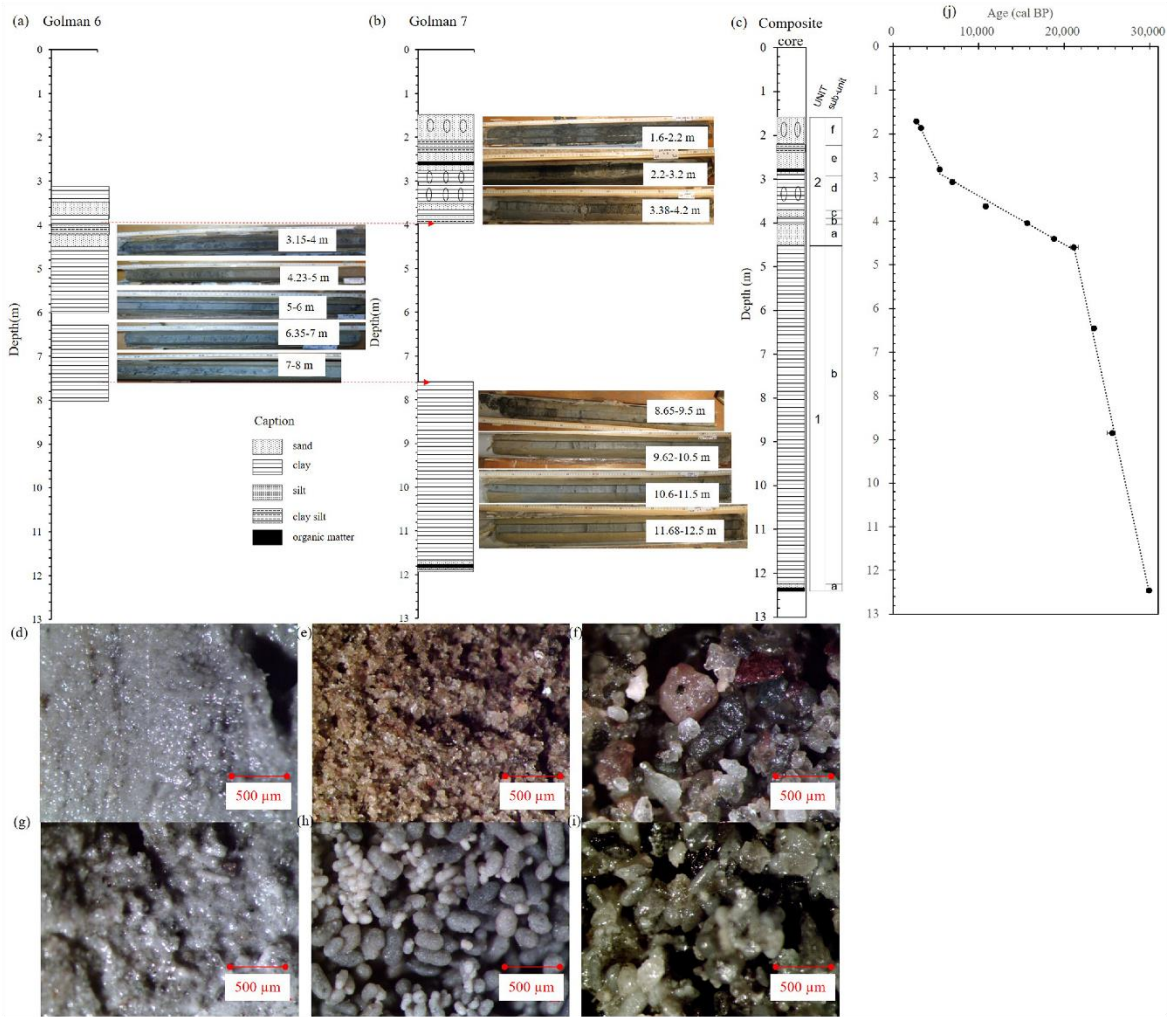

Fig. 2. Down-core variation of simplified lithofacies from Lake Urmia sediments: (a) core Golman 6; (b) core Golman 7; (c) composite core and lithology units, optical microphotograph from composite core for: (d) clay at 12.12 m depth; (e) fine silt at 4.12 m depth; (f) sand at 2.75 m depth; (g) clayish sediment with fecal pellets at 10.92 m depth; (h) fecal pellet rich clayish sediment at 3.09 m depth; (i) sandy sediment with fecal pellet rich at 2.00 m depth (j) the age-depth model for the composite core obtained using AMS ^{14}C in this study.

normalized area of each carbonate to the sum of the standardized areas. Associated to the relative percentages of these carbonates, carbonate crystallinity was measured on the main peak through full width half maximum (FWHM). This index determined by measuring the enlargement of the carbonate peak likely reflects the authigeny of the crystal. Indeed, according to Fontes et al. (1993, 1996), detrital, well crystallized carbonates display thin shape of the peak and thus low values of crystallinity index while for authigenic carbonates that are less well crystallized, this index is high (Fontes et al., 1993; Fontes et al., 1996).

3.2.3. Radiocarbon chronology

The time-scale has been defined through 13 AMS ^{14}C dating both on (i) organic fractions including diffused organic matter and hand-picked charcoal, and (ii) carbonates fractions on inorganic fractions and on hand-picked shrimp's fecal pellets when existing.

Each organic fraction was submitted to the standard chemical protocol for AMS analyses: 3 successive hydrochloric acid/sodium hydroxide/hydrochloric acid baths, followed by several rinses with deionized water up to neutral pH, and gently drying-up at 60 °C overnight.

The CO_2 gas was obtained (i) for organic samples by burning at 860 °C for 30 min, under vacuum, in presence of a mixing of copper(II)-oxide/copper(III)-oxide and silver thread, and (ii) for carbonates, by an H_3PO_4 acid attack under vacuum during one night in a thermostatic bath. Then, AMS-^{14}C targets were obtained by graphitization of the CO_2 gas on powdered iron with hydrogen at 650 °C for 100 min, and graphite compression under analytical plots. Aliquot of the CO_2 gas was then used for associated ^{13}C measurement. Graphite sources were prepared in GEOPS laboratory, and counted by the accelerator mass spectrometer at LSCE laboratory (ECHoMICADAS facility, France).

Analytical uncertainties, including laboratory errors, are ± 0.1 ‰ for δ ^{13}C and between 0.5 and 0.8 pMC for ^{14}C activity. All the dates are converted to calendar ages according to the revised calibration program CALIB 8.2 (Execute Version 8.2 html 2020; Table 2) (Reimer et al., 2013; Reimer et al., 2020; Stuiver et al., 2021).

Table 2 *AMS-^{14}C calibrated ages of Lake Urmia sediments. Sample depth refers to the composite core (see text). All corrections and calibration are detailed in paragraph "^{14}C chronology".*

Sample	Depth (cm)	Type (*)	Sample Nr	F^{14}C (pMC)	σ (b)	Measured ^{14}C ages (BP)	σ (b)	Mineralogy of the carbonate fraction Aragonite (%)	Calcite (%)	Dolomite (%)	Crystallinity of the carbonate fraction Aragonite	Calcite	Dolomite	δ^{13}C (‰ PDB)(c)
Lake surface water			E2476	93,46	0,250	540	20							-1,10
Golman-5 core														
G5	2,34	Charcoal	B2087	0,5824	0,20	4 343	25							-14,50
G5	2,66	Charcoal	B2088	0,5787	0,20	4 394	22							-25,50
Composite core (Golman-6 and Golman-7 cores)														
G7	1,70	$CaCO_3$		0,5580	0,32	4 265	26	94,2	3,8	1,9	0,131	***0,095***	0,370	
G7	1,85	OM	B2295	0,5306	0,002	5 090	25							
G7-S2	2.80	Charcoal	B2097	0,5547	0,40	4 735	22							-26,50
G7-S2	3,07	$CaCO_3$	CaCO3	0,3334	0,42	8 825	34	95,9	3,3	0,7	0,100	***0,130***	***0,150***	
G7-S2	3,09	White FP (**)	A21542	0,3666	0,0035	8060	80	100.0						
G7-S2	3,09	Black FP (**)	A21543	0,3880	0,0036	7600	80	(secondary carbonate precipitation suspected)						
G7-S2	3,09	$CaCO_3$	CaCO3	0,3579	0,41	8 250	33	96,7	2,3	<0,01	0,110	***0,130***	0,230	
G7-S3	3,65	$CaCO_3$	CaCO3	0,2377	0,53	11 540	42	93,9	4,2	1,8	0,143	***0,089***	0,380	
G7	4,05	OM	B2297	0,1529	0,10	15 090	66							-25,3
G6-S2	4,40	OM	B2304	0,1124	0,0011	17 560	76							
G6 S2	4,60	$CaCO_3$	62001	0,0662	0,12	21 810	140	58,3	30,2	11,4	0,100	***0,140***	0,200	
G6-S4	6,45	OM	B2300	0,0689	0,0005	21 490	63							
G7 S6b	8,85	OM	B2099	0,0554	0,12	23 240	170	51,3	21,1	25,7		***0,123***	***0,140***	
G7-S8	12.46	Charcoal	B2301	0,0005	0,001	25 590	96							-25,90

Sample	Depth (cm)	Type (a)	Sample Nr	F^{14}C (pMC)	σ (b)	Measured ^{14}C ages	σ (b)	^{14}C Ages corrected from detrital fraction (yr BP)	^{14}C Ages corrected from a 2-kyr HWE (yr BP)	Calibrated ^{14}C Ages (cal BP)	2σ
Lake surface water		Water	E2476	93,46	0,250	540	20				
Golman-5 core											
G5	2,34	Charcoal	B2087	0,5824	0,20	4 343	25	4 340	4 340	**4 910**	-60/+60
G5	2,66	Charcoal	B2088	0,5787	0,20	4 394	22	4 390	4 390	**4 940**	-75/+100
Composite core (Golman-6 and Golman-7 cores)											
G7	1,70	$CaCO_3$		0,5580	0,320	4 265	26	**4 560**	2 560	**2 720**	-205/+30
G7	1,85	OM	B2295	0,5306	0,002	5 090	25	3 090	3 090	**3 295**	-75/+65
G7-S2	2.80	Charcoal	B2097	0,5547	0,400	4 735	22	4 730	4 730	**5 475**	-145/+105
G7-S2	3,07	$CaCO_3$	CaCO3	0,3334	0,420	8 825	34	**8 730**	6 730	7 595	-80/+70
G7-S2	3,09	Black FP (**)	A21543	0,3880	0,0036	7 600	80	*(secondary carbonate precipitation suspected)*			
G7-S2	3,09	White FP (**)	A21542	0,3666	0,0035	8 060	80	8 060	6 060	**6 920**	-180/+240
G7-S2	3,09	$CaCO_3$	CaCO3	0,3579	0,410	8 300	33	**8 300**	6 300	7 215	-55/+90
G7-S3	3,65	$CaCO_3$	CaCO3	0,2377	0,530	11 540	42	**11 520**	9 520	**10 850**	-245/+225
G7-S3	4,05	OM	B2297	0,1529	0,100	15 090	66	15 090	13 090	**15 695**	-230/+235
G6-S2	4,40	OM	B2304	0,1124	0,0011	17 560	76	17 560	15 560	**18 845**	-135/+135
G6-S2	4,60	$CaCO_3$	62001	0,0662	0,120	21 810	140	**19 470**	17 470	**21 115**	-385/+575
G6-S4	6,45	OM	B2300	0,0689	0,0005	21 490	63	19 490	17 490	**23 510**	-260/+255
G7 S6b	8,85	OM	B2099	0,0830	0,123	23 240	82	23 240	21 240	**25 610**	-555/+375
G7-S8	12.46	Charcoal	B2301	0,0005	0,001	25 590	96	25 590	25 590	**29 950**	-290/+165

(*) Apparent Hard Water Effect (HWE) calculated with a ^{14}C activity of atmosphere of 100 pMC

(a) $CaCO_3$: total carbonate fraction; OM: diffused organic matter; FP: fecal pellets (*Artemia*)

(b) Error bars represent one sigma deviation

(c) Accuracies on ^{13}C measurements are of ±0.05 and ±0.02% PDB for carbonates and organic matter, respectively

(d) *Stuiver, M., Reimer, P.J., and Reimer, R.W., 2021, CALIB 8.2 [WWW program] at* http://calib.org

4. Results

4.1. Catchment area samples

The results of grain size, bulk sediment mineralogy and clay minerals analyses of 8 samples from the main geological formations are presented in Table 3 and Fig. 3. Grain size distribution indicates that the silt fraction predominates in all samples, ranging from 67.5 to 85.2 %. In the silty fraction, coarse silt with 36.3 to 53.9 % presents higher content than the fine one with 15.7 to 38.4 % respectively; only sample 6 shows both two fractions in the same proportions. The second dominant fraction is sand ranging from 9.3 to 28.3 %, while the clayish fraction remains at low contents, i.e. between 2.2 and 5.8 %.

Considering bulk sediment samples, several groups of minerals are identified such as (i) carbonates (calcite and dolomite), (ii) silicates: quartz, mica (muscovite), feldspar (albite, orthoclase, anorthite), amphibole (hornblende), clays (chlorite, kaolinite, illite, smectite and some palygorskite), and (iii) oxides and hydroxides: rutile, magnetite and goethite. Among these minerals, the most frequent ones have been semi-quantified (Table 3 and Fig. 3).

As a whole, calcite and quartz are predominant. Quartz varies between 7.3 and 55.8 % and reaches the highest values (31.7 and 55.8 %) in samples 2, 6 and 7. Calcite prevails in samples 1, 3, 4, 5 and 8, ranging from 53.9 to 79.3 %, while it is absent in sample 6. Dolomite is only present in samples 1, 2, 3, 5 and 8, and varies between 5.8 and 18.5 %. Low values of crystallinity index obtained for calcite and dolomite in all units where they occur (0.08–0.12) indicate that they are well crystallized (Fontes et al., 1993; Fontes et al., 1996).

In all samples, clays, mica and feldspars are in relatively low contents except sample 6, in which the high values are 19.1 %, 29.8 % and 19.3 %, respectively. Further analysis of the clay assemblages in the clay-sized siliceous fraction, which allows more accurate estimates than in the bulk sediment, shows that smectite and illite are the most common (Table 3 and Fig. 3). Smectite is predominant in samples 1 and 7, with 58.2 and 72.7 %, respectively. Meanwhile, the ratios of smectite/illite (S/I) in these two samples are more than 3. Illite prevails in samples 3,5,6 and 8, ranging from 42.4 to 52.0 %, as a consequence of the S/I ratio much smaller than 1. In samples 2 and 4, smectite and illite display similar percentages with a S/I ratio about 1. Kaolinite and chlorite reach lower values as a whole. Chlorite shows the same change pattern with illite and one can observe that chlorite contents are quite high reaching even to 31.9 % in samples where illite dominates. Nevertheless, it is very low in sample 7. Kaolinite remains at about 10 %, with however higher values for samples 5 and 8 (ca 18 %) and lowest value for sample 7 (2.2 %).

The illite chemistry index of all eight samples is less than 0.4 (Table 3 and Fig. 3), suggesting Fe- and Mg-rich illites as it was proposed by Diekmann et al. (1996) and Ehrmann et al. (2005). In addition, smectite and illite crystallinities of these samples are ranging from 0.27 to 0.76 and from 0.17 to 0.30 respectively. Being less than 1.50 for smectite and less than 0.40 for illite, these values indicate well-crystallized clay minerals (Diekmann et al., 1996; Ehrmann et al., 2005).

4.2. Lake sediments

4.2.1. Lithology

The 8-m long Golman 6 core presents two major sedimentary sequences, under and upper the 4.52 m depth (Fig. 2a). In the lower part from 8.00 to 4.52 m depth, quite fine, grey silty and clayish sediments dominate while the above 4.52–4.23 m interval is composed of sandy and silty deposits. In the last section of the upper part in Golman 6 core has been compacted to the 4–3.15 m interval from 4 to 0 m during coring. The Golman 7 sequence is 12.5 m long and also divided into two major sequences separated by an empty interval due to missing sediment between 8.65 and 4.20 m (Fig. 2b). The lower part between 12.50 and 8.65 m depth is mainly composed of grey silts and clays while the above section from 4.20 m to the core top at 1.60 m depth encloses several lithological variations highlighted, similarly as in the Golman 6 core, by changes in the grain size, color and nature of the sediment.

The lacustrine sedimentation depicted in these two cores evidences the same lithological succession, although with slight differences in unit thicknesses. In order to better integrate and therefore interpret all the results as a whole set of data, a single stratigraphic sequence was reconstructed based on lithological changes as well as on carbonate contents and magnetic susceptibility (Tudryn et al., 2021). The composite sequence defined thus displays the complete Lake Urmia

Table 3
Mineralogy including crystallinity of selected minerals, and grain-size parameters on the geological samples collected from the Shahr Chay River catchment (samples from 1 to 8, for details see Table 1).

Sample Number	1	2	3	4	5	6	7	8	
Grain size	Clay (%)	4.5	2.2	4.8	5.2	5.1	5.8	4.2	5.5
	Fine silt (%)	28.5	15.7	30.1	24.1	37.5	38.4	30.5	37.4
	Coarse silt (%)	53.7	53.9	42.1	43.4	45.1	36.3	54.3	47.8
	Silt (%)	82.2	69.6	72.2	67.5	82.6	74.8	84.8	85.2
	Sand (%)	13.3	28.3	23.0	27.4	12.4	19.4	11.0	9.3
	Mode (μm)	27.6	61.8	27.2	25.8	13.4	7.9	31.3	16.1
	Median (μm)	20.0	41.7	21.6	26.8	14.2	14.0	19.4	13.9
	Mean (μm)	42.4	53.5	57.3	77.9	41.1	64.1	33.9	33.7
	Mode/Median	1.4	1.5	1.3	1.0	1.0	0.6	1.6	1.2
Clay minerals	Smectite (%)	58.2	37.6	10.6	45.9	18.8	11.6	72.7	11.8
	Illite (%)	18.9	36.7	47.5	37.3	42.4	51.1	23.3	52.0
	Kaolinite (%)	11.0	9.0	10.1	9.5	18.7	9.4	2.2	17.8
	Chlorite (%)	11.9	16.7	31.9	7.4	20.1	27.9	1.8	18.4
	Smectite crystallinity	0.76	0.57	0.27	0.56	0.29	0.40	0.89	0.33
	Illite crystallinity	0.26	0.18	0.17	0.25	0.30	0.21	0.25	0.27
	Illite chemistry	0.26	0.33	0.31	0.0	0.19	0.20	0.30	0.21
	Smectite/Illite	3.1	1.0	0.2	1.2	0.4	0.2	3.1	0.2
Total mineralogy	Clay (%)	3.6	9.0	4.8	2.7	1.5	19.1	6.2	4.2
	Feldspars (%)	11.3	11.0	9.7	1.5	2.6	19.3	6.9	1.9
	Quartz (%)	24.4	38.6	16.8	13.4	7.3	31.7	55.8	16.1
	Mica (%)	1.0	7.5	1.6	2.0	1.8	29.8	2.9	1.7
	Carbonate (%)	59.7	33.8	67.1	80.4	86.8	0.0	28.2	76.2
	Dolomite (%)	5.8	11.8	12.9	0.0	7.5	0.0	0.0	18.5
	Dolomite crystallinity	0.12	0.12	0.10	/	0.12	/	/	0.08
	Calcite (%)	53.9	22.0	54.2	80.4	79.3	0.0	28.2	57.7
	Calcite crystallinity	0.12	0.11	0.12	0.08	0.11	/	0.11	0.11

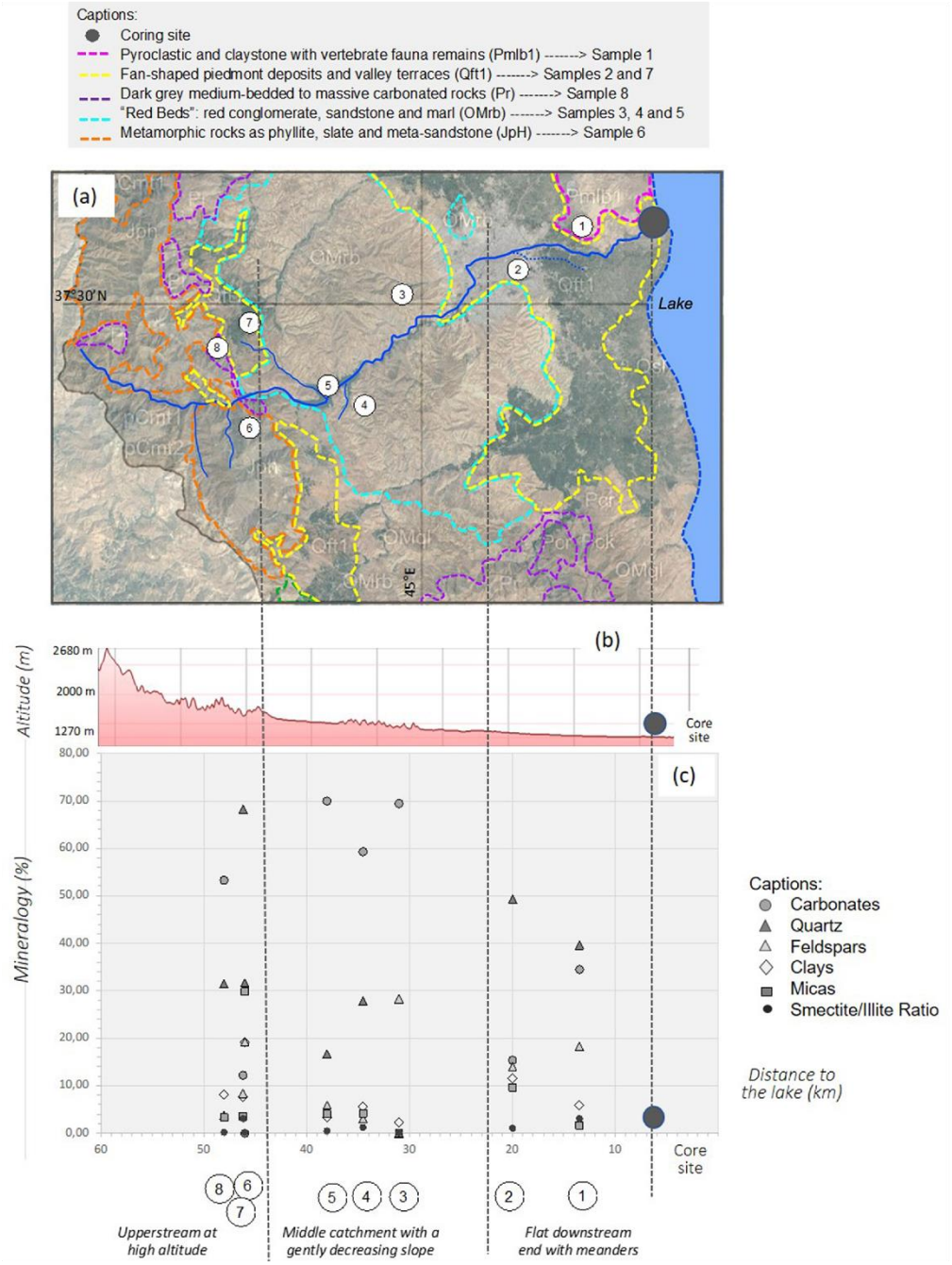

Fig. 3. Mineralogy and clay parameters of geological samples collected from the Shahr Chay River catchment: (a) distribution of samples in the catchment and according to the geology, (b) topographic profile along the catchment, (c) mineralogical distribution of catchment samples (see Table 1 for sample location and Table 3 for data).

sedimentation from 12.50 m depth to the core top at 1.60 m depth with the following major lithological units (Fig. 2c).

The lower unit 1 between 12.50 and 4.52 m depth begins with sub-unit 1a, from the core base to 12.38 m depth, consisting in brownish sand followed by a dark grey, organic-rich black event at 12.48–12.43 m interval and then by grey silt above. From 12.38 to 4.52 m, the sub-unit 1b consists of grey silty/clayish deposits (Fig. 2d) containing some 1-mm thick sandy levels interbedded and an interval between 8.87 and 8.65 m marked by higher contents of silt and sand. Unit 2 presents a much more heterogeneous pattern with successive sub-sections as follows: (i) sub-unit 2a between 4.52 and 4.02 m depth consisting in brown sand and silt (Fig. 2e); (ii) sub-unit 2b from 4.02 to 3.85 m, made of homogeneous grey silts and clays; (iii) sub-unit 2c comprised between 3.85 and 3.73 m, containing grey and dark grey sand; (iv) sub-unit 2d at 3.73–2.87 m

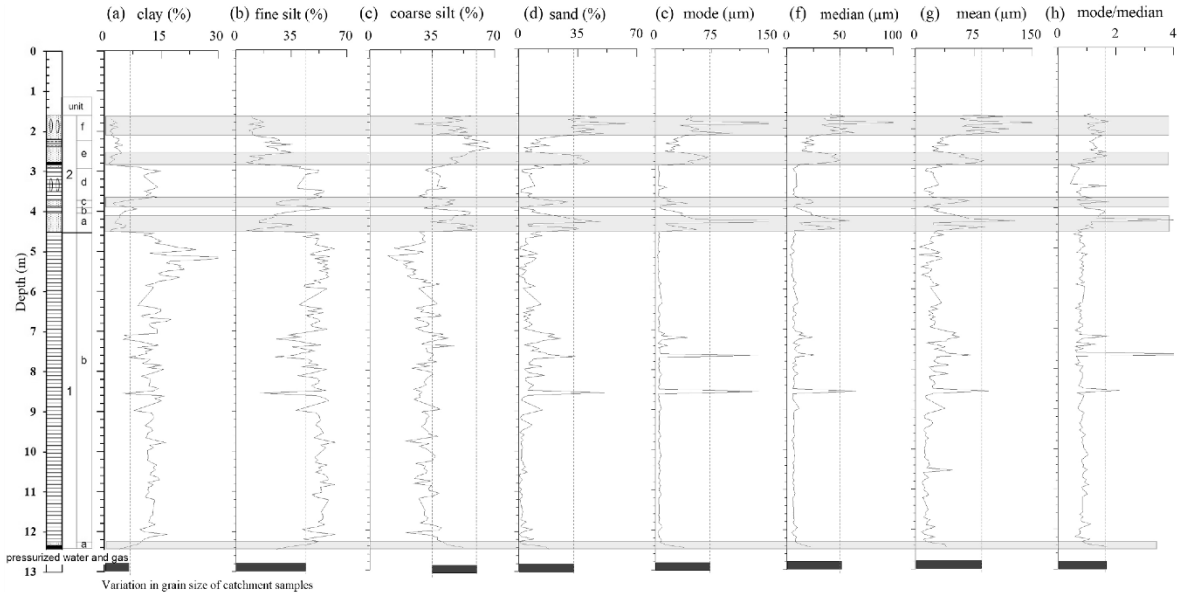

Fig. 4. Down-core variation in lithology and in grain size distribution of Lake Urmia sediments and of catchment samples.

depth and formed by homogeneous grey clayish levels; (v) sub-unit 2e made of sandy and silty layers from 2.87 to 2.20 m depth (Fig. 2f), overlaying a 8-cm dark grey and black organic rich level, and (vi) sub-unit 2f that consists in grey sand from 2.20 to the core top at 1.60 m depth.

In addition, the two sub-units 2d and 2f contain lots of fecal pellets from the development of the brine shrimp *Artemia urmiana* in the lake (Fig. 2g-i). These pellets are white, sometimes dark, and they constitute almost 90 % of many levels of sub-unit 2d (Fig. 2h). In the lower unit 1, fecal pellets are absent except for only few thin levels, in which some white pellets have been observed at 9.86 m and 10.92 m depth. These 50–200 μm, white fecal capsules of brine shrimp *Artemia* are considered as authigenic sedimentary component, although composed of a mixture of carbonates with minor amounts of siliclastic particles (Kelts and Shahrabi, 1986; Sharifi et al., 2018). According to Kelts and Shahrabi (1986), fecal pellets are composed of more than 80 % aragonite in modern sediment beds, while when they are darker in color, it is suggested that fecal pellets are older reworked. According to the studies in Great Salt Lake, the presence of fecal pellets in the sediment indicates that *Artemia* thrives in the water salinity between 100 and 300 $g.L^{-1}$ but its tolerance of salinities can extend up to about 340 $g.L^{-1}$ (Post and Youssef, 1977; Sharifi et al., 2018). For a water salinity lower than 100 $g.L^{-1}$, the decrease in the shrimps population is explained by increasing predators, while in a water salinity more than 300 $g.L^{-1}$, *Artemia* can hardly live (Wurtsbaugh and Gliwicz, 2001; Agh et al., 2008; Esmaeili Dahesht et al., 2010). In addition, when the lake water temperature is less than ca 3 °C, the shrimps are completely absent (Wurtsbaugh and Gliwicz, 2001).

4.2.2. *Grain-size distribution*

The distribution patterns of major grain-size classes for the siliclastic fraction of Lake Urmia sediments are shown in Fig. 4. The results reveal that silt is the dominant size fraction throughout the sequence as the whole, ranging from 33.3 % to 93.1 %. The lower sequence in the 12.38–4.52 m interval, presents higher contents and a more stable composition of clays and silts than that of the upper sequence (4.52–1.60 m), which is marked by a saw tooth increase in sand content and by a low clay fraction however broadly correlated to the silt content.

The core base between 12.50 and 12.38 m depth (sub-unit 1a), is characterized by the predominance of sandy and coarse silty fractions. The following section between 12.38 and 4.52 m (sub-unit 1b), presents a broadly stable grain size distribution with 49.8 % of fine silt, 31.5 % of coarse silt, 12.5 % of clay and 6.2 % of sand. Nevertheless, at the top of this section (6.00–4.52 m), the clayish fraction increases while coarse silt decreases. The whole sequence exhibits low and unvaried values of mode, median and mean.

Between 4.52 and 1.60 m, grain size displays sharp changes, quite well correlated with the identified lithological unit 2 and as a whole, with increasing coarse silt and sandy fractions when compared with the lower unit 1. The clayish fraction is low and follows the fine silt pattern that reaches its highest content in sub-unit 2d and relative high content in sub-unit 2b. The most important variations are pointed out by the sandy and fine silty fractions varying between 4.52 and 4.02 m and between 3.85 and 3.73 m in levels 2a and 2c, respectively. These two grain sizes, as well as mode and median highlight the bi-modal sub-unit 2e with increased sandy fraction in its lower part and increased fine silts in its upper part. In combination with mode, the most frequently-occurring particle diameter, as well as median, corresponding to the 50 percentile on a cumulative curve, the mode/median ratio could indicate the predominate particles as fine, coarse, or equal contents of both. As presented in Fig. 4, the mode/median ratio at 12.38–4.52 m and 3.73–2.87 m intervals is less than 1, reflecting the dominant fine fraction while other depths are characterized by coarse fraction.

Finally, the different proportions of clay, silt and sand in lake sediments and in the catchment area, reflect the sorting of the detrital material during the river transport and depositional conditions.

4.2.3. *Mineralogy*

In combination with Fig. 5 and Fig. 6, XRD analyses on samples from the composite core indicate the present of (i) silicates dominated by quartz, feldspars (orthoclase, albite), mica (muscovite) and clay minerals (chlorite, illite, kaolinite, smectite and some palygorskite), all identified in the whole set of samples, and in some specific levels, minerals from amphibole and pyroxene groups as well as iron oxides (magnetite) that are of detrital origin; (ii) carbonates that can be detrital, biomediated or chemically precipitated whether in evaporitic environments or not; (iii) evaporitic minerals as halite and gypsum, and (iv) other minerals such as iron sulfides (greigite and pyrite) that are of

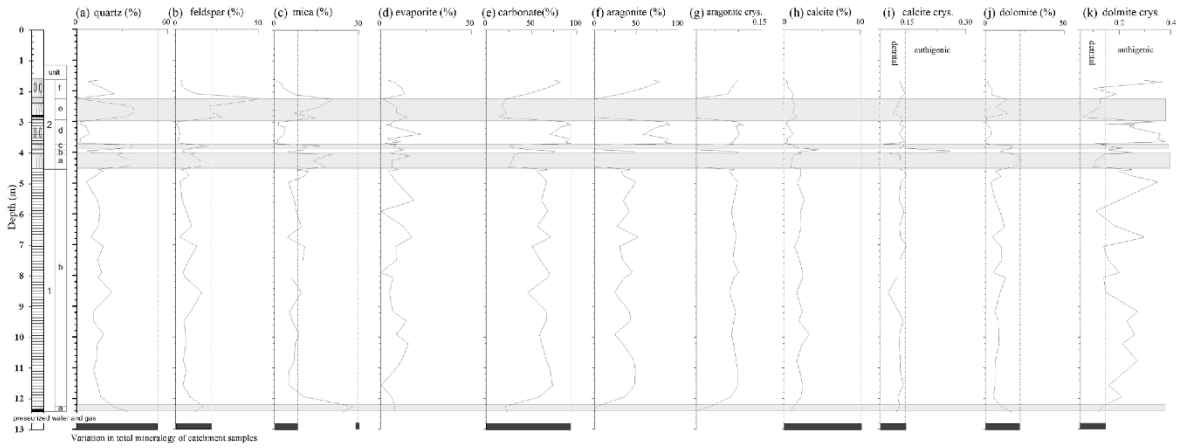

Fig. 5. Down-core variation in lithology and in total mineralogy of Lake Urmia sediments and of catchment samples with percentages of minerals in (a), (b), (c), (d), (e), (f), (h), (j), and mineral crystallinity index in (g) (i) (k).

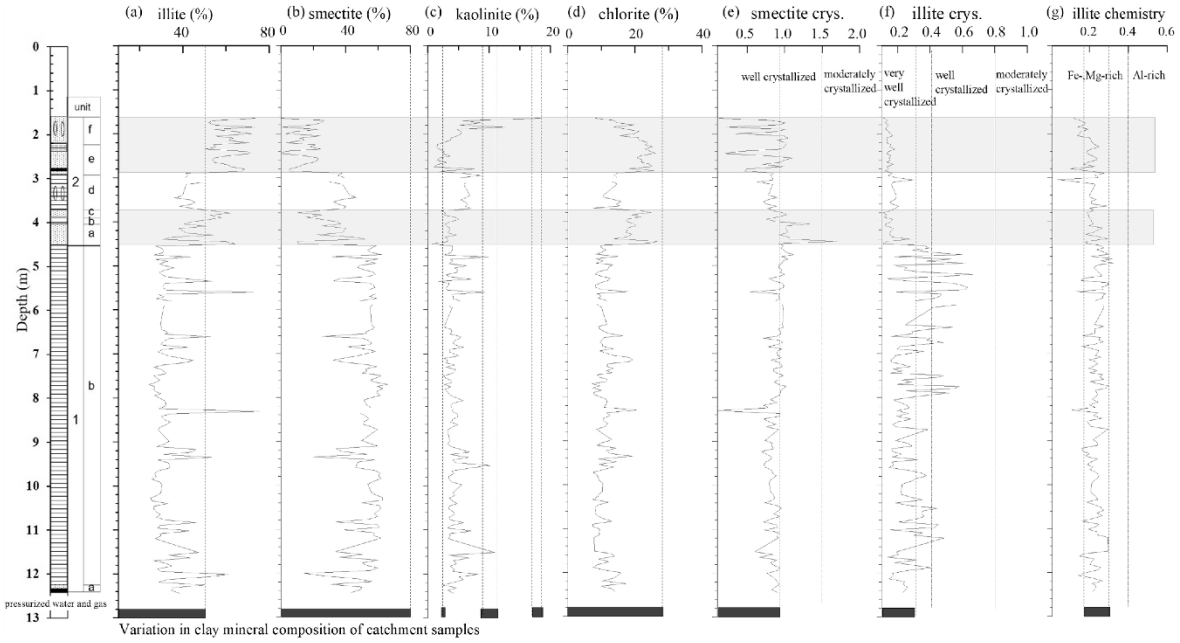

Fig. 6. Down-core variation in lithology and in clay mineral composition of Lake Urmia sediments and of catchment samples with percentages of clay minerals in (a), (b), (c), (d), smectite and illite crystallinity index in (e), (f), and illite chemistry in (g).

early diagenetic origin.

The presence of evaporitic minerals, such as halite and gypsum in almost all the samples, points out relatively saline to highly saline conditions in the lake during all concerned period (Fig. 5d).

4.2.3.1. Quartz, feldspars and mica. Quartz, as well as feldspars and mica display the same pattern with increased contents at the core bottom (sub-unit 1a), and in three above sections of the unit 2 (sub-units 2a, c and e), with 38 %, 27 % and 28 % of the total sediment respectively (Fig. 5 and Table 3). The lowest contents of these minerals, even less than 1 %, are recorded in sub-unit 2d. According to the results obtained from the catchment area, the geological formation 6 and possibly some others (formations 2, 7) represent important sources for these three minerals. When these minerals are in lower contents, their origin cannot be clearly identified, but one can observe that the lowest contents of this mineralogical assemblage as in the sub-unit 2d, are in the geological formations 4, 5 and 8.

4.2.3.2. Clay minerals. Among all clay minerals in the clay-sized siliceous fraction, illite and smectite dominate the lake sedimentation (Fig. 6 and Table 3), less abundant chlorite fluctuates similarly to illite, kaolinite shows lowest percentages. Sediments from unit 1 (12.50–4.52 m), are characterized by relatively stable proportions of different clay minerals with the predominance of smectite (51.9 %), followed by illite (33.2 %), chlorite (11 %) and kaolinite (4.3 %). The upper unit 2 demonstrates more contrasted clay minerals pattern. Sediments in the 4.52–3.73 m interval that correspond to sub-units 2a, 2b and 2c, exhibit (i) increasing proportions of illite (up to 62.0 %) and chlorite, (ii)

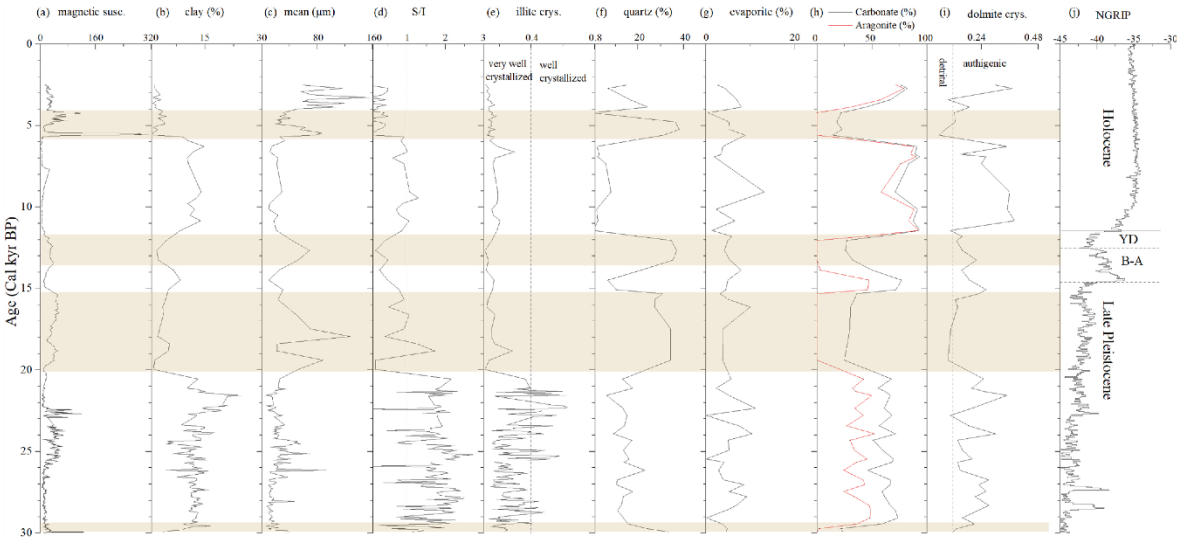

Fig. 7. Evolution of sedimentological parameters against a ^{14}C time scale: (a) magnetic susceptibility (susc.), (b) clay fraction (%), (c) mean grain size (, (d) smectite/illite ratio, (e) illite crystallinity (crys.), (f) quartz percentage (%), (g) evaporate percentage (%), (h) carbonate and aragonite percentages (%), (i) dolomite crystallinity(crys.), and (j) NGRIP curve (NGRIP, 2004).

decreasing contents of smectite (until 10.3 %), and (iii) low and stable proportions of kaolinite. In sediments comprised between 3.73 and 2.87 m, i.e. sub-unit 2d, both smectite and illite present relatively stable and equal proportions of 40 %. The two last units 2e and 2f units exhibit broadly the same pattern with relatively low, changing contents of smectite (13.7 %) and high, fluctuating contents of illite (61.3 %). Chlorite reaches its highest values of 26.2 % in sub-unit 2e before decreasing while kaolinite stays low overall the whole core and just increases up to 18.4 % at the top sequence. The composition variations of different minerals throughout the whole composite core reflect quite a good agreement with different lithological formations from the catchment area. Indeed, high contents of smectite in the lake sediment are also recorded in the catchment area for geological formations represented by samples 1, 2, 4 and 7. Illite rich sediments that display increased contents of chlorite too, are present in samples 3 and 6, but also in 2, 5 and 8. Finally, the high contents of kaolinite in the upper part of the core are also recorded in samples 5 and 8.

Smectite crystallinity index is around 0.8 in the lower part of the core (unit 1) and scales further above but still remaining below 1.5. Meanwhile illite crystallinity in the under lying unit 1, varying values between 0.2 and 0.5 that reflect very well- to well- crystallized illite, suggests some chemical transformations (Ehrmann et al., 2005). As values obtained for samples from the catchment area (Fig. 6), they indicate well crystallized smectite and illite (Ehrmann et al., 2005). In the upper sequence named as unit 2, illite crystallinity index remains stable and low, equaling to 0.1–0.2 that indicates very well crystallized illite, which is well correlated with samples in the catchment area. Illite chemistry index fluctuates around 0.2 all throughout the sediments. This parameter when lower than 0.4, reflects Fe and Mg-rich illite (Diekmann et al., 1996; Ehrmann et al., 2005). The illite chemistry as well as illite and smectite crystallinities in the core sediments present values identical to those of the formations of the catchment area, thus suggesting the high stability and detrital origin of the clays, acting rather by erosion than chemical weathering.

4.2.3.3. Carbonates. Carbonate contents display values from ca 20 to 93 % and their variations are correlated with defined lithological units (Fig. 5e). Unit 1 starts with low values of about 20 % that increase at the beginning of sub-unit 2b up to 60 % and remain relatively stable throughout the core. Above unit 1, carbonate contents clearly fluctuate: they decrease to 20–25 % in sub-units 2a, 2c, 2e and increase in 2b, 2d and 2f reaching the highest values of 93 % in sub-unit 2d. The carbonate curve evidences the same succession of environmental changes to that obtained by Tudryn et al. (2021), although due to different method used, either the calculations from XRD diagrams applied in the present study or the Mélières mono-calcimeter (Tudryn et al., 2021), the values are different. The former might be slightly overestimated due to a fraction of non-crystalline material that may be present in the sample, while the latter allows calcium carbonate to be measured but not the most resistant dolomite.

Carbonate fraction consists of three minerals: calcite, aragonite and dolomite (Fig. 5). Aragonite is absent in sub-units 1a, 2a, 2c and 2e, whereas it is present elsewhere in the sediment either as mud or as major component of fecal pellets. Aragonite represents the major part of the carbonate fraction with percentages even as high as 92 % where shrimp's fecal pellets are particularly abundant (sub-unit 2d, Fig. 2h) and its general pattern is similar to that of total carbonate. Calcite and dolomite evolve as a whole between 0 and 15 %. In the very narrow sub-unit 2b calcite reaches the highest content of 38 % and then contains low and stable content from sub-unit 2d to the core top, it displays inversed pattern to that of aragonite. Dolomite also displays such inversed pattern to aragonite all along the sequence with clear increases of percentages in sub-units 1a, 2a, 2c and 2e (Fig. 5).

The calcite crystallinity index presents values of about 0.10 along the core. A single level is characterized by the highest calcite crystallinity index of 0.26 shown in sub-unit 2b (Fig. 5). Since (i) the higher value the crystallinity index, the worse the carbonate is crystallized, and (ii) calcite crystallinity obtained for samples from the catchment area ranges between 0.08 and 0.12, it appears that most of the calcite in the core sediments present the same good crystallinity and is thus of detrital origin. According to Fontes et al. (1993, 1996), only the calcite found at depths from the sub-unit 2b can be considered as authigenic rapidly precipitated through biogenic activity or through direct chemical precipitation in lake water.

The crystallinity index of dolomite in lake sediments displays scattered values between 0.06 and 0.38 while it is evolving from 0.08 to 0.12 in samples from the catchment area. Following the example of calcite, well-crystallized dolomite is thus of detrital origin (low index value; sub-

units 1a, 2a, 2c and 2e), while its poor crystallinity is related to authigenic conditions of precipitation (high index value; sub-units 1b, 2b, 2d and 2f). The formation of dolomite requires drastic chemical conditions rarely found in lacustrine environments except when occurring as in situ replacement product of calcium carbonate sediments, particularly in evaporitic sites (Pierre et al., 1984). However, dolomite precipitation is driven by both high alkalinities and low Ca^{2-}/Mg^{2+} and SO_4^{2-} concentrations in the solution, the two latter resulting of massive calcium minerals precipitation (carbonates, sulfates) and/or a bacterial sulfate reduction (Lippmann, 1973). In Lake Urmia composite core, the direct crystallization of dolomite from aqueous solutions could be considered in relation with highly evaporative phases (alkaline status of the lake) as observed in the Coorong area in Australia or in the Deep Spring Lake basin in California (Alderman and Skinner, 1957; Alderman and Von Der Borch, 1960, 1961, 1963; Peterson et al., 1963; Skinner, 1963; von Der Borch, 1965; Peterson and Bien, 1966; Clayton and Jones, 1968; Von der Borch and Jones, 1976). Moreover, dolomite precipitation occurs concomitantly with the formation of aragonite that (i) displays high crystallinity index (Fig. 5k), (ii) requires a high Mg^{2-} content in waters to become the stable species of calcium carbonate and (iii) can be related to the chemical or biochemical precipitation, both reflecting evaporative conditions (Müller et al., 1972; Eugster and KELTS, 1983; Kelts and Shahrabi, 1986; Fontes et al., 1993; Fontes et al., 1996).

4.2.4. Chronology

The ^{14}C AMS dating performed both on organic fractions (diffused organic matter and hand-picked charcoal) and on inorganic and biomediated (i.e. fecal pellets) carbonates from cores Golman 6 and Golman 7 are presented in Table 2.

Considering all the data gathered on the carbonate fraction over the composite core and on the catchment as well as the modern hydrogeochemical lake system, we have to implement two age corrections: (i) the first one related to the detrital carbonate fraction in the dated samples, and (ii) the second one taking into account the hard-water effect of the modern lake surface water, considering that authigenic materials such as inorganic carbonates and organic matter are formed in the lake upper water layer.

(i) Correction 1 is applied on bulk samples when a detrital carbonate fraction is evidenced; the ^{14}C activity of the authigenic carbonates can be written as $A_M = X^*A_{AC} + A_{DC}^*(1- X)$ with A_M, the measured ^{14}C activity on the total carbonate fraction; X, the percentage of authigenic carbonate in the bulk sample; A_{AC} and A_{DC}, the ^{14}C activities of the authigenic and detrital carbonates respectively. Assuming that detrital carbonate originating from the watershed is ^{14}C-free ($A_{DC} = 0$), we can state $A_{AC} = A_M /X$ as proposed by Fontes et al. (Fontes et al., 1993; Fontes et al., 1996). This correction is applied on all the dated samples containing a detrital fraction, either calcite or calcite and dolomite through XRD half-width of the main peak for each mineral (Table 2): both of dolomite and calcite are considered as detrital (authigenic) when their crystallinity indexes are lower (higher) than 0.12 according to the crystallinity index of catchment samples.

(ii) Correlation 2 is applied on ^{14}C dates established from carbonate activities after correction 1 if a detrital fraction is present in the bulk sample; knowing that the ^{14}C activity of atmosphere CO_2 was measured at 101.8 pMC in 2016 (Hua et al., 2021), the present-day ^{14}C activity of the lake water is 680 yr. The most common hypothesis is to consider that this reservoir effect in the past (Fontes et al., 1993; Fontes et al., 1996; Gasse, 2000). However, when ^{14}C dates are plotted against depth, a consistent evolution appears with all carbonate and organic levels dated above 6 m depth (above 22 kry BP). With respect to the ages defined on charcoal which represent the equilibrium with atmospheric CO_2, a different of 2000 years can be defined which can be applied to all the other ages.

From 12.5 to 4.52 m depth, the ^{14}C AMS chronology is based on 4 dating that are in agreement with the lithostratigraphy, with a sedimentary rate (msr) of 0.89 $mm.yr^{-1}$ (Table 2, Fig. 2j). This msr is relatively high due to the presence of unrecovered muddy sections during coring, which artificially increase the sedimentation rate. From 4.52 m depth to the core top, two phases are recorded, i.e. 4.52–2.87 m and 2.87–1.6 m intervals, associated to msr of 0.12 and 0.40 $mm.yr^{-1}$ respectively.

5. Discussion

5.1. The paleoenvironmental history of lake Urmia

Lake Urmia is a complex hydrological system governed not only by the climatic evolution in the eastern Mediterranean area and Western Asia, but also by local factors. Among local factors, the topography, geology and tectonics in the catchment area as well as the lake basin hydrology, which is driven by the net effect of precipitation, surface runoff, evaporation, and evapotranspiration processes (Eugster and Jones, 1979), are of upmost significance during depositional processes in the lake. In its southwestern part of Lake Urmia concerned by this study, the contrasting topography and differences in altitude of more than 1500 m between the most distant sources of detrital material and the lake favor erosional processes independently of the climate and water availability. Magmatic, metamorphic and sedimentary rocks are present in the catchment and minerals from these rocks constitute an important part of the lake sediments. Carbonates, feldspars and mica undergo chemical alteration relatively easily among all these minerals (Chamley, 1989). These detrital minerals are dramatically poor in two sub-units of the unit 2 (2b: 4.02–3.85 m; 2d: 3.73–2.87 m), while elsewhere they represent a major part of the sediments and highlight rather erosional processes in the catchment area than chemical ones. Additionally, the authigenic carbonate integrating the aragonite fraction either chemically or biological mediation precipitated, represents a significant part of the lake sediments. Halite and gypsum indicate the evaporitic conditions in the lake basin as a whole. Iron sulfides identified in several parts of the sediment highlight the early diagenesis in the sediment in anoxic, sulfate-reducing environment (Tudryn et al., 2021). Despite the complexity of ^{14}C signatures of authigenic carbonate and from organic matter samples (either terrestrial or lacustrine) we established a reliable chronology of the lake evolution for the last 30 kyr. As the age scale of composite core is presented in Fig. 7, the data reflect the lake history both general climate trends and fundamental changes in local hydrology through well-defined intervals.

5.1.1. The lake at ca 30 cal kyr BP

The interval starts with light brown sandy sediments and is followed by coarse silt of blackish to dark grey color due to abundant vegetation remains. This sequence is characterized by high contents of detrital silicates, including both predominant coarse particles (such as quartz, feldspars and mica) and few fine particles (Fig. 7). In addition, a low abundance of aragonite-free carbonates is recorded with the presence of calcite and dolomite, both from detrital origin. Such a sedimentary composition dominated by coarse grain sizes indicates the direct influence of the Shahr Chay River at the coring site and erosional processes in the catchment rather than chemical weathering that implies water availability. Silicates originating principally from phyllite and sandstone, are present in the upper part of the catchment area (geological formation sample 6 in Table 3), while calcite and dolomite derive from carbonate rich formations 3 and 8. According to Tudryn et al. (2021), the light brown sand at the beginning of the interval and the presence of detrital magnetite highlight well oxygenated conditions during the sedimentation at the coring site. Moreover, pressurized gas and brine are captured in this sand with less water salinity than in today's lake waters. Above the sandy level, blackish and dark grey silts are rich in plant remains identified as C_3 plants with $\delta^{13}C$ around −25 ‰ PDB (Table 2) and in greigite, an authigenic iron sulfide that indicates the anoxic and sulfate-reducing conditions within the sediment (Curtis, 1987). Greigite being magnetic mineral, its presence is highlighted by high magnetic

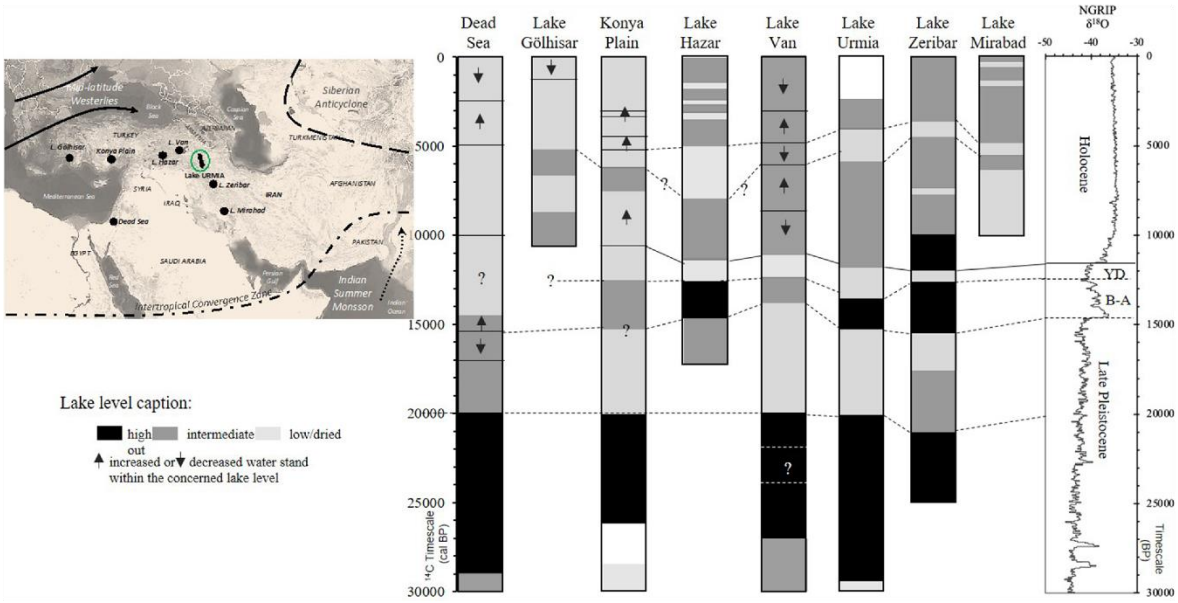

Fig. 8. Location map of selected lakes surrounding Lake Urmia (Northwestern Iran) and tentative synthetic reconstruction of past lake levels at the Middle East since 30 kyr BP, with a comparison with the NGRIP curve (NGRIP, 2004), references for lakes water level reconstruction are as follows: Dead Sea (Bartov et al., 2003; Bookman (Ken-Tor) et al., 2004; Stein et al., 2010); Lake Gölhisar (Eastwood et al., 2007); Konya Plain (Fontugne et al., 1999; Kuzucuoğlu et al., 1999); Lake Hazar (Ön et al., 2018); Lake Van (Kuzucuoğlu et al., 2010; Çağatay et al., 2014); Lake Zeribar (Wasylikowa et al., 2006); Lake Mirabad (Stevens et al., 2006).

susceptibility on Fig. 7a. As noted by Tudryn et al. (2021), the high organic content here may reflect an increased input of organic detritus from the river, although the decreasing grain size of the sediment and its poor oxygenation more likely suggest the development of a saltmarsh with high biological productivity rather than a higher riverine activity.

Such a start of the sedimentary sequence reflects erosional processes in the catchment and a low lake level, without lacustrine or very shallow conditions in the coring area, reflecting rather dry conditions and a low water availability on the catchment area.

5.1.2. The 29.9–20.2 cal kyr BP interval

The grey, homogeneous sedimentation is dominated by fine silts and clays, with some interbedded millimetric levels of coarse silt and sand. Detrital silicates (mainly quartz, mica and feldspars) represent about 30 % of the sediment. In the clay fraction, well-crystallized smectite dominates reaching the highest contents of the whole sequence (12 % in total sediment). The ratio smectite *versus* illite stays close to 2, indicating broadly invariable proportions of these minerals all along the interval (Fig. 7). This is compatible with the erosion of the geological formations 7 and 1, as well as 4 and 2, that bring abundant smectite from the catchment area enough to explain the high smectite contents (Table 3). However, chemical ongoing weathering or precipitation in the lake salty environment (Chamley, 1989) cannot be totally excluded since (i) halite is present here (but also all along the core), and (ii) smectite related to the chemical weathering especially in the formations 7 and 1, would indicate enough water in the catchment for such process. In addition, carbonates account for 62 % in the suite of minerals with 38 % of aragonite, 16 % of calcite, and 8 % of dolomite, in which aragonite is of authigenic origin and calcite is of detrital one, while dolomite has both authigenic and detrital origins according to their respective crystallinity indexes.

Such detrital fraction in the core sediment suggests that the environment is still dominated by physical weathering and erosion on the catchment area, with nevertheless, low transport energy conditions, reflecting lacustrine conditions established in the coring site. At the beginning of the interval, aragonite that was absent before at the core base appears and increases rapidly from 25 to 50 % of the sediment, while authigenic dolomite occurs in several parts of the interval, both constituting the carbonaceous mud. The formation of both aragonite and dolomite requires a high Mg^{2+} content in waters to become the stable species of calcium and magnesium carbonates, and thus reflect evaporative lacustrine conditions (Alderman and Skinner, 1957; Alderman and Von Der Borch, 1960, 1961, 1963; Peterson et al., 1963; Skinner, 1963; Peterson and Bien, 1966; Clayton and Jones, 1968; Müller et al., 1972; Eugster and KELTS, 1983; Kelts and Shahrabi, 1986), as do halite and gypsum. The intensity of evaporative conditions probably experienced several fluctuations that can be deduced from the decrease of evaporate minerals and the simultaneously decrease of authigenic dolomite between 26.5 and 24.3 kyr BP, and at ca 22.9 kyr BP (Fig. 7g and i).

Detrital and authigenic fractions of the sediment show a clearly lacustrine environment established at the coring site during this interval. Meanwhile, the quite small grain size suggests low transport energy conditions in phase with a relatively high water level. The water salinity fluctuation is highlighted by simultaneous changes in the authigenic dolomite contents and evaporites. The interval is characterized by relatively wet although cold conditions that favor erosional processes in the catchment area even if chemical weathering was probably acting too.

In addition, according to previous studies (Wurtsbaugh and Gliwicz, 2001; Abbaspour and Nazaridoust, 2007; Agh et al., 2008; Esmaeili Dahesht et al., 2010), the absence of fecal pellets could be attributed to (i) very low lake level and thus too highly saline conditions for shrimps development (more than 300 $g.L^{-1}$), or (ii) a very high water level with too low salinity (below 100 $g.L^{-1}$) implying the presence of predators that do not allow the shrimps development, or (iii) very cold lake water that also do not allow the shrimps development (ca 3 °C). However, this sequence (apart two thin levels) could reflect a very high water level with cold temperature.

Finally, Tudryn et al. (2021) showed that magnetic minerals point out early diagenetic processes in anoxic sediment and possibly a bad ventilation of the bottom water, in good agreement with a high lake

level. Additionally, the decrease of illite crystallinity within this time interval could also be related to the specific post-deposition environment in the lake sediments. The data thus indicate that after a low lake stand at ~ 30 cal kyr BP, the lake level increased and, nevertheless some fluctuations, remained high until 20.2 cal kyr BP.

5.1.3. The 20.2–15.3 cal kyr BP phase

Sediments of the 20.2–15.3 kyr BP interval consist in (i) brown sands and silts with high contents of silicates as quartz, mica and feldspars, quick and short time illite and chlorite peaks, decrease of smectite and (ii) low carbonate contents with no aragonite, some calcite and more dolomite, both of detrital origin as indicated by their low crystallinities. These parameters thus indicate detrital input into the core site associated to physical weathering with erosion from geological formation 6 and dolomite-rich formations 3 and/or 8 (Table 3), and with no authigenic minerals. It is suggested that sediments during this period were deposited in relatively dry conditions, a low lake level and a well-oxygenated environment.

5.1.4. The 15.3–13.3 cal kyr BP interval

This following sequence is characterized by increasing clays and fine silt, in which silicates as quartz, mica and feldspars, only account for 20 % (Fig. 7). With 66.2 % of total sediment, the carbonate mud is made of aragonite (31.6 %), calcite (23.5 %) and dolomite (11.1 %). According to the crystallinity index values, both dolomite and calcite are entirely of authigenic origin. Meanwhile these parameters clearly indicate lacustrine conditions as the same with 29.9–20.2 cal kyr BP interval. In contrast, the presence of the authigenic calcite between 15.3 and 13.3 cal kyr BP suggests less evaporative conditions than before, without authigenic calcite (Müller et al., 1972). Even if slightly advanced, two thousand years lasting in this interval shows timing in good agreement with the Bölling/Alleröd warming within Post-Glacial period as observed through Greenland ice cores (Fig. 7j).

5.1.5. The 13.3–11.8 cal kyr BP interval

The environmental conditions are similar to those recorded between 20.2 and 15.3 cal kyr BP. Indeed, sediments are marked by an increase in grain sizes and detrital silicates input, the dominance of illite and chlorite in the clayish fraction and the decrease in carbonate contents. Within carbonate fraction, aragonite is absent while few calcite and abundant dolomite of detrital inputs are present. All these parameters as well as the presence of magnetite indicate a well-oxygenated and close to the river mouth environment at the coring site, indicating a very low lake level. This regressive stage of the lake corresponds to the Younger Dryas cooling before the Holocene (Fig. 7j).

5.1.6. The 11.8–5.6 cal kyr BP interval

The sequence is characterized by fine-grained sediments, with very low contents of detrital minerals and the predominance of an authigenic carbonate fraction, indicating clearly the re-establishment of open lacustrine conditions. The detrital fraction of this section has higher clay mineral contents than the underlying section, and contains equal proportions of smectite and illite, with some added detrital calcite. In the carbonate fraction, authigenic dolomite and huge contents of aragonite are present in the calcareous mud, mainly under the form of aragonite shrimp fecal pellets that are the dominant component of the sediment (Figs. 2 and 7). The presence of these minerals indicates a lacustrine environment with high water salinity as like the period recorded at 29.8–20.2 cal kyr BP during which nevertheless, the presence of the shrimps *Artemia* is not recorded. According to previous studies, the abundance of *Artemia* fecal pellets is related to the water salinity between 100 and 300 $g.L^{-1}$ and other parameters including temperature, that make favorable conditions for shrimp's development (Wurtsbaugh and Gliwicz, 2001; Agh et al., 2008; Esmaeili Dahesht et al., 2010; Sharifi et al., 2018). In several levels, dark and white pellets are mixed, the dark ones being older and reworked according to Kelts and Sharabi (1986). The presence of some iron sulfides, suggests a bad ventilation of the bottom water (Tudryn et al., 2021). The end of this section is marked by sharp changes in the lithology and all parameters (Fig. 2c and 7).

5.1.7. The 5.6–4.1 cal kyr BP spell

This interval is divided into two parts. The lower part is characterized by coarse, sandy black sediment with abundant organic remains and authigenic iron sulfide, i.e. greigite. The ^{14}C dating performed on charcoal at 2.80 m depth gives an age of 5.5 cal kyr BP, in good agreement with the 4.9 cal kyr BP age also obtained on charcoal and collected from the neighboring core Golman 5 at 2.66 m depth indicated by Tudryn et al. (2021). In the upper part of this sequence, silty and detrital minerals prevail, mainly with quartz, feldspar, mica, illite, and few carbonate-calcite and dolomite being of detrital origin too. This suggests the drying out or very shallow conditions at the coring site similarly to what is recorded at the beginning of the sequence i.e. at ~ 30 cal kyr BP. Nevertheless, contrary to the core bottom, the dated charcoal samples exhibit distinct $\delta^{13}C$ values of −26.5, −25.5 ‰ and of −13.5, −14.5 ‰ vs PDB (Table 2), characterizing C_3 and C_4 plants respectively and emphasizing that both coexist on the watershed at the time of deposition. The C_4 vegetation episode seems to have lasted at least 600 years, between 5.6 and 4.1 cal kyr BP, and likely indicates a warmer and drier episode than the one occurring at 30 cal kyr BP.

5.1.8. The 4.1–2.3 cal kyr BP interval

Abundant shrimp fecal pellets are found in this last sequence, reflecting the lake level rise and thus a recover of open lacustrine environment at the coring site. The predominant sandy fraction made of detrital silicates reflects a high energy transport from the nearest inflow, Shahr Chay River. Furthermore, the high carbonate content gathers authigenic aragonite and dolomite as well as some detrital calcite. Authigenic carbonates and shrimp fecal pellets indicate a high evaporation rate, with a water salinity comprised between 100 and 300 $g.L^{-1}$, and temperature high enough to allow the shrimp development (Sharifi et al., 2018).

5.2. Lake Urmia history at a regional scale

The results obtained here show the importance of detrital input related to the physical weathering in the catchment area and indicate several Lake Urmia low and high stands. The intense erosional processes have also been described by Mirzapour et al. (2021a; 2021b). The lake water level changes clearly mark the alternation of relatively dry and wetter periods in the lake catchment, but still with high evaporation conditions and saline lake waters even in the wettest periods.

After the low stand at ca 30 cal kyr BP, the lake level increased and remained high until the Last Glacial Maximum at ca 20 cal kyr BP at the coring site. Our results confirm those obtained by Djamali et al. (2008a) who proposed a high water level during the last glacial period, on the opposite to Stevens et al. (2012) that indicated no perennial lake and clearly arid climate at Lake Urmia.

From 20.2 to 2.3 cal kyr BP, the lake experienced water level fluctuations with three relatively high stands (i) between 15.3 and 13.3 cal kyr BP during the warming Bölling/Alleröd event, (ii) from 11.82 to 5.64 cal kyr BP, during the Early and Mid-Holocene and (iii) during the 4.1–2.3 cal kyr BP, Late Holocene interval registered in our cores. These intervals were separated by low lake stands with completely dried-out or close to the lake water line conditions at a coring site (i) after the Last Glacial Maximum between 20.2 and 15.3 cal kyr BP, (ii) during the Younger Dryas from 13.3 to 11.8 cal kyr BP, and (iii) at the transition from Mid to Late Holocene, during the 5.6–4.1 cal kyr BP interval (Fig. 7).

Previous studies by Kelts and Shahrabi (1986) on Lake Urmia identified 3 relatively high lacustrine stands and 2 low ones for the Late Pleistocene and Holocene, and proposed ca 9–7.5 kyr BP for the lacustrine period that certainly corresponds to that between 11.8 and 5.6 cal

kyr BP in our record; indeed, authors highlighted the lack of readily dateable material in their study. Stevens et al. (2012) indicated dry conditions with the short-term lacustrine episode at ~ 14 kyr, drying out probably marking the Younger Dryas and no re-establishment of lacustrine conditions until ca 10 kyr. Holocene reconstructions by Sharifi (2018) suggested wet early Holocene and frequent dry episodes during Mid-Late Holocene.

The synthetized water level evolution of Lake Urmia from 30 kyr BP to present-day is presented on Fig. 8, where selected lakes from the Middle East region are also shown. Lakes Gölhisar, Konya Plain, Hazar and Van represent the W-E line from East Mediterranean Sea to Lake Urmia. The Dead sea related to the East Mediterranean area and Lakes Zeribar and Mirabad to the S and SE from Lake Urmia are also presented. In Fig. 8, the lake water level is expressed as high, intermediate and low, the latter including drying. The results from Lake Urmia are in good agreement with evolution of surrounding lakes, Lakes Van and Zeribar. At a greater distance, whether West or South, some similarities but also differences appear in the evolution of the lakes.

Considering the Late Pleistocene from 30 cal kyr BP, all lakes displayed broadly the same evolution. At about 28 kyr cal BP, the water level increased in all lakes and they reached their highest level ever recorded until today, with this high level continued until 20 cal kyr BP. After 20 cal kyr BP, they all recorded a clear lowering followed by a water level increase that can be related to Bölling/Alleröd warming and its subsequent decrease during the Younger Dryas cooling (Fig. 8). Such homogeneity in the evolution of the lakes argues for a generalized distribution of moisture or aridity throughout the region. Timing of water level change is consistent with global climate change during the late Pleistocene as shown in Fig. 8.

During the Holocene, the overall pattern is more contrasted through different parts of region, generally displaying lower increases in water levels than before and many dryings. After the dry Younger Dryas during which a general lowering or even a complete drying was recorded, the beginning of the Holocene is characterized by milder conditions with an increase in humidity implying a rise in the lake water level or at least, the appearance of marshes (Konya Plain). Only Lake Mirabad and Dead Sea present an opposite pattern and low lake level conditions at that time. Lakes Zeribar, Urmia, and Van are clearly under lacustrine environment during the Early-Mid Holocene, while other lakes display water level changes before a general lowering and even drying out in the Mid-Holocene. This dry phase is likely linked to the drought event recorded at 5.2 cal kyr BP that was evidenced in the speleothem record of the Soreq Cave (Bar-Matthews et al., 1997) and around 5.2 and 4.2 cal kyr BP in many sites over the eastern Mediterranean and Asia (Staubwasser and Weiss, 2006).

Finally, the Upper Holocene is generally characterized by unstable lake levels, whether they were fluctuating (Lake Hazar), very low (Lake Gölhisar) or even dried out (Konya Plain), all of these sites being located west of Lake Van. In contrast, the levels observed at Lake Van and further east in Iran seem to be more stable. All these data likely highlight an Early Holocene wetter than the Late Holocene. Furthermore, the Early Holocene appears to be less humid in Western Anatolia than in Inner Anatolia and Western Iran, a situation that tends to become more pronounced during the Late Holocene. This distribution of moisture may be related to the decreasing influence of the Indian monsoon towards the west, and its greater impact during the Early Holocene. Indeed, according to Jones and co-authors (2008), during the Early Holocene, phases of relatively high humidity rate in Anatolia are connected with an increase in Indian monsoon rainfall, and this relation is no more observed during the Late Holocene.

This interpretation seems rather appealing, but it must be taken with caution: other factors must be taken into account that include (i) the topography, (ii) the obvious influence of westerly winds as it is the case today, and (iii) the interaction between these westerlies, the Indian monsoon and the extension of the Siberian high in the distribution of humidity. Indeed, according to Bottema (1986), climate of Inner Anatolia and Western Iran where Lakes Van, Urmia and Zeribar are located, is largely impacted by the surrounding mountains Furthermore, the relatively wet Early Holocene inferred from the paleoenvironmental record of these three lakes contrasts with the pronounced delay in postglacial forest expansion in the Southwest Asia at the Early Holocene that has been highlighted by many authors (Djamali et al., 2008b; Jones and Roberts, 2008; Aubert et al., 2019). To explain this delay, these authors emphasized the importance of the seasonal moisture supply, with westerlies bringing moisture in winter and early spring, resulting in a dry summer that does not allow vegetation to develop well, whereas the Indian monsoon, if it reaches this region, brings enough moisture in late spring and summer, which favors vegetation development. Our data on Lake Urmia allowed us to reconstruct the history of the lake water fluctuations in relation to the available moisture, but do not permit to clearly identify the origin of the air humidity and/or the season producing the most effective rainfall for water resources in Lake Urmia basin.

6. Conclusion

In this paper, we conducted systematic investigations on grain size and mineralogy of detrital and authigenic compounds that includes detailed analyses of carbonate and clays assemblages on the sedimentary sequence retrieved from the southwestern part of Lake Urmia. Our results show important changes in the lake water level for the past ~ 30 kyr, likely attributed to the available humidity. Although further interpretation of the hydrogeochemical characteristics and mixing processing in the lake basin is needed, the consistency of the AMS ^{14}C chronology between 22 and 2 cal kyr BP enabled us to estimate a reservoir effect for the past, which is particularly rare for such salt lakes. This reservoir age of about 2000 years has made possible to define a reliable chronology in agreement with the lithostratigraphy but also matching with the major regional environment phases.

Our work benefitted from highly reliable, precise multi-proxy data. The paleoenvironmental reconstruction suggests a humid Late Pleistocene before the Last Glacial Maximum, followed by frequent drier/wetter episodes from that time until today, including the humid early Holocene period and evaporative conditions during the Mid to Late Holocene transition.

Being today on the eastern limit of the Mediterranean zone, NW Iran links Southern Europe, North Africa and Asia, and thus could be submitted to the respective influences of the air masses from the North Atlantic, the Indian monsoon, the Ponto-Caspian region and the Siberian anticyclone. Our results suggest that an atmospheric teleconnection existed between North Atlantic and the Western Iran during the last 30 kyr BP and will be of high interest for global understanding of climatic change in the past.

Declaration of Competing Interest

The authors declare that they have no known competing financial interests or personal relationships that could have appeared to influence the work reported in this paper.

Data availability

Data will be made available on request.

Acknowledgement

This work was supported by the French-Iranian project Gundishapur, the Center for International Scientific Studies and Collaboration (CISSC), TelluS Program of CNRS/INSU and China Scholarship Council (CSC). Two anonymous reviewers are thanked for their suggestions in improving the manuscript.

References

Abbaspour, M., Nazaridoust, A., 2007. Determination of environmental water requirements of Lake Urmia, Iran: an ecological approach. International Journal of Environmental Studies 64, 161–169.

Agh, N., Van Stappen, G., Bossier, P., Sepehri, H., Lotfi, V., Rouhani, S., Sorgeloos, P., 2008. Effects of salinity on survival, growth, reproductive and life span characteristics of Artemia populations from Urmia Lake and neighboring lagoons. Pakistan journal of biological sciences: PJBS 11, 164–172.

AghaKouchak, A., Norouzi, H., Madani, K., Mirchi, A., Azarderakhsh, M., Nazemi, A., Nasrollahi, N., Farahmand, A., Mehran, A., Hasanzadeh, E., 2015. Aral Sea syndrome desiccates Lake Urmia: Call for action. Journal of Great Lakes Research 41, 307–311.

Ahmady-Birgani, H., Mirnejad, H., Feiznia, S., McQueen, K.G., 2015. Mineralogy and geochemistry of atmospheric particulates in western Iran. Atmospheric Environment 119, 262–272.

Ahmady-Birgani, H., Ravan, P., Schlosser, J.S., Cuevas-Robles, A., AzadiAghdam, M., Sorooshian, A., 2020. On the chemical nature of wet deposition over a major desiccated lake: Case study for Lake Urmia basin. Atmospheric Research 234, 104762.

Alderman, A., Skinner, H.C.W., 1957. Dolomite sedimentation in the south-east of South Australia. American Journal of Science 255, 561–567.

Alderman, A., Von Der Borch, C., 1960. Occurrence of hydromagnesite in sediments in South Australia. Nature 188, 931.

Alderman, A., Von der Borch, C., 1961. Occurrence of magnesite–dolomite sediments in South Australia. Nature 192, 861.

Alderman, A., Von Der Borch, C., 1963. A dolomite reaction series. Nature 198, 465–466.

Alipour, S., 2006. Hydrogeochemistry of seasonal variation of Urmia Salt Lake. Iran. Saline systems 2, 1–19.

Asem, A., Mohebbi, F., Ahmadi, R., 2012. Drought in Urmia Lake, the largest natural habitat of brine shrimp Artemia. World aquaculture 43, 36–38.

Aubert, C., Djamali, M., Jones, M., Lahijani, H., Marriner, N., Naderi-Beni, A., Sharifi, A., Ponel, P., Gandouin, E., 2019. A major hydrobiological change in Dasht-e Arjan Wetland (southwestern Iran) during the late glacial–early Holocene transition revealed by subfossil chironomids. Canadian journal of earth sciences 56, 848–856.

Bar-Matthews, M., Ayalon, A., Kaufman, A., 1997. Late Quaternary paleoclimate in the eastern Mediterranean region from stable isotope analysis of speleothems at Soreq Cave, Israel. Quaternary Research 47, 155–168.

Bartov, Y., Goldstein, S.L., Stein, M., Enzel, Y., 2003. Catastrophic arid episodes in the Eastern Mediterranean linked with the North Atlantic Heinrich events. Geology 31, 439–442.

Bookman (Ken-Tor), R., Enzel, Y., Agnon, A., Stein, M., 2004. Late Holocene lake levels of the Dead Sea. Geological Society of America Bulletin 116, 555-571.

Bottema, S., 1986. A late Quaternary pollen diagram from Lake Urmia (northwestern Iran). Review of Palaeobotany and Palynology 47, 241–261.

Çağatay, M.N., Öğretmen, N., Damcı, E., Stockhecke, M., Sancar, Ü., Eriş, K.K., Özeren, S., 2014. Lake level and climate records of the last 90ka from the Northern Basin of Lake Van, eastern Turkey. Quaternary Science Reviews 104, 97–116.

Chamley, H., 1989. Clay Sedimentology pp. 21-50.

Clayton, R.N., Jones, B.F., 1968. Isotope studies of dolomite formation under sedimentary conditions. Geochimica et Cosmochimica Acta 32, 415–432.

Curtis, C., 1987. Mineralogical consequences of organic matter degradation in sediments: inorganic/organic diagenesis. Marine clastic sedimentology. Springer 108–123.

Diekmann, B., Petsehick, R., Gingele, F., Fütterer, D., Abelmann, A., Brathauer, U., Gersonde, R., Mackensen, A., 1996. Clay mineral fluctuations in Late Quaternary sediments of the southeastern South Atlantic: implications for past changes of deep water advection. The South Atlantic. Springer 621–644.

Djamali, M., de Beaulieu, J.-L., Shah-hosseini, M., Andrieu-Ponel, V., Ponel, P., Amini, A., Akhani, H., Leroy, S.A.G., Stevens, L., Lahijani, H., Brewer, S., 2008a. A late Pleistocene long pollen record from Lake Urmia, Nw Iran. Quaternary Research 69, 413–420.

Djamali, M., Kürschner, H., Akhani, H., de Beaulieu, J.L., Amini, A., Andrieu-Ponel, V., Ponel, P., Stevens, L., 2008b. Palaeoecological significance of the spores of the liverwort Riella (Riellaceae) in a late Pleistocene long pollen record from the hypersaline Lake Urmia, NW Iran. Review of Palaeobotany and Palynology 152, 66–73.

Djamali, M., Akhani, H., Andrieu-Ponel, V., Braconnot, P., Brewer, S., de Beaulieu, J.-L., Fleitmann, D., Fleury, J., Gasse, F., Guibal, F., 2010. Indian Summer Monsoon variations could have affected the early-Holocene woodland expansion in the Near East. The Holocene 20, 813–820.

Eastwood, W.J., Leng, M.J., Roberts, N., Davis, B., 2007. Holocene climate change in the eastern Mediterranean region: a comparison of stable isotope and pollen data from Lake Gölhisar, southwest Turkey. Journal of Quaternary Science: Published for the Quaternary Research Association 22, 327–341.

Eastwood, W., Roberts, N., Lamb, H., Tibby, J., 1999. Holocene environmental change in southwest Turkey: a palaeoecological record of lake and catchment-related changes. Quaternary Science Reviews 18, 671–695.

Ehrmann, W., Setti, M., Marinoni, L., 2005. Clay minerals in Cenozoic sediments off Cape Roberts (McMurdo Sound, Antarctica) reveal palaeoclimatic history. Palaeogeography, Palaeoclimatology, Palaeoecology 229, 187–211.

Erfan, S., Rezaei, K., Lak, R., Alcali, S.M., 2017. Clay mineralogy and sediment grain-size variations as climatic signals in southern part of Urmia Lake cores, North West of Iran. Journal of Research in Biology 7, 2266–2281.

Esmaeili Dahesht, L., Negarestan, H., Eimanifar, A., Mohebbi, F., Ahmadi, R., 2010. The fluctuations of physicochemical factors and phytoplankton populations of Urmia Lake. Iran. Iranian Journal of Fisheries Sciences 9, 361–381.

Esquevin, J., 1969. Influence de la composition chimique des illites sur leur cristallinité. Bull. Centre Rech. Pau-SNPA 3, 147–153.

Eugster, H., KELTS, K., 1983. Lacustrine chemical sediments. Chemical sediments and geomorphology, 321-368.

Eugster, H.P., Jones, B.F., 1979. Behavior of major solutes during closed-basin brine evolution. American journal of science 279, 609–631.

Fontes, J.C., Mélières, F., Gibert, E., Qing, L., Gasse, F., 1993. Stable isotope and radiocarbon balances of two Tibetan lakes (Sumxi Co, Longmu Co) from 13,000 BP. Quaternary Science Reviews 12, 875–887.

Fontes, J.C., Gasse, F., Gibert, E., 1996. Holocene environmental changes in Lake Bangong basin (Western Tibet). Part 1: Chronology and stable isotopes of carbonates of a Holocene lacustrine core. Palaeogeography, Palaeoclimatology, Palaeoecology 120, 25–47.

Fontugne, M., Kuzucuoğlu, C., Karabiyikoğlu, M., Hatte, C., Pastre, J.F., 1999. From Pleniglacial to Holocene: a 14C chronostratigraphy of environmental changes in the Konya Plain, Turkey. Quaternary Science Reviews 18, 573–591.

Galicki, S.J., Doerner, J.P., 2010. Holocene lake evolution in the Elmali basin, southwest Turkey. Physical Geography 31, 234–253.

Gasse, F., 2000. Hydrological changes in the African tropics since the Last Glacial Maximum. Quaternary Science Reviews 19, 189–211.

Ghalibaf, M.B., Moussavi, Z., 2014. Development and environment in Urmia Lake of Iran. European Journal of Sustainable Development 3, 219.

Holtzapffel, T., 1985. Les minéraux argileux. Préparation. Analyse diffractométrique et détermination. Société Géologique Nord. Publication 12, 136 p.

Hua, Q., Turnbull, J.C., Santos, G.M., Rakowski, A.Z., Ancapichún, S., De Pol-Holz, R., Hammer, S., Lehman, S.J., Levin, I., Miller, J.B., 2021. Atmospheric radiocarbon for the period 1950–2019. Radiocarbon 1–23.

Jalali, B., Sicre, M.A., Bassetti, M.A., Kallel, N., 2016. Holocene climate variability in the north-western Mediterranean Sea (gulf of lions). Climate of the Past 12, 91–101.

Jones, M.D., Roberts, C.N., 2008. Interpreting lake isotope records of Holocene environmental change in the Eastern Mediterranean. Quaternary international 181, 32–38.

Jones, M.D., Roberts, C.N., Leng, M.J., Türkeş, M., 2006. A high-resolution late Holocene lake isotope record from Turkey and links to North Atlantic and monsoon climate. Geology 34, 361–364.

Jones, M.D., Roberts, C.N., Leng, M.J., 2007. Quantifying climatic change through the last glacial–interglacial transition based on lake isotope palaeohydrology from central Turkey. Quaternary Research 67, 463–473.

Kelts, K., Shahrabi, M., 1986. Holocene sedimentology of hypersaline Lake Urmia, northwestern Iran. Palaeogeography, Palaeoclimatology, Palaeoecology 54, 105–130.

Kuzucuoğlu, C., Bertaux, J., Black, S., Denefle, M., Fontugne, M., Karabiyikoğlu, M., Kashima, K., Limondin-Lozouet, N., Mouralis, D., Orth, P.J.G.J., 1999. Reconstruction of climatic changes during the Late Pleistocene, based on sediment records from the Konya Basin (Central Anatolia. Turkey) 34, 175–198.

Kuzucuoğlu, C., Christol, A., Mouralis, D., Doğu, A.F., Akköprü, E., Fort, M., Brunstein, D., Zorer, H., Fontugne, M., Karabiyikoğlu, M., 2010. Formation of the upper pleistocene terraces of Lake Van (Turkey). Journal of Quaternary Science 25, 1124–1137.

Lippmann, F., 1973. Crystal chemistry of sedimentary carbonate minerals. Sedimentary Carbonate Minerals. Springer 5–96.

McKenzie, D., 1976. The East Anatolian Fault: a major structure in eastern Turkey. Earth and Planetary Science Letters 29, 189–193.

Mirzapour, B., Lak, R., Aleali, M., Djamali, M., Shahbazi, R., 2021a. Identifying the effects of climate changes on sedimentary environments and determining the sedimentation rate of south wetlands of Lake Urmia during Late Pleistocene and Holocene. Pollution 7, 113–127.

Mirzapour, B., Lak, R., Aleali, M., Djamali, M., Shahbazi, R., 2021b. Mineralogical reconstruction of Late Pleistocene - Holocene climate and environmental changes in southern wetlands of Lake Urmia. Geopersia 11, 205–218.

Müller, G., Irion, G., Förstner, U., 1972. Formation and Diagenesis of Inorganic Ca-Mg Carbonates. Naturwissenschaften 59, 158–164.

Ngrip, 2004. High-resolution record of Northern Hemisphere climate extending into the last interglacial period. Nature 431, 147–151.

Ön, Z.B., Akçer-Ön, S., Özeren, M.S., Eriş, K.K., Greaves, A.M., Çağatay, M.N., 2018. Climate proxies for the last 17.3 ka from Lake Hazar (Eastern Anatolia), extracted by independent component analysis of μ-XRF data. Quaternary International 486, 17–28.

Pengra, B., 2012. The drying of Iran's Lake Urmia and its environmental consequences. United Nations Environmental Progamme (UNEP), Global Environmental Alert Service (GEAS) Bulletin.

Peterson, M., Bien, G., 1966. Growth of dolomite crystals. American Journal of Science 264, 257–272.

Peterson, M., Bien, G., Berner, R., 1963. Radiocarbon studies of recent dolomite from Deep Spring Lake, California. Journal of Geophysical Research 68, 6493–6505.

Petschick, R., 2000. MacDiff 4.2.2. (Online). Available: http://servermac.geologie.un-frankfurt.de.Reiner.html. (Cited 01-12-2001).

Pierre, C., Ortlieb, L., Person, A., 1984. Supratidal evaporitic dolomite at Ojo de Liebre Lagoon; mineralogical and isotopic arguments for primary crystallization. Journal of Sedimentary Research 54, 1049–1061.

Post, F., Youssef, N., 1977. A procaryotic intracellular symbiont of the Great Salt Lake brine shrimp Artemia salina (L.). Canadian Journal of Microbiology 23, 1232–1236.

Reimer, P.J., Bard, E., Bayliss, A., Beck, J.W., Blackwell, P.G., Ramsey, C.B., Buck, C.E., Cheng, H., Edwards, R.L., Friedrich, M., 2013. IntCal13 and Marine13 radiocarbon age calibration curves 0–50,000 years cal BP. Radiocarbon 55, 1869–1887.

Reimer, P.J., Austin, W.E., Bard, E., Bayliss, A., Blackwell, P.G., Ramsey, C.B., Butzin, M., Cheng, H., Edwards, R.L., Friedrich, M., 2020. The IntCal20 Northern Hemisphere radiocarbon age calibration curve (0–55 cal kBP). Radiocarbon 62, 725–757.

Roberts, N., Reed, J., Leng, M., Kuzucuoğlu, C., Fontugne, M., Bertaux, J., Woldring, H., Bottema, S., Black, S., Hunt, E., 2001. The tempo of Holocene climatic change in the eastern Mediterranean region: new high-resolution crater-lake sediment data from central Turkey. The Holocene 11, 721–736.

Roberts, N., Jones, M., Benkaddour, A., Eastwood, W., Filippi, M., Frogley, M., Lamb, H., Leng, M., Reed, J., Stein, M., 2008. Stable isotope records of Late Quaternary climate and hydrology from Mediterranean lakes: the ISOMED synthesis. Quaternary Science Reviews 27, 2426–2441.

Sharifi, A., Shah-Hosseini, M., Pourmand, A., Esfahaninejad, M., Haeri-Ardakani, O., 2018. The Vanishing of Urmia Lake: a geolimnological perspective on the hydrological imbalance of the world's second largest hypersaline lake.

Sharifi, A., Pourmand, A., Canuel, E.A., Ferer-Tyler, E., Peterson, L.C., Aichner, B., Feakins, S.J., Daryaee, T., Djamali, M., Beni, A.N., Lahijani, H.A.K., Swart, P.K., 2015. Abrupt climate variability since the last deglaciation based on a high-resolution, multi-proxy peat record from NW Iran: The hand that rocked the Cradle of Civilization? Quaternary Science Reviews 123, 215–230.

Skinner, H.C.W., 1963. Precipitation of calcian dolomites and magnesian calcites in the southeast of South Australia. American Journal of Science 261, 449–472.

Solaymani Azad, S., 2009. Evaluation de l'aléa sismique pour les villes de Téhéran, Tabriz et Zandjan dans le NW de l'Iran: approche morphotectonique et paléosismologique. University Montpellier 2, France. Doctoral dissertation.

Staubwasser, M., Weiss, H., 2006. Holocene climate and cultural evolution in late prehistoric–early historic West Asia. Quaternary Research 66, 372–387.

Stein, M., Torfstein, A., Gavrieli, I., Yechieli, Y., 2010. Abrupt aridities and salt deposition in the post-glacial Dead Sea and their North Atlantic connection. Quaternary Science Reviews 29, 567–575.

Stevens, L.R., Ito, E., Schwalb, A., Wright, H.E., 2006. Timing of atmospheric precipitation in the Zagros Mountains inferred from a multi-proxy record from Lake Mirabad. Iran. Quaternary research 66, 494–500.

Stevens, L.R., Djamali, M., Andrieu-Ponel, V., de Beaulieu, J.L., 2012. Hydroclimatic variations over the last two glacial/interglacial cycles at Lake Urmia. Iran. Journal of Paleolimnology 47, 645–660.

Stuiver, M., Reimer, P., Reimer, R., 2021. CALIB 8.2 [WWW program] at http://calib.org.

Talebi, T., Ramezani, E., Djamali, M., Lahijani, H.A.K., Naqinezhad, A., Alizadeh, K., Andrieu-Ponel, V., 2016. The Late-Holocene climate change, vegetation dynamics, lake-level changes and anthropogenic impacts in the Lake Urmia region, NW Iran. Quaternary International 408, 40–51.

Tudryn, A., Tucholka, P., Özgûr, N., Gibert, E., Elitok, O., Kamaci, Z., Massault, M., Poisson, A., Platevoet, B., 2013. A 2300-year record of environmental change from SW Anatolia, Lake Burdur, Turkey. Journal of paleolimnology 49, 647–662.

Tudryn, A., Motavalli-Anbaran, S.H., Tucholka, P., Gibert-Brunet, E., Lankarani, M., Ahmady-Birgani, H., Kong, T., Noret, A., Miska, S., Massault, M., Dufaure, O., 2021. Late Quaternary environmental changes of Lake Urmia basin (NW Iran) inferred from sedimentological and magnetic records. Quaternary International 589, 83–94.

Turner, R., Roberts, N., Jones, M., 2008. Climatic pacing of Mediterranean fire histories from lake sedimentary microcharcoal. Global and Planetary Change 63, 317–324.

von Der Borch, C., 1965. The distribution and preliminary geochemistry of modern carbonate sediments of the Coorong area, South Australia. Geochimica et Cosmochimica Acta 29, 781–799.

Von der Borch, C.C., Jones, J.B., 1976. Spherular modern dolomite from the Coorong area, South Australia. Sedimentology 23, 587–591.

Wasylikowa, K., Witkowski, A., Walanus, A., Hutorowicz, A., Alexandrowicz, S.W., Langer, J.J., 2006. Palaeolimnology of Lake Zeribar, Iran, and its climatic implications. Quaternary Research 66, 477–493.

Wurtsbaugh, W.A., Gliwicz, Z.M., 2001. Limnological control of brine shrimp population dynamics and cyst production in the Great Salt Lake, Utah. Saline Lakes. Springer 119–132.

Chapter 4: Sediment flux and early diagenesis inferred from high-resolution XRF-CS data and iron and arsenic sulfides during the last 30 kyr in Lake Urmia, Iran: implications for studies of hypersaline lakes

XRF core scanning provides a rapid and non-destructive record of elemental variations in sediments and has recently been used quite frequently in studies of marine and lacustrine sediments. However, this method is still rarely used for specific environments such as hypersaline lakes like Lake Urmia.

In this chapter, results of XRF analyses of Lake Urmia for the last 30 kyr are presented. Previously obtained XRF and mineralogical data allowed discussion of physical versus chemical weathering in the lake's catchment, of the carbonate and sulphate fraction precipitated in the lake water, and of the sulphide authigenesis in the bottom sediment during the early anoxic diagenesis. Thanks to XRF analyses, arsenic was identified in specific sections of the sediment and correlated with iron sulphides previously identified through magnetic parameters and XRD analyses. Arsenic is rarely reported in marine and lacustrine studies and may be result of anthropogenic activity. In lake Urmia, it occurs naturally and readily identifies anoxic sections of the sediment/lake bottom conditions.

Sediment flux and early diagenesis inferred from high-resolution XRF-CS data and iron and arsenic sulfides during the last 30 kyr in Lake Urmia, Iran: implications for studies of hypersaline lakes

Ting Kong [a], Alina Tudryn [a, *], Elisabeth Gibert-Brunet [a], Piotr Tucholka [a], Seyed-Hani Motavalli-Anbaran [b], Mohammad Lankarani [c], Hesam Ahmady-Birgani [d]

[a] University Paris-Saclay, CNRS, UMR 8148-GEOPS, 91405, Orsay, France

[b] Institute of Geophysics, University of Tehran, Tehran, Iran

[c] School of Geology, University-College of Science, University of Tehran, Tehran, Iran

[d] Faculty of Natural Resources, Urmia University, Urmia, Iran

Submitted to Sedimentary Geology

Abstract

Geochemical studies on lake sediments are the most effective in obtaining precise information on the variable influence on weathering conditions of the watershed and related sedimentary fluxes to the lake. Authigenic versus allogenic sedimentation occur both in the water column and at the water-sediment interface, the latter being particularly important in hypersaline lake's basins. Here, we investigated the continuous sedimentary elemental compositions of a 12.5-m-long sediment composite core collected from Lake Urmia (NW Iran) by high resolution X-Ray fluorescence core scanning (XRF CS). In combination with mineralogical investigations including clays, carbonates and magnetic minerals as well as grain size distributions, our study presents a continuous 30 cal kBP record of the lake's evolution. The CS XRF elemental data show three groups that correlate closely with the three mineralogical categories of sediments: the Si group (*e.g.* Si, Al, Ti, Fe, Mn), including mostly aluminosilicates, the Ca-Sr group

representing Ca, Sr and Mg carbonates, and the Cl-S group gathering halite minerals, sulfates and sulfides (*e.g.* Fe, As).

High values of ln(K/Ti), ln(Ca/Ti) and ln(Sr/Ca) and low ln(Rb/Sr) highlight increasing chemical weathering in the catchment in conjunction with increasing authigenic carbonate precipitation in Lake Urmia and reflect both wet conditions and high lake water levels. In contrast, increasing ratios of Rb/Sr associated with decreasing ln(K/Ti), ln(Ca/Ti) and ln(Sr/Ca) values indicate enhanced erosion in the catchment linked to drier conditions and lower lake water levels. Moreover, according to As-XRF CS pattern and magnetic parameters, we identify iron and naturally-occurring arsenic sulfides rarely reported from saline lakes; they are acting as specific indicators of anoxic conditions in the lake bottom environment. This work highlights the effectiveness of the method that can be applied to the studies of salt lakes environments.

Beyond Lake Urmia, these new data fill an important gap in the Middle East paleoclimate records, provide unique and continuous 30 cal kBP information on the possible driving mechanisms of the observed changes to be compared to the paleoenvironmental and climate evolution at regional and global scales and to be used in global circulation models.

Keywords: XRF CS geochemistry; iron and arsenic sulfides; early diagenesis; anoxic environment; environmental sedimentology; paleoclimatology; salty lake

4.1. Introduction

Understanding climate change affecting geographical regions with high population density makes the study of continents a direct and significant issue, especially to ensure the accessibility to natural water resources as well as to ecological services. The continents and their margins provide both an essential spatial resolution for attempting to reconstruct environmental changes on a regional scale, and because of their relatively high sedimentation rates, a human-scale temporal resolution.

Within the framework of multidisciplinary projects, the reconstruction of paleoenvironments

in the continental domain, and consequently the prediction of the current and future evolution of climate change impacts, requires two essential steps: (i) obtaining accurate and reliable correlations from one site to another, and distributed as equitably as possible both in latitude and longitude, and (ii) establishing data sets under the form of databases accessible to all and being the starting point for comparison with a general circulation model (GCM's).

Among all continental markers and despite the fact that they are sometimes governed by local hydrogeological factors and sometimes unrelated to global climate fluctuations, endorheic lakes, relatively well distributed in the world, give an access to a very high temporal resolution, with a sedimentation rate much higher than that encountered in the marine domain. They thus allow the detection of very rapid paleoclimate variations, sometimes annual and even seasonal (Clement and Peterson, 2008).

Finally, lakes are privileged recorders of both climate change at the regional scale and the evolution of surface conditions at the local scale. Therefore, the cored lake sequences constitute reliable paleoenvironmental records, whose signal is often continuous, precise and sensitive over time. This is particularly interesting for closed lake basins for which variations in water balance are essentially and/or directly linked to climatic fluctuations.

In order to reconstruct past environments in a closed basin, geochemical studies on lake sediments are the most effective in obtaining precise information on the variable influence of authigenic versus allogenic sedimentary processes (Löwemark et al., 2011) as well as on, either, physical or chemical weathering conditions of the watershed. Among all available methods, scanning X-ray fluorescence spectrometry (XRF) offers an opportunity to interpret past environmental and climate changes. This method with the advantages of both the preservation of samples and the possibility of obtaining a continuous recording at high resolution of the elemental analyzes has been routinely used (Evans et al., 2019; Hennekam et al., 2019; Guo et al., 2021; Peti and Augustinus., 2022).

The elemental composition of lake sediment is controlled both (i) by the geochemistry of the detrital supply, itself determined by the geology and the hydrodynamic sorting, (ii) by the history of weathering and erosion on the watershed, and as well as (iii) by the different sedimentary

processes occurring both in the water column and at the water-sediment interface. The combination and comparison of several high-resolution XRF data sets provide information 1- on detrital inputs with analyzes of the elements such as Ti, Fe, Si, Al, Rb and K (Kylander et al., 2011; Croudace and Rothwell, 2015; Davies et al., 2015); 2- on the chemical weathering and erosion of watersheds, with for example the evolution of K/Ti (Xie et al., 2014); 3- on the composition and content of the carbonate procession and on the variations of evaporates when present with elements such as Ca, Sr and S, and ratios as Ca/Ti and Sr/Ca (Davies et al., 2015), as well as 4- on the salinity of the lake water in chlorite (Cl), when studying saline lakes (Brisset et al., 2018).

Within the framework of the Lake Urmia (Western Iran) project (Tudryn et al., 2021) aiming at deciphering the patterns and trends of the lake's past environmental evolution in relation with natural *versus* anthropogenic impacts and at integrating the results into sustainable water and ecosystem management strategies, we present here the results of XRF core scanning (XRF CS) performed on lacustrine cored sequences from Lake Urmia. Although being the world's second largest hypersaline lake for years, Lake Urmia experienced significant changes in its water level that rapidly fell from 1278 m to 1270 m above mean sea level from 1995. Since it developed in closed basin, the main causes behind the pronounced 8-m lake level drop are likely the shortage of riverine inflow and/or excess outflow through evaporation, which maybe be caused by anthropogenic alteration including dam construction, channel deviation, groundwater pumping (Tourian et al., 2015), and climate changes through reducing precipitation and/or higher temperature. Although anthropogenic factors have been widely discussed (Chaudhari et al., 2018; Asem et al., 2019; Khazaei et al., 2019; Ahmady-Birgani et al., 2020), the lack of high-resolution sedimentary records in the past limits the understanding of actual processes under present-day climate variations.

Lake Urmia sedimentary archives are ideal for the application of XRF methodology and can be extensively explored to reconstruct climatic and environmental changes at high resolution. In connection with the lake hydrological regime, the objectives of this study are therefore (i) to highlight correlations, if existing, between the results of the elementary XRF CS analyzes as well

as their variation according to the timescale, and by combining mineralogical indicators already published (Tudryn et al., 2021; Kong et al., 2022), and (ii) to reconstruct the evolution of sediment origin/influx and water levels of Lake Urmia over the past 30,000 years. Finally, this work will assess the potential of these XRF elemental analyzes for the determination of the intensity of erosion and chemical weathering on the catchment of the lake and it will help to understand the climatic history at a more regional to global scale during the late Pleistocene and Holocene, in relation to climatic conditions.

4.2. General setting

Iran lies in Western Asia, and is surrounded by (i) the Caspian Sea and borders of Azerbaijan, Armenia and Turkmenistan to the north, (ii) Turkey and Iraq borders to the west, (iii) the littoral of the Persian Gulf and the Sea of Oman in the south, and (iv) its east abuts Pakistan and Afghanistan (Fig. 1a). Forming the 2/3 of Iran, the Iranian plateau is an important geological formation between the Middle East and Central Asia (Allen et al., 2013), bordered by the Zagros Mountains in the South-west with both a high seismic and faulting activities and development of volcanoes, and by the Alborz range and the Kopet-Dag in the north.

Located in a subsiding tectonic basin in the northwestern part of the Iranian plateau, Lake Urmia, is a hypersaline endorheic lake lying at 1270 m a.s.l. and extending approximately between 45°00′ and 46°00′ east longitudes and 37°00′ to 38°16′ north latitudes. As a consequence, the geological settings of the lake basin is comprised of a variety of rock formations ranging from Precambrian metamorphic complexes to Quaternary mud deposits as presented in Fig. 1b (Kelts and Shahrabi, 1986). The paleozoic metamorphic rocks characterize the Zagros Mountains in the west of the basin while intrusive rocks occur in the southern, western, and northwestern areas of the basin. The volcanic to volcano-sedimentary formations dominate in the eastern and northeastern basin. Moreover, the carbonate sedimentary units prevail in southern and western basin, and evaporitic sedimentary units occurs in the northeastern basin (Kelts and Shahrabi, 1986).

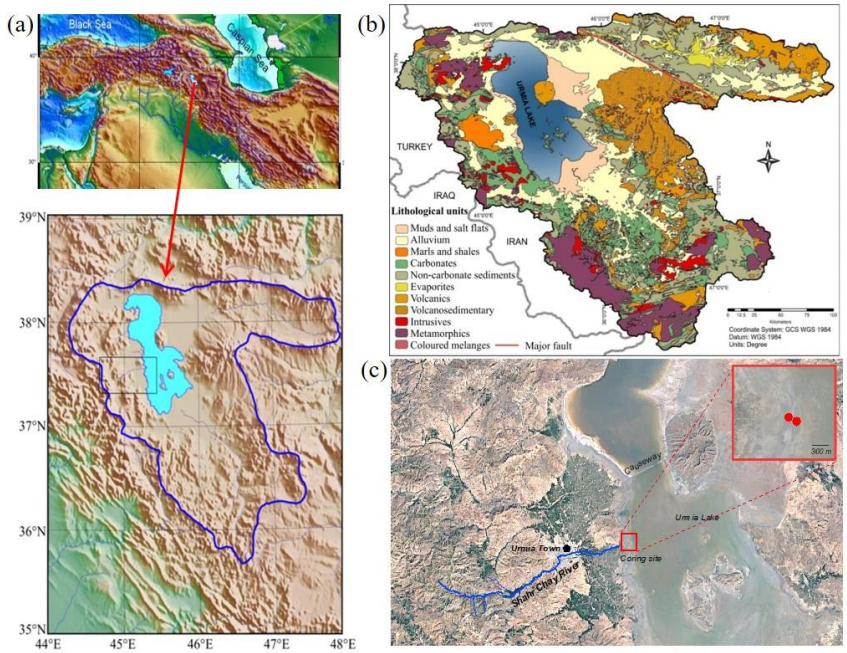

Fig. 1. *Lake Urmia: (a) location of the lake and lake's catchment area: blue lines indicate Lake Urmia basin (Aubert et al., 2017); (b) simplified geological map of Lake Urmia catchment area (after Sharifi et al., 2018, modified in Tudryn et al, 2021); (c) location of coring-red circle indicates the G6 and G7 coring sites; support from Google Earth.*

4.3. Materials and methods

4.3.1. Sediment core and previous results

Integrated in the Franco-Iranian research projects, the present work is based on the study of a composite sedimentary sequence presenting a continuous record of Lake Urmia evolution for the last 30,000 years. A 12.5-m long composite core has been reconstructed from two cores Golman 6 (37° 35′ 28.854″ N, 45° 16′ 33.834″ E) and Golman 7 (37° 35′ 28.746″ N, 45° 16′ 33.75″ E) taken from the mouth of the Shahr Chay River in the recently dried out part of the west coast of the lake (Fig. 1c) (Tudryn et al., 2021). Collected in the same area, core Golman 5 duplicates the most recent part of the sequence and the main peaks, especially for magnetic susceptibility, were exactly correlated (for details, see Tudryn et al., 2021).

The records of many environmental parameters such as (i) magnetic susceptibility allowing the estimation of the ferromagnetic minerals of detrital and/or authigenic origin, (ii) grain size reflecting either the transport energy, *i.e.* the distance from detrital sources, as well as (iii) the mineralogy along specific study of the clays and carbonate fractions, allowed for the definition of several successive environmental phases clearly defined and dated since 30 cal kBP to present day (Tudryn et al., 2021; Kong et al., 2022).

At about 30 cal kBP, all proxies indicate low lake stand and even drying out at the core site, followed by a rise in water level with open conditions between 29.9 and 20.2 cal kBP. Thereafter, all data suggests very unstable lake conditions. Lacustrine low stands were recorded during the intervals 20.2-15.3, 13.3-11.8 and 5.6-4.1 cal kBP while lake conditions recovered at 15.3-13.3, 11.8-5.6 and 4.1-2.3 cal kBP.

The lake high stand recorded between 15.3 and 13.3 cal kBP is likely attributed to the Bölling/Alleröd warming, and the following regressive phase during the 13.3-11.8 cal kBP period would correspond to the Younger Dryas period. In the Early-Mid Holocene, the lacustrine environment from 11.8 to 5.6 cal kBP was characterized by high aragonite and salt contents, highlighting more evaporative environment when compared with that during the 29.9-20.2 cal kBP phase.

4.3.2. XRF methodology

The elemental composition of bulk sediments was non-destructively analyzed every 5 mm on the U-channel core with a 4th generation Avaatech XRF core scanner (Laboratoire des Sciences du Climat et de l'Environnement -LSCE-, Gif sur Yvette, France; GEOPS/LSCE PANOPLY platform). Before the measurement the sediment surface of each section was carefully smoothed and covered with 4-µm thick Ultralene foil to protect the measurement triangle and prevent desiccation of the sediment. Elemental intensities were obtained at 10 kV (current of 200 µA, no filter, under helium flow) for the light elements (Mg, Al, Si, P, S, Cl, K, Ca, Ti), and at 30 kV (current of 150 µA, thin Palladium filter, under air) for heavier elements (Mn, Fe, Ni, Cu, Zn,

As, Br, Rb, Sr, Zr,). The measuring window is 5 mm (downcore) by 10 mm (crosscore), and the counting time is 10 s for each target sample and both runs. The SARM4 certified standard, *i.e.* so-called "Monitor scan", was measured at 10 kV between each core section to ensure the scanner has no technical issue (*e.g.* absence of helium leak affecting the counts of light elements).

The chemical composition of the sediment is measured by the XRF scanner as element intensities in total counts (cnts). The relative changes of elemental data based on XRF CS results, are recorded as the elemental profiles, rather than as absolute concentrations.

4.4. XRF element results

To quantify the strength of association among measured elements, a correlation matrix is constructed. As each element can occur in many different minerals while the similar variation of elemental intensity could reflect good relationships among the same minerals, strong correlations ($r>0.8$) are highlighted in red in the matrix (Table 1).

In agreement with the correlation matrix, two groups of elements highly correlated with each other can be individualized: (i) the Si group including Al, K, Ti, Fe, Rb, Mg, Mn and Zn, and (ii) the Ca–Sr group. Some other elements represented as (iii) the Cl-S group that includes As, do not display clear correlations but appear to be significant components of the lake sediments.

The Si group

Elements from this group usually represent the silicate and aluminosilicate minerals among which quartz, feldspars, mica, and clays. Individually, some of these elements can also reflect other groups of minerals, such as oxides (*e.g.* Al, Fe, Ti, Mn), carbonates (*e.g.* Mg, Mn), sulfides (*e.g.* Fe, Zn). However, the good correlations of these elements with Si and Al suggest their dominant affiliation to aluminosilicates. Besides, Si can also be related to biogenic sources as amorphous silica forming diatom frustules (Peinerud, 2000), but its strong correlation with Al (Table 1, Fig. 2a), which is not affected by biological action, rules out its biogenic origin. The group thus presents principally the siliclastic fraction of the sediment, whose time-scale

distribution is presented for four elements: Ti, K, Fe and Mg (Fig. 3a, 3b, 3c, 3d). Potassium is one from three most correlated elements, *i.e.* Si, Al and K, with a correlation coefficient of more than 0.96 (Table 1). Titanium is considered as less chemically affected than potassium and therefore represents more resistant to chemical weathering minerals (Wei et al., 2003). Iron is sensitive to redox changes while magnesium could belong partly to the carbonate fraction of the sediment. K, Fe and Ti display relatively high intensities at the beginning of the sequence although still remaining but still relatively high and stable as Mg do. This occurs until ca 20.2 cal kBP for K and Mg, both progressively decreasing until 15.3 cal kBP while Ti and Fe stay stable until ca 15.3 cal kBP. After 15.3 cal kBP and to the top of the sequence four elements present quite similar changes.

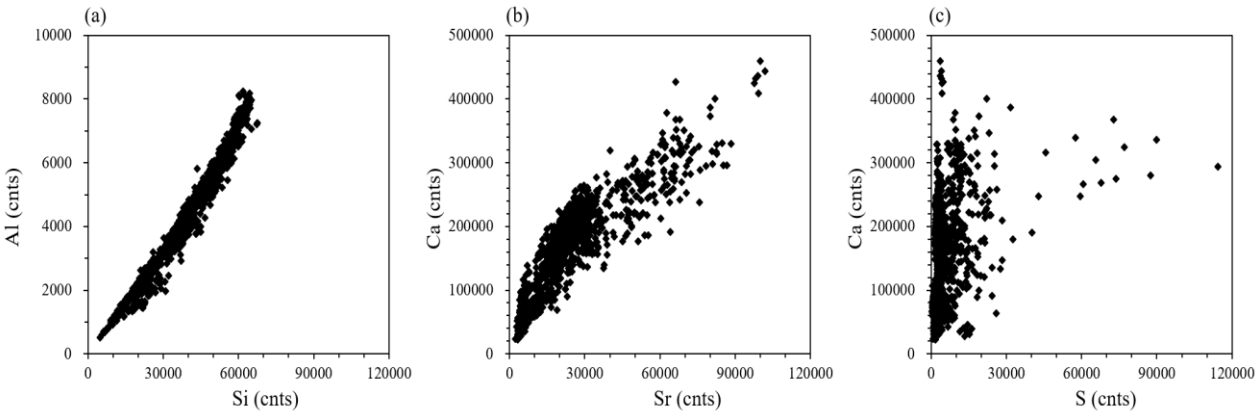

Fig. 2. *Elemental XRF CS data in Lake Urmia sediments: correlations of (a) Si vs Al; (b) Sr vs Ca; (c) S vs Ca.*

The Ca-Sr group

Due to its occurrence mainly in minerals such as silicates, carbonates and sulfates, Ca can be associated to these minerals. In lake sediments, Ca either comes from the watershed as supplied minerals or dissolved ions, or represents minerals that precipitate chemically or biologically in the lake. In Lake Urmia, Ca is clearly not correlated with silicates (Table 1). Therefore, Ca mainly represents carbonate minerals, *i.e.* aragonite, calcite and dolomite, and can also be linked to gypsum. Moreover, Ca displays the positive linear relationship with Sr with a correlation coefficient of 0.86 (Table 1, Fig. 2b). In lake sediments, Sr can originate from celestine ($SrSO_4$)

but also tracks Sr-rich aragonite that precipitates either chemically or by biomediation in lake water, in highly evaporated environments (Böning and Bard, 2009; Brisset et al., 2018). This correlation thus suggests that Ca is closely related to aragonite.

Considering the low correlation between Ca and S (Table 1, Fig. 2c), Ca is weakly representing gypsum, which supports the link of Ca with the aragonite. The poor correlation between S and Sr data, along with the absence of celestine in mineralogical assemblages (Kong et al. 2022), could also certify that Sr does track aragonite while S records other mineral abundance. Of course, to a lesser extent, Ca can also be correlated to calcite, dolomite and gypsum. Among carbonates, there is no clear correlation between Ca and Mg, the latter being well correlated with elements from the Si group (Table 1). The changes in Ca and Sr with time (Fig. 3e and 3f) show an antisymmetric pattern with respect to the siliclastic elements. After low contents at the beginning of the sequence, they increase and remain constant until 20.2 cal kBP. Between 20.2 and 11.8 cal kBP, they decrease with the short increase at 15.3 cal kBP. From 11.8 to 5.6 cal kBP, they display changing but highest values while they decrease from 5.6 to 2.3 cal kBP and finally increase to the core top.

The Cl-S group

In saline lakes such as Lake Urmia, Cl intensity principally represents halite abundance in the bulk sediment and thus reflects the salinity of the water. This element shows relatively high and stable values in the oldest part of the sediment, until ca 20.2 cal kBP (Fig. 3g). After that time, Cl concentration is more variable but generally maintains higher values than before, apart from two periods, between 20.2 and 17.8 cal kBP, and between 13.3 and 10.0 cal kBP (with a brief increase at 12.0 cal kBP), indicating freshening of the water (fresh water input, possible proximity of the river). The presence of sulfur can commonly be related to sulfates as gypsum and/or to iron sulfides. S is generally higher and more variable in the upper part of the sediment, from 12.0 cal kBP onwards (Fig. 3h) but it is not correlated with other elements. Finally, XRF analyses detected As at the beginning of the sequence and in its upper part (Fig. 3i). Since its content is generally very low in lacustrine deposits, As is usually not taken into account in XRF

analyses. However, its increased intensities appear to be significant in some levels and partly correlated with increased S intensities.

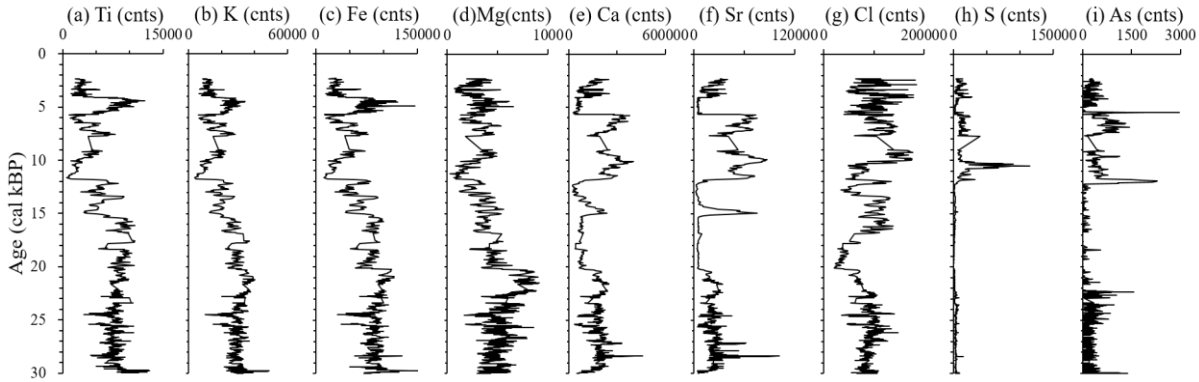

Fig. 3. *Elemental XRF CS profiles of Lake Urmia composite core against the ^{14}C timescale: (a) Ti; (b) K; (c) Fe; (d) Mg; (e) Ca; (f) Sr; (g) Cl; (h) S; (i) As.*

Table 1 *Correlation indexes among XRF CS elements: Mg, Al, Si, P, S, Cl, K, Ca, Ti, Mn, Fe, As, Ni, Cu, Zn, Br, Rb, Sr and Zr.*

	Mg	Al	Si	P	S	Cl	K	Ca	Ti	Mn	Fe	As	Ni	Cu	Zn	Br	Rb	Sr	Zr
Mg	1																		
Al	0.895	1																	
Si	0.860	0.985	1																
P	0.650	0.691	0.673	1															
S	-0.343	-0.419	-0.462	-0.162	1														
Cl	-0.052	-0.256	-0.281	-0.062	0.166	1													
K	0.850	0.965	0.963	0.654	-0.471	-0.154	1												
Ca	0.332	0.184	0.119	0.494	0.242	0.171	0.068	1											
Ti	0.613	0.795	0.824	0.460	-0.475	-0.105	0.883	-0.238	1										
Mn	0.756	0.785	0.776	0.646	-0.401	0.018	0.825	0.216	0.744	1									
Fe	0.789	0.890	0.893	0.626	-0.464	-0.076	0.954	0.014	0.907	0.875	1								
As	-0.170	-0.207	-0.233	-0.009	0.296	0.219	-0.217	0.173	-0.250	-0.192	-0.202	1							
Ni	0.740	0.740	0.724	0.713	-0.270	0.045	0.741	0.457	0.539	0.750	0.722	-0.018	1						
Cu	0.543	0.650	0.651	0.578	-0.323	-0.045	0.691	0.175	0.604	0.622	0.671	-0.073	0.674	1					
Zn	0.700	0.816	0.822	0.559	-0.448	-0.074	0.883	-0.038	0.857	0.781	0.899	-0.133	0.700	0.692	1				
Br	0.469	0.355	0.310	0.440	0.011	0.579	0.374	0.414	0.264	0.506	0.403	0.135	0.576	0.363	0.376	1			
Rb	0.316	0.504	0.547	0.071	-0.433	-0.130	0.620	-0.612	0.772	0.356	0.614	-0.261	0.173	0.329	0.623	-0.003	1		
Sr	-0.022	-0.189	-0.258	0.182	0.369	0.246	-0.299	0.865	-0.525	-0.130	-0.341	0.272	0.113	-0.118	-0.369	0.242	-0.756	1	
Zr	0.000	0.125	0.166	-0.106	-0.220	-0.041	0.207	-0.520	0.497	0.096	0.257	-0.169	-0.099	0.047	0.247	-0.089	0.570	-0.514	1

4.5. Discussion

In Lake Urmia sediments, the main mineralogical phases that have been identified (Tudryn et al., 2021; Kong et al., 2022) are (i) detrital siliclastic minerals (*e.g.* quartz, feldspars, mica, clay minerals), (ii) oxides (magnetite), (iii) carbonates such as aragonite, calcite and dolomite, these two latter being either detrital or authigenic, (iv) evaporites (gypsum and halite) formed within the lake water body, and (v) iron sulfides (greigite, pyrite) that crystallize under specific conditions either at the sediment-water interface or within the sediments.

These mineralogical data allowed us to identify the significance of the XRF CS elemental analysis in terms of the representativeness of the elements, and even their environmental significance in terms of geochemical processes occurring on the catchment and in the lake.

4.5.1. What happens in the catchment area?

As shown on Fig. 1c, the coring site is located close to the mouth of River Shahr Chay, whose catchment is thus the dominant supplier of both solid and dissolved material into the lake. Rocks in the catchment area are of various ages, origins and nature, and include metamorphic and magmatic rocks as well as carbonate and evaporite sedimentary units (Fig. 1b). Other sources of material that are related to the water circulation in the lake and to the intensity of airborne arrivals may also play a role.

According to XRF CS data, the similar change pattern in the defined elements of the Si group that includes Al, Si, Fe, K, Rb and Ti is recorded in Lake Urmia sediments, these elements clearly reflecting the detrital siliclastic signal from the catchment area (Kylander et al., 2011; Davies et al., 2015). In addition, significant intensities of Ca that evolve broadly antisymmetrically to silicates (Fig 3), suggests the presence of this element in the carbonate fraction of the sediment whether of detrital or authigenic origin.

Within the population of elements representing the silliclastic fraction of the sediment, Si, Al, Ti are relatively stable and are considered to be inert elements while K and Rb, which is associated with

K, are quite mobile and can enter the lake sediment in mineral form from the catchment area (*e.g.* K-feldspars, mica, illite) or in the form of an ion state when chemical weathering is acting. Thus, the value of ln(K/Ti) can reflect erosional processes in the watershed from different sources of detrital material, but it can also be an indicator of chemical weathering (Xie et al., 2014; Croudace and Rothwell, 2015). According to Xie et al. (2014), high K/Ti reflect abundant K-rich minerals, especially illite as a result of chemical weathering, and conversely low K/Ti values mean low illite content but abundant Ti-rich heavy minerals.

In addition, Ca-bearing carbonates and sulfates in natural fractionation process are easy to breakdown compared to the K-bearing minerals, so that Ca-Sr minerals are leached much more easily than K-Rb minerals (Xu et al., 2010). Therefore, chemical weathering in the catchment area results in lower values of ln(Rb/Sr), ln(K/Sr), ln(Rb/Ca) and ln(K/Ca) in lake deposits whereas lake sediments characterized by a higher fraction of silliclastic detritus exhibit higher values for the same ratios. Based on these findings, the ln(K/Ti) and ln(Rb/Sr) values of lake sediments could serve as a potential indicator of the intensity of chemical weathering in the watershed, the former being higher while the latter is lower as chemical weathering increases.

As presented in Fig. 4, ln(K/Ti) and ln(Rb/Sr) values are closely associated with the sedimentary units and reflect quite well the grain size and mineralogy in the composite core. The ln(K/Ti) parameter is well correlated with the evolution of clay and fine silt fraction in the sediment and with dominant clay minerals, i.e. smectite and illite (Fig. 4a, 4b, 4c). Its higher values highlight either increased erosion of fine deposits from the catchment area or chemical weathering within the siliclastic fraction. The high values of ln(Rb/Sr) are clearly correlated both with increased silliclastic minerals as quartz, feldspars and mica, and with coarse grain sizes indicating low chemical weathering (high erosional processes) at about 30 cal kBP and during the intervals from 20.2 to 15.3, from 13.3 to 11.8 and from 5.6 to 4.1 cal kBP. On the opposite, phases of moderate and low ln(Rb/Sr) after 29.9 and to 20.2, from 15.3 to 13.3, and between 11.8 and 5.6 cal kBP, as well as at the core top between 4.1 and 2.3 cal kBP, are correlated thus with increased chemical weathering in the catchment (Fig. 4d, 4e, 4f).

These data clearly indicate variations in the intensity of erosion and chemical weathering in the

watershed, with chemical weathering only occurring efficiently in the presence of sufficient water. According to these data, we observe that fine sediments deposited in Lake Urmia are related to increased humidity/moisture over the catchment area while the increased amounts of coarse clastic material were deposited during drier conditions. These increased amounts of clastic material are therefore not related to a generally wetter climate but correspond to drier conditions when the lake level was lower and when more erodible material was exposed in the catchment, as also observed in Dead Sea (Migowski et al., 2006).

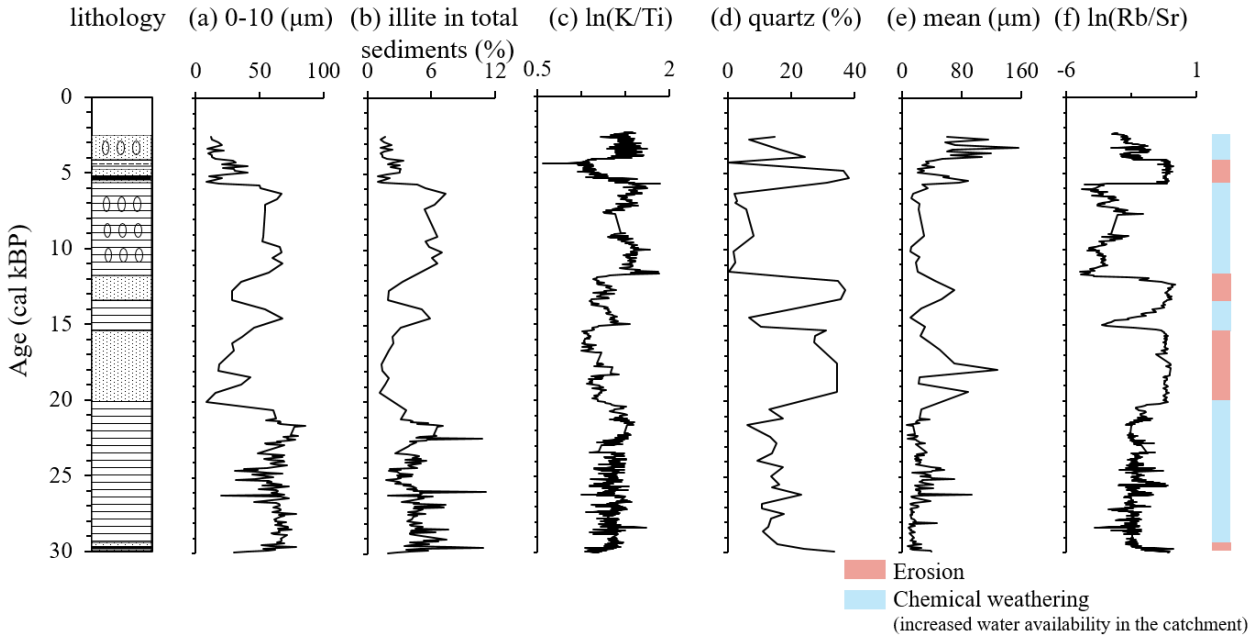

Fig. 4. *Comparison of elemental XRF CS and mineralogical data of Lake Urmia composite core against the ^{14}C timescale: (a) grain-size fraction from 0 to 10 μm; (b) illite percentages in bulk samples; (c) ln(K/Ti); (d) quartz percentages in bulk samples; (e) mean sediment grain size; (f) ln(Rb/Sr). Mineralogical and grain size data after Kong et al. (2022).*

4.5.2. What happens in the lake?

As in a closed-basin lake, the water level of Lake Urmia is principally controlled by the precipitation-evaporative water balance in its catchment area, including the lake itself. The main markers of different evaporation rates in relation to ionic concentrations within the water body are carbonate, gypsum and halite. In addition, iron sulfides are good indicators of anoxic conditions in the sediment and at the water-sediment interface. XRF CS elemental data of Ca, S, Cl and Fe integrate

all the information on these minerals that have been identified in Lake Urmia sediments (Tudryn et al., 2021; Kong et al., 2022). Additionally, XRF CS data indicate that As is a no-negligible component of the sediment, contrary to what is generally reported from lacustrine environments. The high Cl contents throughout the core, but especially in its upper part (Fig. 3g), reflect the presence of halite and point out highly evaporative conditions in the lake. Other elements may belong indifferently to either of the mineralogical groups. We will just deal below with carbonates, sulfates and sulfides.

5.2.1. Calcium: carbonates

The carbonate fraction consists of a mixture of both detrital carbonate, *i.e.* resulting from erosion, and authigenic carbonate directly precipitating in the lake water. In such a case, Ca/Ti could act as a proxy of the relative proportions, and hence changes, between carbonate and siliclastic terrigenous fluxes (Davies et al., 2015). Furthermore, as Sr is closely associated with aragonite that precipitates both chemically or biologically in lake water (Böning and Bard, 2009; Brisset et al., 2018), the increase in ln(Sr/Ca) may be an indicator of the presence of aragonite in the sediment. In Lake Urmia, ln(Ca/Ti) value are well correlated with the carbonate contents in general and ln(Sr/Ca) indicates the presence of aragonite (Fig. 5a, 5b, 5c) which has been previously identified as part of calcareous mud, and more specifically in the upper part of the core, as part of brine shrimp fecal pellets as well (Kong et al., 2022). Since the majority of carbonates is composed of aragonite, variations in ln(Ca/Ti) and ln(Sr/Ca) values with time follow a similar pattern.

In addition, calcite and dolomite have been identified as either detrital or authigenic depending on the level in the sedimentary sequence, through XRD analyses (Kong et al., 2022). Their detrital contributions to the overall sediment are quite well expressed by ln(Ca/Sr), inverse value to that discussed above ln(Ca/Ti). However, it was not possible to further identify these minerals and their authigenic and/or detrital origins through XRF CS.

In Lake Urmia, aragonite is mainly correlated with fine silliclastic minerals (Fig. 4a and 5b) deposited during the increase in chemical weathering in the catchment suggested by ln(Rb/Sr) (Fig. 4f). Its formation requires the supply of bicarbonate and Ca^{2+} through freshwater flows (Stein et al., 1997). Consequently, the presence of aragonite in the lake sediments indicates relatively humid

climatic conditions. This interpretation of aragonite as an indicator of more humid conditions is specific to highly saline environments and has been proposed for the Dead Sea sediments (Stein et al., 1997). As highlighted by Neugebauer (2016), such an indication of a relatively wet environment by aragonite is generally not valid since in freshwater lakes and under humid conditions, calcite precipitates, whereas a shift towards aragonite formation reflects drier conditions, more saline water and lower lake level. The presence of aragonite in Lake Urmia indicates thus relatively humid conditions and high lake water level, as proposed Tudryn et al. (2021) and Kong et al. (2022). The increase in aragonite contents and water level is in good agreement with phases of increased chemical weathering recorded in the catchment area and fine grain sedimentation in the lake while the absence of aragonite and the increased amount of clastic deposits are related to generally drier conditions and low lake level.

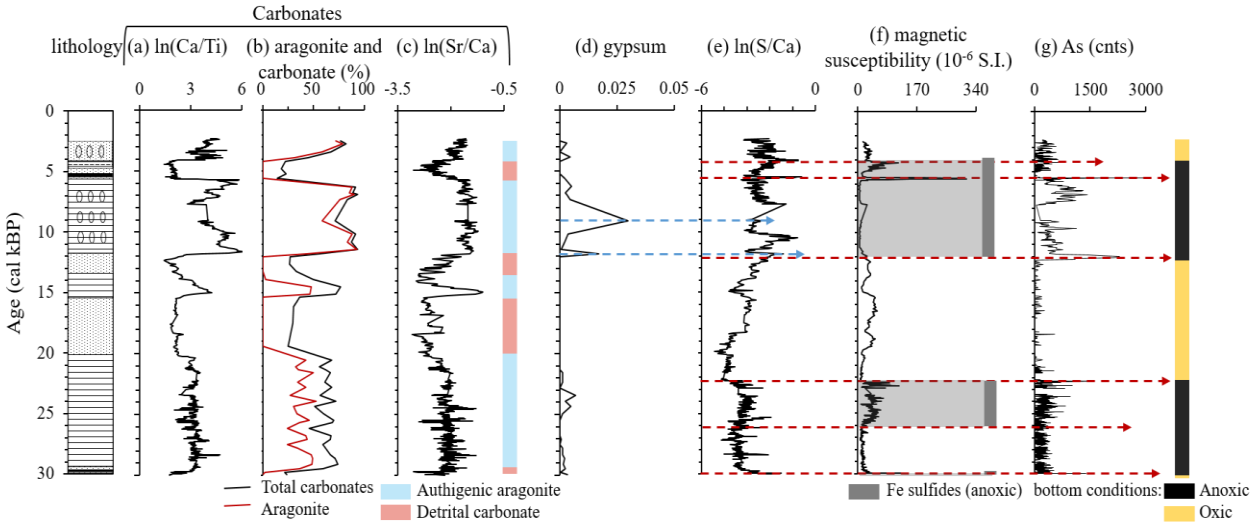

Fig. 5. *Comparison of elemental XRF CS and mineralogical and magnetic data of Lake Urmia composite core against the ^{14}C timescale: (a) ln(Ca/Ti); (b) carbonate and aragonite percentages in bulk samples; (c) ln(Sr/Ca); (d) gypsum percentages in bulk samples; (e) ln(S/Ca); (f) magnetic susceptibility; (g) Arsenic profile.*

5.2.2. Sulfur: Sulfates and sulfides

According to Chéron et al. (2016), XRF CS sulfur data have been rarely reported in previous studies, because of a poor XRF CS detection efficiency and low elemental abundance and hence leading to count rates associated with a large counting statistic error. However, in lacustrine environments, XRF CS sulfur data are used to identify gypsum precipitation, the presence of pyrite,

or soil leaching as summarized by Davis and colleagues (2015). In saline lake sediments, sulfur displays quite high values and can be hosted either by sulfates (*e.g.*, gypsum, anhydrite), or by sulfides (*e.g.*, pyrite, marcasite, greigite), and it can also occur in pore water as dissolved sulfate and sulfide forms.

Gypsum

In Dead Sea sediments, gypsum layers are reflected in the S/Ca value (Neugebauer et al., 2016) and the presence of gypsum is interpreted as the result of the mixing of the water column during more extreme dry years with higher evaporation (Stein et al., 1997). In Lake Urmia sediments, two individual layers of gypsum seem to be in phase with an increase in sulfur content and the ln(S/Ca) value, but overall, these parameters are only weakly correlated with the presence of gypsum (Fig. 5e, Fig. 3h). The evolution of sulfur and ln(S/Ca) value are therefore clearly dependent on another parameter.

Iron sulfides

Previous studies have reported the presence of iron sulfides, *i.e.* greigite and pyrite, and of iron oxide, *i.e.* magnetite, in Lake Urmia sediments (Tudryn et al., 2021). The results of the mineral distribution are presented synthetically in Fig. 5f through magnetic susceptibility and magnetic mineralogy. One can observe that magnetic susceptibility integrates information on these iron-bearing minerals but cannot allow their identification in different sections of the sediment.

Both authigenic sulfides (greigite and pyrite) precipitate in an anoxic, bacterial sulfate-reducing environment (Berner, 1981; Curtis, 1987; Jelinowska et al., 1995; Roberts, 1995; Tudryn et al., 2010). Being a magnetic mineral, greigite is revealed by an increased magnetic susceptibility when present in relatively high contents (two peaks occurring in organic-rich dark levels at 5.5 and 29.9 cal kBP, and between ca 26.0 and 22.5 cal kBP) while it is not the case for its low contents or when only pyrite is present (between ca 12.0 and 5.6 cal kBP; Fig. 5). Magnetite is of detrital origin and indicates oxygenated depositional environments. Changes of its contents are recorded through both high and low magnetic susceptibility values (Fig. 5f). Indeed, according to Tudryn et al. (2021), the low

magnetic susceptibility values after 29.9 and before ca 26.0 cal kBP are due to the small amounts of magnetite that underwent partial dissolution during bacterial reduction under anoxic conditions in the sediments after deposition while elsewhere, magnetite remains in oxic environments and is thus not dissolved (Fig. 5f). The presence of both iron sulfides and an anoxic environment at the water-sediment interface or in the sediment coincides with an increase in sulfur but this coincidence is only confirmed after further analyses (*e.g.*, X-Ray diffractometry or magnetism) and not just when sulfur is compared to magnetic susceptibility or iron XRF CS pattern that reflects mainly detrital iron-bearing silicates and oxides (Fig. 5e, 5f, Fig. 3c). Additionally, XRF CS analyses reveal another element that correlates well with sulfur and with iron sulfides: arsenic. Indeed, arsenic contents that are generally close to the detection limit of XRF analyses and are often therefore not investigated, show values clearly distinct from the XRF background and in relation to sulfur and iron contents (Fig. 5e, 5f, 5g).

Arsenic and iron sulfides

Arsenic is a toxic element and its presence in sediments, groundwater and surface water results from its mobilization from As-containing rocks by both natural processes and anthropogenic activities. Smedley and Kinniburgh (2002) proposed a detailed review of As sources, behavior and distribution. Mine-wastes, floodplain deposits, peat soils, lake and sea sediments can be As-contaminated (Kulp et al., 2006; Le Pape et al., 2017). Since iron sulfide minerals have a high capability to adsorb or co-precipitate arsenic during bacterial sulfate-reducing early diagenesis in anoxic sediment or sediment-water interface, iron sulfides (pyrite, greigite) represent a major host for As, and arsenic sulfide (arsenopyrite, FeAsS, realgar, As_4S_4) can also precipitate (Rodriguez‐Freire et al., 2016; Le Pape et al., 2017). Natural and anthropogenic enrichment in arsenic, often related to iron sulfides, is known in hypersaline lakes as Lake Urmia and from organic-rich sediments. A seasonal hypersaline Lake Maharlu (Southwestern Iran) receives wastewater of various types produced in the basin through seasonal rivers that drain the lake's catchment (Khosravi et al., 2019). According to these authors, dissolved As concentrations at the sediment–water interface are mainly controlled by evaporation, by interactions between the lake water and shallow sediment pore water, and by redox processes

allowing Fe and As sulfide precipitation within the first cm of lake sediments. Hypersaline Lakes Mono and Searles (California) contain naturally high concentrations in dissolved arsenic originating from volcanic rocks, these concentrations having been studied for bacterial respiratory reduction of arsenate and sulfate (Kulp et al., 2006). The results showed that (i) reduction can occur in anoxic water and sediment, and (ii) the strongest reduction occurred in surface sediments, gradually decreasing with burial to undetectable levels. Anoxic conditions in organic-rich environments that favor arsenic immobilization through arsenic-iron sulfides associations are well known in continental and marine sediments. Indeed, As-rich sulfides have been reported, for example, in Holocene Mediterranean sapropel units (Thomson et al., 2006) and in the Pleistocene Hetao paleolake Basin (North China) that started to shrink due to climate change in the early Late Pleistocene (ca 120 kyr) and became a salt marsh both rich in organic matter and in As-Fe sulfide association (Wang et al., 2021).

According to these results, the increase in As and Fe sulfides precipitation occurs in anoxic bottom and top lake sediments and therefore, when present in the top of the sedimentary sequence, they can be identified as pollution of anthropogenic origin (Croudace et al., 2019). In Lake Urmia, high contents of iron sulfides and arsenic are highlighted on Fig. 5e, 5f and 5g. In addition, arsenopyrite is identified in the sample dated at ca 4.4 cal kBP for which Tudryn et al. (2021) demonstrated the presence of greigite and pyrite by X-ray diffraction analysis (Fig. 6). These minerals are recorded in ancient sediments, and are therefore of natural rather than anthropogenic origin. As-XRF CS high values thus show natural processes evidencing clearly anoxic conditions both (i) in lake bottom sediments during high lake water levels that settled just after 29.9 and up to 22.0 cal kBP and from ca 12 to just before 5.5 cal kBP, and (ii) in organic-rich levels that have been identified as high biological productivity salt marshes developed at the coring site during the lake low stands at 29.9 and 5.5 cal kBP (Tudryn et al., 2021).

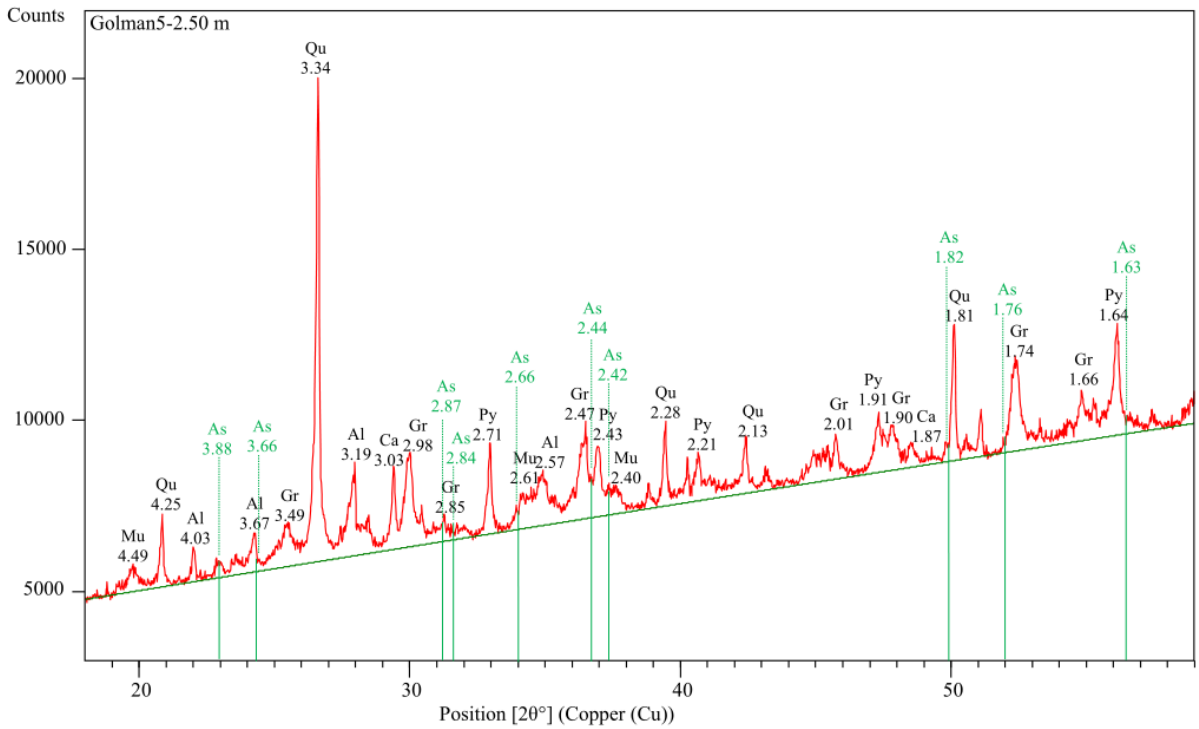

Fig. 6. *X-ray diffraction pattern obtained for magnetic extract from core Golman 5 at 2.50 m depth with mean identified minerals: arsenopyrite (As), which is highlighted by vertical green lines, greigite (Gr), albite (Al), calcite (Ca), chlorite (Ch), muscovite (Mu), pyrite (Py), quartz (Qu). After Tudryn et al. (2021).*

4.5.3. Which implications at the regional scale?

On the lake basin scale to a more regional Middle East scale, the data from Lake Urmia fill an important gap in the paleoclimatic records. Indeed, existing lake records are often discontinuous or very short, or on very large time scale with relatively low resolutions. They include records for Lake Urmia (Kelts and Shahrabi, 1986; Djamali et al., 2008a; Djamali et al., 2008b; Stevens et al., 2012; Talebi et al., 2016), Lake Zeribar south of Lake Urmia (Wasylikowa et al., 2006) and Anatolian lakes such as Van, Gölhisar, Eski Acigöl, Nar, Burdur (Roberts et al., 2001; Jones et al., 2006; Jones et al., 2007; Roberts et al., 2008; Turner et al., 2008; Kuzucuoğlu et al., 2010; Tudryn et al., 2013; Ön et al., 2018). The XRF CS data that are available for Lakes Van and Neor as well as for the Black Sea partially or totally cover the last 30 cal kBP (Fig. 7). In Lake Van, two independently obtained ln(Ca/K) and ln(Ca/Fe) records exhibit a relationship between authigenic carbonate precipitation and siliciclastic material input from the drainage basin (Çağatay et al., 2014; Kwiecien et al., 2014).

Higher ln(Ca/K) and ln(Ca/Fe) values (Fig. 7c, 7d) have been attributed to higher amounts of authigenic carbonate during warm and wet periods characterized in the catchment by the presence of a dense vegetation cover which would reduce erosion rates. On the opposite, lower ln(Ca/K) and ln(Ca/Fe) values have been related to both increased detrital input, cold and dry climate and evaporative regression of the lake level. Lake's Neor peripheral peat data for the last 13000 cal kBP (Sharifi et al., 2015) indicate that the transition occurred from dry and dusty conditions during the Younger Dryas to a relatively wetter period with low aeolian input during the Early Holocene (Fig. 7a). This period was followed by relatively drier and dustier conditions, with the prevalence of numerous episodes of strong aeolian input spanning a few decades to millennia, during the Middle to Late Holocene. Finally, according to many authors, the variability in the XRF-Ca profiles and carbonate contents in the Black Sea sediments (Fig. 7e) represent a record of the variability of productivity in Black Sea "Lake" surface waters in relation with climate change (Major et al., 2002; Bahr et al., 2005; Kwiecien et al., 2009; Soulet et al., 2011; Constantinescu et al., 2015). Indeed, from ca 30 to 15 cal kBP, an extremely reduced primary productivity and the detrital origin of carbonates have been recorded ((Major et al., 2002; Bahr et al., 2005; Kwiecien et al., 2009; Soulet et al., 2011). After that time, the Bølling–Allerød and Early Holocene warm oscillations have been geochemically characterized by remarkable maxima in XRF-Ca intensities and $CaCO_3$ content that is mainly composed of authigenic calcite (Major et al., 2002; Bahr et al., 2005; Soulet et al., 2011; Constantinescu et al., 2015; Tudryn et al., 2016) as it is also recorded in Lakes Van and Urmia. Such homogeneous changes recorded in Lakes Van and Urmia, in the Black Sea, as well as in other sites from the Middle East (Soulet et al., 2011; Çağatay et al., 2014; Kwiecien et al., 2014; Constantinescu et al., 2015; Pickarski et al., 2015; Sharifi et al., 2015) reflecting climate change as in the North Greenland ice core (Fig. 7f), provide evidence of the climate evolution in relation with the North Atlantic climatic system over the last 30 cal kBP.

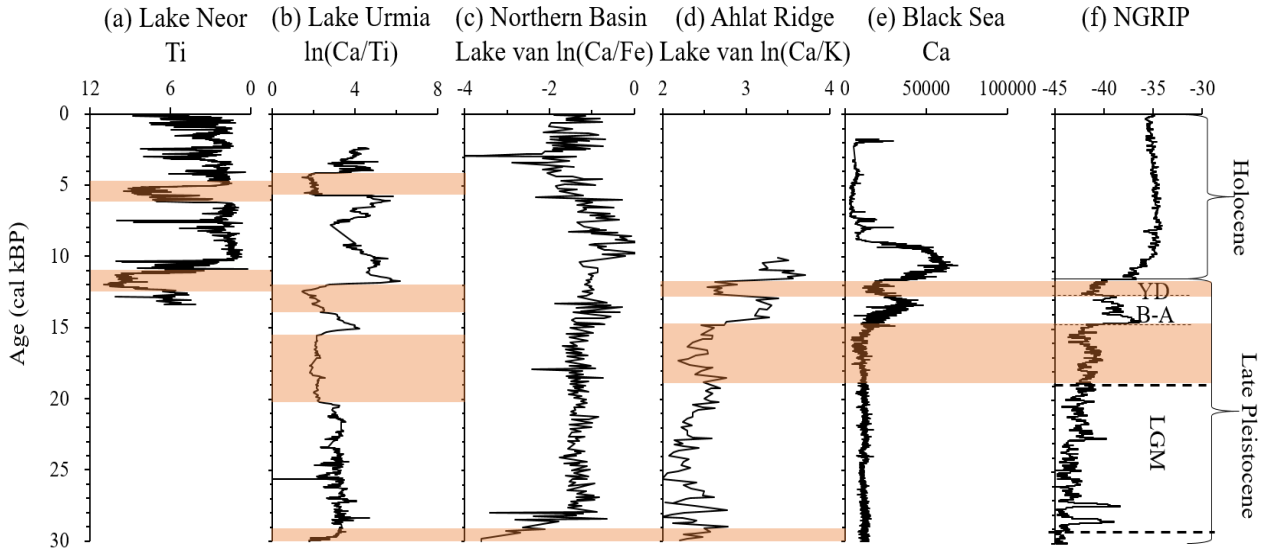

Fig. 7. *Comparison of elemental XRF CS profile of: (a) Ti in Lake Neor's peat (Sharifi et al., 2015); (b) ln(Ca/Ti) in Lake Urmia sediments; (c) ln(Ca/Fe) in North Basin sediments from Lake Van after Çağatay et al. (2014); (d) ln(Ca/K) in Ahlat Ridge sediments from Lake Van after Kwiecien et al. (2014) and Pickarski et al. (2015); (e) Ca in Black Sea sediments (Soulet et al., 2011; Constantinescu et al., 2015); (f) NGRIP curve (NGRIP, 2004).*

4.6. Conclusion

The results of the XRF elemental analyses of Lake Urmia sediments in combination with mineralogy, magnetic susceptibility and others sedimentological records, present a continuous 30 cal kBP record of the lake's evolution.

Superimposed to these results, XRF data on Lake Urmia deposits revealed the presence of arsenic of natural origin and in concentrations above background at the lake-sediment interface or in the first cm of sediments. Moreover, arsenic appears to be systematically associated with iron sulfides.

Both being of early diagenetic origin, they indicate anoxic conditions (i) in lake bottom sediments during high lake water levels after 29.9 and up to 22.0 cal kBP and from ca 12 to just before 5.5 cal kBP, and (ii) in organic-rich levels during the lake low stands at 29.9 and 5.5 cal kBP.

Our results have been compared to the evolution of other water bodies in the Middle East and we show that the environmental phases determined at Lake Urmia fit well into the evolution of the Anatolian sub-region, especially during the wet and dry spells of Bölling-Alleröd and Younger Dryas

respectively, as well as at the beginning of the Holocene Optimum.

Focusing on the interest of geochemical XRF SC analyses for reconstructions of past environments, all these data through elemental data and/or ratios, are clearly highly valuable for deciphering and defining the successive sedimentary and environmental phases in saline lake sediments, especially to precisely determine the periods of chemical or physical weathering. If present in the sediments even at levels slightly above background, specific elements such as arsenic can be revealed by XRF CS analyses. Although it is difficult to generalize this type of results from one lake basin to another, even with identical geological or hydrogeochemical characteristics, our results showed that As (i) can be an indicator of natural early diagenesis processes in lake bottom sediments, and (ii) is a more efficient marker to characterize sulfate-reducing anoxic environments than the detection of iron sulfides alone, by XRD and/or magnetic analyses. This insight on arsenic and iron sulfide, markers of early diagenesis at the time scale considered, suggests the possibility of highlighting short events of anoxic conditions, these events being of utmost importance for both paleoenvironmental reconstructions during the Late Quaternary and the present-day management of ecological resources.

Acknowledgement

This work was supported by the French-Iranian project Gundishapur, the Center for International Scientific Studies and Collaboration (CISSC, Iran), TelluS Program of CNRS/INSU and China Scholarship Council (CSC). We are very grateful to Aline Govin (Laboratoire des Sciences du Climat et de l'Environnement, CEA-CNRS-UVSQ, France) for fruitful discussions.

References

Ahmady-Birgani, H., Ravan, P., Schlosser, J.S., Cuevas-Robles, A., AzadiAghdam, M., Sorooshian, A., 2020. On the chemical nature of wet deposition over a major desiccated lake: Case study for Lake Urmia basin. Atmospheric Research 234, 104762.

Allen, M., Saville, C., Blanc, E.P., Talebian, M., Nissen, E., 2013. Orogenic plateau growth: Expansion of the Turkish‐Iranian Plateau across the Zagros fold‐and‐thrust belt. Tectonics

32, 171-190.

Asem, A., Eimanifar, A., van Stappen, G., Sun, S.C., 2019. The impact of one-decade ecological disturbance on genetic changes: a study on the brine shrimp Artemia urmiana from Urmia Lake, Iran. Peerj 7.

Aubert, C., Brisset, E., Djamali, M., Sharifi, A., Ponel, P., Gambin, B., Akbari Azirani, T., Guibal, F., Lahijani, H., Naderi Beni, A., 2017. Late glacial and early Holocene hydroclimate variability in northwest Iran (Talesh Mountains) inferred from chironomid and pollen analysis. Journal of Paleolimnology 58, 151-167.

Bahr, A., Lamy, F., Arz, H., Kuhlmann, H., Wefer, G., 2005. Late glacial to Holocene climate and sedimentation history in the NW Black Sea. Marine Geology 214, 309-322.

Berner, R.A., 1981. A new geochemical classification of sedimentary environments. Journal of Sedimentary Research 51, 359-365.

Böning, P., Bard, E., 2009. Millennial/centennial-scale thermocline ventilation changes in the Indian Ocean as reflected by aragonite preservation and geochemical variations in Arabian Sea sediments. Geochimica et Cosmochimica Acta 73, 6771-6788.

Brisset, E., Djamali, M., Bard, E., Borschneck, D., Gandouin, E., Garcia, M., Stevens, L., Tachikawa, K., 2018. Late Holocene hydrology of Lake Maharlou, southwest Iran, inferred from high-resolution sedimentological and geochemical analyses. Journal of Paleolimnology 61, 111-128.

Çağatay, M.N., Öğretmen, N., Damcı, E., Stockhecke, M., Sancar, Ü., Eriş, K.K., Özeren, S., 2014. Lake level and climate records of the last 90ka from the Northern Basin of Lake Van, eastern Turkey. Quaternary Science Reviews 104, 97-116.

Chaudhari, S., Felfelani, F., Shin, S., Pokhrel, Y., 2018. Climate and anthropogenic contributions to the desiccation of the second largest saline lake in the twentieth century. Journal of Hydrology 560, 342-353.

Chéron, S., Etoubleau, J., Bayon, G., Garziglia, S. and Boissier, A., 2016. Focus on sulfur count rates along marine sediment cores acquired by XRF Core Scanner. X‐Ray Spectrometry 45, 288-298.

Clement, A.C., Peterson, L.C., 2008. Mechanisms of abrupt climate change of the last glacial period. Reviews of Geophysics 46.

Constantinescu, A., Toucanne, S., Dennielou, B., Jorry, S., Mulder, T., Lericolais, 2015. Evolution of the Danube deep-sea fan since the last glacial maximum: new insights into Black Sea water-level fluctuations. Marine Geology 367, 50-68.

Croudace, I.W., Rothwell, R.G., 2015. Micro-XRF Studies of Sediment Cores: Applications of a non-destructive tool for the environmental sciences, 17. Springer.

Croudace, I.W., Teasdale, P.A., Cundy, A.B., 2019. 200-year industrial archaeological record preserved in an Isle of Man saltmarsh sediment sequence: Geochemical and radiochronological evidence. Quaternary International 514, 195-203.

Curtis, C., 1987. Mineralogical consequences of organic matter degradation in sediments: inorganic/organic diagenesis, Marine clastic sedimentology. Springer, pp. 108-123.

Davies, S.J., Lamb, H.F., Roberts, S.J., 2015. Micro-XRF Core Scanning in Palaeolimnology: Recent Developments, Micro-XRF Studies of Sediment Cores. Developments in Paleoenvironmental Research, pp. 189-226.

Djamali, M., de Beaulieu, J.-L., Shah-hosseini, M., Andrieu-Ponel, V., Ponel, P., Amini, A., Akhani, H., Leroy, S.A.G., Stevens, L., Lahijani, H., Brewer, S., 2008a. A late Pleistocene long pollen record from Lake Urmia, Nw Iran. Quaternary Research 69, 413-420.

Djamali, M., Kürschner, H., Akhani, H., de Beaulieu, J.L., Amini, A., Andrieu-Ponel, V., Ponel, P., Stevens, L., 2008b. Palaeoecological significance of the spores of the liverwort Riella (Riellaceae) in a late Pleistocene long pollen record from the hypersaline Lake Urmia, NW Iran. Review of Palaeobotany and Palynology 152, 66-73.

Evans, G., Augustinus, P., Gadd, P., Zawadzki, A., Ditchfield, A., 2019. A multi-proxy μ-XRF inferred lake sediment record of environmental change spanning the last ca. 2230 years from Lake Kanono, Northland, New Zealand. Quaternary Science Reviews 225, 106000.

Guo, F., Clemens, S., Liu, X., Long, Y., Li, D., Tan, L., Liu, C., Yan, H., Sun, Y., 2021. Application of XRF scanning to different geological archives. Earth and Space Science 8, e2020EA001589.

Hennekam, R., Sweere, T., Tjallingii, R., de Lange, G.J., Reichart, G.-J., 2019. Trace metal analysis of sediment cores using a novel X-ray fluorescence core scanning method. Quaternary International 514, 55-67.

Jelinowska, A., Tucholka, P., Gasse, F., Fontes, J.-C., 1995. Mineral magnetic record of environment in late Pleistocene and Holocene sediments, Lake Manas, Xinjiang, China. Geophysical Research Letters 22, 953-956.

Jones, M.D., Roberts, C.N., Leng, M.J., 2007. Quantifying climatic change through the last glacial–interglacial transition based on lake isotope palaeohydrology from central Turkey. Quaternary Research 67, 463-473.

Jones, M.D., Roberts, C.N., Leng, M.J., Türkeş, M., 2006. A high-resolution late Holocene lake isotope record from Turkey and links to North Atlantic and monsoon climate. Geology 34, 361-364.

Kelts, K., Shahrabi, M., 1986. Holocene sedimentology of hypersaline Lake Urmia, northwestern Iran. Palaeogeography, Palaeoclimatology, Palaeoecology 54, 105-130.

Khazaei, B., Khatami, S., Alemohammad, S.H., Rashidi, L., Wu, C., Madani, K., Kalantari, Z., Destouni, G., Aghakouchak, A., 2019. Climatic or regionally induced by humans? Tracing hydro-climatic and land-use changes to better understand the Lake Urmia tragedy. Journal of Hydrology 569, 203-217.

Khosravi, R., Zarei, M., Sracek, O., Bigalke, M., 2019. Geochemical and hydrological controls of arsenic concentrations across the sediment–water interface at Maharlu Lake, Southern Iran. Applied geochemistry 102, 88-101.

Kong, T., Tudryn, A., Gibert-Brunet, E., Tucholka, P., Motavalli-Anbaran, S-H., Ahmady-Birgani, H., Lankarani, M., Miska, S., Noret, A., Dufaure, O., 2022. 30,000 years of the southwestern Lake Urmia (Iran) evolution inferred from mineralogical indicators. Journal of Asian Earth Sciences, 105387.

Kulp, T., Hoeft, S., Miller, L., Saltikov, C., Murphy, J., Han, S., Lanoil, B., Oremland, R., 2006. Dissimilatory arsenate and sulfate reduction in sediments of two hypersaline, arsenic-rich soda lakes: Mono and Searles Lakes, California. Applied and environmental microbiology 72, 6514-6526.

Kuzucuoğlu, C., Christol, A., Mouralis, D., Doğu, A.F., Akköprü, E., Fort, M., Brunstein, D., Zorer, H., Fontugne, M., Karabiyikoğlu, M., 2010. Formation of the upper pleistocene terraces of Lake Van (Turkey). Journal of Quaternary Science 25, 1124-1137.

Kwiecien, O., Arz, H.W., Lamy, F., Plessen, B., Bahr, A., Haug, G.H., 2009. North Atlantic control on precipitation pattern in the eastern Mediterranean/Black Sea region during the last glacial. Quaternary Research 71, 375-384.

Kwiecien, O., Stockhecke, M., Pickarski, N., Heumann, G., Litt, T., Sturm, M., Anselmetti, F., Kipfer, R., Haug, G.H., 2014. Dynamics of the last four glacial terminations recorded in Lake Van, Turkey. Quaternary Science Reviews 104, 42-52.

Kylander, M.E., Ampel, L., Wohlfarth, B., Veres, D., 2011. High-resolution X-ray fluorescence core scanning analysis of Les Echets (France) sedimentary sequence: new insights from chemical proxies. Journal of Quaternary Science 26, 109-117.

Le Pape, P., Battaglia-Brunet, F., Parmentier, M., Joulian, C., Gassaud, C., Fernandez-Rojo, L., Guigner, J.-M., Ikogou, M., Stetten, L., Olivi, L., 2017. Complete removal of arsenic and zinc from a heavily contaminated acid mine drainage via an indigenous SRB consortium. Journal of Hazardous Materials 321, 764-772.

Löwemark, L., Chen, H.F., Yang, T.N., Kylander, M., Yu, E.F., Hsu, Y.W., Lee, T.Q., Song, S.R., Jarvis, S., 2011. Normalizing XRF-scanner data: a cautionary note on the interpretation of high-resolution records from organic-rich lakes. Journal of Asian Earth Sciences 40, 1250-1256.

Major, C., Ryan, W., Lericolais, G., Hajdas, I., 2002. Constraints on Black Sea outflow to the Sea of Marmara during the last glacial–interglacial transition. Marine Geology 190, 19-34.

Migowski, C., Stein, M., Prasad, S., Negendank, J.F., Agnon, A., 2006. Holocene climate variability and cultural evolution in the Near East from the Dead Sea sedimentary record. Quaternary Research 66, 421-431.

Neugebauer, I., Schwab, M., Waldmann, N.D., Tjallingii, R., Frank, U., Hadzhiivanova, E., Naumann, R., Taha, N., Agnon, A., Enzel, Y., 2016. Hydroclimatic variability in the Levant during the early last glacial (∼ 117–75 ka) derived from micro-facies analyses of deep Dead Sea sediments. Climate of the Past 12, 75-90.

NGRIP, 2004. High-resolution record of Northern Hemisphere climate extending into the last interglacial period. Nature 431, 147-151.

Ön, Z.B., Akçer-Ön, S., Özeren, M.S., Eriş, K.K., Greaves, A.M., Çağatay, M.N., 2018. Climate proxies for the last 17.3 ka from Lake Hazar (Eastern Anatolia), extracted by independent component analysis of μ-XRF data. Quaternary International 486, 17-28.

Peinerud, E.K., 2000. Interpretation of Si concentrations in lake sediments: three case studies. Environmental Geology 40, 64-72.

Peti, L., Augustinus, P.C., 2022. Micro-XRF-inferred depositional history of the Orakei maar lake sediment sequence, Auckland, New Zealand. Journal of Paleolimnology 67, 327-344.

Pickarski, N., Kwiecien, O., Djamali, M., Litt, T., 2015. Vegetation and environmental changes during the last interglacial in eastern Anatolia (Turkey): a new high-resolution pollen record from Lake Van. Palaeogeography, Palaeoclimatology, Palaeoecology 435, 145-158.

Roberts, A.P., 1995. Magnetic properties of sedimentary greigite (Fe3S4). Earth and Planetary Science Letters 134, 227-236.

Roberts, N., Jones, M., Benkaddour, A., Eastwood, W., Filippi, M., Frogley, M., Lamb, H., Leng, M., Reed, J., Stein, M., 2008. Stable isotope records of Late Quaternary climate and hydrology from Mediterranean lakes: the ISOMED synthesis. Quaternary Science Reviews 27, 2426-2441.

Roberts, N., Reed, J., Leng, M., Kuzucuoğlu, C., Fontugne, M., Bertaux, J., Woldring, H., Bottema, S., Black, S., Hunt, E., 2001. The tempo of Holocene climatic change in the eastern Mediterranean region: new high-resolution crater-lake sediment data from central Turkey. The Holocene 11, 721-736.

Rodriguez‐Freire, L., Moore, S.E., Sierra‐Alvarez, R., Root, R.A., Chorover, J., Field, J.A., 2016. Arsenic remediation by formation of arsenic sulfide minerals in a continuous anaerobic bioreactor. Biotechnology and Bioengineering 113, 522-530.

Sharifi, A., Pourmand, A., Canuel, E.A., Ferer-Tyler, E., Peterson, L.C., Aichner, B., Feakins, S.J., Daryaee, T., Djamali, M., Beni, A.N., Lahijani, H.A.K., Swart, P.K., 2015. Abrupt climate variability since the last deglaciation based on a high-resolution, multi-proxy peat record from NW Iran: The hand that rocked the Cradle of Civilization? Lake Neor. Quaternary Science Reviews 123, 215-230.

Soulet, G., Ménot, G., Garreta, V., Rostek, F., Zaragosi, S., Lericolais, G., Bard, E., 2011. Black Sea "Lake" reservoir age evolution since the Last Glacial—Hydrologic and climatic implications. Earth and Planetary Science Letters 308, 245-258.

Stein, M., Starinsky, A., Katz, A., Goldstein, S.L., Machlus, M., Schramm, A., 1997. Strontium isotopic, chemical, and sedimentological evidence for the evolution of Lake Lisan and the Dead Sea. Geochimica et Cosmochimica Acta 61, 3975-3992.

Stevens, L.R., Djamali, M., Andrieu-Ponel, V., de Beaulieu, J.L., 2012. Hydroclimatic variations over the last two glacial/interglacial cycles at Lake Urmia, Iran. Journal of Paleolimnology 47, 645-660.

Talebi, T., Ramezani, E., Djamali, M., Lahijani, H.A.K., Naqinezhad, A., Alizadeh, K., Andrieu-Ponel, V., 2016. The Late-Holocene climate change, vegetation dynamics, lake-level changes and

anthropogenic impacts in the Lake Urmia region, NW Iran. Quaternary International 408, 40-51.

Thomson, J., Croudace, I., Rothwell, R., 2006. A geochemical application of the ITRAX scanner to a sediment core containing eastern Mediterranean sapropel units. Geological Society, London, Special Publications 267, 65-77.

Tourian, M., Elmi, O., Chen, Q., Devaraju, B., Roohi, S., Sneeuw, N., 2015. A spaceborne multisensor approach to monitor the desiccation of Lake Urmia in Iran. Remote Sensing of Environment 156, 349-360.

Tudryn, A., Leroy, S.A., Toucanne, S., Gibert-Brunet, E., Tucholka, P., Lavrushin, Y.A., Dufaure, O., Miska, S., Bayon, G., 2016. The Ponto-Caspian basin as a final trap for southeastern Scandinavian Ice-Sheet meltwater. Quaternary Science Reviews 148, 29-43.

Tudryn, A., Motavalli-Anbaran, S.H., Tucholka, P., Gibert-Brunet, E., Lankarani, M., Ahmady-Birgani, H., Kong, T., Noret, A., Miska, S., Massault, M., Dufaure, O., 2021. Late Quaternary environmental changes of Lake Urmia basin (NW Iran) inferred from sedimentological and magnetic records. Quaternary International 589, 83-94.

Tudryn, A., Tucholka, P., Gibert, E., Gasse, F., Wei, K., 2010. A late Pleistocene and Holocene mineral magnetic record from sediments of Lake Aibi, Dzungarian Basin, NW China. Journal of Paleolimnology 44, 109-121.

Tudryn, A., Tucholka, P., Özgûr, N., Gibert, E., Elitok, O., Kamaci, Z., Massault, M., Poisson, A., Platevoet, B., 2013. A 2300-year record of environmental change from SW Anatolia, Lake Burdur, Turkey. Journal of paleolimnology 49, 647-662.

Turner, R., Roberts, N., Jones, M., 2008. Climatic pacing of Mediterranean fire histories from lake sedimentary microcharcoal. Global and Planetary Change 63, 317-324.

Wang, H., Göttlicher, J., Byrne, J., Guo, H., Benning, L.G., Norra, S., 2021. Vertical redox zones of Fe–S–As coupled mineralogy in the sediments of Hetao Basin–Constraints for groundwater As contamination. Journal of Hazardous Materials 408, 124924.

Wasylikowa, K., Witkowski, A., Walanus, A., Hutorowicz, A., Alexandrowicz, S.W., Langer, J.J., 2006. Palaeolimnology of Lake Zeribar, Iran, and its climatic implications. Quaternary Research 66, 477-493.

Wei, G., Liu, Y., Li, X., Shao, L., Liang, X., 2003. Climatic impact on Al, K, Sc and Ti in marine sediments: evidence from ODP Site 1144, South China Sea. Geochemical Journal 37, 593-602.

Xie, X., Zheng, H.B., Qiao, P.J., 2014. Millennial climate changes since MIS 3 revealed by element records in deep-sea sediments from northern South China Sea. Chinese Science Bulletin 59, 776-784.

Xu, H., Liu, B., Wu, F., 2010. Spatial and temporal variations of Rb/Sr ratios of the bulk surface sediments in Lake Qinghai. Geochemical Transactions 11, 1-8.

Chapter 5: Stable isotopes of authigenic carbonates and organic matter for deciphering environmental conditions on Lake Urmia basin (NW Iran) and surrounding region during the Late Quaternary

This chapter focuses on isotope geochemistry of inorganic carbonates and organic matter. We present a two-step correction model for stable isotopes on carbonate that allows obtaining the real isotopic composition of the authigenic fraction in such saline environments as Lake Urmia is. Beyond the reconstruction of the paleoenvironmental evolution of the lake through these parameters and in combination with mineralogical records, this study will provide a new insight on the interpretation and validity of isotopic contents defined on bulk samples gathering at the same time information on the origin and nature of carbonates (authigenic/detrital, mixing of different carbonate species).

Stable isotopes of authigenic carbonates and organic matter for deciphering environmental conditions on Lake Urmia basin (NW Iran) and surrounding region during the Late Quaternary

Ting Kong [a], Elisabeth Gibert-Brunet [a, *], Alina Tudryn [a], Piotr Tucholka [b], Aurélie Noret [a], Seyed-Hani Motavalli-Anbaran [c], Mohammad Lankarani [d], Hesam Ahmady-Birgani [e], Serge Miska [a]

[a] University Paris-Saclay, CNRS, UMR 8148-GEOPS, 91405, Orsay, France

[b] Warsaw University, Department of Geology, Warsaw, Poland

[c] Institute of Geophysics, University of Tehran, Tehran, Iran

[d] School of Geology, University-College of Science, University of Tehran, Tehran, Iran

[e] Faculty of Natural Resources, Urmia University, Urmia, Iran

5.1. Introduction

Stable isotope contents of authigenic carbonates, of chemical or biogenic origin, are widely used to study and reconstruct paleoenvironmental phases deduced from various recorders, and in particular from lake basins, including in-lake processes and multiple pathways at the watershed scale (Kelts and Talbot, 1990; Aravena *et al.*, 1992; Fontes *et al.*, 1993; Fontes *et al.*, 1996; Valero-Garcés *et al.*, 1996; Gibert *et al.*, 1999; Gibert *et al.*, 2002; Lamb *et al.*, 2002; Zanchetta *et al.*, 2007; Develle *et al.*, 2010; McCormack *et al.*, 2019; Vystavna *et al.*, 2021). However, recent studies have highlighted the difficulty of validating these parameters when confronted with mixtures of carbonate compounds that may be, one by one, (i) authigenic or detrital, or (ii) early-diagenetic precipitates or completely recrystallized after burial. Superimposed on these processes, crystallization is subjected to different fractionation factors with respect to the crystalline phase involved that may have an impact on the stable isotopic contents (Roberts *et al.*, 2001; Çağatay *et al.*, 2014; Dean *et al.*, 2015; McCormack *et al.*, 2019).

Although dolomite is often considered as a detrital mineral, it can be of authigenic, early diagenetic and of fully diagenetic origins. As pointed out by McCormack et al. (2019), authigenic aragonite, calcite, and Mg-calcite when mixed with diagenetic minerals can compromise interpretations of lacustrine $\delta^{18}O$ and $\delta^{13}C$ signals obtained from bulk materials. In such a context, the global study of the lake and its watershed is of utmost importance to determine the system end-members (Fontes *et al.*, 1996) and to be able to access the initial parameters, these poles being able to be sedimentological and/or geochemical.

This paper focuses on stable isotope records of inorganic carbonates and organic matter from the salty Lake Urmia (northwestern Iran). Salt lakes have always been the subject of particular studies for a long time, notably because of the particularity of the geochemical processes that take place (Langbein, 1961). In saline environments with brackish water, the carbonate species that precipitate are usually aragonite or strongly magnesium calcite. Fractionation factors in this case are much greater than when carbonates precipitate from freshwater lakes: -0.6‰ and +3 ‰ relative to calcite for aragonite and dolomite, respectively (Tarutani *et al.*, 1969; Land, 1980; Clark and Fritz, 1997).

Recent climate change and continued human needs have shown that inland water bodies are highly sensitive to water storage changes in response to declining precipitation and enhancing evaporation particularly in Central Asia, the Middle East, and North Africa, where the loss of water storage is currently a factor of 2-4 higher than previous estimates (Wang *et al.*, 2018). Although the hydrological modifications of the water balance are still poorly understood, the response of closed basins can be reached through the study of (i) the modern reference hydrogeological system, and (ii) past sedimentary records that allow for reconstruction of present and past environmental fluctuations through specific multi-disciplinary parameters.

As a closed salty lake, Lake Urmia is part of these large water bodies whose large fluctuations in their water level and salinity are the global response to (i) changing precipitating air masses, (ii) changes in river discharge from neighboring mountains, (iii) variations in the precipitation-evaporation balance over the basin, and/or to a lesser extent except in specific areas (iv) tectonic or geomorphological events (Fontes *et al.*, 1993; Stevens *et al.*, 2012; McCormack *et al.*, 2019). As recently demonstrated by Vystavna et al. (2021) and whatever the climatic zone, the main constraints

on lake isotope composition and evaporation in arid zones are precipitation amount, parameters at the catchment scale -limnicity and free water surface, wind speed, relative humidity, and the solar radiation. Beyond the dynamics of precipitating air masses that are particularly specific to northern Iran, the geomorphological and hydrological parameters of the Urmia basin are of significant importance in understanding the evolution of the lake.

Initiated in 2016-2017, our Lake Urmia Project brought results for last 30 kBP lake history and highlighted that the maximum lake extent is between ~29.9 and 20.2 kBP, while major regressive periods but lasting only a few centuries are recorded at ~20.2, ~13.3 and ~5.6 kBP. Warmer and wetter conditions prevailed in the Lake Urmia basin during the Bølling/Allerød oscillation of the latest Pleistocene, and during the early and middle Holocene, with three major wet pulses at ~15.3, ~11.8 and ~4.1 kBP (Tudryn *et al.*, 2021; Kong *et al.*, 2022).

As an important part of our project, this paper described the stable isotope data obtained on inorganic carbonates and on organic fractions from Lake Urmia cored sequences and from the catchment sediments and in a detailed ^{14}C timescale (Kong *et al.*, 2022). The significance of these isotopic chronicles is discussed in a geochemical approach considering the carbon poles on the catchment and the related corrections to be applied, and then compared to regional records.

5.2. Site description

Lake Urmia, located in the northwestern Iran at an altitude of about 1270 m above sea level, was the second largest endorheic saline lake before its drop that started at 1995, just after the Caspian Sea in Western Asia (Fig. 1a). The geological setting of the lake is quite diverse with a drainage basin that is comprised of a variety of rock formations of various ages, ranging from the Precambrian metamorphic complexes to carbonated formations and to Quaternary mud deposits (Tudryn *et al.*, 2021; Kong *et al.*, 2022). At the catchment scale, the closed Lake Urmia is fed by both direct precipitation and river inflows, the latter including nine major tributaries: Zarineh Rud, Gader Chay, Baranduz Chay, Nazlu Chay, Mahabad Chay, Simineh Rud, Aji Chay, Shahar Chay and Zola Chay shown in Fig. 1b (Sharifi *et al.*, 2018). All the sedimentary materials from the catchment area are

mainly transported by rivers and deposited by gravity, although aeolian deposits may occur during the most arid periods such as these last decades with the aridification of the region.

The climate of Urmia region is governed by complex interactions implying mid-latitude Westerlies in the west, the Siberian Anticyclone in the north and east, and the Indian Ocean Summer Monsoon in the south. However, both the Mediterranean Sea and Atlantic Ocean are the predominant sources of precipitations in Iran through cyclonic disturbances transmitted by the polar front toward the east (Taha *et al.*, 1981; Bartholy *et al.*, 2009) with a slight participation of vapor that originates from the Black and Caspian Seas in the north as well as from the Persian Gulf in the far south (Alijani and Harman, 1985).

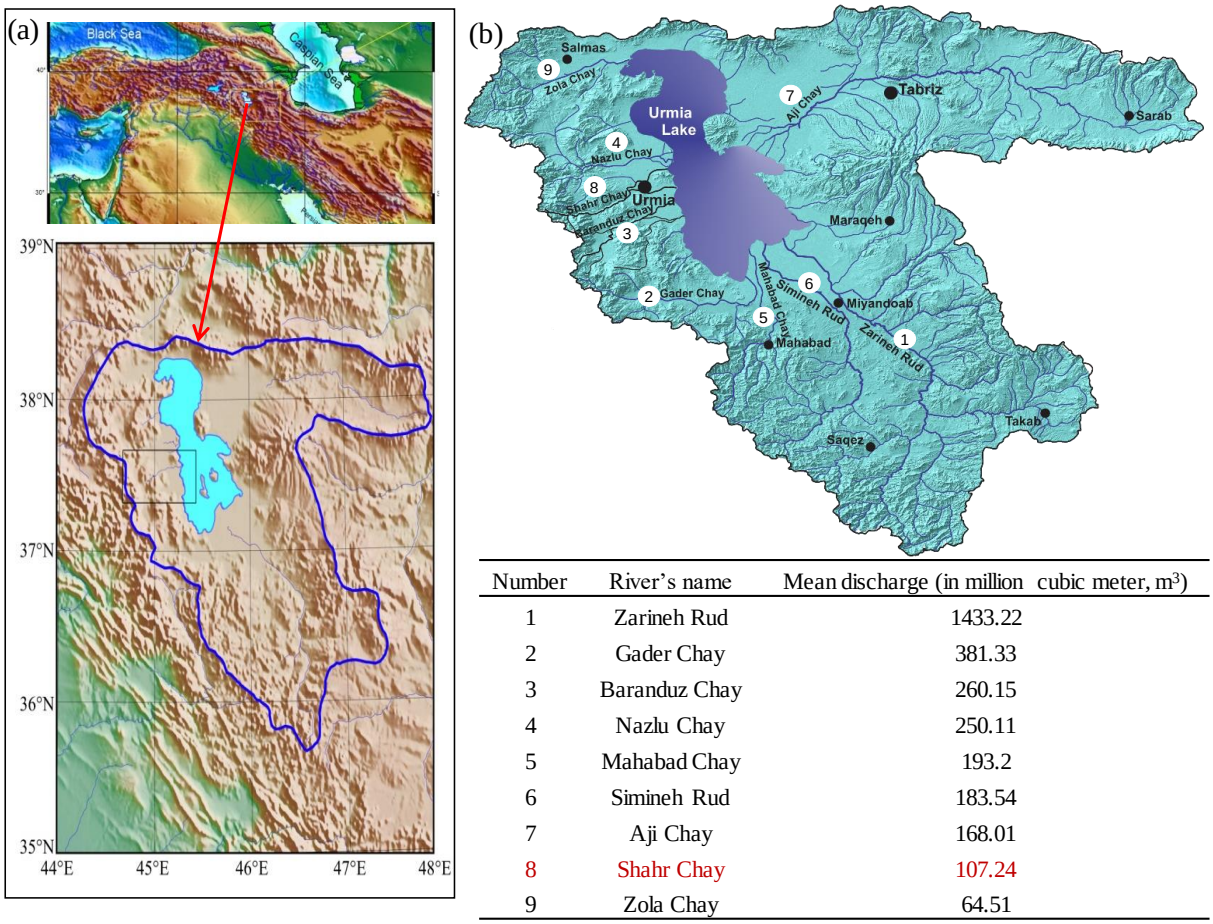

Number	River's name	Mean discharge (in million cubic meter, m^3)
1	Zarineh Rud	1433.22
2	Gader Chay	381.33
3	Baranduz Chay	260.15
4	Nazlu Chay	250.11
5	Mahabad Chay	193.2
6	Simineh Rud	183.54
7	Aji Chay	168.01
8	Shahr Chay	107.24
9	Zola Chay	64.51

Fig. 1. *Lake Urmia: (a) location of the lake and lake's catchment area, black rectangle indicates study area; (b) Urmia Lake watershed area, 9 major tributaries and their annual mean river discharge (in million cubic meters, m^3).*

5.3. Material and previous results

5.3.1. Sediment sampling

During the 2017 field campaign, very close sediment cores have been drilled out from recently dried out part of the lake near the city of Urmia and the modern hydrological system was constrained by surface and groundwater sampling and in situ measurements (Gibert-Brunet et al. submitted).

From the two longest sedimentary sequences, Golman 6 and Golman 7 of 8.0 m and 12.5 m depth, a reference profile was defined based on mineralogy and magnetic susceptibility (Tudryn *et al.*, 2021; Kong *et al.*, 2022). This 12.5-m composite core present successive sedimentary phases with silt and clay-silt particles distribution with transitions to sand or silty sand. Additionally, plant samples have been collected from the lake catchment close to the coring site.

In 2021, in order to find lake sediment sources of our cores, eight samples have been collected according to the main geological formations of the catchment area of the Shahr Chay River, which is the major supplier of detrital material into the lake at the coring location (Fig. 2a).

5.3.2. Previous mineralogical analyses: methods and results

Details of X-Ray diffractometry (XRD) on the bulk sediment samples from composite core and catchment area are presented in chapter 3, however, we recall them for clear data presentation. The mineralogical assemblages of both bulk samples and more specifically on the carbonate fraction have been performed though XRD analyses on a routine manner at the GEOPS laboratory via an X'Pert Pro PANalytical diffractometer, Cu- Kα1 source, 2Θ range 5-80°, 4 h runs, and by using both the PANalytical HighScore software with crystallography open database and ICDD PDF-4/Minerals database (Kong *et al.*, 2022). Specific carbonates are identified through mainly analyzing peaks with 2Θ range 24°-33° and the semi-quantification of the carbonate group was obtained by normalizing the areas of the main diffraction peaks of identified minerals (aragonite 3.39 Å; calcite 3.03 Å; Mg-calcite 2.99 Å; dolomite 2.88 Å). Owing to similar structure, these four carbonates overlap at the

same 2Theta (2Θ) position, resulting in untrue normalized area of each carbonate. In order to obtain the real percentage of carbonate in our samples, use carbonate standard samples (25% aragonite + 25% calcite + 25% Mg-calcite + 25% dolomite) were used to calculate the correlation coefficient of main peaks of aragonite, calcite, Mg-calcite and dolomite. Based on five times repeatable experiments, the correlation coefficient of aragonite, calcite, Mg-calcite and dolomite are 0.0309, 0.3542, 0.2530, 0.3618 respectively. Through correlation coefficient, the relative percentages of four carbonates are calculated.

The crystallinity of each carbonate species determined on the same spectra, corresponds to full width half maximum (FWHM) and is considered as a parameter reflecting the authenticity of carbonates (Fontes *et al.*, 1993; Fontes *et al.*, 1996). Indeed, a low crystallinity index, *i.e.* a thin main peak, will denote well-crystallized detrital carbonates, whereas less well-crystallized authigenic carbonates will show a high value of their crystallinity.

XRD analyses of samples from the catchment area indicate that the dominant minerals are quartz, feldspars, clays and carbonates (calcite and dolomite), present in varying proportions depending on the lithological units (Kong *et al.*, 2022). As presented in Table 1, these 8 samples display relatively low dolomite percentages, *i.e.*, from 5.8 to 18.5 % while calcite has higher propositions from 28.2 to 86.7. Crystallinity indexes display values for both calcite and dolomite from 0.08 to a maximum of 0.12.

Data obtained for the composite core highlight an alternation of detrital and authigenic origin of minerals. The sediment is mainly composed of quartz, clays and feldspars originating from the Shahr Chay watershed but also carbonates whose composition is a mixing between the 3 major calcareous phases: aragonite, calcite and dolomite, as well as sulfates and sulfides (gypsum, iron sulfides, arsenic and iron sulfides; Tudryn et al., 2021; Kong et al., 2022). Authigenic aragonite and a mixture of calcite and dolomite are encountered in specific levels (Fig. 2b). As developed in Kong et al. (2022), these two latter carbonates may be detrital and/or authigenic. Only crystallinity then allows the origin of these carbonate fractions to be deciphered. Indeed, the crystallinity values obtained for the watershed carbonates, calcite and dolomite, define the limit beyond which these two species can be considered authentic. These data will allow us to correct the stable isotope content measured on the

bulk samples of the composite core, in relation to the respective percentages of the 3 carbonate species encountered.

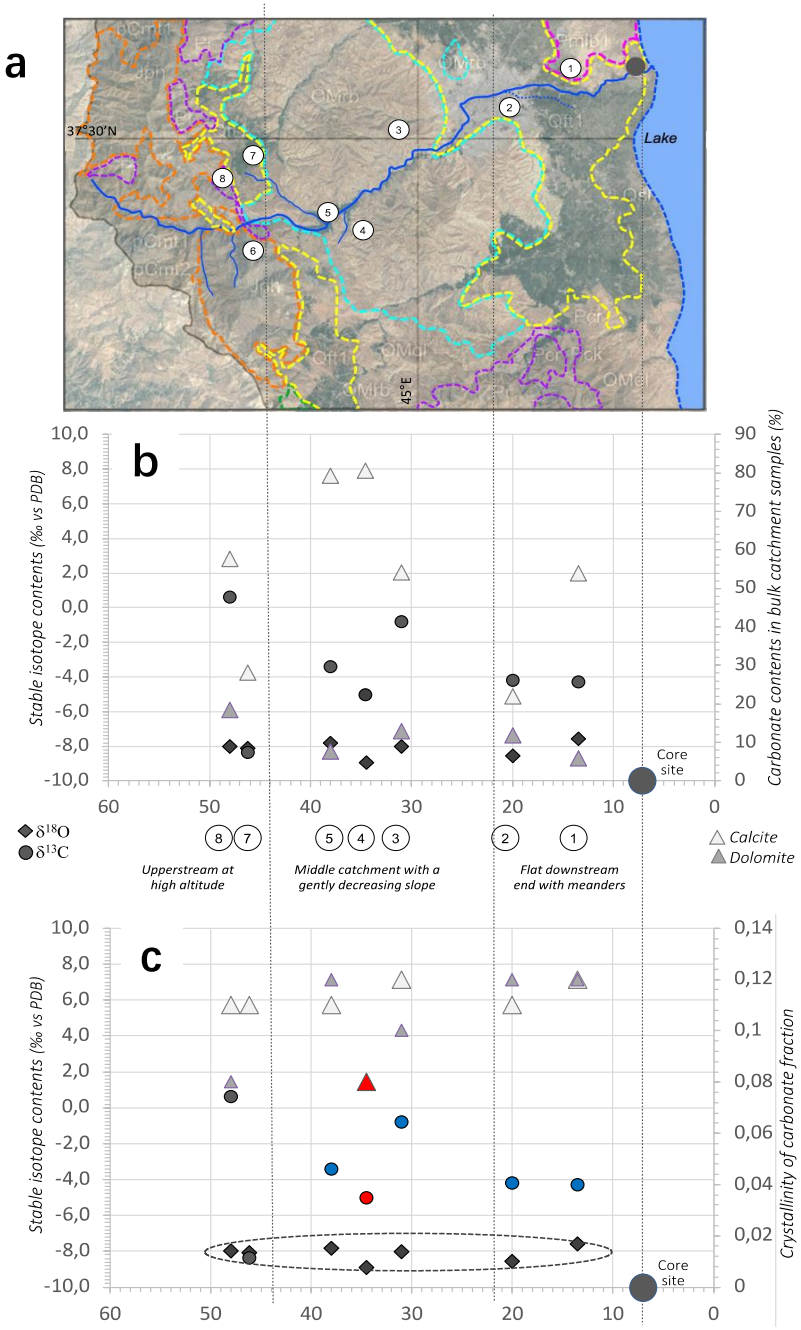

Fig. 2. *(a) Geological formation and related sample locations on the Shahr Chay River catchment as well as location of the coring site;(b) $\delta^{13}C/\delta^{18}O$ values and carbonate species percentages of the catchment samples according the Shahr Chay River flow line; (c) $\delta^{13}C/\delta^{18}O$ values and crystallinity of carbonate species of the catchment samples along the Shahr Chay River flow line.*

Table 1 *Mineralogical composition of the carbonate fraction and isotopic contents of catchment samples (see Fig. 2 for samples location).*

Sample Number	Distance to lake shore (km)	Carbonates in bulk sediment (%)	Calcite in bulk sediment (%)	Calcite crystallinity	Dolomite in bulk sediment (%)	Dolomite crystallinity	$\delta^{18}O$ (‰ vs VPDB)	$\delta^{13}C$ (‰ vs VPDB)
lake	0							
1	13.5	59.7	53.9	0.12	5.8	0.12	-7.6	-4.3
2	20	33.8	22	0.11	11.8	0.12	-8.55	-4.22
3	31	67.1	54.2	0.12	12.9	0.1	-8.04	-0.83
4	34.5	80.4	80.4	0.08	-	-	-8.93	-5.06
5	38	86.8	79.3	0.11	7.5	0.12	-7.84	-3.43
6	46	-	-	-	-	-	-	-
7	46.2	28.2	28.2	0.11	-	-	-8.1	-8.37
8	48	76.2	57.7	0.11	18.5	0.08	-8	0.61

5.4. Methods

5.4.1. Stable isotopes on inorganic carbonates

Samples for measurements of carbon and oxygen stable isotope ratios on bulk carbonates from both catchment and lake sediment samples were carried out using standard analytical procedures at the GEOPS laboratory. Prior to stable isotope measurements, carbonate contents were parallelly determined by XRD and measurements with the Mélières mono-calcimeter (Tudryn *et al.*, 2021). Although the values compared are slightly different due to either a small fraction of non-crystalline material or incomplete reaction of dolomite when present, the carbonate contents vary from about 10 to 70%. This then allows the weighting of a precise fraction of sediment corresponding to the 100 µg of carbonate required for analysis, *i.e.*, for each sample in the composite sequence, from 140 to 1000 µg (0.14-1.00 mg).

The CO_2 from carbonate samples was generated by reaction under vacuum with 100% phosphoric acid in individual inverted y-tube vials at 25 °C to avoid the risk of cross-contamination from one sample to the other through an automated carbonate preparation system, which is connected on-line to the isotope ratio mass spectrometer. The reaction was carried out in a water bath at 25 °C for 24 hours. A particular attention was paid to the completion of the reaction, *i.e.* the full dissolution of all

the carbonated species, especially for dolomite which is slower and more difficult to solubilize than calcite for a given grain size and crystallinity (Epstein *et al.*, 1964; Al-Aasm *et al.*, 1990).

Samples were then measured on a Finnigan Mat MS-252 mass spectrometer at the LSCE laboratory (Gif sur Yvette, France). Both stable isotopes (^{13}C and ^{18}O) were calibrated by two international standards (IAEA-CO8 and NBS-19) and an internal standard after the background was removed from an internal standard of LSCE. The isotopic composition is reported in the conventional scale in ‰ vs VPDB with reference to the international standard Vienna-*Belemnitella americana* from the Peedee formation of North Carolina (USA).

5.4.2. Stable isotopes on organic matter

Plant samples collected in the vicinity of today's lake level as well as sediment samples taken directly during the core opening, were stored in cold room, and then were subjected to the standard GEOPS laboratory chemical protocol for stable isotopes measurements, *i.e.,* acid (HCl 10%)-alkali (NaOH 10%)-acid (HCl 10%) successive treatments at room temperature in order to remove the carbonate fraction and humic acids. In between each step, sample were washed with deionized water up to neutral pH.

After drying-up at 60 °C overnight, samples were mechanically crushed into homogenized power, weighted and encapsulated into a tin capsule then placed inside the 32-position tray of the MAS 200R autosampler. Based on repeated measurements, the calibration of the elemental and isotopic values for both carbon and nitrogen was made by analyzing 3 international standards (USGS-40 and IAEA-600, and an in-lab working standard GG-IPG) that allow for the definition of linear regression equations whom blank subtraction followed linearity tests. The Carbon (%), Nitrogen (%) and stable isotope analyses were conducted on an Elemental Analyser (EA, Thermo Scientific Flash HT plus) coupled with Isotope Ratio Mass Spectrometry (IRMS, Thermo Scientific Delta V Advantage) under continuous flow mode at the GEOPS laboratory (Orsay, France).

Results are expressed in standard δ notation (%) relative to the Vienna Pee Dee Belemnite (VPDB) (Coplen, 1995), and nitrogen values are reported with respect to atmospheric nitrogen (AIR) for

carbon and nitrogen isotope values respectively. Analytical precision is ±0.8% for $\delta^{15}N$ and ±0.4% for $\delta^{13}C$. C/N ratios are expressed as weight percent.

5.5. Results

5.5.1. The carbonate fraction and the two-step correction model

The isotope data from the catchment area present values from -7.60 to -8.93 for $\delta^{18}O_{carb}$ and varying values between 0.61 and -8.37 for $\delta^{13}C_{carb}$ (Table 1; Fig. 2b and 2c). These data from the sediment core roughly display values from -4.49‰ and 1.30‰, with an average of -1.39‰, and between -8.37‰ and -0.18‰, with an average of -3.19‰, for $\delta^{18}O_{carb}$ and $\delta^{13}C_{carb}$ respectively (Fig. 3d and 3c).

Since Lake Urmia samples present a quite non-neglectable carbonate detrital fraction (Tudryn *et al.*, 2021; Kong *et al.*, 2022), we need to correct theses isotope values to reach the original isotopic record of authigenic carbonates.

The principle of the correction is based on the knowledge of the percentages of each of the carbonate fractions and their associated crystallinity determined by XRD analyses, as well as the mean isotopic composition of the carbonate species found in the geological formations of the watershed (Fig. 2c). The correction equations are therefore as follows:

$$\delta^{13}C_M = X*\delta^{13}C_{A\text{-}Carbonates} + \delta^{13}C_{D\text{-}Carbonates}*(1- X)$$

$$\delta^{18}O_M = X*\delta^{18}O_{A\text{-}Carbonates} + \delta^{18}O_{D\text{-}Carbonates}*(1- X)$$

with X, the fraction of authigenic carbonate in the carbonate phase; (1-X), the fraction of detrital carbonate in the carbonate phase; $\delta^{13}C_{A\text{-}Carbonates}$ and $\delta^{18}O_{A\text{-}Carbonates}$, isotopic composition for authigenic carbonates determined by XRD; $\delta^{13}C_{D\text{-}Carbonates}$ and $\delta^{18}O_{D\text{-}Carbonates}$, isotopic composition of detrital carbonates inferred from stable isotope values of catchment samples.

$$\delta^{13}C_{A\text{-}Carbonates}= [\delta^{13}C_M - \delta^{13}C_{D\text{-}Carbonates}*(1- X)]/X$$

$$\delta^{18}O_{A\text{-}Carbonates}= [\delta^{18}O_M - \delta^{18}O_{D\text{-}Carbonates}*(1-X)]/X$$

Authigenic carbonates in the composite core: previous studies have shown that aragonite is always authigenic and occurs as *Artemia* shrimp fecal pellets and/or calcareous mud (Kelts and Talbot, 1990; Djamali *et al.*, 2010; Kong *et al.*, 2022) whereas calcite and dolomite can have either detrital or authigenic origin. The determination of the authigeny of the carbonate fraction is essential for the correction of stable isotope contents. The crystallinity index is a valuable parameter that allows this discrimination knowing that calcite and dolomite are detrital and therefore well crystallized, when they have low crystallinity indices (Fontes *et al.*, 1993; Fontes *et al.*, 1996). Crystallinity indices obtained for calcite and dolomite in samples from the Lake Urmia watershed show crystallinities of 0.08 to 0.12 for both detrital carbonate species. All calcite and dolomite fractions with IC values above 0.12 will be therefore considered as authigenic in the composite core samples.

Carbon-13 composition for detrital carbonates: the $\delta^{13}C$ value of detrital carbonates is quite difficult to attempt since there are several parameters have to be taken into account. As shown in Fig. 2b, samples 4 and 7 from the watershed contain only calcite and the related $\delta^{13}C$ values, although very different, could be considered as those of detrital calcites from different parts of the watershed. Although this solution could be unfortunately very complex to implement and would require an independent marker to differentiate the exact origin of the detrital fraction on the watershed, we can argue that the geological formation of sample 7 seems to less impact the load of the Shahr Chay River main stream (low carbonate content). As a consequence, sample 4 located in the middle catchment where the slope gently decreasing to the lake suggests higher erosional processes is considered as the most interesting reference. On another hand, all other samples show $\delta^{13}C$ enrichment with the presence of dolomite, even in small amounts (Fig. 3b), also highlighting that the higher the crystallinity of the dolomite, the lower the $\delta^{13}C$ values. Considering all these points, the mean isotopic composition of -3.65 ‰ calculated from samples 1 to 5 is chosen for the $\delta^{13}C$ values of detrital carbonates.

Oxygen-18 composition for the catchment samples: except for sample 6 which is $CaCO_3$-free, the $\delta^{18}O$ compositions of both calcite and dolomite in the catchment samples are plotted around the single value of -8.15 ‰ (n=7) whatever the carbonate composition of the samples and with a very low standard deviation (-0.5/+0.8 ‰). This value will be used as the $\delta^{18}O$ content for detrital carbonate

fraction.

In order to disentangle and interpret the isotopic contents of the authigenic carbonate fractions, an additional correction must be considered, namely that corresponding to the ^{18}O fractionation factor of +3‰ for dolomite relatively to calcite (Land, 1980; Clark and Fritz, 1997; Roberts *et al.*, 2001). When in high concentration, early-diagenetic/authigenic dolomite can really affect the isotope contents by inducing higher $\delta^{18}O$ values especially for bulk samples records (Roberts *et al.*, 2001; Çağatay *et al.*, 2014; McCormack *et al.*, 2019). Some authors subtracted this +3 ‰ ^{18}O-fractionation factor from the isotopic contents of bulk samples proportionally to their dolomite amounts in the carbonate fraction (*e.g.*, Roberts et al., 2001). Considering that dolomite percentages in the Lake Urmia composite core are comprised from 1 up to almost 74 % within the carbonate fraction, the deviation for $\delta^{18}O$ values ranges from a minimum of 0.03 ‰ to a maximum of 2.2 ‰ vs VPDB. Because the latter content cannot be considered negligible, the ^{18}O data must incorporate this second correction (Fig. 2). Variations in ^{18}O contents are exacerbated by this second correction and are much better defined as in particular the Bölling-Alleröd and Younger Dryas episodes identified by Kong et al. (2022) are much more visible. The maximum corrections of $\delta^{18}O$ value are taking place during the Younger Dryas phase, at around 14 cal kBP (Fig. 3).

Finally, the two-step correction of the $\delta^{13}C$ and $\delta^{18}O$ values of the bulk samples defines the true ^{18}O and ^{13}C contents of the authigenic carbonate fraction that will be referred to as $\delta^{13}C_A$ and $\delta^{18}O_A$ from now on, and which range from -4.5‰ to +1.6‰ and from -8.50‰ to +3.00‰ respectively. As shown on Fig. 3 (vs depth) and 4 (vs time), aragonite and dolomite abundances are in phase opposition along the sedimentary sequence. While aragonite contents and the Sr/Ca ratio determined by XRF are in phase, they are also in phase opposition with the Mg/Ca ratio (chapter 4). Knowing that carbonate precipitation follows a definite order, with aragonite first, then calcite and finally dolomite as the Mg/Ca ratio increases, the dolomite precipitation suggests an environment with a high evaporation/precipitation ratio and thus drier conditions with lake water concentration.

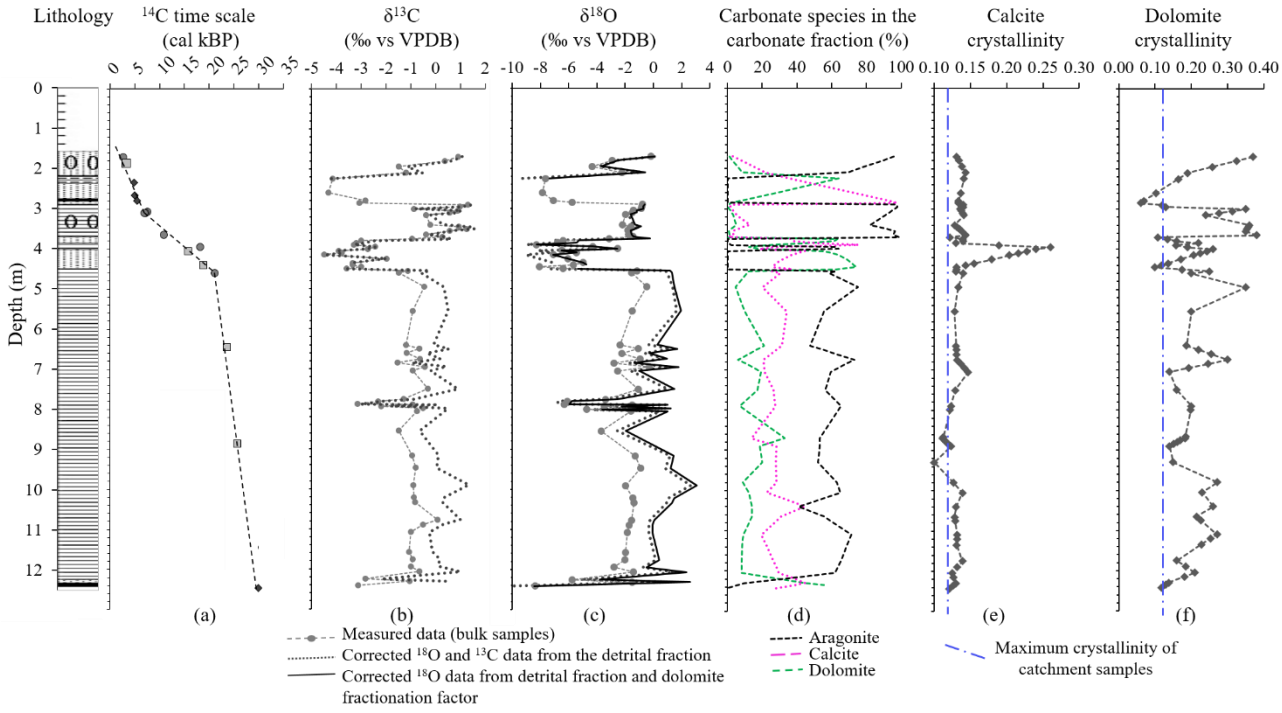

Fig. 3*. Down-core variation in lithology, carbonate mineralogy and stable isotopes of Lake Urmia sediments: (a) age-depth model;(b) and (c) $\delta^{13}C$ and $\delta^{18}O$ (‰ vs VPDB) in bulk samples and after the two-step correction (detrital fraction and dolomite fractionation factor); (d) aragonite, calcite and dolomite percentages in the carbonate fraction determined by XRD; (e) calcite crystallinity; (f) dolomite crystallinity. Data for d to f profiles are from Tudryn et al. (2021) and Kong et al. (2022).*

5.5.2. Stable oxygen and carbon isotope distribution of carbonate

The isotopic record of authigenic carbonates shows a quite great variability with depth. After a paleosol phase at the core base (12.5-12.38 m) characterized by detrital carbonates and plant remains indicating palustrine conditions, an extremely rapid enrichment is observed at 12.2 m depth with $\delta^{18}O$ contents reaching the highest values observed over the entire sequence, *i.e.*, between -2 and +2.5 ‰, and $\delta^{13}C$ contents of +1‰ at a maximum. This leads a very rapid water input to the lake, with the establishment of evaporative conditions leading to the concentration of Ca and Mg ions in the water and thus to the precipitation of authigenic aragonite up to 4.5 m depth. These relatively enriched $\delta^{18}O$ values can therefore be related to the evolution of isotopic contents observed in the carbonates of Lake Lisan and the Dead Sea, the latter being more depleted than the former due to the effect of salinity in a closed lake (Katz *et al.*, 1977; Gat, 1995). The stable isotope balance and fractionation

seem not to be highly affected by the salinity in brackish and moderately saline solutions (Gat, 1995). However, this influence is more important in lakes with salinity largely exceeding that of seawater, with the appearance of so-called "salinity effects" on the isotopic fractionation in relation with (i) humidity that will reach higher values over a brine for any given atmospheric vapor pressure, (ii) the effect of salt that modifies the isotopic fractionation factor at the solution-vapor equilibrium, and (iii) salinity that can alter lake water dynamics and lead to mixing and stratification, with all the implications for authigenic precipitation (Gat, 1995). In Lake Urmia, although with no indication on the water chemistry, the conductivity of the lake surface water reaches 190 to 207 $mS.cm^{-1}$ in 2016 (Tudryn *et al.*, 2021) up to almost 4 times that of sea water. The stable isotope contents of Lake Urmia authigenic carbonates, even corrected for the detrital fraction and from the dolomite fractionation factor, are therefore likely to be affected by an error related to these salinity effects. Furthermore, recent studies show that the much sought-after and often assumed isotopic equilibrium between carbonates and the water in which they crystallize is almost never achieved (Daëron *et al.*, 2019). In this case and in the impossibility of sampling other modern waters of the lake basin, we can only consider that we are approaching as close as possible the real isotopic compositions of our samples and whose fluctuations can be interpreted in terms of palaeohydrological evolution.

Usually driven by interactions with terrestrially-derived dissolved carbon, the corresponding carbon-13 contents in lacustrine carbonates are likely linked to processes such as (i) the exchange/re-equilibration of the TDIC with atmospheric CO_2 whose 2015-^{13}C composition is equal to ~ -8.4 ‰ in an overall decreasing trend (Graven *et al.*, 2020), and (ii) the carbon depletion due to lake primary productivity, especially in lakes with a high residence time (McKenzie, 1985; Leng *et al.*, 1999; Graven *et al.*, 2020). The corresponding ^{13}C contents are thus showing increasing values from -0.5 to +1.5 ‰ indicating the re-equilibration with the atmosphere.

This phase between 12.38 and 4.5 m depth thus corresponds to the lake settlement, with water still subjected to evaporation, and with input of dissolved elements from the watershed. Throughout this phase, lake level fluctuations are relatively large and marked by highly rapid events such as during the 9.2-8.85 m phase and from 7.1 to 6.45 m depth. If the first spell reflects an abrupt lake flood event with $\delta^{13}C$ and $\delta^{18}O$ values around -3‰ and -6 ‰ respectively indicating a marked influence of soil

CO_2, detrital calcite and dolomite inputs and unevaporated water, the second one evidenced the establishment of clear lacustrine conditions with authigenic dolomite and stable isotope contents of carbonates at around 0 ‰ for both $\delta^{13}C$ and $\delta^{18}O$ that fingerprint the equilibrium with atmospheric CO_2. These results mark however the complexity/timing of the water inputs to the lake and the related status in the lake surface water in Fig. 4.

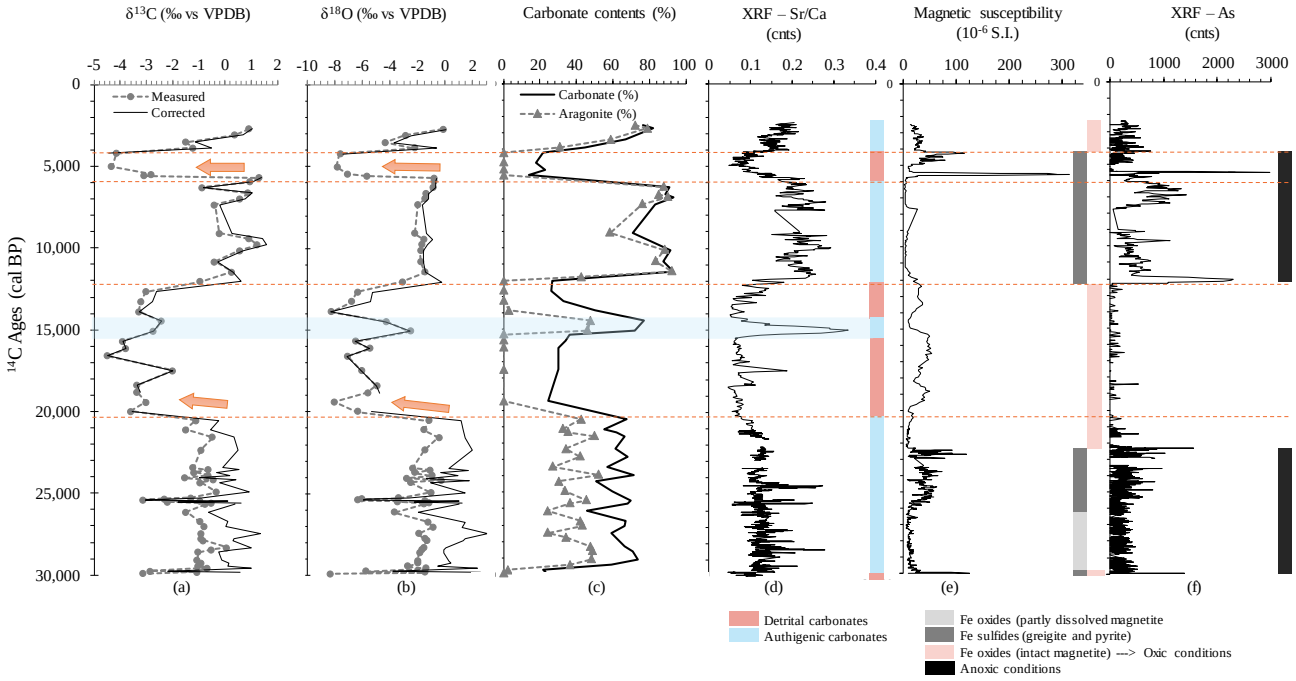

Fig. 4. *Down-core variation in (a) and (b) $\delta^{13}C$ and $\delta^{18}O$ (‰ vs VPDB) in bulk samples and after the two-step correction (detrital fraction and dolomite fractionation factor); (c) carbonate and aragonite content (%); (d) XRF-Sr/Ca; (e) Magnetic susceptibility; (f) XRF-As in Lake Urmia sediments with respect to time.*

In the $\delta^{13}C_{A\ vs}\ \delta^{18}O_A$ diagram (Fig. 5), we observed a moderately significant covariation of isotope data ($Y = 0.39 * X + 0.14$; $R^2 = 0.59$). However, when considering the two major sedimentary sections on the composite core, *i.e.*, form the core base to 4.5 m depth ($R^2 = 0.83$) and from 4.5 m depth to the core top ($R^2 = 0.72$), rather better correlations exist in agreement with the generally admitted evolution of hydrologically closed lakes in relation with temperature, pH or dissolved carbon reservoirs (Talbot, 1990; Li and Ku, 1997). These covariance degrees are relatively high, indicating that the lake remained a closed lake with a long residence time throughout the two sedimentary periods with predominantly evaporation and exchange processes (Leng *et al.*, 1999).

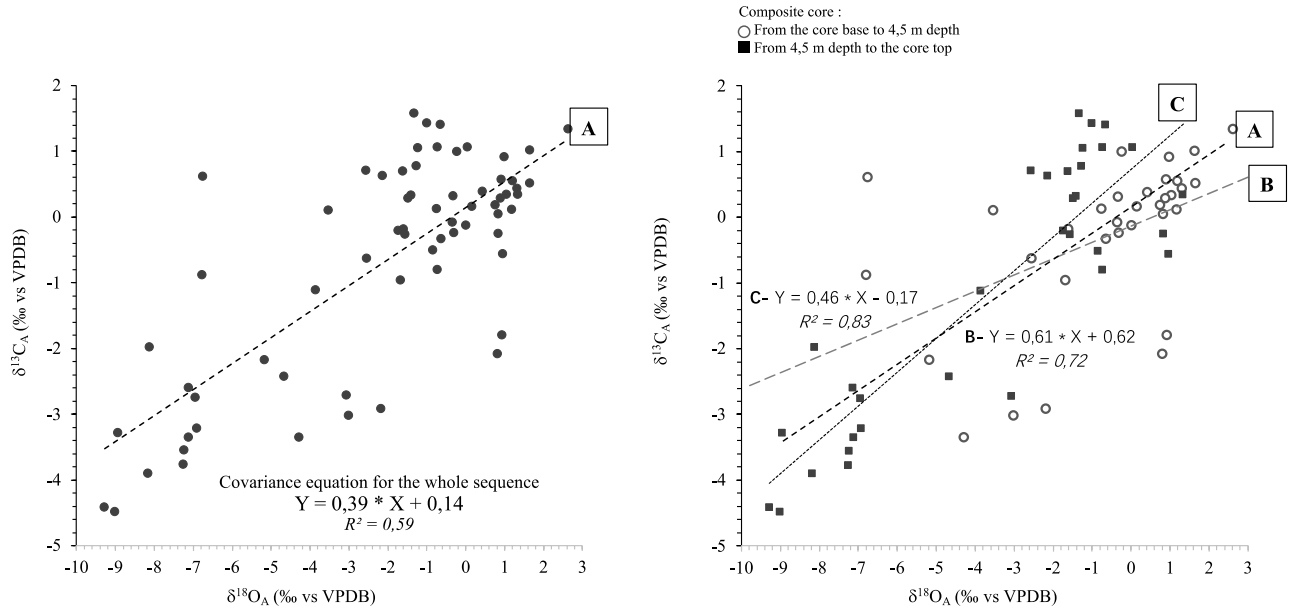

***Fig. 5**. Diagram $\delta^{13}C_A$ vs $\delta^{18}O_A$ (‰ vs VPDB) in authigenic carbonate of samples from the Lake Urmia composite core (regression line A) and with distinction of the two major sub-sections: a- empty circles for the 12.5-4.5 m depth section (regression line B), and b- black square for the section from 4.5 m depth to the core top (regression line C).*

5.5.3. TOC, total nitrogen (TN), C/N, $\delta^{13}C$, and $\delta^{15}N$ of organic matter

In order to define the organic matter inputs from the current Shahr Chay River watershed, three samples of modern vegetation growing around the coring site were collected. Their ^{13}C values range from -21.9 to -10.3 ‰ (Table 2).

Because the sources and qualities of organic matter are environmentally dependent, C and N contents and stable isotope compositions will be highly variable and should theoretically reflect the relative proportions of the sources of this organic matter (Meyers, 1997; Olsen *et al.*, 2013). Terrestrial C_3 plants constitute approximately 90% of all vegetation, with $\delta^{13}C$ values generally ranging from -35‰ to -23‰ while C_4 vegetation have ^{13}C contents of -17‰ to -9‰ (Deines, 1980; Cerling *et al.*, 1993). Freshwater aquatic plants generally have values that range from -50‰ to -11‰ (Osmond *et al.*, 1981; Keeley and Sandquist, 1992). The third CAM pathway that combines features of the C_3 and C_4 pathways, have an intermediate ^{13}C composition of -28‰ to -11‰ (Schleser, 1995)

and gathers succulent plants, which are adapted to water stress (Cerling *et al.*, 1993). The modern global ecosystem has a significant component of C_4 plants, primarily in tropical savannas, temperate grasslands, and semi-desert scrub. Several pollen studies indicate that Lake Urmia sediments are rich in pollen concentration as well as in diversity, in relation with its huge catchment and geomorphology (Djamali *et al.*, 2008a; Djamali and Cilleros, 2020). At the basin scale, the vegetation mainly consists in halophytic grasses and halotolerant vegetation (Talebi *et al.*, 2016), with montane steppe in the northern part, scrub and open forest communities in the south (Zohary, 1973) while wetlands are present in fluvial-lacustrine environments of river mouths, particularly in the northeastern and southern parts of the lake (Djamali *et al.*, 2008b). In such a saline and complex environment, the ^{13}C levels of modern plants highlight that the vegetation of Lake Urmia is mainly of C_4-type, consistent with the salinity and aridity of the environment.

Table 2 *Modern vegetation around Lake Urmia coring site.*

Sample	$\delta^{13}C$ (‰)	TOC	TN	$\delta^{15}N$ (‰)	C/N
URMIA-plant_1	-21.9	42.94	0.38	6.8	114.51
URMIA-plant_2	-18.3	44.42	1.16	6.2	38.39
URMIA-plant_3	-10.3	45.67	2.15	16	21.23

From a general point of view in Fig. 6, the records of carbon and nitrogen contents in the whole samples do not really show any significant evolution, except at specific levels that correspond to layers enriched in organic matter such as the paleo-soil at the core base or much more importantly, the 2.8-m depth level. Indeed, the total organic contents (TOC) vary between 0.05% and 6.10%, with an average of 0.50% while total nitrogen contents (TN) display values from 0.005% to 0.247%, with an average of 0.035%. In a first approach, $\delta^{15}N$ values declines upwards through the core while $\delta^{13}C$ values remains approximately constant. However, the $\delta^{15}N$ curve shows several cyclic fluctuations with increasing contents during the 12.2-11.4 m, 8.8-5.2 m, 5.2-4.8 m and 4.8-2.8 m intervals (Fig. 6). These intervals are roughly anticorrelated with detrital inputs from the catchment as represented by quartz percentages (Tudryn *et al.*, 2021; Kong *et al.*, 2022).

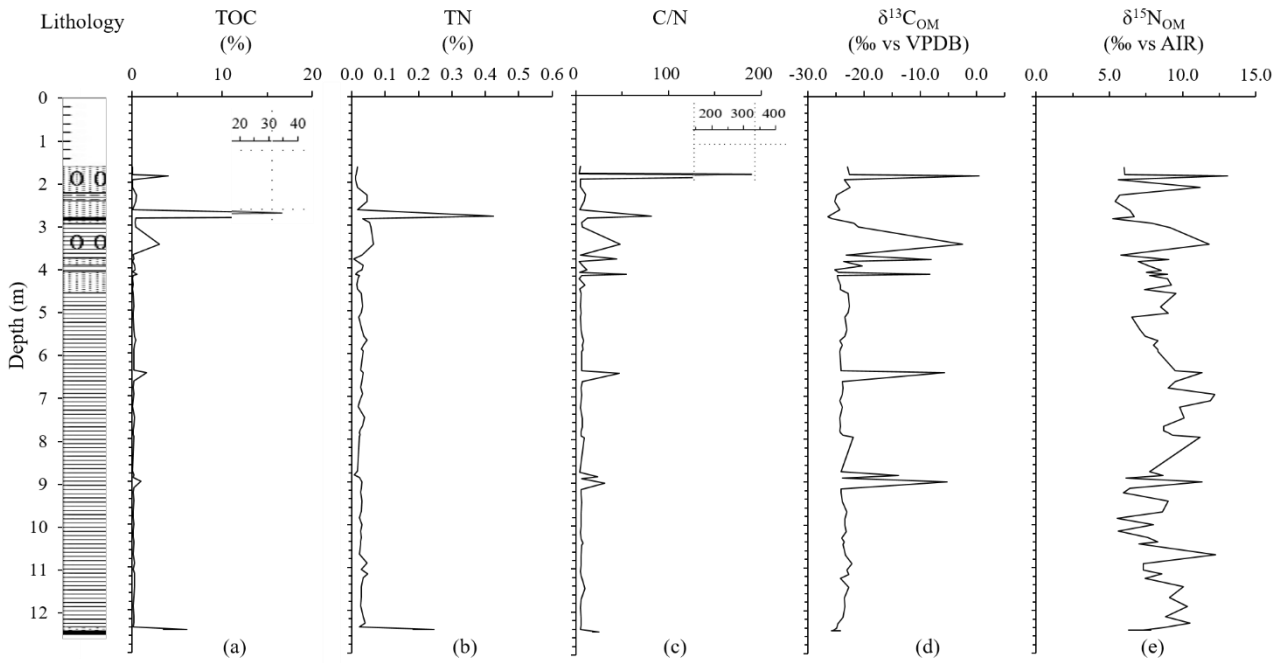

Fig. 6. *Down-core variation of organic fraction and its stables isotope contents in Lake Urmia sediments: (a) Total organic carbon (TOC, %); (b) Total nitrogen (TN; %); (c) carbon versus nitrogen ratio; (d) $\delta^{13}C$ (‰ vs VPDB) in organic matter (OM); (e) $\delta^{15}N$ (‰ vs AIR).*

Several cross-checking diagrams are represented on Fig. 7. In the $\delta^{15}N$ vs $\delta^{13}C$ diagram (Fig. 7a), nearly all data are plotted along a horizontal line indicating highly stable ^{13}C contents of organic matter along the core, with the exception of some levels that show ^{13}C enrichment up to +2‰. Although the two typical soil levels recognized at 12.46 and 2.80 m depth are characterized by elevated TN and TOC contents (Fig. 7c and d), they fall within the average of the sediment sequence data for $\delta^{13}C$ and $\delta^{15}N$ values. The apparent ^{13}C enrichment as a function of $\delta^{15}N$ that appears to be defined for specific levels (noted with their depth on the diagram) does not define a regression line because it is uncorrelated with lithology but represents rapid episodes of changing hydrological conditions. Indeed, these ^{13}C values associated to low TOC can be indicative of low organic inputs from the catchment, leading to the appearance of drier hydrological conditions in a more arid environment (Forbes *et al.*, 2021).

In the $\delta^{13}C$ vs C/N diagram (Fig. 8), the analytical points are plotted following three main pathways: (i) the first one corresponds to the main group of data plotted in a very restricted area between marine and freshwater algae, likely indicating autochthonous organic matter in an open-lake although saline

system; (ii) the second evolution originates from this group and evolves towards the C_4 terrestrial plant area; however, on the opposite to Forbes et al. (2021) who suggest OM decomposition for the evolution towards both decreasing C/N values and increasing ^{13}C contents, levels of the composite core characterized by high $\delta^{13}C$ and $\delta^{15}N$ values are associated with high C/N ratios (Forbes *et al.*, 2021). This may imply the establishment of a typical C_4 vegetation on the catchment which primarily consist of tropical savanna grasses, semi-desert shrublands, desert and salt marsh plants (Stuiver, 1975; Cerling *et al.*, 1993), notably during periods of reduced P/E budget (lacustrine low stands). It has to be noted that the most ^{13}C-enriched levels may be associated with the almost complete degradation of organic compounds that released all labile fractions and kept the most resistant ones such as cellulose or lignin (Deines, 1980; Mariotti *et al.*, 1991); (iii) the third process shows an evolution towards the C_3 group of terrestrial plants that have a greater sensitivity to environmental factors such as atmospheric CO_2 concentration; peaks in ^{13}C-enriched levels can therefore be reasonably related to the rapid replacement of C_3-dominated vegetation by C_4 plants, either due to drier climatic conditions or due to the better adaptation of C_4 plants to lower atmospheric CO_2 concentration as during the last glacial maximum (Meyers and Horie, 1993; Street-Perrott *et al.*, 1997; Gibert *et al.*, 1999; Tyson, 2012). Despite the highly variable C/N values of vegetation in small watersheds due to potentially large fluctuations in plant nitrogen content (Lamb *et al.*, 2006), the fluctuations in Lake Urmia levels can be compared to those of coastal lakes and the tempestology study described in Jahan et al. (2021) showing that the global organic parameter (GOP) can reflect saltwater or freshwater inputs to the lake (Jahan *et al.*, 2021). Indeed, these authors point out that seawater inundation causes an enrichment of ^{13}C and ^{15}N contents with little or no change in C/N ratios, whereas freshwater inflow leads to both a depletion of ^{15}N and an increase in C/N ratios.

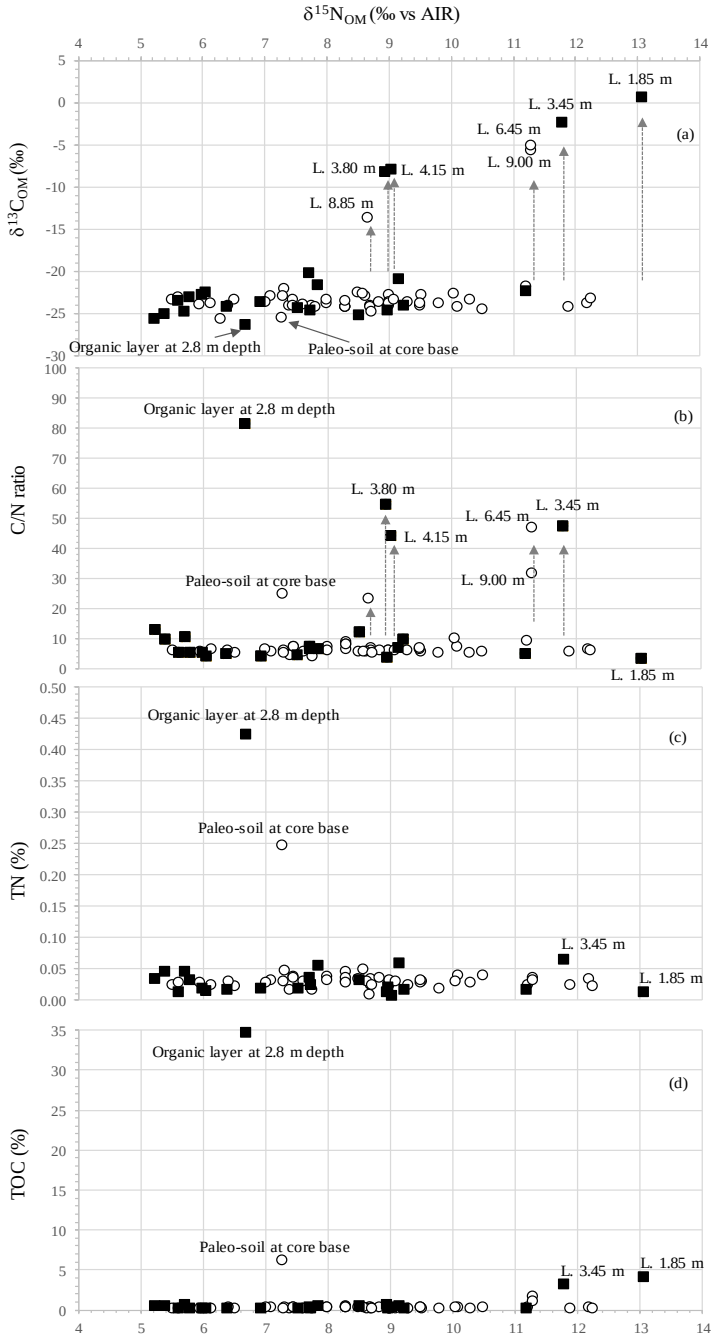

Fig. 7. *Cross-check variations of (a) $\delta^{13}C$ (‰ vs VPDB) in organic matter versus $\delta^{15}N$ (‰ vs AIR); (b) the ratio of C/N versus $\delta^{15}N$; (c) TN (%) versus $\delta^{15}N$; (d) TOC (%) versus $\delta^{15}N$. Empty circles correspond to the 12.5-4.5 m depth section and black square to the section from 4.5 depth to the core top.*

For the present-day Urmia Lake basin which has mainly C_4 vegetation (Table 2), only freshwater inputs from Shahr Chay River will be recorded in the organic parameters. But Fig. 7 shows that for most of the peaks encountered, high ^{13}C values coincide with high ^{15}N values and high C/N ratios. These peaks can be interpreted as recording either saline or freshwater organic species, taking into

account that Lake Urmia is far above ocean salinity and its organic matter could have fingerprints equivalent to marine OM markers with typically higher ^{13}C and ^{15}N values compared to terrestrial vegetation (Lamb *et al.*, 2006). In contrast, the levels of both paleosols, *i.e.*, at the base of the core and at 2.8 m depth, follow a classical evolution with high C/N ratios but low isotopic contents, emphasizing the clear characteristics of C_3 vegetation.

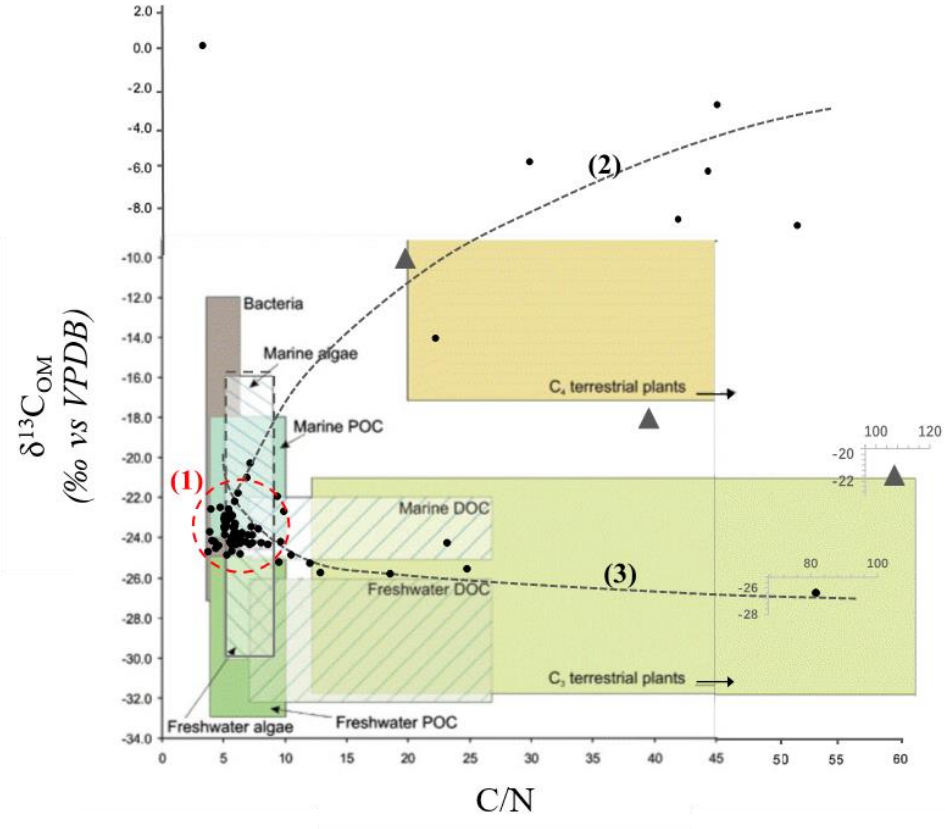

Fig. 8. *Organic matter analyses (black dots) of Lake Urmia composite core sediments and of modern vegetation (grey triangles) from the Shahr Chay River basin plotted in a $\delta^{13}C$ vs C/N ratio diagram. All colored boxes are from Lamb et al. (2006).*

5.6. Discussion

Sedimentary processes occurring in Lake Urmia are clearly recorded in the composite core lithostratigraphy and all the isotope contents on authigenic phases define several major environmental fluctuations during the past 30,000 years. These phases are detailed on Fig. 9.

Phase I (~30 cal kBP) is characterized by low isotope contents indicating inputs from the watershed in agreement with coarse detrital inputs (Tudryn *et al.*, 2021; Kong *et al.*, 2022). The lake level is

considered to be very close to the coring site due to the existence of a paleosol with high organic carbon content. This can be considered as the first stage of lake filling.

Phase II (29.9-26 cal kBP): during this phase, the lake level rise is very rapid with the appearance of authigenic carbonates, all together with detrital carbonates. Stable isotope $\delta^{13}C$ contents highlight the equilibrium with the atmosphere while $\delta^{18}O$ values of the authigenic carbonates are the highest in the entire composite core (up to +3‰), indicating an evaporated open water surface. Comparison with the modern analog of the lake extension indicates that the lake level is above the core site and most likely above since the ^{14}C ages of groundwater from Hajilar wells near the town of Urmia on the Shahr Chay watershed have the same geochemical fingerprints as the muddy water rinsing-up at this depth (Appendix 2). This is also consistent with previous work on sedimentological and elemental parameters that show lower inputs of detrital material from the Shahr Chay watershed, low energy transport and anoxic conditions at the lake bottom (Tudryn *et al.*, 2021; Kong *et al.*, 2022) as well as results of Djamali et al (2008a) describing a high lake stand with lower salinities and higher surface water temperatures.

Phase III (26-25.2 cal kB) corresponds to a short-time dry period characterized by a drastic drop in both ^{18}O and ^{13}C contents and correlated with the disappearance of detrital carbonates. Depleted $\delta^{13}C$ and $\delta^{18}O$ values indicate CO_2 input from soil or salt marsh vegetation, and non-evaporated, low water input from the Shahr Chay river or from the shallow aquifer (Appendix 2).

Phase IV (25.2-20.2 cal kBP) sees the reappearance of lacustrine conditions, similar to those of Phase II, although the onset of this period is more turbulent with very short and sharp peaks probably indicating rapid climate fluctuations and water availability on the catchment.

During Phase V (20.2-15.3 cal BP), the lake level again undergoes a decline, likely implying drier conditions as evidenced by low authigenic carbonate contents and detrital carbonate inputs related to a significant rate of watershed erosion (Tudryn *et al.*, 2021). Depleted $\delta^{13}C$ values indicate a CITD of waters marked by soil organic inputs by and rapid decreasing ^{18}O contents underscore the establishment of a salt marsh environment. This indicates decreasing precipitation on the surrounding mountains and very little on the basin itself, with likely a disappearance of the river stream in the very flat plain before the lake shore (high detrital contents in quartz at the core site).

Phase VI (15.3-13.3 cal kBP) corresponds to the Bølling-Allerød optimum, with an episode of lake rise (deepening of the lake at the coring site). This episode is very well evidenced by all studied parameters (Tudryn *et al.*, 2021; Kong *et al.*, 2022) with increasing Sr/Ca contents, authigenic carbonate precipitation and reduced detrital inputs in relation with the increasing distance of the coring site from the lake shore.

Phase VII: 13.3-11.8 cal kBP is clearly marked in the Lake Urmia sediments, combining the decreasing authigenic aragonite, low ^{18}O contents and a very strong and rapid increase in the quartz fraction. The lake level was lower than before, probably at its minimum for the entire core, although we were unable to recover the most recent sediments for comparison with the present regressive environment.

Phase VIII (11.8-5.6 cal kBP) is characterized by the reappearance of lacustrine conditions with the highest $\delta^{13}C$ values linked to the complete equilibration with the atmosphere and thus a high residence time of the lake surface water. Corresponding $\delta^{18}O$ values are quite stable (mean value of -1.2 ‰ ± 0.6) and point out a relatively low evaporation rate compared to phases II and IV.

A very important regression in water availability is recorded during phase IX (5.6-4.1 cal kBP), with the total disappearance of authigenic carbonates, the highest quartz fraction deposited at the core site (up to 38%) but associated with low clay contents, the two latter roughly highlighting drastic flooding events at the core site.

Phase X represents the core top ending at around 2.3 cal kBP and divided into two spells in an overall increase in stable isotope contents of authigenic carbonates, likely indicating the re-establishment of lacustrine conditions.

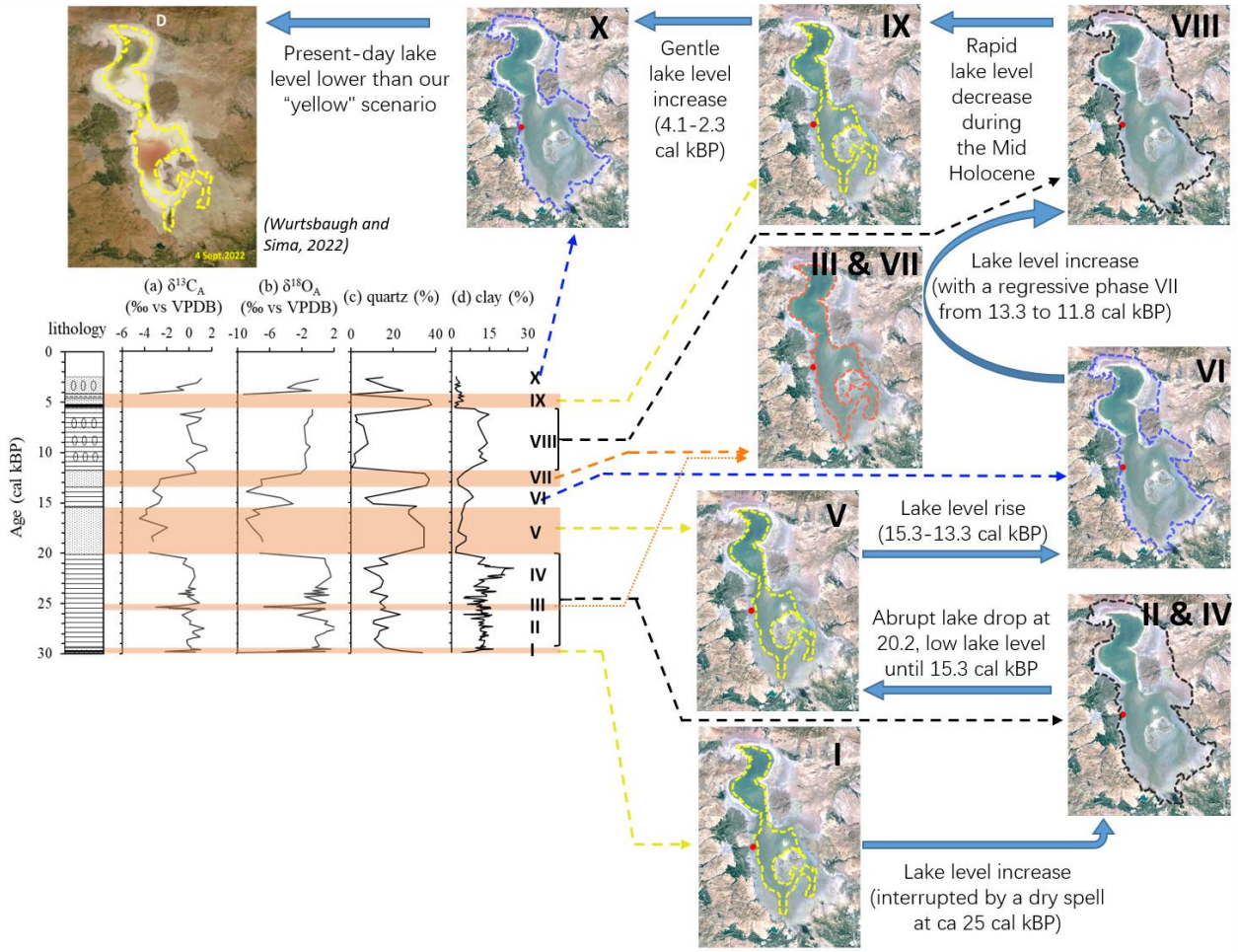

Fig. 9. *Schematic reconstruction of Lake Urmia water level evolution since 30 cal kBP, based on observed analogues since 1984 (Google Earth satellite photo), and in relation to environmental phases inferred from stable isotope contents of authigenic carbonates (a- $\delta^{13}C_A$ ‰ vs VPDB; b- $\delta^{18}O_A$ ‰ vs VPDB) and mineralogical parameters (c- quartz %; d-clay %).*

At a more regional scale, our results can be related to $\delta^{18}O$ records from the Soreq Cave in Israel (Bar-Matthews *et al.*, 1997), Zeribar and Mirabad lakes in Central Iran (Stevens *et al.*, 2006; Wasylikowa *et al.*, 2006; Djamali *et al.*, 2010), Lake Van in Turkey to the East (Çağatay *et al.*, 2014), and at a global scale, we tentatively compare Lake Urmia record to the NGRIP ice core record (NGRIP, 2004) and to the East Mediterranean $\delta^{18}O$ values of sea surface water (Almogi-Labin *et al.*, 2009).

At around 30 kyr BP, Lake Van reached its highest water level to date, a level that was maintained until 20 kyr BP (Çağatay *et al.*, 2014). At the same time, (as for the Dead Sea lake level (Lake Lisan) (Bartov *et al.*, 2003; Stein *et al.*, 2010), the ^{18}O record of Soreq Cave is similar to that of the eastern

Mediterranean Sea, with positive and stable $\delta^{18}O$ values during the Last Glacial Maximum (LGM). The LGM is recorded almost identically in Lake Van and Lake Urmia, except that the depletion of ^{18}O content is much more drastic in Lake Urmia sediments. This LGM regressive phase reaches its maximum in Urmia basin between 20 and 18.5 cal kBP with the complete disappearance of authigenic carbonates, the increase of coarse detrital load and almost no clay deposition at the coring site implying water inflow in the form of ice breakups or floods whom only the most important reached the lake. The coring site would have probably located in the Shahr Chay River channel. At the same time, the evolution is much smoother at Lake Van, since this high-altitude lake probably received water inputs from a smaller catchment area. In comparison, the Soreq cave records show decreasing $\delta^{18}O$ values until the Younger Dryas (Bar-Matthews *et al.*, 1997) and without any clear mark of the LGM, as for the NGRIP curve.

It is from the end of the LGM that the environmental histories of Lakes Van and Urmia separate. Indeed, on the opposite to Lake Urmia for which the two major climatic phases, *i.e.*, Bölling-Alleröd warming (B-A) and Younger Dryas cooling (YD), are well defined with respect to the NGRIP record, high $\delta^{18}O$ values of authigenic carbonate of Lake Van records are evidenced during these two stages, pointing out high levels in Lake Van during these stages (Çağatay *et al.*, 2014). According to these authors, even though Eastern Mediterranean seawater has been considered to be an important source of vapor for winter precipitation in eastern Anatolia, $\delta^{18}O_{G.ruber}$ values show opposite trends with $\delta^{18}O$ values in Lake Van during the Late Pleistocene to early Younger Dryas (30-13 kyr). They suggest that factors other than the source effect are important in understanding the $\delta^{18}O$ record of high-altitude Lake Van during these intervals. Although surrounded by Zagros Mountains and even if Lake Urmia is a continuously saline lake, these factors could have also impacted Lake Urmia fluctuations even in a lesser manner.

Compared to Western Anatolia, which experiences a drier climate, Early Holocene appears to be wetter in Inner Anatolia and Western Iran, in relation with a high humidity rate in Anatolia due to increased Indian monsoon precipitation, a situation that is no longer observed in the Late Holocene (Jones and Roberts, 2008). Comparison of these sequences shows that during the Holocene, $\delta^{18}O$ value at Lake Urmia and Lake Mirabad shows opposite trends. The major decrease in Indian monsoon

rainfalls recorded in the northern Oman speleothem records occurred at around 6.3 kyr BP (Fleitmann *et al.*, 2007) while an increase in Saharan dust was recognized at around 5.5 kyr BP. This period corresponds to lower $\delta^{18}O$ values in Lake Urmia, which was correlated with Lake Zeribar located in the south of Lake Urmia.

All of these sequences have previously been interpreted primarily in terms of fluctuations in regional water balance. However, the specific hydroclimatic controls on each lake system may, nonetheless, be more complex than simply precipitation-minus-evaporation.

5.7. Conclusion

The present study documents the results of stable isotopes on carbonates and organic matter of 12.5 m-long composite cores covering 30 cal kBP. The comparison involves stable oxygen and carbon isotopes and organic matter with XRF elemental and XRD mineralogical results.

In a closed, fresh-water lake, ^{18}O contents of the lake water is controlled by the balance between precipitation and evaporation. Therefore, higher $\delta^{18}O$ values of authigenic carbonates can be attributed to four conditions: (i) heavy isotope enrichment of precipitation linked to the origin and to the type of condensation of air moisture; (ii) long residence time, (iii) higher average air temperature and (iv) lower relative humidity, the last three leads to stronger evaporation and thus heavy isotope enrichment (Fontes *et al.*, 1996). Opposite variations of these parameters and increasing snow falling on the mountainous catchment areas, lighter precipitation or lighter runoff into the river mouth result in a decrease of $\delta^{18}O$ value in authigenic carbonates (Çağatay *et al.*, 2014). Increase in $\delta^{13}C$ value of authigenic carbonates precipitated in the lake water can be related to either a long residence time of the water allowing the equilibration of the water TDIC with the atmospheric CO_2 and/or higher organic productivity leads to light carbon isotopes into organic matter and thus increase $\delta^{13}C$ value of the TDIC in lake water. Low ^{13}C content of authigenic carbonates may be due to the opposite above cited factors, and/or to oxidation of bottom organic matter (Fontes *et al.*, 1996).

In Lake Urmia, Steven et al. (2012) investigated $\delta^{18}O$ record of sediment core spanning the last 180 kyr constructed from aragonite-rich fecal pellets, while there are only three $\delta^{18}O$ data over the

last 30 kyr. The $\delta^{18}O$ values for the last 80 kyr were stable and fluctuated around 0 ‰ and three $\delta^{18}O$ values of 1‰ at 28 cal kBP, 0‰ at 12 cal kBP and -1‰ at 10 cal kBP are totally the same with our corrected $\delta^{18}O$ values. The $\delta^{18}O$ values in our composite core sediments, shows high positive correlation with $\delta^{13}C$ values which further certifies that Lake Urmia has no outlets, and these variations are mainly controlled by the balance of precipitation and evaporation (Talbot and Kelts, 1990; Roberts *et al.*, 2008).

Owing to Lake Urmia as a shallow and hypersaline like, the abrupt decrease of $\delta^{18}O$ value at 20.2 cal kBP, possibly attributes to no precipitation, our coring site near the river mouth was drying out, and fresh runoff into the lake went through our core, decreasing $\delta^{18}O$ value of authigenic carbonate. This period of lower $\delta^{18}O$ value lasted until 15.3 cal kBP. During the warm period of Bølling-Allerød, $\delta^{18}O$ value was associated to weaker evaporation of the lake waters. During the Younger Dryas period, the $\delta^{18}O$ value gradually increased is related to higher evaporation in arid condition.

Generally, higher $\delta^{18}O$ values is related with higher evaporation and thus a lower lake level, while correlations between the abundance of $\delta^{18}O$ values and high lake level in Lake Urmia during the Early-Mid Holocene, suggest that other climate parameters such as lake water temperature, rainfall amount and moisture source inferred from the seasonality of precipitation may also affect lake water $\delta^{18}O$. Owing to geological location of Lake Urmia, the principal moisture source of winter precipitation originates from the storm tracts in the North Atlantic, which is strongly modified in the Eastern Mediterranean just like Lake Van region in north way or similar with Dead Sea in south way (Karaca *et al.*, 2000; Stevens *et al.*, 2001). For spring precipitation, the Black Sea and Caspian Sea may also be a vapour source of $\delta^{18}O$-enriched rains (Djamali *et al.*, 2010a; Roberts *et al.*, 2011). In contrast, summer precipitation mainly attributes to southern Indian monsoons from Indian Sea. Different moisture source contains different $\delta^{18}O$, and generally an increasing contribution of summer precipitation results in higher $\delta^{18}O$ values compared with winter precipitation. Stevens et al. (2001) stated that a reduction in spring and summer precipitation and increase in winter precipitation at Lake Zeribar resulted in a negative shift of annual $\delta^{18}O$ value of precipitation at around 4.5 kyr. Thus, such a decrease of $\delta^{18}O$ values in authigenic carbonate contributes to a shift of winter precipitation in Lake Urmia during the 5.6-4.1 cal kBP. In general, increasing temperature enriches the isotopic

composition of precipitation in the heavy isotope by condensation and isotope partitioning during phase transitions (*i.e.*, evaporation and condensation) (Cole *et al.*, 1999). Subsequently, increase of $\delta^{18}O$ values during the 4.1-2.3 cal kBP was likely associated with increasing temperature and thus stronger evaporation.

References

Al-Aasm, I.S., Taylor, B. and South, B., 1990. Stable Isotope Analysis of Multiple Carbonate Samples Using Selective Acid Extraction. Chemical Geology: Isotope Geoscience Section, 80(2): 119-125.

Alijani, B. and Harman, J.R., 1985. Synoptic Climatology of Precipitation in Iran. Annals of the Association of American Geographers, 75(3): 404-416.

Almogi-Labin, A., Bar-Matthews, M., Shriki, D., Kolosovsky, E., Paterne, M., Schilman, B., Ayalon, A., Aizenshtat, Z. and Matthews, A., 2009. Climatic Variability During the Last∼ 90 Ka of the Southern and Northern Levantine Basin as Evident from Marine Records and Speleothems. Quaternary Science Reviews, 28(25-26): 2882-2896.

Aravena, R., Warner, B.G., MacDonald, G.M. and Hanf, K.I., 1992. Carbon Isotope Composition of Lake Sediments in Relation to Lake Productivity and Radiocarbon Dating. Quaternary Research, 37(3): 333-345.

Bar-Matthews, M., Ayalon, A. and Kaufman, A., 1997. Late Quaternary Paleoclimate in the Eastern Mediterranean Region from Stable Isotope Analysis of Speleothems at Soreq Cave, Israel. Quaternary Research, 47(2): 155-168.

Bartholy, J., Pongrácz, R. and Pattantyús-Ábrahám, M., 2009. Analyzing the Genesis, Intensity, and Tracks of Western Mediterranean Cyclones. Theoretical Applied Climatology, 96(1): 133-144.

Bartov, Y., Goldstein, S.L., Stein, M. and Enzel, Y., 2003. Catastrophic Arid Episodes in the Eastern Mediterranean Linked with the North Atlantic Heinrich Events. Geology, 31(5): 439-442.

Çağatay, M.N., Öğretmen, N., Damcı, E., Stockhecke, M., Sancar, Ü., Eriş, K.K. and Özeren, S., 2014. Lake Level and Climate Records of the Last 90ka from the Northern Basin of Lake Van, Eastern Turkey. Quaternary Science Reviews, 104: 97-116.

Cerling, T.E., Wang, Y. and Quade, J., 1993. Expansion of C4 Ecosystems as an Indicator of Global Ecological Change in the Late Miocene. Nature, 361(6410): 344-345.

Clark, I. and Fritz, P., 1997. Environmental Isotopes in Hydrology. Lewis Publishers Boca Raton, Fla.

Cole, J.E., Rind, D., Webb, R.S., Jouzel, J. and Healy, R., 1999. Climatic Controls on Interannual Variability of Precipitation Δ18o: Simulated Influence of Temperature, Precipitation Amount, and Vapor Source Region. Journal of Geophysical Research: Atmospheres, 104(D12): 14223-14235.

Coplen, T., 1995. Reporting of stable carbon, hydrogen, and oxygen isotopic abundances. Reference intercomparison materials for stable isotopes of light elements 825, 31-34.

Daëron, M., Drysdale, R.N., Peral, M., Huyghe, D., Blamart, D., Coplen, T.B., Lartaud, F. and Zanchetta, G., 2019. Most Earth-Surface Calcites Precipitate out of Isotopic Equilibrium. Nature Communications, 10(1): 1-7.

Dean, J.R., Jones, M.D., Leng, M.J., Noble, S.R., Metcalfe, S.E., Sloane, H.J., Sahy, D., Eastwood, W.J. and Roberts, C.N., 2015. Eastern Mediterranean Hydroclimate over the Late Glacial and Holocene, Reconstructed from the Sediments of Nar Lake, Central Turkey, Using Stable Isotopes and Carbonate Mineralogy. Quaternary Science Reviews, 124: 162-174.

Deines, P., 1980. The Isotopic Composition of Reduced Organic Carbon. In: Fritz, P., Fontes, J.C. (Eds.), Handbook of Environmental Isotopic Geochemistry, Vol. 1, The Terrestrial Environment. Elsevier, Amsterdam: pp. 329–406.

Develle, A.-L., Herreros, J., Vidal, L., Sursock, A. and Gasse, F., 2010. Controlling Factors on a Paleo-Lake Oxygen Isotope Record (Yammoûneh, Lebanon) since the Last Glacial Maximum. Quaternary Science Reviews, 29(7-8): 865-886.

Djamali, M., Akhani, H., Andrieu-Ponel, V., Braconnot, P., Brewer, S., de Beaulieu, J. L., Fleitmann, D., Fleury, J., Gasse, F. and Guibal, F., 2010. Indian Summer Monsoon Variations Could Have Affected the Early-Holocene Woodland Expansion in the near East. The Holocene, 20(5): 813-820.

Djamali, M. and Cilleros, K., 2020. Statistically Significant Minimum Pollen Count in Quaternary Pollen Analysis; the Case of Pollen-Rich Lake Sediments. Review of Palaeobotany Palynology, 275: 104156.

Djamali, M., de Beaulieu, J.L., Shah-hosseini, M., Andrieu-Ponel, V., Ponel, P., Amini, A., Akhani, H., Leroy, S.A.G., Stevens, L., Lahijani, H. and Brewer, S., 2008a. A Late Pleistocene Long Pollen Record from Lake Urmia, Nw Iran. Quaternary Research, 69(03): 413-420.

Djamali, M., Kürschner, H., Akhani, H., de Beaulieu, J.L., Amini, A., Andrieu-Ponel, V., Ponel, P. and Stevens, L., 2008b. Palaeoecological Significance of the Spores of the Liverwort Riella (Riellaceae) in a Late Pleistocene Long Pollen Record from the Hypersaline Lake Urmia, Nw Iran. Review of Palaeobotany and Palynology, 152(1-2): 66-73.

Epstein, S., Graf, D.L. and Degens, E.T., 1964. Oxygen Isotope Studies on the Origin of Dolomites.

Fleitmann, D., Burns, S.J., Mangini, A., Mudelsee, M., Kramers, J., Villa, I., Neff, U., Al-Subbary, A.A., Buettner, A. and Hippler, D., 2007. Holocene Itcz and Indian Monsoon Dynamics Recorded in Stalagmites from Oman and Yemen (Socotra). Quaternary Science Reviews, 26(1-2): 170-188.

Fontes, J.-C., Gasse, F. and Gibert, E., 1996. Holocene Environmental Changes in Lake Bangong Basin (Western Tibet). Part 1: Chronology and Stable Isotopes of Carbonates of a Holocene Lacustrine Core. Palaeogeography, Palaeoclimatology, Palaeoecology, 120(1-2): 25-47.

Fontes, J.C., Mélières, F., Gibert, E., Qing, L. and Gasse, F., 1993. Stable Isotope and Radiocarbon Balances of Two Tibetan Lakes (Sumxi Co, Longmu Co) from 13,000 Bp. Quaternary Science Reviews, 12(10): 875-887.

Forbes, M., Cohen, T., Jacobs, Z., Marx, S., Barber, E., Dodson, J., Zamora, A., Cadd, H., Francke, A. and Constantine, M., 2021. Comparing Interglacials in Eastern Australia: A Multi-Proxy Investigation of a New Sedimentary Record. Quaternary Science Reviews, 252: 106750.

Gat, J.R., 1995. Stable Isotopes of Fresh and Saline Lakes. In: Physics and Chemistry of Lakes. Springer: pp: 139-165.

Gibert, E., Bergonzini, L., Massault, M. and Williamson, D., 2002. Ams-14c Chronology of 40.0 Cal Ka Bp Continuous Deposits from a Crater Lake (Lake Massoko, Tanzania): Modern Water Balance and Environmental Implications. Palaeogeography, Palaeoclimatology, Palaeoecology, 187(3-4): 307-322.

Gibert, E., Travi, Y., Massault, M., Chernet, T., Barbecot, F. and Laggoun-Défarge, F., 1999. Comparing Carbonate and Organic Ams-14c Ages in Lake Abiyata Sediments (Ethiopia): Hydrochemistry and Paleoenvironmental Implications. Radiocarbon, 41(3): 271-286.

Graven, H., Keeling, R.F. and Rogelj, J., 2020. Changes to Carbon Isotopes in Atmospheric Co2 over the Industrial Era and into the Future. Global Biogeochemical Cycles, 34(11): e2019GB006170.

Jahan, S., Wang, Y., Burnett, W.C., Means, G.H. and Sun, F., 2021. Evaluating Organic Geochemical Proxies for Application to Coastal Lake Sediments Along the Gulf Coast of Florida for Paleotempestology. Quaternary Science Reviews, 266: 107077.

Jones, M.D. and Roberts, C.N., 2008. Interpreting Lake Isotope Records of Holocene Environmental Change in the Eastern Mediterranean. Quaternary International, 181(1): 32-38.

Karaca, M., Deniz, A. and Tayanç, M., 2000. Cyclone Track Variability over Turkey in Association with Regional Climate. International Journal of Climatology: A Journal of the Royal Meteorological Society, 20(10): 1225-1236.

Katz, A., Kolodny, Y. and Nissenbaum, A., 1977. The Geochemical Evolution of the Pleistocene Lake Lisan-Dead Sea System. Geochimica et Cosmochimica Acta, 41(11): 1609-1626.

Keeley, J.E. and Sandquist, D., 1992. Carbon: Freshwater Plants. Plant, Cell, Environmental Development, 15(9): 1021-1035.

Kelts, K. and Talbot, M., 1990. Lacustrine Carbonates as Geochemical Archives of Environmental Change and Biotic/Abiotic Interactions. In: Large Lakes. Springer: pp: 288-315.

Kong, T., Tudryn, A., Gibert-Brunet, E., Tucholka, P., Motavalli-Anbaran, S.-H., Ahmady-Birgani, H., Lankarani, M., Miska, S., Noret, A. and Dufaure, O., 2022. 30,000 Years of the Southwestern

Lake Urmia (Iran) Paleoenvironmental Evolution Inferred from Mineralogical Indicators from Lake and Watershed Sediments. Journal of Asian Earth Sciences: 105387.

Lamb, A.L., Leng, M.J., Lamb, H.F., Telford, R.J. and Mohammed, M.U., 2002. Climatic and Non-Climatic Effects on the Δ18o and Δ13c Compositions of Lake Awassa, Ethiopia, During the Last 6.5 Ka. Quaternary Science Reviews, 21(20-22): 2199-2211.

Lamb, A.L., Wilson, G.P. and Leng, M.J., 2006. A Review of Coastal Palaeoclimate and Relative Sea-Level Reconstructions Using Δ13c and C/N Ratios in Organic Material. Earth-Science Reviews, 75(1-4): 29-57.

Land, L.S., 1980. The Isotopic and Trace Element Geochemistry of Dolomite: The State of the Art. Concepts and models of dolomitization.: pp.87-110.

Langbein, W.B., 1961. Salinity and Hydrology of Closed Lakes: A Study of the Long-Term Balance between Input and Loss of Salts in Closed Lakes. US Government Printing Office.

Leng, M.J., Roberts, N., Reed, J.M. and Sloane, H.J., 1999. Late Quaternary Palaeohydrology of the Konya Basin, Turkey, Based on Isotope Studies of Modern Hydrology and Lacustrine Carbonates. Journal of Paleolimnology, 22(2): 187-204.

Li, H.-C. and Ku, T.-L., 1997. Δ13c–Δ18c Covariance as a Paleohydrological Indicator for Closed-Basin Lakes. Palaeogeography, Palaeoclimatology, Palaeoecology, 133(1-2): 69-80.

Mariotti, A., Gadel, F. and Giresse, P., 1991. Carbon Isotope Composition and Geochemistry of Particulate Organic Matter in the Congo River (Central Africa): Application to the Study of Quaternary Sediments Off the Mouth of the River. Chemical Geology: Isotope Geoscience Section, 86(4): 345-357.

McCormack, J., Nehrke, G., Jöns, N., Immenhauser, A. and Kwiecien, O., 2019. Refining the Interpretation of Lacustrine Carbonate Isotope Records: Implications of a Mineralogy-Specific Lake Van Case Study. Chemical Geology, 513: 167-183.

McKenzie, J.A., 1985. Carbon Isotopes and Productivity in the Lacustrine and Marine Environment. Chemical processes in lakes: 99-118.

Meyers, P.A., 1997. Organic Geochemical Proxies of Paleoceanographic, Paleolimnologic, and Paleoclimatic Processes. Organic geochemistry, 27(5-6): 213-250.

Meyers, P.A. and Horie, S., 1993. An Organic Carbon Isotopic Record of Glacial-Postglacial Change in Atmospheric Pco2 in the Sediments of Lake Biwa, Japan. Palaeogeography, Palaeoclimatology, Palaeoecology, 105(3-4): 171-178.

NGRIP, 2004. High-Resolution Record of Northern Hemisphere Climate Extending into the Last Interglacial Period. Nature, 431(7005): 147-151.

Olsen, J., Anderson, N.J. and Leng, M.J., 2013. Limnological Controls on Stable Isotope Records of Late-Holocene Palaeoenvironment Change in Sw Greenland: A Paired Lake Study. Quaternary Science Reviews, 66: 85-95.

Osmond, C., Valaane, N., Haslam, S., Uotila, P. and Roksandic, Z., 1981. Comparisons of Δ13c Values in Leaves of Aquatic Macrophytes from Different Habitats in Britain and Finland; Some Implications for Photosynthetic Processes in Aquatic Plants. Oecologia, 50(1): 117-124.

Roberts, N., Jones, M., Benkaddour, A., Eastwood, W., Filippi, M., Frogley, M., Lamb, H., Leng, M., Reed, J. and Stein, M., 2008. Stable Isotope Records of Late Quaternary Climate and Hydrology from Mediterranean Lakes: The Isomed Synthesis. Quaternary Science Reviews, 27(25-26): 2426-2441.

Roberts, N., Reed, J., Leng, M., Kuzucuoğlu, C., Fontugne, M., Bertaux, J., Woldring, H., Bottema, S., Black, S. and Hunt, E., 2001. The Tempo of Holocene Climatic Change in the Eastern Mediterranean Region: New High-Resolution Crater-Lake Sediment Data from Central Turkey. The Holocene, 11(6): 721-736.

Schleser, G.H., 1995. Parameters Determining Carbon Isotope Ratios in Plants. Problems of Stable Isotopes in Tree-Rings, Lake Sediments and Peat-Bogs as Climatic Evidence for the Holocene, Palaeoclim. Res, 15: 71-96.

Sharifi, A., Shah-Hosseini, M., Pourmand, A., Esfahaninejad, M. and Haeri-Ardakani, O., 2018. The Vanishing of Urmia Lake: A Geolimnological Perspective on the Hydrological Imbalance of the World's Second Largest Hypersaline Lake. pp: 1-3.

Stein, M., Torfstein, A., Gavrieli, I. and Yechieli, Y., 2010. Abrupt Aridities and Salt Deposition in the Post-Glacial Dead Sea and Their North Atlantic Connection. Quaternary Science Reviews, 29(3-4): 567-575.

Stevens, L.R., Djamali, M., Andrieu-Ponel, V. and de Beaulieu, J.L., 2012. Hydroclimatic Variations over the Last Two Glacial/Interglacial Cycles at Lake Urmia, Iran. Journal of Paleolimnology, 47(4): 645-660.

Stevens, L.R., Ito, E., Schwalb, A. and Wright, H.E., 2006. Timing of Atmospheric Precipitation in the Zagros Mountains Inferred from a Multi-Proxy Record from Lake Mirabad, Iran. Quaternary Research, 66(3): 494-500.

Stevens, L.R., Wright, H.E. and Ito, E., 2001. Proposed Changes in Seasonality of Climate During the Lateglacial and Holocene at Lake Zeribar, Iran. The Holocene, 11: 747-755.

Street-Perrott, F.A., Huang, Y., Perrott, R.A., Eglinton, G., Barker, P., Khelifa, L.B., Harkness, D.D. and Olago, D.O., 1997. Impact of Lower Atmospheric Carbon Dioxide on Tropical Mountain Ecosystems. Science, 278(5342): 1422-1426.

Stuiver, M., 1975. Climate Versus Changes in 13c Content of the Organic Component of Lake Sediments During the Late Quarternary. Quaternary Research, 5(2): 251-262.

Taha, M., Harb, S., Nagib, M. and Tantawy, A., 1981. The Climate of the near East. In: Climates of Southern and Western Asia. Elsevier Amsterdam: pp: 183-255.

Talbot, M., 1990. A Review of the Palaeohydrological Interpretation of Carbon and Oxygen Isotopic Ratios in Primary Lacustrine Carbonates. Chemical Geology: Isotope Geoscience Section, 80(4): 261-279.

Talbot, M. and Kelts, K., 1990. Paleolimnological Signatures from Carbon and Oxygen Isotopic Ratios in Carbonates, from Organic Carbon-Rich Lacustrine Sediments: Chapter 6.

Talebi, T., Ramezani, E., Djamali, M., Lahijani, H.A.K., Naqinezhad, A., Alizadeh, K. and Andrieu-Ponel, V., 2016. The Late-Holocene Climate Change, Vegetation Dynamics, Lake-Level Changes and Anthropogenic Impacts in the Lake Urmia Region, Nw Iran. Quaternary International, 408: 40-51.

Tarutani, T., Clayton, R.N. and Mayeda, T.K., 1969. The Effect of Polymorphism and Magnesium Substitution on Oxygen Isotope Fractionation between Calcium Carbonate and Water. Geochimica et Cosmochimica Acta, 33(8): 987-996.

Tudryn, A., Motavalli-Anbaran, S.H., Tucholka, P., Gibert-Brunet, E., Lankarani, M., Ahmady-Birgani, H., Kong, T., Noret, A., Miska, S., Massault, M. and Dufaure, O., 2021. Late Quaternary Environmental Changes of Lake Urmia Basin (Nw Iran) Inferred from Sedimentological and Magnetic Records. Quaternary International, 589: 83-94.

Tyson, R.V., 2012. Sedimentary Organic Matter: Organic Facies and Palynofacies. Springer Science and Business Media.

Valero-Garcés, B.L., Grosjean, M., Schwalb, A., Geyh, M., Messerli, B. and Kelts, K., 1996. Limnogeology of Laguna Miscanti: Evidence for Mid to Late Holocene Moisture Changes in the Atacama Altiplano (Northern Chile). Journal of Paleolimnology, 16(1): 1-21.

Vystavna, Y., Harjung, A., Monteiro, L.R., Matiatos, I. and Wassenaar, L.I., 2021. Stable Isotopes in Global Lakes Integrate Catchment and Climatic Controls on Evaporation. Nature Communications, 12(1): 1-7.

Wang, J., Song, C., Reager, J.T., Yao, F., Famiglietti, J.S., Sheng, Y., MacDonald, G.M., Brun, F., Schmied, H.M. and Marston, R.A., 2018. Recent Global Decline in Endorheic Basin Water Storages. Nature Geoscience, 11(12): 926-932.

Wasylikowa, K., Witkowski, A., Walanus, A., Hutorowicz, A., Alexandrowicz, S.W. and Langer, J.J., 2006. Palaeolimnology of Lake Zeribar, Iran, and Its Climatic Implications. Quaternary Research, 66(3): 477-493.

Zanchetta, G., Borghini, A., Fallick, A.E., Bonadonna, F.P. and Leone, G., 2007. Late Quaternary Palaeohydrology of Lake Pergusa (Sicily, Southern Italy) as Inferred by Stable Isotopes of Lacustrine Carbonates. Journal of Paleolimnology, 38(2): 227-239.

Zohary, M., 1973. Geobotanical Foundations of the Middle East. Fischer.

General conclusions and perspectives

Lake Urmia basin, located in Western Asia, is a significant continental position in the eastern Mediterranean zones, nowadays influenced by North Atlantic, mid-latitude subtropical high pressure and Siberian high pressure systems. The main objectives of this research were to reconstruct the paleoclimate of Lake Urmia over the last 30 kyr, which helps us to understand the climate evolution at the regional scale in terms of identifying its causal mechanisms during the Late Pleistocene and the whole Holocene.

In this study, we present systematic investigations of sedimentological, magnetic, mineralogical, geochemical and chronological records on 12.5-m composite core from the southwestern part of Lake Urmia with catchment samples on the way of river Shahr Chay close to the coring site. The relatively content of detrital and authigenic compounds that includes detailed analyses of carbonate and clays assemblages on the sedimentary sequence retrieved show important changes in the lake water level for the past ~30 kyr. After the establishment of the lake water balance through an extensive study of surface and groundwater on the Lake Urmia basin, a reservoir effect about 2000 years for the past was defined and allow the validation of the consistency of the AMS ^{14}C chronology between 22 and 2 cal kBP, in agreement with the lithostratigraphy and matching with the major regional environment phases.

The paleoenvironmental reconstruction suggests a humid Late Pleistocene during 29.2-20.2 cal kBP period, followed by drier episode before warm and humid Bölling-Alleröd period, the following dry spell of Younger Dryas, the humid early Holocene period and evaporative conditions during the Mid to Late Holocene transition. The past 30 cal kBP was divided into two main conditions: drier conditions at ca 30-29.9, 20.2-15.3, 13.3-11.8, 5.6-4.1 cal kBP and humid conditions at intervals of 29.9-20.2, 15.3-13.3, 11.8-5.6 and 4.1-2.3 cal kBP.

Other analyses of element and stable isotopes with reliable ^{14}C dating verify this pattern and trends of environmental change in Lake Urmia basin over the last 30 kyr. In combination with mineralogy results, XRF core scanning data on Lake Urmia deposits indicated the presence of arsenic is systematically associated with iron sulfides as natural origin. Both arsenic and iron sulfides being of

early diagenetic origin, they indicate anoxic conditions (i) in lake bottom sediments during high lake water levels in phase of 29.9-22 and ca. 12-5.5 cal kBP and (ii) in organic-rich levels during the lake low stands at 29.9 and 5.5 cal kBP.

Our results have been compared to the evolution of other water bodies in the Middle East and we show that the environmental phases determined at Lake Urmia fit well into the evolution of the eastern Mediterranean and the Anatolian sub-region, particularly during the Late Pleistocene wet period, as well as the early Holocene Optimum. It suggests that an atmospheric teleconnection dominated between the North Atlantic and western Iran during the last 30 kyr BP. In the early Holocene, an Indian monsoon influence cannot be excluded.

Fig. 1. *(next page): Lake level record during the Late Quaternary with special attention to (1) high lake level in humid phases marked in blue recorded during LGM, Bølling-Allerød, Early and Late Holocene, and (2) low lake level in dry phases marked in earthy yellow recorded during Late glacial, Younger Dryas and Mid-Holocene for the last 30 kyr*

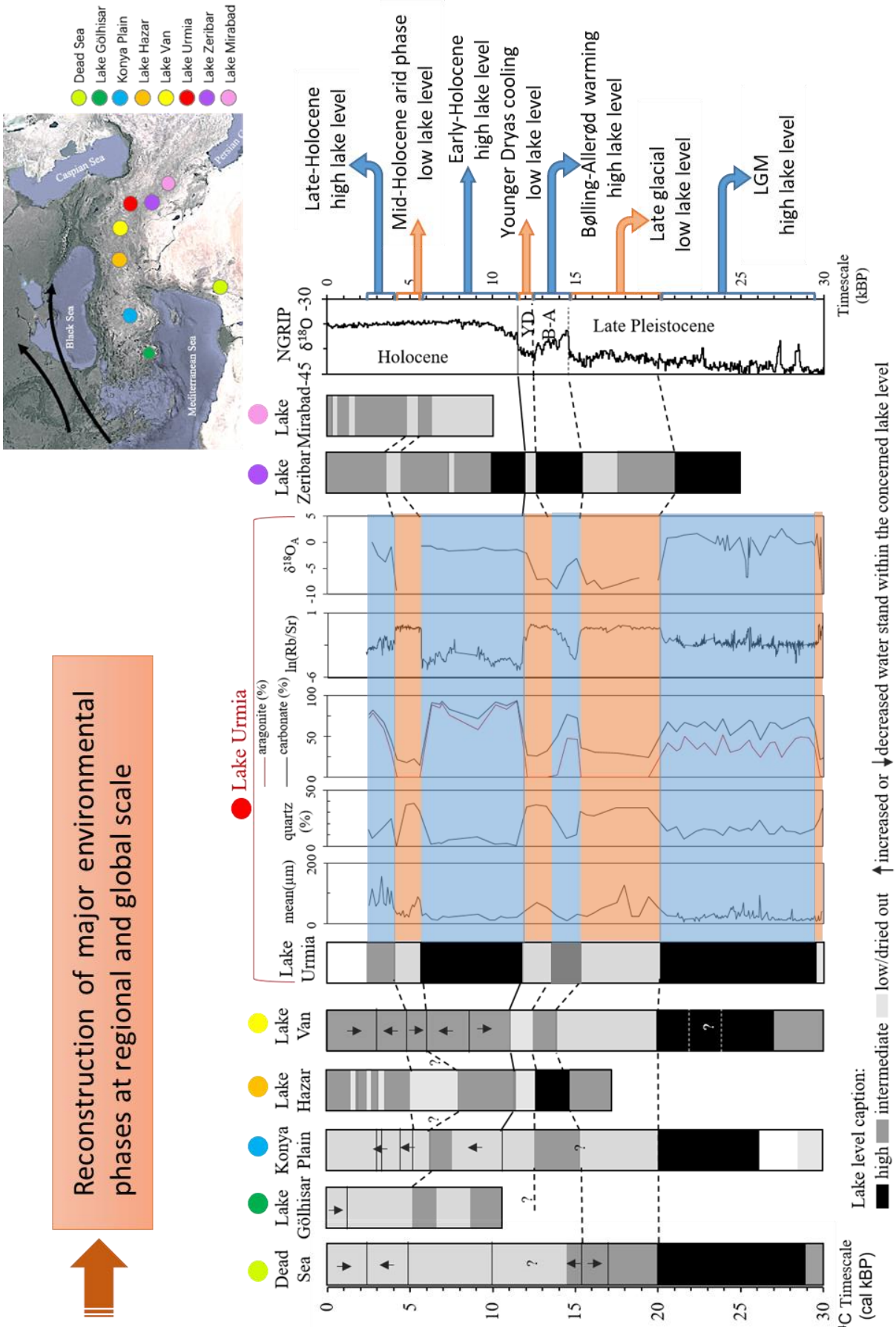
Reconstruction of major environmental phases at regional and global scale
Dead Sea
Lake Gölhisar
Konya Plain
Lake Hazar
Lake Van
Lake Urmia
Lake Zeribar
Lake Mirabad
Caspian Sea
Black Sea
Mediterranean Sea
Late-Holocene high lake level
Mid-Holocene arid phase low lake level
Early-Holocene high lake level
Younger Dryas cooling low lake level
Bølling-Allerød warming high lake level
Late glacial low lake level
LGM high lake level
Timescale (kBP)
NGRIP δ18O
Holocene
YD
B-A
Late Pleistocene
Lake Mirabad
Lake Zeribar
Lake Urmia
aragonite (%)
carbonate (%)
δ18OA
ln(Rb/Sr)
quartz (%)
mean(µm)
Lake Van
Lake Hazar
Konya Plain
Lake Gölhisar
Dead Sea
14C Timescale (cal kBP)
Lake level caption:
high
intermediate
low/dried out
increased or
decreased water stand within the concerned lake level

As a conclusion:

Lake Urmia provides a unique record for the region…

Beyond major changes descripted, the study of Lake Urmia emphasizes:

- At local scale, in conjunction with all mineralogical records:
  - The identification of short-time environment changes around two-three hundred years as highlighted through XRF elements;
  - The specification of carbonate system and the validation of the chronology via the two-step corrections.
- At regional and global scale:
  - The good correlation with the climate evolution of the northern hemisphere, and
  - Evidences of teleconnection with North Atlantic atmospheric system.

Unfortunately, our data stops at around 2000 years. We therefore do not have access to the most recent periods and therefore impacted by human activities.

The perspective for future researches on Lake Urmia basin would be:
(1) To continue the multidisciplinary study of the most recent sediments covering the last 2000 years (i.e. Golman 4 core that could allow for the deciphering of sedimentary and geochemical processes occurring at the lake-water interface),
(2) To implement pollen analysis that can provide insights on vegetation evolution. Indeed, although the analysis of biomarkers has already been undertaken in other parts of the basin, the study of pollens on our composite sequence could be quite relevant in relation to the parameters already acquired and clarify the share of human influence on the basin (landscape modification, pastoralism, etc.).

Both perspectives are linked with the human history and with environmental impacts on Lake Urmia evolution.

But according to the recent trend of climate change and the numerous studies on the Urmia Lake basin, we believe that the future of Lake Urmia is still at stake. In combination with previous studies, it is the relevance and interaction of global and regional factors, including climate change and local water management, that will determine the fate of Lake Urmia. Based on the hydrogeological balance and scientifically based future projections (modeling), water management already undertaken through a series of local agricultural water savings for the restoration and conservation of Lake Urmia, immediate water savings as well as optimization of agricultural practices.

References

Abbaspour, M., Nazaridoust, A., 2007. Determination of environmental water requirements of Lake Urmia, Iran: an ecological approach. International Journal of Environmental Studies 64, 161-169.

AghaKouchak, A., Norouzi, H., Madani, K., Mirchi, A., Azarderakhsh, M., Nazemi, A., Nasrollahi, N., Farahmand, A., Mehran, A., Hasanzadeh, E., 2015. Aral Sea syndrome desiccates Lake Urmia: Call for action. Journal of Great Lakes Research 41, 307-311.

Ahmady-Birgani, H., Ravan, P., Schlosser, J.S., Cuevas-Robles, A., AzadiAghdam, M., Sorooshian, A., 2020. On the chemical nature of wet deposition over a major desiccated lake: Case study for Lake Urmia basin. Atmospheric Research 234, 104762.

Al-Aasm, I.S., Taylor, B., South, B., 1990. Stable isotope analysis of multiple carbonate samples using selective acid extraction. Chemical Geology: Isotope Geoscience Section 80, 119-125.

Alijani, B., Harman, J.R., 1985. Synoptic climatology of precipitation in Iran. Annals of the Association of American Geographers 75, 404-416.

Alipour, S., 2006. Hydrogeochemistry of seasonal variation of Urmia Salt Lake, Iran. Saline systems 2, 1-19.

Alizade Govarchin Ghale, Y., Altunkaynak, A., Unal, A., 2017. Investigation Anthropogenic Impacts and Climate Factors on Drying up of Urmia Lake using Water Budget and Drought Analysis. Water Resources Management 32, 325-337.

Alizadeh-Choobari, O., Ahmadi-Givi, F., Mirzaei, N., Owlad, E., 2016. Climate change and anthropogenic impacts on the rapid shrinkage of Lake Urmia. International Journal of Climatology 36, 4276-4286.

Amiri, M., Eslamian, S., 2010. Investigation of climate change in Iran. Journal of Environmental Science Technology 3, 208-216.

Asem, A., Eimanifar, A., Djamali, M., Rios, P.D.l., Wink, M., 2014. Biodiversity of the Hypersaline Urmia Lake National Park (NW Iran). Diversity 6, 102-132.

Asem, A., Eimanifar, A., van Stappen, G., Sun, S.C., 2019. The impact of one-decade ecological disturbance on genetic changes: a study on the brine shrimp Artemia urmiana from Urmia Lake, Iran. Peerj 7.

Berberian, M., Arshadi, S., 1976. On the evidence of the youngest activity of the North Tabriz Fault and the seismicity of Tabriz city. Geol. Surv. Iran Rep 39, 397-418.

Bottema, S., 1986. A late Quaternary pollen diagram from Lake Urmia (northwestern Iran). Review of Palaeobotany and Palynology 47, 241-261.

Chaudhari, S., Felfelani, F., Shin, S., Pokhrel, Y., 2018. Climate and anthropogenic contributions to the desiccation of the second largest saline lake in the twentieth century. Journal of Hydrology 560, 342-353.

Cohen, J., Screen, J.A., Furtado, J.C., Barlow, M., Whittleston, D., Coumou, D., Francis, J., Dethloff, K., Entekhabi, D., Overland, J., 2014. Recent Arctic amplification and extreme mid-latitude weather. Nature geoscience 7, 627-637.

Coplen, T., 1995. Reporting of stable carbon, hydrogen, and oxygen isotopic abundances. Reference intercomparison materials for stable isotopes of light elements 825, 31-34.

Djamali, M., de Beaulieu, J.-L., Shah-hosseini, M., Andrieu-Ponel, V., Ponel, P., Amini, A., Akhani, H., Leroy, S.A.G., Stevens, L., Lahijani, H., Brewer, S., 2008a. A late Pleistocene long pollen record from Lake Urmia, Nw Iran. Quaternary Research 69, 413-420.

Djamali, M., Kürschner, H., Akhani, H., de Beaulieu, J.L., Amini, A., Andrieu-Ponel, V., Ponel, P., Stevens, L., 2008b. Palaeoecological significance of the spores of the liverwort Riella (Riellaceae) in a late Pleistocene long pollen record from the hypersaline Lake Urmia, NW Iran. Review of Palaeobotany and Palynology 152, 66-73.

Djamali, M., Ponel, P., Delille, T., Thiéry, A., Asem, A., Andrieu-Ponel, V., de Beaulieu, J.L., Lahijani, H., Shah-Hosseini, M., Amini, A., 2010. A 200,000-year record of the brine shrimp Artemia (Crustacea: Anostraca) remains in Lake Urmia, NW Iran. International Journal of Aquatic Science 1, 14-18.

Eimanifar, A., Mohebbi, F., 2007. Urmia Lake (Northwest Iran): a brief review. Saline Syst 3, 1-8.

Epstein, S., Graf, D.L., Degens, E.T., 1964. Oxygen isotope studies on the origin of dolomites.

Erfan, S., Rezaei, K., Lak, R., Aleali, S.M., 2017. Clay mineralogy and sediment grain-size variations as climatic signals in southern part of Urmia Lake cores, North West of Iran. Journal of Research in Biology 7, 2266-2281.

Esquevin, J., 1969. Influence de la composition chimique des illites sur leur cristallinité. Bull. Centre Rech. Pau-SNPA 3, 147-153.

Finné, M., Holmgren, K., Sundqvist, H.S., Weiberg, E., Lindblom, M., 2011. Climate in the eastern Mediterranean, and adjacent regions, during the past 6000 years–A review. Journal of archaeological science 38, 3153-3173.

Ghaheri, M., Baghal-Vayjooee, M., Naziri, J., 1999. Lake Urmia, Iran: a summary review. International Journal of Salt Lake Research 8, 19-22.

Golabian, H., 2010. Urumia Lake: Hydro-ecological stabilization and permanence, Macro-engineering seawater in unique environments. Springer, pp. 365-397.

Habibi, M., Babaeian, I., Schöner, W., 2021. Changing Causes of Drought in the Urmia Lake Basin—Increasing Influence of Evaporation and Disappearing Snow Cover. Water 13, 3273.

Hammer, U.T., 1986. Saline lake ecosystems of the world. Springer Science & Business Media.

Holtzapffel, T., 1985. Les minéraux argileux. Préparation. Analyse diffractométrique et détermination. Publication-Société géologique du Nord.

Jalili, S., Hamidi, S.A., Ghanbari, R.N., 2016. Climate variability and anthropogenic effects on Lake Urmia water level fluctuations, northwestern Iran. Hydrological Sciences Journal 61, 1759–1769.

Jalili, S., Kirchner, I., Livingstone, D.M., Morid, S., 2012. The influence of large-scale atmospheric circulation weather types on variations in the water level of Lake Urmia, Iran. International Journal of Climatology 32, 1990-1996.

Kehl, M., 2009. Quaternary climate change in Iran – the state of knowledge. Erdkunde 63, 1-17.

Kelts, K., Shahrabi, M., 1986. Holocene sedimentology of hypersaline Lake Urmia, northwestern Iran. Palaeogeography, Palaeoclimatology, Palaeoecology 54, 105-130.

Khazaei, B., Khatami, S., Alemohammad, S.H., Rashidi, L., Wu, C., Madani, K., Kalantari, Z., Destouni, G., Aghakouchak, A., 2019. Climatic or regionally induced by humans? Tracing hydro-climatic and land-use changes to better understand the Lake Urmia tragedy. Journal of Hydrology 569, 203-217.

Manaffar, R., Zare, S., Agh, N., Siyabgodsi, A., Soltanian, S., Mees, F., Sorgeloos, P., Bossier, P., Van Stappen, G., 2011. Sediment cores from Lake Urmia (Iran) suggest the inhabitation by parthenogenetic Artemia around 5,000 years ago. Hydrobiologia 671, 65-74.

Mehran, A., AghaKouchak, A., Nakhjiri, N., Stewardson, M.J., Peel, M.C., Phillips, T.J., Wada, Y., Ravalico, J.K., 2017. Compounding impacts of human-induced water stress and climate change on water availability. Scientific Reports 7, 1-9.

Messager, M.L., Lehner, B., Grill, G., Nedeva, I., Schmitt, O., 2016. Estimating the volume and age of water stored in global lakes using a geo-statistical approach. Nature communications 7, 1-11.

Micklin, P., 2007. The Aral sea disaster. Annual review of Earth planetary sciences 35, 47-72.

Mirzapour, B., Lak, R., Aleali, M., Djamali, M., Shahbazi, R., 2021a. Identifying the effects of climate changes on sedimentary environments and determining the sedimentation rate of south wetlands of Lake Urmia during Late Pleistocene and Holocene. Pollution 7, 113-127.

Mirzapour, B., Lak, R., Aleali, M., Djamali, M., Shahbazi, R., 2021b. Mineralogical reconstruction of Late Pleistocene - Holocene climate and environmental changes in southern wetlands of Lake Urmia. Geopersia 11, 205-218.

Nhu, V.H., Mohammadi, A., Shahabi, H., Shirzadi, A., Al-Ansari, N., Ahmad, B.B., Chen, W., Khodadadi, M., Ahmadi, M., Khosravi, K., Jaafari, A., Nguyen, H., 2020. Monitoring and Assessment of Water Level Fluctuations of the Lake Urmia and Its Environmental Consequences Using Multitemporal Landsat 7 ETM(+) Images. International journal of environmental research and public health 17.

Pengra, B., 2012. The drying of Iran's Lake Urmia and its environmental consequences, United Nations Environmental Programme (UNEP), Global Environmental Alert Service (GEAS) Bulletin.

Petschick, R.J.R.h., 2000. MacDiff 4.2. 2 [online] Available: http://servermac. geologie. un-frankfurt. de.

Richter, T.O., Van der Gaast, S., Koster, B., Vaars, A., Gieles, R., de Stigter, H.C., De Haas, H., van Weering, T.C., 2016. The Avaatech XRF Core Scanner: technical description and applications to NE Atlantic sediments. Geological Society, London, Special Publications 267, 39-50.

Ruddiman, W.F., 2008. Earth's Climate: past and future. Macmillan.

Schagerl, M., 2021. Saline Lakes. Encyclopedia of Inland Waters, 453-464.

Schagerl, M., Renaut, R.W., 2016. Dipping into the soda lakes of East Africa, soda lakes of East Africa. Springer, pp. 3-24.

Schulz, S., Darehshouri, S., Hassanzadeh, E., Tajrishy, M., Schuth, C., 2020. Climate change or irrigated agriculture - what drives the water level decline of Lake Urmia. Sci Rep 10, 236.

Shahrabi, M., 1981. Holocene lacustrine facies and climatic cycles in the hypersaline lake Urmieh Basin, Northwest Iran, Diplomarb. Abt. Naturwiss. ETH Zürich.

Sharifi, A., Shah-Hosseini, M., Pourmand, A., Esfahaninejad, M., Haeri-Ardakani, O., 2018. The Vanishing of Urmia Lake: a geolimnological perspective on the hydrological imbalance of the world’s second largest hypersaline lake, pp. 1-38.

Solaymani Azad, S., 2009. Evaluation de l'aléa sismique pour les villes de Téhéran, Tabriz et Zandjan dans le NW de l'Iran: approche morphotectonique et paléosismologique. Montpellier 2.

Stevens, L.R., Djamali, M., Andrieu-Ponel, V., de Beaulieu, J.L., 2012. Hydroclimatic variations over the last two glacial/interglacial cycles at Lake Urmia, Iran. Journal of Paleolimnology 47, 645-660.

Stevens, L.R., Wright, H.E., Ito, E., 2001. Proposed changes in seasonality of climate during the Lateglacial and Holocene at Lake Zeribar, Iran. The Holocene 11, 747-755.

Stuiver, M. and Reimer, P.J., 1993, Radiocarbon, 35, 215-230.

Stuiver, M. and Reimer, P.J., Reimer, R.W., 2021. CALIB Radiocarbon Calibration, URL: http://calib.

Talebi, T., Ramezani, E., Djamali, M., Lahijani, H.A.K., Naqinezhad, A., Alizadeh, K., Andrieu-Ponel, V., 2016. The Late-Holocene climate change, vegetation dynamics, lake-level changes and anthropogenic impacts in the Lake Urmia region, NW Iran. Quaternary International 408, 40-51.

Tudryn, A., Motavalli-Anbaran, S.H., Tucholka, P., Gibert-Brunet, E., Lankarani, M., Ahmady-Birgani, H., Kong, T., Noret, A., Miska, S., Massault, M., Dufaure, O., 2021. Late Quaternary environmental changes of Lake Urmia basin (NW Iran) inferred from sedimentological and magnetic records. Quaternary International 589, 83-94.

Wang, J., Song, C., Reager, J.T., Yao, F., Famiglietti, J.S., Sheng, Y., MacDonald, G.M., Brun, F., Schmied, H.M., Marston, R.A., 2018. Recent global decline in endorheic basin water storages. Nature geoscience 11, 926-932.

Wurtsbaugh, W.A., Miller, C., Null, S.E., DeRose, R.J., Wilcock, P., Hahnenberger, M., Howe, F., Moore, J., 2017. Decline of the world's saline lakes. Nature Geoscience 10, 816-821.

Yechieli, Y., Wood, W.W., 2002. Hydrogeologic processes in saline systems: playas, sabkhas, and saline lakes. Earth-Science Reviews 58, 343-365.

Zoljoodi, M., Didevarasl, A., 2014. Water-Level Fluctuations of Urmia Lake: Relationship with the Long-Term Changes of Meteorological Variables (Solutions for Water-Crisis Management in Urmia Lake Basin). Atmospheric and Climate Sciences 04, 358-368.

Appendix 1

Quaternary International 589 (2021) 83–94

Contents lists available at ScienceDirect

Quaternary International

journal homepage: www.elsevier.com/locate/quaint

Late Quaternary environmental changes of Lake Urmia basin (NW Iran) inferred from sedimentological and magnetic records

Alina Tudryn [a,*], Seyed-Hani Motavalli-Anbaran [b], Piotr Tucholka [a], Elisabeth Gibert-Brunet [a], Mohammad Lankarani [c], Hesam Ahmady-Birgani [d], Ting Kong [a], Aurélie Noret [a], Serge Miska [a], Marc Massault [a], Olivier Dufaure [a]

[a] University Paris-Saclay, CNRS, UMR 8148-GEOPS, 91405, Orsay, France
[b] Institute of Geophysics, University of Tehran, Tehran, Iran
[c] School of Geology, University-College of Science, University of Tehran, Tehran, Iran
[d] Faculty of Natural Resources, Urmia University, Urmia, Iran

ARTICLE INFO

Keywords:
Lake urmia
Late Quaternary palaeoenvironments
Water level change
Carbonates
Magnetic minerals
Electric conductivity

ABSTRACT

The ongoing changes affecting Lake Urmia (NW Iran) are revealed by the lake water level decrease (~7 m in the last 20 yr) that was attributed to natural and anthropogenic causes but the exact impact of these factors on the state of the lake is still not identified. Indeed, lack of detailed record of environmental evolution of the lake in the past limits the understanding of actual and future processes. Our project aims to obtain a high-temporal resolution record of environmental changes in the lake area for the last ~30 kyrs. Sediment cores have been obtained from the recently dried out part of the lake near Urmia City, and surface and ground waters have been measured for electric conductivity. This paper presents results of water and sediments analyses. Six ^{14}C AMS dating on organic fractions provide a chronological framework and indicate that the record covers the last ~30 cal kyr BP. During this period, evaporitic conditions were prevailing in the lake. The electric conductivity of brines from the sediment highlights changes in the lake water salinity. The data indicate a lake-level low stand at ~30 cal kyr BP that was followed by a water level rise and establishment of lacustrine conditions for the next ~9 kyr, this phase representing the highest lake level recorded since that time to date. From the LGM, the lake experienced several fluctuations of the water level. The relatively long-term lacustrine condition established during the Early Holocene before the water level decrease between ~5.5 and 4.9 cal kyr BP. Sediments from the two dry events at ~30 cal kyr BP and at 5.5–4.9 cal kyr BP are characterized by the presence of greigite, which indicates anaerobic early diagenetic conditions in the sediment.

1. Introduction

Registered in the International Ramsar Convention and National Park in NW Iran, Lake Urmia (Fig. 1) is one of the largest saline lakes in the world displaying a unique, highly valuable biodiversity (Asem et al., 2014). The lake plays a major role in creating the mild climate favouring a highly productive agriculture and brine shrimp farming, both making the region as one of the most important economical poles of Iran. However, since the end of the 1990's, Lake Urmia's water level dropped drastically, and by more than 7 m during the last 20 years (Fig. 1b) causing water hyper salinization, desertification and dust storms threatening health condition of millions of people at a regional scale (Alipour, 2006; Pengra, 2012; Ahmady-Birgani et al., 2018, 2020). Although, subjected to controversies, the water level fall has been attributed to rainfall declining by ~10% and to anthropogenic causes such as the construction of many dams on rivers feeding the lake (Fig. 1c) and intense groundwater pumping (Alipour, 2006; Pengra, 2012; Jalili et al., 2016; Sharifi et al., 2018).

Despite evident water overexploitation, the role of natural *versus* anthropogenic factors influencing the lake hydrology is still not quantified. The lack of detailed records of environmental evolution in the past limits the understanding of actual processes and the capability to develop integrated management of this water resource. As a matter of fact, the lake deposits have not been extensively explored for palaeoenvironmental reconstructions. Already existing sedimentological, geochemical and pollen studies of Pleistocene and Holocene sequences

* Corresponding author.
E-mail addresses: alina.tudryn@universite-paris-saclay.fr, alina.tudryn@u-psud.fr (A. Tudryn).

https://doi.org/10.1016/j.quaint.2021.03.024
Received 28 June 2020; Received in revised form 11 March 2021; Accepted 15 March 2021
Available online 29 March 2021

are scarce. They cover large time scale (200 kyr) with a low resolution, generally missing the Holocene (Djamali et al., 2008a, 2008b, 2010; Stevens et al., 2012) or focus on the Holocene with a low temporal resolution (Kelts and Shahrabi, 1986; Bottema, 1986), or just concern its youngest part (Talebi et al., 2015). However, all these studies show the highest amplitude lake-level variations at a glacial-interglacial time scale with a dry open mountain steppe dominating during the glacial periods and a steppe-forest environment during interglacials. An increase in tree pollens during the Holocene was recorded at the transition from Early to Mid-Holocene, at 6.5 kyr B.P., and similar to today's vegetation established. The vegetation reached its maximum destruction due to increasing human impact during the last centuries. Saline deposition seems almost continuous during the Holocene with clear water level changes but no visible total desiccation of Lake Urmia.

The Franco-Iranian project initiated by bilateral Gundishapur program (2016–2017) on Lake Urmia aims to obtain high temporal resolution records of past environmental and climate changes in the SW lake area for the Late Pleistocene and Holocene, and to identify natural and human impacts on the past hydro-environments of the lake and its catchment area. The process integrates hydrogeological, hydrogeochemical and lake sediments studies. The obtained results will be useful for the integrated approach of future Lake Urmia management and restoration of its environment, and for studies of the past climate evolution at a larger, south Eurasian scale. Indeed, the area is a place of choice being on the junction of the different air mass circulation systems from the West (Atlantic, Mediterranean and North Sea) and from the East (Siberian and Indian monsoon).

In this paper are presented the first results of water in-situ measurements (electric conductivity, pH and temperature) and measurements on five collected sediment cores. The chronological framework is based on six ^{14}C datings. The sedimentary sequence has been analyzed for water contents in sediment and corresponding relative salinity, grain size, magnetic minerals, mineralogy of bulk sediment by X-Ray diffraction (XRD) and carbonate contents and mineralogy. The goal of the study is (i) to provide the record of environmental changes in Lake Urmia basin, mainly in terms of the lake water changes for the last ~30 cal kyr BP., (ii) to complement the existing information on the evolution of the lake basin at the local scale and that of the Middle East, and (iii) to contribute to a better understanding of relation between local environment and the climate change.

2. Setting

2.1. Lake Urmia

Lake Urmia is an endorheic hypersaline lake located in a subsiding tectonic basin in NW Iran (Fig. 1). Before the recent water level fall, it was the largest lake in the region after the Caspian Sea and the second largest salt lake on Earth, and presented similar in physical, chemical and biological aspects to the Great Salt Lake in the USA (Kelts and Shahrabi, 1986). Lake Urmia was approximately 140 km long and 85 km wide, with a deeper northern basin (maximal depth of ~16 m) and shallower southern one, salinity varying between 140 and more than 220 g.L ^{1} on an annual basis, a surface area of 5000 to 6000 km^2 and a catchment area of approximately 52,500 km^2 (Sharifi et al., 2018). Although its salinity varied between 140 and more than 220 g.L^{-1} on an annual basis, the lake was geochemically homogeneous due to mixing by strong water currents, particularly during spring (Alipour, 2006; Sharifi et al., 2018). Nevertheless, Sharifi et al. (2018) show that in spring, the hydrochemistry of the southern part of the lake at the vicinity of Simineh Rud and Zarrineh Rud river mouths (Fig. 1) becomes different due to fresh water inflow to the lake, some stratification in water column was also observed (report by Azarbaidjan Regional Mining Cooperation, 1995). Lately, both basins were separated by the Kalantari causeway, an east-west dike-type highway constructed in the 1980s–1990s that stretches on 15 km across the center of the lake with a gap of ~1.5 km on

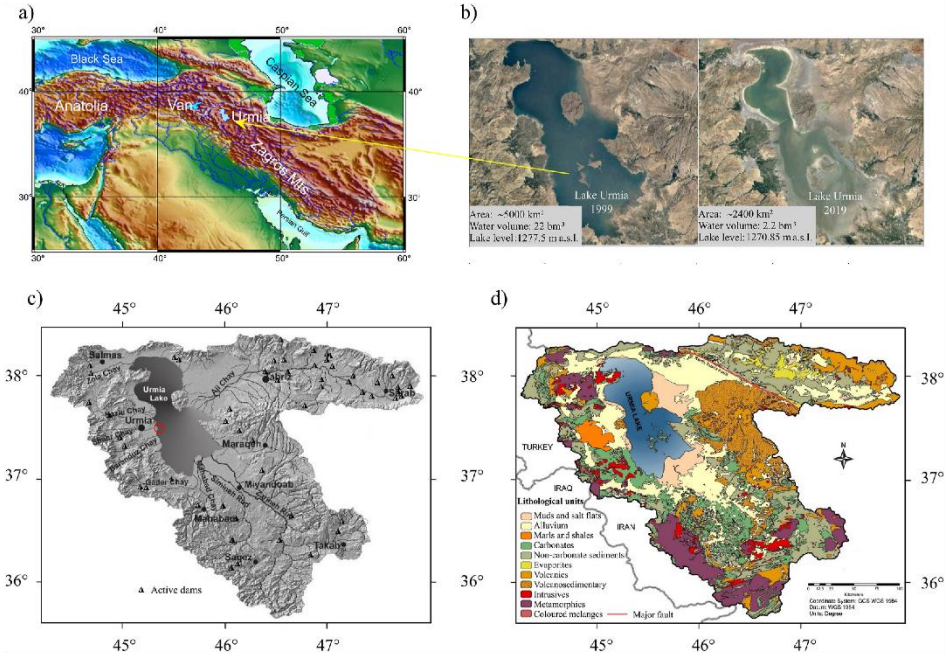

Fig. 1. Lake Urmia: a) location of the lake, b) lake in 1999 on the left and in 2019 on the right (after Ahmady-Birgani et al., 2020), c) lake's catchment area, hydrography and dams (after Sharifi et al. et al., 2018), red circle indicates coring area, d) simplified geological map of Lake Urmia catchment area (after Sharifi et al., 2018, completed with information from Geological Map of Iran, Sheet No 1 North-West Iran). (For interpretation of the references to color in this figure legend, the reader is referred to the Web version of this article.)

which a bridge was constructed (1998–2008).

The lake basin is situated in a semi-arid zone. Prevailing winds are westerlies during winter, northeasterlies during summer and strong southwesterlies during spring (Djamali et al., 2008a).

Today, the lake is supplied by direct precipitation (~300 mm.yr ^{1}), inflow from 13 permanent rivers and also from periodic discharge into the lake by seasonal rivers and creeks (Alipour, 2006). According to Kelts and Shahrabi (1986), ancient terraces show evidence of large fluctuations in lake level during Pleistocene. Historical documents and analysis of recent satellite images show fluctuations ranging from 1.0 to 3.5 m, with an estimated lowest lake level during the Little Ice Age (~XIV-XIX centuries; Kelts and Shahrabi, 1986; Alipour, 2006). Nevertheless, from its highest level in the mid-1990s (1278 m a.s.l.), the lake level has decreased by 7 m to 1271 m a.s.l. in 2010, reducing the surface of the lake from 5700 km^2 to 4610 and after that to ~2400 km^2 (Fig. 1b), resulting in the salinity increase above 300 g.L^{-1} and dramatic ecologic consequences for the lake catchment area (Alipour 2006; Asem et al., 2014).

2.2. Geological setting

Iran lies in the Alpine-Himalayan orogenic belt. The North-West of the country, where Lake Urmia is located, is a part of the Turkish–Iranian Plateau with an average altitude of around 2000 m a.s.l. and is situated in the center of the Arabian-Eurasian collision zone. The crustal deformation since the upper Miocene is dominated by N–S shortening and E-W extension (Solaymani, 2009). This resulted in faulting, seismic activities and the forming of volcanoes which are the highest mountains on the plateau. As other lakes in the area, Lake Urmia is located in a tectonic depression related to the large zones of faulting. The Tabriz fault system limits this depression to the North-East while the Sahand volcano (3695 m a.s.l.; 3rd highest volcano on the plateau), dominates the east of the lake area. About 100 km to the west of the lake lies the active Zagros thrust belt. This tectonic activity results in intense seismicity. The archives show that since 600 BC, more than 450 big earthquakes happened in the region. Recent and historic data since 858 AD record a high seismic activity in the area of Urmia, especially associated

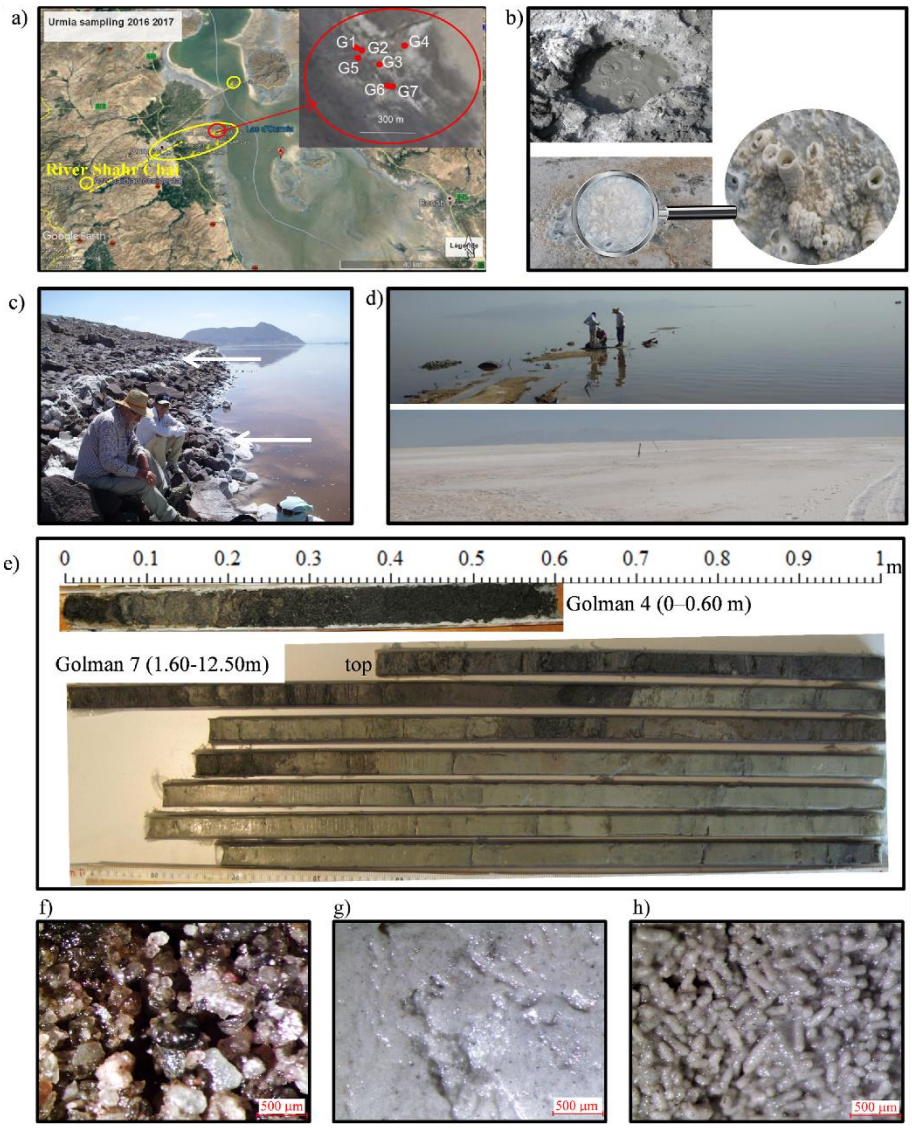

Fig. 2. Study area: a) location of coring - red circle (Golman coring sites are labeled as G and numbers from G1 to G7), surface- and groundwater sampling - yellow circles and line, Google Earth map (geographic coordinates for all sites are indicated on Table 1), b) upper picture - gas and under-pressure mud rising up along the borehole Golman 2 after coring in May 2016, lower pictures - crystallization of muddy salt on the borehole surface, September 2017, c) lake water sampling site at the foot of the east-west dike-type highway in May 2016; arrows indicate two salty lines that highlight water level change in spring 2016, d) lake water sampling site close to the coring Golman 4: above - May 2016, below - September 2017, e) sediment cores Golman 4 and Golman 7 obtained from recently dried out part of the lake, optical microphotograph from core Golman 7 for: f) sand at 12.49 m depth, g) fine silty, carbonate rich sediment at 10.66 m depth, h) fecal pellet rich sediment at 3.62 m depth. (For interpretation of the references to color in this figure legend, the reader is referred to the Web version of this article.)

with the Tabriz fault. In this time span, at least 12 major catastrophic earthquakes destroyed the town of Tabriz (Solaymani 2009).

Lake Urmia catchment area is composed of rocks ranging from Precambrian to Quaternary. Volcanic and volcano-sedimentary formations dominate in the east and northeast of the catchment area. Intrusive rocks, as well as metamorphic rocks, are mainly found in the south, west, and northwest (Fig. 1d). Carbonate sedimentary units are mainly found in southern and western parts, and evaporite sedimentary units are present to the northeast of the watershed area. According to Kelts and Shahrabi (1986), Lake Urmia sediments are principally composed of detrital particles of varying grain size (clays-silts-sand-gravel), chemically precipitated aragonite, shrimp fecal pellet sands, thin aragonite crusts, ooids, and evaporites.

3. Materials and methods

3.1. Material collection

During the fieldwork campaigns in 2016 and 2017, seven sediment cores (0.6 m–14.2 m long) have been drilled out from recently dried out part of the lake near the city of Urmia. Water sampling and in-situ measurements were performed on the lake and river as well as on groundwater (Fig. 2, Table 1). The shortest 0.6 m long core Golman 4 has been taken manually, directly to the plastic tube and close to the today's lake shoreline, for the retrieval of the lake-sediment interface. This provided a sampling of the undisturbed, continuous top sedimentary sequence of the lake. Six other cores have been taken with a mechanic corer and casing of the borehole at a distance from the today's shoreline allowing safe using of the corer. Therefore, all cores have been taken from the recently dried out lake bottom (Fig. 2a). Below the surficial crust, the uppermost sediment was soft sand-rich, and was collected either as compacted (Golman 5 and Golman 6) or incomplete sequence (Golman 3 and Golman 7). The two longest cores, *i.e.* Golman 3 and Golman 7, were empty in their middle part; too liquid, either sandy or clayish sediment being impossible to be taken out, the solid lower sequence was lightly compacted during coring. When coring reached the depth of ~5 m, H_2S gas began bubbling (Fig. 2b). Corings Golman 3 and Golman 7 were stopped when pressurized water with mud and gas with an intense H_2S odor rose up from the boreholes to the sediment surface. Cores Golman 1 and Golman 2 were very incomplete and only small and disturbed fragments of sediment were collected but not analyzed. In-situ parameters such as temperature, pH and conductivity have been measured on surface water (Lake Urmia and Shahr Chai River at several locations) and on groundwater (rising-up muddy water from coring wells as well as 6 surrounding wells distributed according to a potential flow line). Samples from all water points have been taken for chemical (major anions and cations) and stable isotope analyses ($^{18}O_{watcr}$, $^{2}H_{water}$). During fieldworks, we observed important lake water level changes both in seasonal and annual scale. In May 2016, the lake water level decreased by ~1 m just due to the end of the winter/spring intense rainfall period and the increase of the evaporation rate (Fig. 2c). In September of 2017, the water level had lowered so that the lake water sampling sites from 2016 had become dry (Fig. 2d).

3.2. Methods

On the field temperature, water electric conductivity and pH of were measured with WTW 3210 conductivity meter and pH-meter respectively. Sediment characteristics have been obtained through laboratory analyses as presented below.

3.2.1. Measurements of water contents and salinity

Water content in sediment was obtained through the difference of weighted humid, immediately taken from fresh core sediment samples and the same samples weighted after drying for 3 day at 80 °C in a laboratory oven.

The salinity measurements had to take into account the fact that salt is present both in the solution and in the solid part of sediment. Therefore, the total salt content was obtained by washing the salts from the dried out sediments three times with distilled water and weighting the remaining dried fraction. The difference between the mass of dried out sample and the mass of the dried out sample after washing gives the quantity of salt which we normalized by the water content. In the following equation, the numerator corresponds to the quantity of solu-

Table 1
Location of sampling sites, both water and sediment in the vicinity of Urmia City, and the results of in situ measurements of pH, temperature and electric conductivity. Measurements of surface water, groundwater from wells and groundwater rising-up from coring well Golman 5, have been done in May 2016 or in September 2017. Measurements of groundwater rising-up from coring wells Golman 1, Golman 2 and Golman 3, have been done in May 2016 and in September 2017.

	Site name	comment on sampling	latitude	longitude	altitude	pH	temp.	conduct.
					m asl ±1 m		°C	mS.cm^{-1}
river	BARDESOOR	above dam, near Silvana City, September 2017	37°26′14.592″	44°49′26.92″	1606	8.38	13.8	0.299
SHAHR CHAI	SHAH 1	Urmia City, May 2016	37°31′35.24″	45°02′50.53″	1354	8.41	14.2	0.249
	SHAH 2	between Urmia City and the river outlet, May 2016	37°33′16.93″	45°16′12.26″	1276	7.83	16.9	3.40
well	SALEH ABAD	in "Amir's garden", September 2017	37°31′16.626″	45°10′52.812″	1294	7.28	14.2	0.884
	KESH 1	Kesh Tiban, September 2017	37°32′28.788″	45°14′07.224″	1281	8.13	19.9	0.575
	GOLMAN 0	close to GOLMAN coring site, May 2016	37°35′15.44″	45°15′19.70″	1278	7.35	15.3	1.18
	HAJILAR 1	1st after sampling SHAH 2, May 2016	37°33′22.00″	45°16′17.51″	1277	6.29	15.4	3.12
	HAJILAR 2a	Double well - large well, May 2016	37°33′09.07″	45°16′08.95″	1276	6.12	15.1	12.22
	HAJILAR 2 b	Double well - small well, May 2016	37°33′09.07″	45°16′08.95″	1276	6.63	16.2	12.39
coring well	GOLMAN 1	9 m deep, May 2016	37°35′35.86″	45°16′26.77″	1270	6.84	29.6	222.0
	GOLMAN 1	9 m deep, September 2017	37°35′35.86″	45°16′26.77″	1270	6.05	30.1	227.0
	GOLMAN 2	14 m deep, May 2016	37°35′35.09″	45°16′28.60″	1270	5.80	29.2	219.0
	GOLMAN 2	14 m deep, September 2017	37°35′35.09″	45°16′28.60″	1270	5.80	31.8	217.0
	GOLMAN 5	5.25 m deep, September 2017	37°35′33.4″	45°16′27.6″	1270	6.04	26.6	222.0
	GOLMAN 3	14.2 m deep, presurized water, May 2016	37°35′33.09″	45°16′31.20″	1270	6.48	25.0	141.1
	GOLMAN 3	14.2 m deep, inside coring tubing, May 2016	37°35′33.09″	45°16′31.20″	1270	6.35	20.2	147.1
	GOLMAN 3	14.2 m deep, inside coring tubing, September 2017	37°35′33.09″	45°16′31.20″	1270	6.24	18.9	142.0
	GOLMAN 3	14.2 m deep, outside tubing, May 2016	37°35′33.09″	45°16′31.20″	1270	6.61	27.5	158.8
	GOLMAN 3	14.2 m deep, outside tubing, September 2017	37°35′33.09″	45°16′31.20″	1270	6.29	19.1	140.0
	GOLMAN 4	0.6 m deep	37°35′37.31″	45°16′38.38″	1270			
	GOLMAN 6	8 m deep	37°35′28.854″	45°16′33.834″	1270			
	GOLMAN 7	12.5 m deep, presurized water	37°35′28.746″	45°16′33.75″	1270			
lake	GOLMAN	near coring GOLMAN 4, May 2016	37°35′37.31″	45°16′38.38″	1270	8.02	21.3	207.0
	Dam-bridge1	N side of the causeway, May 2016	37°46′31.62″	45°19′47.04″	1270	7.53	27.9	190.2
tap water	Urmia city	May 2016						0.323

ble material washed out of the sediment and the denominator to the water content.

$$S = \frac{W_{Bdry} - W_{WOdry}}{W_B - W_{Bdry}}$$

where:

W_B, mass of bulk fresh sample
W_{WOdry}, mass of washed out and dried sample
W_{Bdry}, mass of bulk dried sample

3.2.2. Grain size, carbonate content and bulk sediment mineralogy

Grain-size distribution measurements of organic matter and carbonate-free sediment were carried out on a Malvern Mastersizer 2000 apparatus. The carbonate content ($CaCO_3 + MgCO_3$) was obtained using a Mélières mono-calcimeter: 100 mg of dried and homogenized bulk sample was reacted with 3 mL of 1 N hydrochloric acid (HCl) in a closed vessel and the resulting pressure of CO_2 gas was measured by a manometer. The calibration was conducted by reacting 100 mg of pure calcium carbonate as standard with 3 mL of 1 N HCl, implying a 1 atm pressure read on the manometer. These measurements were done at GEOPS laboratory (University Paris-Saclay, Orsay, France).

Identification of mineralogical components was performed by XRD on the whole sediment powder at GEOPS laboratory. The XRD pattern was recorded with an X'Pert Pro PANalytical diffractometer, Cu-Kα source, 2Θ range 5°–80°, 4-h runs and identification phase using PANalytical HighScore software and crystallography open database following the laboratory routine at GEOPS laboratory. Specific carbonates were identified through analyzes during 45 min with 2Θ range 24°–33°. The semi-quantification of the carbonates was obtained by normalizing the areas of the diffraction peaks with respect to the percentage of areas coming from an equi-mass mixture of carbonates, then setting the ratio of the normalized area of each carbonate to the sum of the standardized areas.

3.2.3. Magnetic parameters

Low field magnetic susceptibility (χ) was measured with a Bartington Instruments MS-2 susceptibility bridge directly on the sediment surface of the half-core. The thermomagnetic behavior of the bulk sediment samples was determined on a horizontal force translation Curie balance. Analyses were performed under normal air atmosphere, in a magnetic field of 0.375 T and with a linear temperature increase of 10 °C min^{-1}. The XRD pattern of the magnetic extracts was recorded with an X'Pert Pro PANalytical diffractometer, Cu-Kα source, 8-h runs and Panalytical Low background substrate, *i.e.* a 32-mm silicon single crystal substrate for measurements of small amounts of sample material that require low background intensity. Magnetic susceptibility, XRD and Curie balance experiments were carried out at GEOPS laboratory. Magnetic hysteresis measurements of the bulk sediment samples were performed at room temperature with an alternating gradient magnetometer (AGM 2900 – Micromag) at LSCE laboratory, CNRS/CEA at Gif-sur-Yvette, France. A peak - applied field of 1 T was used for hysteresis measurements. The values of saturation magnetization (Ms), saturation remanent magnetization (Mrs) and coercive force (Bc) were estimated from the slope corrected hysteresis loop. Parameters Ms and Mrs were mass normalized. Coercivity of remanence (Bcr) was obtained by step-wise application of back-fields to remove the saturation remanence.

Magnetic susceptibility was measured on all sediment cores while other parameters were measured systematically on core Golman 7 and additionally in some other sequences.

3.2.4. Radiochronology

Six AMS datings have been done on organic fractions (diffused organic matter and hand-picked charcoal).

Each fraction has been submitted to the standard chemical protocol for AMS analyses for organic remains, *i.e.* cleaning treatment via successive hydrochloric acid/sodium hydroxide/hydrochloric acid baths respectively, and rinsed with deionized water up to neutral pH. Samples were then gently dried at 60 °C overnight. CO_2 gas was obtained according to the AMS protocol of burning at 860 °C for 30 min, under vacuum, in presence of a mixing of copper(II)-oxide/copper(III)-oxide and silver thread. Then, AMS-^{14}C targets were obtained by graphitization of the CO_2 gas on powdered iron with hydrogen at 650 °C for 100 min, and graphite compression under analytical plots. Aliquot of the CO_2 gas was then used for associated ^{13}C measurement. These were measured on a VG SIRA 10 IRMS (Isotope Ratio Mass Spectrometer) at the GEOPS laboratory. Graphite sources were also prepared at GEOPS laboratory, and counted by the accelerator mass spectrometer at LSCE laboratory (ECHoMICADAS facility, France).

Analytical uncertainties, including laboratory errors, are ±0.1‰ for δ^{13}C and between 0.5 and 0.8 pMC for ^{14}C activity. All the dates are converted to calendar ages according to the revised calibration program CALIB 7.10 (Reimer et al., 2013, Execute Version 1.10html 2020).

4. Results

4.1. Water measurements

Results of in-situ measured electric conductivity (EC), pH and temperature on surface water and groundwater are presented in Table 1. At a first glance, data from both field campaigns (May 2016 and September 2017) show that lake's basin waters present a wide range of EC values, varying from 0.25 mS cm^{-1} for the Shahr Chai River far from the lake, to 227 mS cm^{-1} for the coring muds. Considering the flow line of the Shahr Chai River, the conductivity and temperature remain low close to its source above the dam and in the city of Urmia (0.30 and 0.25 mS cm^{-1}, ~14 °C, respectively) and increase between the city and the river outlet (3.40 mS cm^{-1} and ~17 °C respectively) while pH shows opposite trend. Groundwater from wells presents temperatures varying between 14.2 and 19.9 °C, pH evolving from 6.1 to 8.1 and conductivity comprised between 0.58 and 12.39 mS cm^{-1}. Lake surface water temperature reaches even 28 °C; its conductivity and pH are respectively ~200 mS cm^{-1} and 7.5 to 8.0, depending of the measurement site. Groundwater (more or less muddy) rising up to the sediment surface in the boreholes, presents very high conductivity and relatively low pH.

Water samples taken upstream from the town of Urmia show EC values in agreement with drinking water standards, either of good quality (until 0.80 mS cm^{-1}) or acceptable (up to 2.50 mS cm^{-1} at a maximum; Drinking Water Directive of European Commission, 2021). About 10 km downstream from Urmia city and towards the lake, EC values evolve from 3.40 mS cm^{-1} to 207.0 mS cm^{-1}, indicating an increase in the evaporation rate. Three of the wells used for drinking water until 2016 are now abandoned. Lake Urmia brine's points out a measured conductivity of 207 mS cm^{-1}. Such a high conductivity has been also found in waters rising up from coring wells, and likely representing captive brines they are markers of ancient lake state. In a pH vs EC diagram (Fig. 3a), two different clusters of conductivity are highlighted and in relation with the two captive brines values. The first (A) displays mean value of 221 ± 4 mS cm^{-1} and characterizes waters rising steeply from intermediated depths during coring (below 4.5–5 m), while the second one (B), with mean value of 146 ± 8 mS cm^{-1}, characterizes highly pressurized water coming from the bottom of core Golman 3. Similar pressurized water was coming from the bottom of the Golman 7 coring tube but unfortunately could not be sampled.

4.2. Sedimentary record

Sediments obtained from cores Golman consist of fine – silty/clayish and sandy deposits with some gravel levels and some sections that contain ooids and fecal pellets of the brine shrimp *Artemia urmiana* (Fig. 2e–h). The shortest core Golman 4 (Figs. 2e and 4a) presents

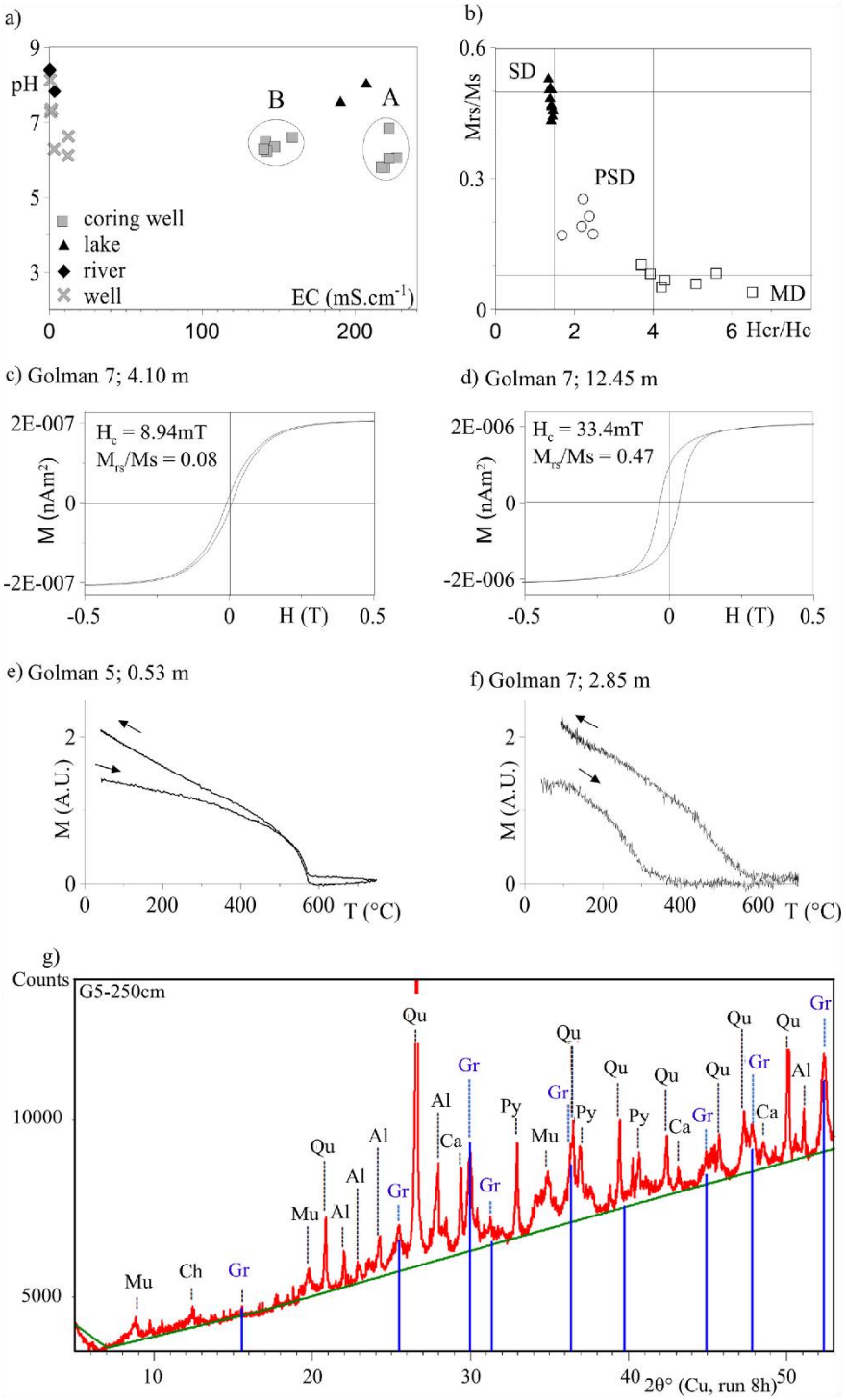

Fig. 3. Parameters measured on water (in-situ measurements) and on sediments: a) electric conductivity *versus* pH for water samples from Lake Urmia, River Shahr Chai, wells between Urmia City and the lake border, coring wells, A – captive brine rising-up from intermediated depth (below 4.5–5 m), B – captive brine rising-up from the bottom of the core, b) classification of magnetic minerals in terms of magnetization and coercivity ratios after Day et al. (1977); sediments from cores Golman 5 and Golman 7: black triangles - SD magnetic grain sizes, circles - PSD-like and squares - MD magnetic grain, typical magnetic hysteresis loop of bulk sediment samples with c) MD magnetic grain sizes and d) SD magnetic grain sizes, typical thermomagnetic curve of bulk sediment samples with e) magnetite and f) greigite, g) X-ray diffraction pattern obtained for magnetic extract from core Golman 5 at 2.50 m depth with mean identified minerals: greigite (Gr), which is highlighted by vertical blue lines, albite (Al), calcite (Ca), chlorite (Ch), muscovite (Mu), pyrite (Py), quartz (Qu). (For interpretation of the references to color in this figure legend, the reader is referred to the Web version of this article.)

continuous sequence of top 0.60 m sediment. The cores Golman 3 and Golman 7 are, respectively, 14.20 and 12.50 m long sequences but present an important gap in the middle due to the liquidity of sandy and clayish/silty sediments (Fig. 4c and d). Sedimentary sequences of both cores display the same pattern although Golman 7 is more complete. Sequences of the cores Golman 5 and Golman 6 (3 and 8 m long, respectively, Fig. 4b, e), are in good agreement with those for cores Golman 4 and Golman 7. Moreover, the section between 8.00 and 4.20

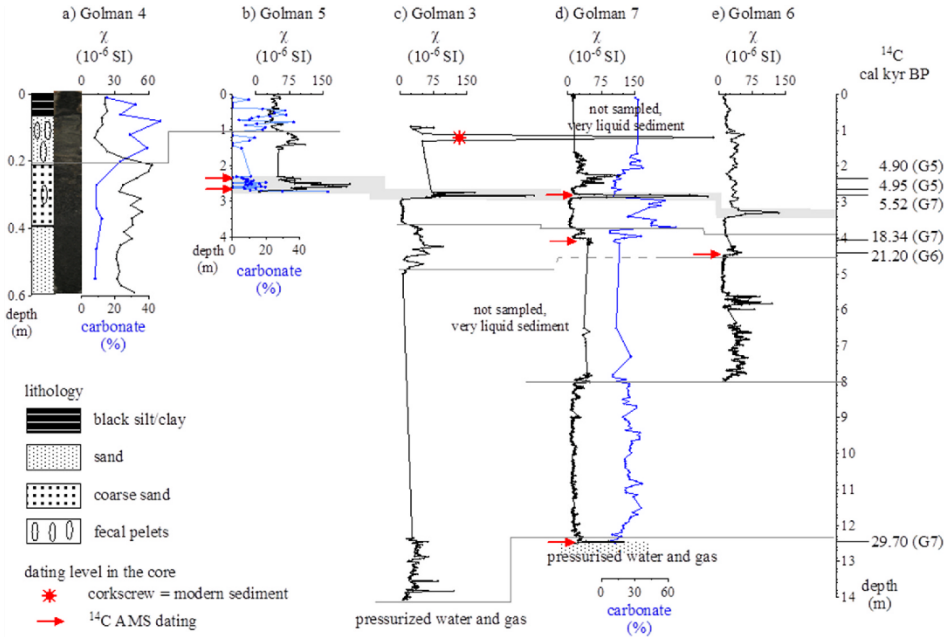

Fig. 4. Down-core variation in magnetic susceptibility (black line) and carbonate contents (blue line) for cores: a) Golman 4, b) Golman 5, c) Golman 3, d) Golman 7 and e) Golman 6. Depth scale for core Golman 4 is different from common scale for others cores. Lithological log is presented for core Golman 4. ^{14}C dating for cores Golman 5 (G5), Golman 6 (G6) and Golman 7 (G7) are indicated on the common depth scale and as red arrows on corresponding cores. Grey band that shows increased magnetic susceptibility through cores, and grey solid and dashed lines indicate correlations between different cores. Sequences compressed during coring are presented after linear decompression. (For interpretation of the references to color in this figure legend, the reader is referred to the Web version of this article.)

m depth of the core Golman 6 completes the gap in the core Golman 7 (Fig. 4f and g), both cores have been collected very close to each other (Fig. 2a).

4.2.1. Correlations between cores, reconstruction of the composite core and lithology

The reconstruction of a complete sequence is based on detailed sedimentary description, carbonate contents and magnetic susceptibility, and the correlation, in a reliable and precise way, of characteristic levels between different cores. This composite sequence will allow us to integrate, and therefore to interpret, all the data on a single stratigraphic sequence.

In the uppermost part of the lake sedimentary sequence (i.e. core Golman 4; Fig. 4a), the magnetic susceptibility relatively high in the lower, sandy part of the section, decreases at ~0.20 m depth and stays low to the top in fine grained sediments while the carbonate contents present the inverse evolution, i.e. low at the beginning and increasing up to ~0.20 m depth. Similar pattern and change are recorded in the core Golman 5 at ~1 m depth (Fig. 4b). Above this change, in both cores, fecal pellets are very abundant. Magnetic susceptibility of the upper sediment in cores Golman 3, 5, 6 and 7, shows varying values with an increase at the depth of ~3 m that is easily correlated between all cores and is highlighted by a grey band on Fig. 4. This increase corresponds to the presence of blackish sandy sediment rich in organic remains, and to the decrease of the carbonate contents recorded in cores Golman 5 and Golman 7 (Fig. 4b, d). Three different changes of the magnetic susceptibility below this section are indicated by grey lines on Fig. 4. The increased magnetic susceptibility recorded in the lowermost sediments of cores Golman 3 and Golman 7 as well as pressurized water and gas rising from the bottom to the sediment surface there, allow the correlation of both beginnings of cores. The highest value of the susceptibility was recorded at ~1 m depth in the sandy sediment of the core Golman 3. This, due to a piece of a broken corkscrew found in this level during sediment sampling, clearly indicates modern age for this sediment (Fig. 4c).

Cores Golman 7 and Golman 6 display the complete sequence of the sediment from 12.5 to 1.60 m depth. The sediment between 12.50 and 12.38 m depth is sandy (Fig. 2f) and silty. The color of the lowest, sandy ~2 cm layer is light brown while above, it is black and rich in plant remains (between 12.47 and 12.44 m) and dark grey. From 12.38 to 4.52 m depth, the sediment consists of quite soft and grey silt/clay (Fig. 2g), with some fine (~1 mm thick), dark grey sandy laminae. After a clear change at 4.52 m, the upper sediment is more complex with alternation of sands, silts and clays of different colors and some discontinuities. The 4.52–3.73 m interval presents brownish, coarse silty quite compact sediments (4.52–4.02 m), clayish/silty grey and brown deposits (4.02–3.85 m) and dark grey sand (3.85–3.73 m). Above, between 3.73 and 2.87 m depth, the sediment is quite homogeneous, made of grey fine silt and clay that is very rich in shrimp's fecal pellets (Fig. 2h). It begins as a hard 2 cm thick horizon clearly separated from lower dark grey sand, and becomes quite soft in the middle. The last few centimeters are light grey, quite dry and end sharply at 2.87 cm depth below the 8 cm thick black and sandy sediment that is rich in organic remains including plant fragments. Above, the sandy sediment, more or less dark and devoid of fecal pellets, continue until 2.20 m. The upper 2.20–1.60 m sands and silts contain varying concentrations of fecal pellets.

4.2.2. Radiochronology

Four ^{14}C AMS datings have been obtained from charcoal and two others, from organic matter (Table 2). Dating for core Golman 7 present ages of 29.70, 18.34 and 5.52 cal kyr BP at 12.46 m, 4.05 m and 2.80 m depth respectively. Two additional dating performed on core Golman 5 at 2.66 and 2.34 m depth, display ages of 4.95 and 4.90 cal kyr BP respectively. These two dated samples represent the same blackish unit with high magnetic susceptibility values as the one in recognized in core

Table 2
^{14}C AMS and δ^{13}C data for cores Golman 6 (G6), Golman 7 (G7) and Golman 5 (G5). The calibrated ages are the mean ages.

Core	Sample	Depth(m)	Analyze Nr	Nature	^{14}C Age (yr BP)	σ (yr)	Cal ^{14}C Age (cal yr BP) (*)	σ (yr)	δ^{13}C (‰ PDB)
G6	G6-4.40	4.40	I2553/B2304	OM	17561	76	21 200	210	24.20
G7	G7-S2 2.80	2.80	I2218/B2097	Charcoal	4734	22	5520	100	−26.50/-13.50
	G7-S3 4.05	4.05	I2525/B2297	OM	15 088	66	18 340	190	−25.30
	G7-S8 12.46	12.46	I2524/B2301	Charcoal	25 591	96	29 700	360	−24.60
G5	G5 2.34	2.34	I2141/B2087	Charcoal	4343	25	4900	60	−14.50
	G5 3.66	2.66	I2142/B2088	Charcoal	4394	22	4950	65	−25.50

(*) Reimer et al. (2013). IntCal13 and MARINE13 radiocarbon age calibration curves 0–50000 years cal BP. *Radiocarbon,* 55(4). https://doi.org/10.2458/azu_js_rc.55.16947.

Golman 7 at 2.80 m depth (Fig. 4). Finally, the core Golman 6 sample at 4.40 m depth indicates 21.20 cal kyr BP. This sample and the 4.05 m depth sample from the core Golman 7 belong to the same lithological unit (Fig. 4).

Although we were not able yet to determine whether the lake water is submitted to a hard water effect or not, the strong winds existing the region allow the good mixing of the lake water: in such a system, we may consider at a first glance that the lake water total dissolved inorganic carbon (TDIC) is in equilibrium with the atmospheric CO_2 (MacDonald et al., 1991; Fontes et al., 1993, 1996; Gibert et al., 1999, 2002a, 2002b; Schneider et al., 2019). However, in order to avoid as much as possible any suspicion of bias in our datings, we thus concentrate on authigenic materials (i) without any link with the carbon lake system such as charcoal, and (ii) with a high C-content for planktonic organic matter and no indication of a detrital origin (mineralogical assemblages). All the ^{14}C datings presented are thus considered as fully reliable.

All these datings are in agreement with the stratigraphy (Figs. 4 and 5). Without any information on the hydrogeochemical balance of the sub-basin of the cored sequences, the interpretation of the ^{14}C datings is only discussed within the framework of the internal consistency of the whole chronology with respect to the lithological sequences.

Moreover, the dated samples present associated ^{13}C contents ranging from −26.50 to −13.50‰ vs PDB with a majority of the samples being centered on a value of −25.2‰ vs PDB. This value highlights the predominance of a C3 vegetation over Lake Urmia catchment. The G5-2.34 sample presents a δ^{13}C value corresponding to a C4 vegetation while sample G7-S2-2.80 exhibits two distinct δ^{13}C values of −13.5 and −26.5‰ vs PDB. This latter is explained by the mixing of two fractions of micro-charcoal, one originating from C3 plants and one from C4 plants, both coexisting in the lake basin (including the lake itself, Decolas-Gros, 1985.) at the time of deposition.

4.2.3. *Sediment characteristics*

4.2.3.1. Water contents, salinity and grain size. Water contents in the sediment display values between 12 and 37% (Fig. 5c), and, as commonly seen, are likely correlated to the grain size; lower water percentages characterising sandy sediments while higher ones

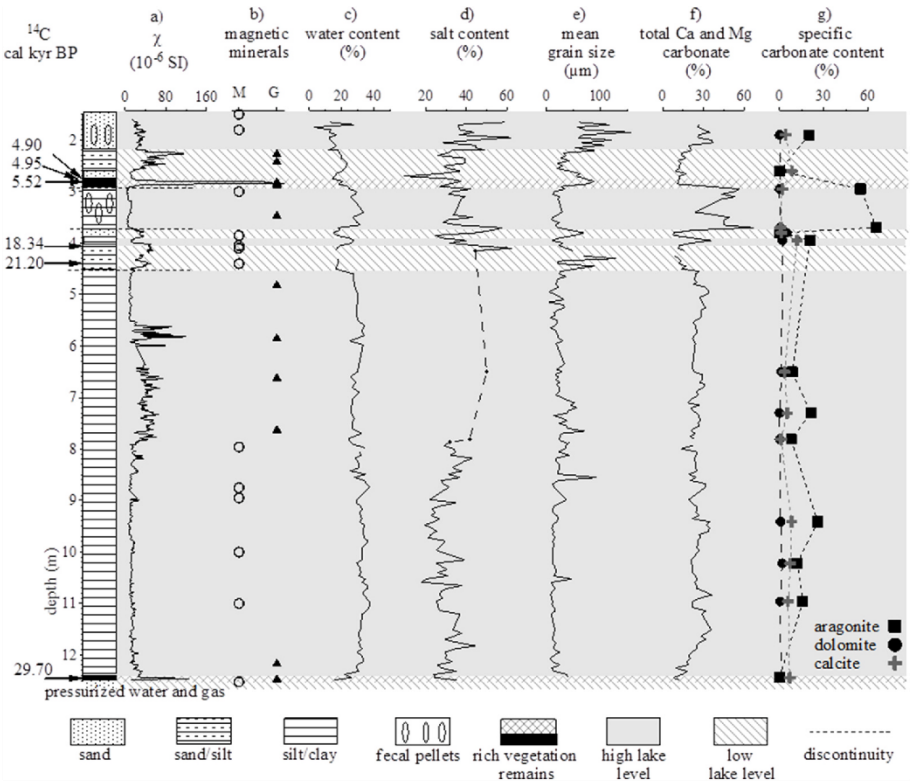

Fig. 5. Down-core variation in lithology and in a) magnetic susceptibility, b) magnetic mineralogy with M for magnetite (circle) and G for greigite (black triangle), c) water contents in the sediment, d) relative salinity on wet sediment samples, e) mean sediment grain size, f) carbonate contents, g) specific carbonate contents. ^{14}C cal BP dates are presented on the left of the depth scale. Lithology, a), b), c), e) and f) present composite data from cores Golman 6 and 7 while d) and g) present data from core Golman 7.

correspond to the silty/clayish levels. The calculated salinity indicates relative changes of the total dissolved salts present in interstitial water and sediment. The obtained pattern indicates less salinity in the lower part of the core, as well as at ~3.90 m and between 3.65 and 2.20 m depth, and higher but changing salinity elsewhere (Fig. 5d). Mean grain size values vary between ~10 and ~160 μm, with a dominant fine silty fraction in the lower part of the core and silty and sandy sediments in its upper part (Fig. 5e). High water contents and low sediment grain sizes, characterize the sequence between 12.38 and 4.52 m depth, from 4.02 to 3.85 m and between 3.73 and 2.87 m depth. These fine-grained sediments are well correlated with the relatively low water salinity. Sandy/silty sediments that are less humid are present at the bottom of the sequence at ~12.50 m depth and in some horizons of its upper 4.52 m (4.52–4.02 m, 3.85–3.73 m, 2.87–2.40 m, and 2.20–1.60 m depth).

Mineralogy and carbonate contents: XRD mineralogy on bulk sediment has been done on 41 samples from cores Golman 3 and Golman 7. Minerals that are identified in all levels are quartz, muscovite, halite and calcite, the two former representing the siliceous detrital fraction. Other carbonates such as aragonite and dolomite were identified in most of the samples. Carbonate contents vary between ~7 and ~66% of the total sediment (Fig. 5f). When existing, aragonite dominates the carbonate fraction and reaches even 65% while calcite and dolomite have low to very low contents varying between 1 and 12% for calcite and around 2% for dolomite (Fig. 5g). Aragonite can be related to the chemical or biochemical precipitation such as calcite, although calcite can be of detrital origin too. Dolomite originates from either chemical precipitation or detrital supply. Microscopic observations and analyses on Lake Urmia sediment by Kelts and Shahrabi (1986) show the predominance of aragonite in the lake sediments. These authors indicate that aragonite is present as mud and at least composes ~80% of the carbonate as shrimps fecal pellets. In our core, aragonite varies greatly and reaches even 65% between 3.73 and 2.87 m depth where shrimp's fecal pellets are particularly abundant.

Magnetic parameters: magnetic susceptibility presents clear changes with alternating sections of low and high values (Fig. 5a). The magnetic hysteresis parameters as Mrs/Ms *versus* Hcr/Hc for samples from cores Golman 7 and Golman 5 are presented in the Day diagram (Day et al., 1977, Fig. 3b). It shows the distribution of the magnetic particle grain sizes in three clusters: SD - magnetic single domain sizes with typical hysteresis loop shape as on Fig. 3d, MD - multi-domain, with hysteresis loop as on Fig. 3c, and PSD - pseudo-single-domain intermediated sizes. The PSD and MD sizes are present in the low magnetic susceptibility sediments; generally, the MD are present in sandy, while PSD, in fine silty ones. The thermomagnetic behavior of samples with PSD and MD magnetic minerals during heating shows clearly the Curie temperature at 580 °C indicating the presence of magnetite (Fe_3O_4), an iron oxide, in the sediments (Fig. 3e). For samples with SD magnetic particles that are mostly correlated with high values of magnetic susceptibility, the Curie balance experiments during heating show a magnetization decrease at ~350 °C. This process is irreversible due to the appearance of new magnetic mineral that is observed during cooling (Fig. 3f). Such a behavior is characteristic for greigite (Fe_3S_4), an iron sulfide (Jelinowska et al., 1997, 1998, 1999; Strechie et al., 2002; Tudryn et Tucholka, 2004; Tudryn et al., 2013, 2014), whose presence is confirmed through XRD analyses of total sediment and magnetic extracts for the concerned depths (Fig. 3g). Magnetic susceptibility presents a correlated pattern to the mean grain size and anti-correlated ones to the carbonates and water contents with however, some independent peaks at sandy/silty depths of ~12.45 m and at ~2.80 m, and larger, silty/clayish section between 8 and 5.5 m depth (Fig. 5). The considered sandy/silty sediment is black and rich in vegetation remains with numerous pieces of wood while silty/clayish section is grey. In sediments characterized by low magnetic susceptibility values, the magnetic hysteresis parameters and Curie balance experiments allowed the identification of low contents of MD and PSD magnetite (squares and circles on Fig. 3b and circles on Fig. 5b) that is of detrital origin while in sections with high magnetic susceptibility, SD greigite appears (black triangles on Figs. 3b and 5b). Greigite is an iron sulfide of early diagenetic origin: it is an intermediated mineral in the authigenesis of the pyrite during the bacterial degradation of the organic matter in the anoxic, sulfate-reducing zone of the sediment or water, where the S/Fe ratio is too low to complete the pyritisation process (Berner, 1980; Curtis, 1987). The presence of greigite is surprising in such a saline environment as Lake Urmia, where sulfate ions are abundant in water. Nevertheless, greigite is well known from other hypersaline lakes as Manas in China (Jelinowska et al., 1995; Tudryn et al., 2010), Dead Sea (Frank et al., 2007) and salt marshes (Cutter and Velinsky, 1987). The presence of greigite in such environments is related to the fresh water supply, high organic matter content or, if methane is present in the environment, an anaerobic oxidation of methane by sulfate reduction (either bacterial or not bacterial; *e.g.* Avrahamov et al., 2014; Neretin et al., 2004). As in Lake Urmia, early diagenetic greigite was often associated with black sediment that is rich in plant fragments including pieces of wood (at depths of ~12.45 m and ~2.80 m), it is related to the bacterial degradation of the organic matter in the anoxic, sulfate-reducing zone rather than to methane oxidation.

5. Discussion

As indicated by all our proxies and during all the time covering the sedimentary sequence, the detrital minerals such as quartz and muscovite have been supplied to the lake and evaporitic conditions, with saline waters and precipitation of halite, were prevailing in the Lake Urmia. The electric conductivity of two-captured brines at different depths during coring highlights changes of its salinity in the past.

The sequence starts with sandy deposits indicating either a high-energy transport related to the fluvial activity of River Shahr Chai or a low water level at the place of coring. The light brown color of the sand and the presence of detrital magnetite (that is MD and in low contents) highlight well oxygenated conditions during the sedimentation. In these deposits, pressurized gas and brine are captured. The brine shows lower electric conductivity than today's lake waters and thus, less water salinity. A few centimeters above the bottom of the core, at ~30 cal kyr BP (12.46 cm depth), the deposits become black, silty, with some calcite and dolomite but without aragonite. They are rich in authigenic greigite and plant remains that, according to $\delta^{13}C$ (Table 2), are identified as C3 plants. The former iron sulfide indicates the anoxic and sulfate reducing conditions within the sediment. The high content of organic material here could reflect an increased input of organic detritus through the river, nevertheless the decreased grain size of the sediment and its bad oxygenation suggest the development of a salt marsh with high biological productivity rather than a high river activity. Such a start of the sedimentary sequence reflects quite low lake water level, without lacustrine or very shallow condition in the coring area (Fig. 5). The above ~8 m thick sequence between 12.38 and 4.52 m depth is quite homogeneous, grey and with high water content. The fine-grained sediment indicates that it was deposited in low energy transport conditions. In this section, carbonate contents reach values of ~20–30%. Some 2–3% of carbonates, either calcite or dolomite, can be of detrital origin according to the distribution of carbonate rocks in the River Shahr Chai catchment area (Fig. 1d). Nevertheless, most of the carbonates are authigenic or bio-mediated as evidenced by the dominance of aragonite mud in the carbonate fraction. According to Kelts and Shahrabi (1986), precipitation of aragonite rather than calcite is a function of the high Mg/Ca molar ratio. Relatively low pore-water salinity values suggest less saline conditions than in the upper part of the sediment. All parameters provide a coherent indication of higher water level than in the beginning of the sequence, and high enough to show clearly lacustrine conditions at the coring site. The magnetic fraction of this sediment is dominated by detrital, PSD magnetite in its lower part until ~8 m depth, and by greigite above. Greigite indicates early diagenetic, sulfate reducing processes in anoxic sediment and possibly bad ventilation of

the bottom water, in good agreement with high lake level. The presence of magnetite could be interpreted as indicating the good ventilation of the basin during its deposition (between 12.38 and 8.00 m), as at the beginning of the sequence at 12.50 m depth where light brown sand with MD magnetite is present and the PSD magnetite here could reflect the different source of the detrital material. Nevertheless, quite homogeneous conditions recorded between 12.38 m and 4.52 m, grey color of the sediment and greigite present above 8.00 m (Figs. 2g and 5) suggest rather anoxic early diagenetic conditions in the magnetite bearing sediments. These conditions without sulfate reduction allowing the iron sulfides precipitation, could favor bacterial reduction of iron oxydes (Curtis, 1987) that resulted in the decrease of their grain size from MD to PSD without their complete dissolution.

These data indicate thus Lake's Urmia low stand at ~30 cal kyr BP. Afterwards the lake level increased and stayed high, probably the highest recorded since that time until today. According to the ^{14}C dating, it finished before 21.20 cal kyr BP (Fig. 5). Djamali et al. (2008a) proposed a high lake water level during the last glacial period while Stevens et al. (2012) indicated a clearly arid climate at Urmia at that time associated to a low lake level and no establishment of a perennial saline lake until ~ 14 kyr. A high stand during the considered part of the glacial period is reported in the region from other lakes such as Lake Zeribar (Wasylikowa et al., 2006) and Lake Van (Kuzucuoglu et al., 2010).

The pattern of all parameters displays several changes in the upper part of the sequence and discontinuities are observed (Fig. 5). It starts, between 4.52 and 4.05 m depth, with water content decreased, brown sandy/silty low-carbonated sediments that contain MD magnetite, and relatively high salinity probably highlighting a low lake level and well oxygenated environment. According to ^{14}C dating, this low lake stand is recorded between 21.2 and 18.3 cal kyr BP and corresponds to the Last Glacial Maximum (LGM). After that, short-time lacustrine conditions indicated by fine sediment grain sizes, decreased water salinity and increased carbonate contents including aragonite mud (up to 20%) were identified between 4.02 and 3.85 m depth before a lowering between the depths of 3.85–3.73 m marked by increased sediment grain sizes and water salinity, and decreased carbonate contents without aragonite. The presence of MD magnetite indicates well oxygenated environment. The re-establishment of clear lacustrine conditions between 3.73 and 2.87 m depth were recorded by fine-grained sediments, carbonate-rich fraction with very high contents of aragonite and abundance of shrimp fecal pellets (Fig. 2h). The presence of some gregite and PSD magnetite, suggest bad ventilation of the bottom water. The beginning and end of this section are marked by sharp change in the lithology, grain size, magnetic susceptibility, carbonate contents and mineralogy. Its lower limit highlighted by the ~2 cm thick dried grey sediment, as well as its upper part clearly indicate drying up, and both limits suggest discontinuities in the sedimentation. Above 2.87 m and until ~2.2 m depth, dark sandy and silty sediment with low carbonate contents but without aragonite was deposited. Between 2.87 and 2.77 m depth, it is black and particularly rich in organic remains and greigite. According to the radiocarbon data of this black sediment, this episode started at ~5.5 cal kyr BP and lasted until at least ~4.9 cal kyr BP. This sediment suggests similar lake low stand to that recorded at the beginning of the sequence *i.e.* at ~30 cal kyr BP, without lacustrine or very shallow condition in the coring site. Moreover, the dated samples exhibit two distinct δ^{13}C values of −26.5, −25.50‰ and of −13.5, −14.50‰ vs PDB (Table 2), the first originating from C3 plants and the second from C4 plants, both coexisting on the watershed at the time of deposition. We observed that the C4 vegetation episode that seems to have lasted at least 600 years, between 5.5 and 4.9 cal kyr BP likely indicates a warmer and drier episode. The latest recorded sandy sediment rich in shrimp fecal pellets (2.20–1.60 m), reflects a lacustrine episode with River's Shahr Chai high energy transport at the place of the coring site. Today, the downstream electric conductivity measurements of River Shahr Chai and of lake water indicate an increase in the evaporation rate with its very high values for the lake. These results are in good agreement with our first hydrogeochemical results on the water samples (E. Gibert-Brunet, pers. comm., Kong et al., 2019). According to these results, including rivers and surrounding wells, the lake is fed not only by direct precipitations and inflow of rivers, but also by groundwater discharge. This present-day discharge has very likely evolved over time in relation with the lake level and could have been more important during the first phases of lake level drop.

According to ^{14}C dates, Lake Urmia evolution from the LGM until today was characterized by lake level fluctuations with three high and three low stands recorded at the coring site (Fig. 5). Kelts and Shahrabi (1986) identified, in the ~4 m thick sedimentary sequence from South Lake Urmia basin, three lacustrine high stands that they named "Aragonite-Pellet-Mud" (APM) and two low ones stamped "Playa-Lake-Mud" (PL). Authors highlighted the lack of readily dateable material in their study, but proposed ~9–7.5 kyr BP for the lake high stand APM-2. This Early Holocene timing is in good agreement with the relatively long-term lacustrine conditions we recorded before ~5.5 cal kyr BP. Previous study by Stevens and coauthors (2012) in the eastern part of Lake Urmia described dry condition during the Late Pleistocene with a short-term lacustrine episode at ~14 kyr, drying out probably in phase with the Younger Dryas and no re-establishment of lacustrine conditions until ~ 10 kyr. Holocene reconstructions by Sharifi (2018) suggested wet Early Holocene and frequent dry episodes during Mid to Late Holocene.

Contrary to the lacustrine records from Zagros Mountains (lakes Zeribar, Mirabad, Dasht-e Arjan) that indicate dry conditions and low lake levels during the Early Holocene (Stevens et al., 2006; Wasylikowa et al., 2006; Aubert et al., 2019), clearly lacustrine conditions dominated in Lake Urmia at that time. Such wetter conditions than those prevailing in the Zagros area, as well as changing ones during the Late Holocene, are in good agreement with data from Lake's Neor area, located in the NW Iran (Sharifi et al., 2015; Aubert et al., 2017).

Transition from Early to Late Holocene in Lake Urmia, was marked by a low lake level and thus dry conditions between ~5.5 and ~4.9 cal kyr BP. Such a dry event was identified during broadly the same time in Zagros Mountains (Stevens et al., 2006) and in Anatolia (Fontugne et al., 1999). It is probably linked to the drought event recorded at 5.2 kyr BP that was evidenced in the Soreq speleothem record (Bar-Matthews et al., 1997) and in many others sites (see in Staubwasser et Weiss, 2006). Jones and co-authors (2013) pointed out the scarcity of information and the problems with identification and timespan of this event in Iran; the complex interplay between natural conditions and humans during much of the Holocene in Iran makes this information difficult to obtain.

6. Conclusion

The sediment cores collected from the SW part of Lake Urmia close to the city of Urmia represent a Late Pleistocene and Holocene record of the paleohydrological evolution of the lake.

Our proxies indicate that during the whole deposition period of the sedimentary sequence, the detrital minerals, such as quartz and muscovite, have been supplied to the lake. Aragonite (if present in the sediment) dominated the carbonate fraction and evaporitic conditions with saline waters and precipitation of halite, were prevailing in the lake.

Our established timescale is based on 6 reliable ^{14}C datings that give chronological anchors for the presented data. A low stand of the lake was identified at about ~30 cal kyr BP (and even drying out at the coring site) and followed by a water level rise leading to establishment of lacustrine conditions, with probably the highest water level from that time until today. According to the ^{14}C dating, the water level decreased prior to the LGM. Lake evolution from the LGM until today was characterized by several changes of the water level with clearly lacustrine conditions and lake low stands. Between ~5.5 and 4.9 cal kyr BP, the lake experienced low stand and even drying out at the coring site. Just

before this, during the Early Holocene, relatively long-term lacustrine conditions were established.

Sediments from two dry events at the coring site recorded at ~30 and at 5.5–4.9 cal kyr BP are characterized by high contents of authigenic greigite associated to the organic matter rich environment. Elsewhere, in sandy sediments, low contents of MD detrital magnetite are present while in fine grained ones, PSD magnetite or greigite dominate. These changes of the magnetic mineralogy reflect differences in the oxygenation state of lake sediment and water.

Our work has allowed presenting a Late Pleistocene and Holocene record of the paleohydrological evolution of Lake Urmia based on the valuable material collected, including sediments and water. Those first results open a wide possibility for further analysis and crosschecking, associated to the strengthening of the ^{14}C chronology to establish a high temporal resolution of the lake evolution. The pluridisciplinary study of Lake Urmia basin will enable to extend the discussion on environmental changes to the regional scale.

Declaration of competing interest

The authors declare that they have no known competing financial interests or personal relationships that could have appeared to influence the work reported in this paper.

Acknowledgement

This work was supported by the French-Iranian project Gundishapur (Project N° 35633ZB), the Center for International Scientific Studies and Collaboration (CISSC, Iran), French Embassy in Iran, TelluS Program of CNRS/INSU (France), and China Scholarship Council (CSC) for one of the coauthors PhD fellowship. We thank Kuadio A., Yilmaz N., Chanon C., Coulibaly S., Belarb S., Convard de Prolles A., Lezeau G. and Randrianarivélo C., students from Paris Sud University who contributed to this work during their Licence and Master traineeship.

References

Ahmady-Birgani, H., Ravan, P., Schlosser, J.S., Cuevas-Robles, A., AzadiAghdam, M., Sorooshian, A., 2020. On the chemical nature of wet deposition over a major desiccated lake: case study for Lake Urmia basin. Atmos. Res. 234, 104762.

Ahmady-Birgani, H., Agahi, E., Ahmadi, S.J., Efranian, M., 2018. Sediment source fingerprinting of the Lake Urmia sand dunes. Sci. Rep. https://doi.org/10.1038/s41598-017-18027-0.

Alipour, S., 2006. Hydrogeochemistry of seasonal variation of Urmia salt lake, Iran. Saline Syst. 2, 9. https://doi.org/10.1186/1746-1448-2-9, 2006.

Asem, A., Eimanifar, A., Djamali, M., De los Rios, P., Wink, M., 2014. Biodiversity of the hypersaline Urmia lake national Park (NW Iran). Diversity 6, 102–132.

Aubert, C., Brisset, B., Djamali, M., Sharifi, A., Ponel, Ph., Gambin, B., Akbari Azirani, T., Guibal, F., Lahijani, H., Naderi-Beni, A., de Beaulieu, J.L., Pourmand, A., Andrieu-Ponel, V., Thiéry, A., Gandouin, E., 2017. Late Glacial and Early Holocene hydroclimate variability in northwest Iran (Talesh Mountains) inferred from chironomid and pollen analysis. Journal of Paleolimnology 58 (2), 151–167. Springer Verlag, 2017.

Aubert, C., Djamali, M., Jones, M., Lahijani, H., Marriner, N., Naderi-Beni, A., Sharifi, A., Ponel, Ph, Gandouin, G., 2019. A major hydrobiological change in Dasht-e Arjan Wetland (southwestern Iran) during the Late Glacial – early Holocene transition revealed by subfossil chironomids. Canadian journal of earth sciences, National Research Council Canada 56 (8), 848–856.

Avrahamov, N., Antler, G., Yechieli, Y., Gavrieli, I., Loye, B., Saxton, M., Turchyn, A.V., Sivan, O., 2014. Anaerobic oxidation of methane by sulfate in hypersaline groundwater of the Dead Sea aquifer. Geobiology 12, 511–528.

Azarbaidjan Regional Mining Cooperation, 1995. Report on the Hydrochemistry of Urmia Lake.

Bar-Matthews, M., Ayalon, A., Kaufman, A., 1997. Late quaternary paleoclimate in the eastern Mediterranean region from stable isotope analysis of speleothems at Soreq Cave, Israel. Quat. Res. 47, 155–168.

Berner, R.A., 1980. Early Diagenesis: a Theoretical Approach. Princeton University Press, Princeton, 1980.

Bottema, S., 1986. A late Quaternary pollen diagram from lake Urmia (Northwestern Iran). Rev. Palaeobot. Palynol. 47, 241–261.

Curtis, C., 1987. Mineralogical consequences of organic matter degradation in sediments: inorganic/organic diagenesis. In: Legget, J.K., Zuffa, G.G. (Eds.), Marine Clastic Sedimentology. Graham and Trotman, London, pp. 108–123.

Cutter, G.A., Velinsky, D.J., 1987. Temporal variation of sedimentary sulfur in a Delaware salt marsh. Mar. Chem. 23, 311–327.

Day, R., Fuller, M., Schmidt, V.A., 1977. Hysteresis properties of titanomagnetites: grain-size and compositional dependence. Phys. Earth Planet. In. 13, 260–267.

Decolas-Gros, C., 1985. La fixation du carbone inorganique par le phytoplancton marin : données bibliographiques sur les carboxylases et le rapport isotopique 13C/12C. Vie Milieu 35 (1), 33–41, 1985.

Djamali, M., de Beaulieu, J.-L., Shah-Hosseini, M., Andrieu-Ponel, V., Ponel, P.H., Amini, A., Akhani, H., Leroy, S.A.G., Stevens, L., Lahijani, H., Brewer, S., 2008a. A late Pleistocene long pollen record from Lake Urmia, NW Iran. Quat. Res. 69, 413–420.

Djamali, M., Kürschner, H., Akhani, H., de Beaulieu, J.L., Amini, A., Andrieu-Ponel, V., Ponel, P., Stevens, L., 2008b. Palaeoecological significance of the spores of the liverwort Riella (Riellaceae) in a late Pleistocene long pollen record from the hypersaline Lake Urmia, NWIran. Rev. Palaeobot. Palynol. 152, 66–73.

Djamali, M., Ponel, Ph, Delille, T., Thiéry, A., Asem, A., Andrieu-Ponel, V., de Beaulieu, J., Lahijani, H., Shah-Hosseini, M., Amini, A., Stevens, L., 2010. A 200,000-year record of Artemia remains (Crustacea, Anostraca) in Lake Urmia, NW Iran. Int. J. Aquat. Sci. 1, 14–18.

Fontes, J.Ch, Mélières, F., Gibert, E., Liu, Qing, Gasse, F., 1993. Stable isotope and radiocarbon balances of two Tibetan lakes (Sumxi Co and Longmu Co) from 13,000 yr B.P. Quat. Sci. Rev. 12, 875–887.

Fontes, J.Ch, Gasse, F., Gibert, E., 1996. Holocene environmental changes in Bangong basin (western Tibet). Part 1 : modern setting, mineralogy, stable isotope of carbonates and radiometric chronology. Palaeoclim., Palaeogeog., Palaeoecol. 120, 25–47.

Fontugne, M., Kuzucuoglu, C., Karabiyikoglu, M., Hatté, C., Pastre, J.-F., 1999. From Pleniglacial to Holocene: a 14C chronostratigraphy ofenvironmental changes in the Konya plain, Turkey. Quat. Sci. Rev. 18, 573–59.

Frank, U., Nowaczyk, N.R., Negendank, J.F.W., 2007. Rock magnetism of greigite bearing sediments from the Dead Sea,Israel, Geophys. J. Intell. 168, 921–934.

Gibert, E., Travi, Y., Massault, M., Chernet, T., Barbecot, F., Laggoun-Defarge, F., 1999. Comparison between carbonate and organic AMS 14C ages in Lake Abiyata sediments (Ethiopia): hydrochemistry and palaeoenvironmental implications. Radiocarbon 41 (3), 251–266.

Gibert, E., Bergonzini, L., Massault, M., Williamson, D., 2002a. AMS-14C chronology of continuous deposits from a crater lake (Lake Massoko, Tanzania): modern water balance and environmental implications. Palaeoclim., Palaeogeog., Palaeoecol. 187, 307–322.

Gibert, E., Travi, Y., Massault, M., Tiercelin, J.-J., Chernet, T., 2002b. AMS-14C chronology of a lacustrine sequence from Lake Langano (Ethiopia): correction and validation steps in relation with volcanism influence, and lake water and carbon balances. Radiocarbon 44, 75–92.

Jalili, S., Hamidi, S.A., Ghanba, R.N., 2016. Climate variability and anthropogenic effects on Lake Urmia water levelfluctuations, northwestern Iran. Hydrol. Sci. J. https://doi.org/10.1080/02626667.2015.1036757.

Jelinowska, A., Tucholka, P., Gasse, F., Fontes, J.Ch, 1995. Mineral magnetic record of environment in late Pleistocene and Holocene sediments, lake Manas, Xinjiang, China. Geophys. Res. Lett. 8, 953–956.

Jelinowska, A., Tucholka, P., Wiçckowski, K., 1997. Magnetic properties of sediments in a Polish lake: evidence of a relation between rock-magnetic properties and environmetal changes in Late Pleistocene and Holocene sediments. Geophys. J. Int. 129, 727–736.

Jelinowska, A., Tucholka, P., Guichard, F., Lefèvre, I., Badaut-Trauth, D., Chalié, F., Gasse, F., Tribovillard, N., Desprairies, A., 1998. Mineral magnetic study of late quaternary south Caspian Sea sediments: palaeoenvironmental implications. Geophys. J. Int. 133, 499–509.

Jelinowska, A., Tucholka, P., Badau-Trauth, D., 1999. Magnetic mineral variations of South Caspian Sea sediments at laminac scale. Phys. Chem. Earth 24 (9), 823–828.

Jones, M., Djamali, M., Stevens, L., Heyvaert, V., Askari, H., Noorollahi, D., Weeks, L., 2013. Mid-Holocene environmental and climatic change in Iran. In: Petrie, C.A (Ed.), Book: Ancient Iran and its Neighbours: Local Developments and Long-Range Interactions in the 4th Millennium BC, Chapter: 1. British Institute for Persian Studies Series, Edition. Publisher: Oxbow books.

Kelts, K., Shahrabi, M., 1986. Holocene sedimentology of hypersaline lake Urmia, NW Iran. Palaeogeogr., Palaeoclim.,Palaeoecol. 54, 105–130.

Kong, T., Tudryn, A., Gibert-Brunet, E., Motavalli-Anbaran, S.-H., Tucholka, P., Lankarani, M., Ahmady-Birgani, H., Noret, A., Massault, M., Miska, S., 2019. Late Quaternary Climate and Environment Reconstruction of Lake Urmia Basin (Iran). Inqua Congress, Dublin, Ireland. Dublin 25-31 july.

Kuzucuoglu, C., Christol, A., Mouralis, D., Dog, A.F., Akköprü, E., Fort, M., Brunstein, D., Zorer, H., Fontugne, M., Karabiyikog, M., Scaillet, S., Reyss, J.L., Guillou, H., 2010. Formation of the upper Pleistocene terraces of lake van (Turkey). J. Quat. Sci. 25 (7), 1124–1137.

MacDonald, G.M., Beukens, R.P., Kieser, W.E., 1991. Radiocarbon dating of limnic sediments: a comparative analysis and discussion. Ecology 72 (3), 1150–1155.

Neretin, L., Böttcher, M.L., Jorgensen, B.B., Volkov, I.I., Lüschen, H., Hilgenfeldt, K., 2004. Pyritization processes and greigite formation in the advancing sulfidization front in the upper Pleistocene sediments of the Black Sea. Geochem. Cosmochim. Acta 68 (9), 2081–2093.

Pengra, B., 2012. The Drying of Iran's Lake Urmia and its Environmental Consequences. UNEP Global Environment Alert Service (GEAS).

Reimer, P.J., Bard, E., Bayliss, A., Beck, J.W., Blackwell, P.G., Bronk Ramsey, C., Buck, C. E., Cheng, H., Edwards, R.L., Friedrich, M., Grootes, P.M., Guilderson, T.P., Haflidason, H., Hajdas, I., Hatté, C., Heaton, T.J., Hogg, A.G., Hughen, K.A., Kaiser, K.F., Kromer, B., Manning, S.W., Niu, M., Reimer, R.W., Richards, D.A., Scott, E.M., Southon, J.R., Turney, C.S.M., van der Plicht, J., 2013. IntCal13 and

Appendix 1

MARINE13 radiocarbon age calibration curves 0-50000 years cal BP. Radiocarbon 55 (4). https://doi.org/10.2458/azu_js_rc.55.16947.

Schneider, L., Pain, C.F., Haberle, S., Blong, R., Alloway, B.V., Fallon, S.J., Hope, G., Zawadzki, A., Heijnis, H., 2019. Evaluating the radiocarbon reservoir effect in lake Kutubu, Papua New Guinea. Radiocarbon 61 (1), 287–308.

Sharifi, A., Pourmand, A., Canuel, E.A., Ferer-Tyler, E., Peterson, L.C., Aichner, B., Feakins, S.J., Daryaee, T., Djamali, M., Beni, A.N., Lahijani, H.A.K., Swart, P.K., 2015. Abrupt climate variability since the last deglaciation based on a high-resolution, multi-proxy peat record from NW Iran: the hand that rocked the Cradle of Civilization? Quat. Sci. Rev. 123, 215–230.

Sharifi, A., Shah-Hosseini, M., Pourmand, A., Esfahanincjad, M., Hacri-Ardakani, O., 2018. The Vanishing of Urmia Lake: A Geolimnological Perspective on the Hydrological Imbalance of the World's Second Largest Hypersaline Lake. The Handbook of Environmental Chemistry, Springer, Berlin, Heidelberg. https://doi.org/10.1007/698_2018_359.

Sharifi, A., 2018. The Urmia lake environmental crisis man vs. Climate. In: The 3rd International Geosciences Congress of Iran, 26/02/2018, Tehran.

Solaymani, S., 2009. Evaluation de l'aléa sismique pour les villes de Téhéran, Tabriz et Zandjan dans le NW de l'Iran. Approche morphotectonique et paléosismologique. Tectonique. Université Montpellier 2 Sciences et Techniques du Languedoc, 2009.

Staubwasser, M., Weiss, H., 2006. Holocene climate and cultural evolution in late prehistoric-early historic West Asia. Quat. Res. 66, 372–387.

Stevens, L.R., Ito, E., Schwalb, A., Wright Jr., H.E., 2006. Timing of atmospheric precipitation in the Zagros Mountains inferred from a multi-proxy record from Lake Mirabad, Iran. Quat. Res. 66, 494–500.

Stevens, L., Djamali, M., Andrieu-Ponel, V., de Beaulieu, J., 2012. Hydroclimatic variations over the last two climatic cycles at Lake Urmia, Iran. J. Paleolimnol. 47, 645–660.

Strechie, C., André, F., Jelinowska, A., Tucholka, P., Guichard, F., Lericolais, G., Panin, N., 2002. Magnetic mineral as indicators of major environmental change in Holocene Black sea sediments: preliminary results. Phys. Chem. Earth 27, 1363–1370.

Talebi, T., Ramezani, E., Djamali, M., Lahijani, H.A.K., Naqinezhad, A., Alizadeh, K., Andrieu-Ponel, V., 2015. The Late-Holocene climate change, vegetation dynamics, lake-level changes and anthropogenic impacts in the Lake Urmia region, NW Iran. Quat. Int. https://doi.org/10.1016/j.quaint.2015.11.070.

Tudryn, A., Tucholka, P., 2004. Magnetic monitoring of thermal alteration for natural pyrite and greigite. Acta Geoph. Polon. 52 (4), 509–520.

Tudryn, A., Tucholka, P., Gibert, E., Gasse, F., Wie, K., 2010. A late Pleistocene and Holocene mineral magnetic record from sediments of lake Aibi, Dzungaria basin, NW China. J. Paleolimnol. 44 (1), 109–121.

Tudryn, A., Chalié, F., Lavrushin, YuA., Antipov, M.P., Spiridonova, E.A., Lavrushin, V., Tucholka, P., Leroy, S.A.G., 2013. Late quaternary Caspian Sea environment: late Khazarian and early Khvalynian transgressions from the lower reaches of the Volga river. Quat. Int. 292, 193–204.

Tudryn, A., Giannesini, P.J., Guichard, F., Badaut-Trauth, D., Tucholka, P., Boomer, I., 2014. The role of iron minerals in laminae formation in Late Pleistocene sediments of the Caspian Sea. Quat. Int. 345, 68–76.

Wasylikowa, K., Witkowski, A., Walanus, A., Hutorowicz, A., Alexandrowich, S.W., Langner, J.J., 2006. Palaeolimnology of lake Zeribar, Iran, and its climatic implications. Quat. Res. 66, 477–493.

Appendix 2

Salt lake's sedimentation and water dynamics impacts on past environmental reconstruction

Elisabeth GIBERT-BRUNET [1,*], Alina TUDRYN [1], Ting KONG [1], Piotr TUCHOLKA [2], Aurélie NORET [1], Seyed-Hani MOTAVALLI-ANBARAN [3], Mohammad LANKARANI [4], Hesam AHMADY-BIRGANI [5], Serge MISKA [1]

[1] University Paris-Saclay, CNRS, UMR 8148-GEOPS, 91405, Orsay, France

[2] Warsaw University, Department of Geology, Warsaw, Poland

[3] Institute of Geophysics, University of Tehran, Tehran, Iran

[4] School of Geology, University-College of Science, University of Tehran, Tehran, Iran

[5] Faculty of Natural Resources, Urmia University, Urmia, Iran

[*] *Corresponding author*

Submitted to Nature Comm;

Introduction

Since some decades, an overall decrease in surface, even salty, water resources, especially in the semi-arid and arid regions of the world, may be both the precursor sign of decrease in groundwater recharge, originating from either the impact of climatic evolution going toward a different repartition of rainfalls and evapotranspiration indices, and/or the increasing fingerprint of anthropogenic activities through both inadequate use of water, extensive pumping, or even population increase in areas already under pressure for fresh water resources (e.g. Wurtsbaugh et al., 2017; Wang et al., 2018).

In salt lake's basins, groundwater is of utmost importance for the maintenance of the lake level as well as for all the activities of the eco-hydrosystems on the watershed (Great Salt Lake USA, Australia, etc.; eg Ashraf et al., 2017). However, the sustainability of these systems comes from the most efficient management of groundwater, in relation to anthropic activities. As emphasized by Vaheddoost and Aksoy (2018), aquifers in saline lake basins are not easily/often studied other than by modelling, due to their very complicated structures as well as the processes they undergo (saltwater intrusion, pollution, etc.), and considering the lacustrine sedimentary deposits (degradation of lacustrine deposits) to which they may or may not be connected.

Finally, accurate comparison of paleoclimate records is essential in order to understand the timing, causality and mechanisms of past climate changes. In addition to the study of the surface-groundwater interactions in salt lake's basin, numerous studies dealt with the reconstruction of Late Quaternary environmental and climatic periods through continental archives such as lacustrine sequences, even with groundwater (eg Fontes et al. 1993, 1996; Gibert et al, 1999, 2000; Jiang et al. 2019). However, when considering lake sediments, the major point arises to define a reliable time scale of the environmental phases and more particularly, to estimate the hard water effect that could distort the radiocarbon chronology in the past. Such a situation is particularly pregnant in complex hydrogeological basins impacted by tectonics, volcanism or even hydrogeochemical processes such as in saline environments.

The salty environments or unfortunately in the process of becoming so under the effect of climate change and anthropic pressure, are essential both for the eco-hydrosystems they represent, and the societies they support. Located in the northwest of Iran, Lake Urmia is a striking example, due to its drying up, which seems to be programmed, and its economic importance for the riparian populations as well as for the preservation of ecosystems and water resources.

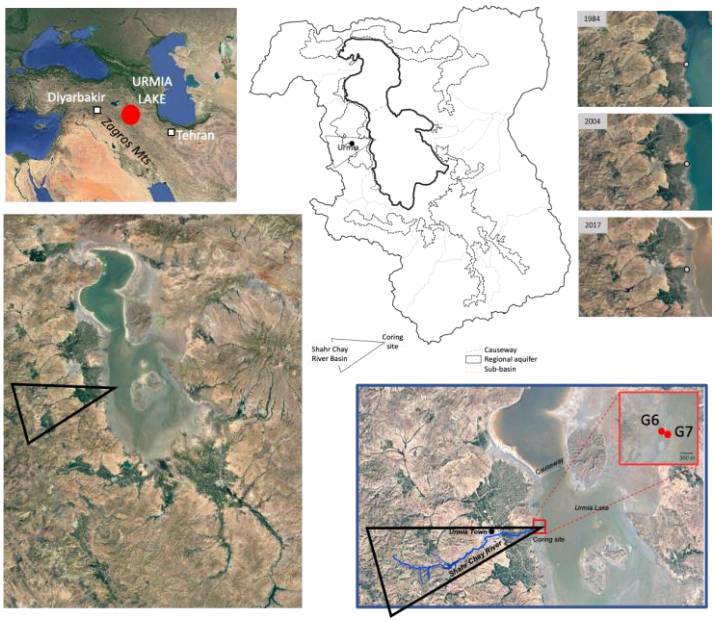

Figure 1: Lake Urmia (north-western Iran) and location of the cored sedimentary sequence at the Shahr Chay River mouth

In connection with the Lake Urmia Restoration Program (ULRP) launched in 2013 by the Iranian

administration, Lake Urmia has been extensively modelled to understand the origin of the drastic drop of more than 8 m in the lake level over the last 20 years, decreasing its surface and volume by 31% and 96% respectively, with the objective of restoring this important lake in terms of assessment and management of water resources and ecological services (eg Alipour, 2006; Marjani and Djamali, 2014; Wurtsbaugh et al., 2017; Ataie-Ashtiani 2019; Javadzadeh et al. , 2020; Parizi et al., 2022). Although controversial, this decline in water level has been attributed to the decrease in rainfall by -10% as well as to anthropogenic impacts due to (i) numerous dams built on its inflowing/feeding streams and illegal surface water abstraction from the catchment area, (ii) very numerous wells implying overuse of groundwater (excessive pumping), (iii) intensive agricultural development but without any effective irrigation techniques. The lake decline has caused soil salinization as well as an increase in dust storms, which implies a decline in ecosystem services with the effect of losses in agricultural production and massive emigration of rural communities (Ahmady-Birgani et al., 2018, 2020; Tudryn et al, 2021). It has recently been shown that even the salinity of groundwater increases due to dams on rivers, as the low flow of rivers downstream of the dams no longer feeds the lake but is subject to intense evaporation and consequent salinization of the water, which seeps very quickly into the shallow aquifer (Mosaffa et al., 2021).

As described by Sheibani et al. (2020), the lack or underestimation of field data as well as the poor consideration of socio-economic parameters do not yet allow fully convincing results to be obtained in actions to reverse the evolution of the lake (Danesh-Yazadi and Ataie-Ashtiani, 2019). Despite the obvious overexploitation of water, the respective role of natural and anthropogenic factors influencing the hydrology of the lake is not yet quantified and the dynamics of this particular “hydro-eco-system” is totally omitted in the proposed restoration efforts. Indeed, the lack of data from modern and past environments limits the understanding of the processes that determine the current state and future evolution of the lake system, which hampers the development of this integrated program of resource management and ecological restoration. Unfortunately, recent modeling in the Lake Urmia basin has shown that the increase in the frequency of dry/hot months could be 4.7 to 24.0% over the period 2060-2080, with meteorological droughts combining low precipitation and high temperatures severely impacting the ecosystem and society (Abbasian et al., 2021).

The comparison of satellite data, field monitoring and land-surface models indicated that over half of the

groundwater loss can be attributed to human impacts (Jookadi et al. 2014). Due to the lack of quantified data, several hydrological modeling based on various scenarios of water use on Lake Urmia catchment or on specific methodologies associating for example the Darcy's law coupled with an inverse modelling to parametrize the lake bed hydraulic conductivity, have highlighted that (i) the surface water baseflows feeding the lake are almost essentially support by shallow groundwater on the whole Lake Urmia catchment, (ii) the lack or underestimation of field data as well as the poor consideration of socio-economic parameters do not yet allow fully convincing results to be obtained in actions to reverse the evolution of the lake, and (iii) only the "stop-of-any-withdrawal-from-lake-Urmia" can achieve the objectives of the lake restoration program (Vaheddoost and Aksoy, 2018; Danesh-Yazadi and Ataie-Ashtiani, 2019; JICA, 2016 in Javadzadeh et al. 2020; Sheibani et al. 2020; Parizi et al. 2022). More recently, Pashaeifar et al (2021) and Mosaffa et al (2021) performed hydrochemical data on aquifers of the Azarshahr, Ajabshir and Qhabestar-Sufyan plains at the north-eastern lakeshore, identifying a Ca-Mg-CO_3-type groundwater facies and salinization due to deforestation, irrigation evaporated return flows and/or rock dissolution on the catchment. Furthermore, Mosaffa et al (2021) conclude that their stable isotope data show that there are no strong interactions between the lake water and the surrounding aquifers.

Part of the controversy regarding the understanding of the drastic decline in the level of Lake Urmia stems from potentially biased modeling of the functioning of this saline lake for which very little geochemical data are available to constrain water fluxes. We therefore present here the first isotopic data ($\delta^{18}O$, $\delta^{13}C$, $\delta^{2}H$) as well as ^{14}C activities on the present-day waters of Lake Urmia in its southwestern part (Shahr Chay River basin) and an attempt to understand the interactions between surface water and groundwater, in order to constrain and validate the radiocarbon chronology established on a composite sequence of sediment cores (Tudryn et al., 2021; Kong et al, 2022).

Joint studies of surface water, groundwater and cored sedimentary sequences

Under the support of the French-Iranian bilateral cooperation Gundishapur program, several sedimentary sequences were retrieved from the recently drained western part of salty Lake Urmia, at the Shahr Chay River mouth (Fig. 1). Several surface and groundwater samples were also collected as well as several geological

samples for the catchment (Tudryn et al., 2021; Kong et al., 2022a). The stratigraphic logs presented in Figure 2 show a succession of well-defined lacustrine deposits and at various depths, “empty” sections in which the material collected corresponds to more or less liquid muds, some of which rose to the surface by artesianism, altogether with significant outgassing with characteristic H_2S smell (and probably other gases) and with the presence of iridescence that could suggest the presence of polycyclic compounds of oil origin. Out of the 6 drillings, 5 gave rise to these upwellings of muddy water, all of them, presented outgassing of various intensity. The sludges were sampled when possible and analyzed for $^{13}C_{TDIC}$ contents and $^{14}C_{TDIC}$ activities.

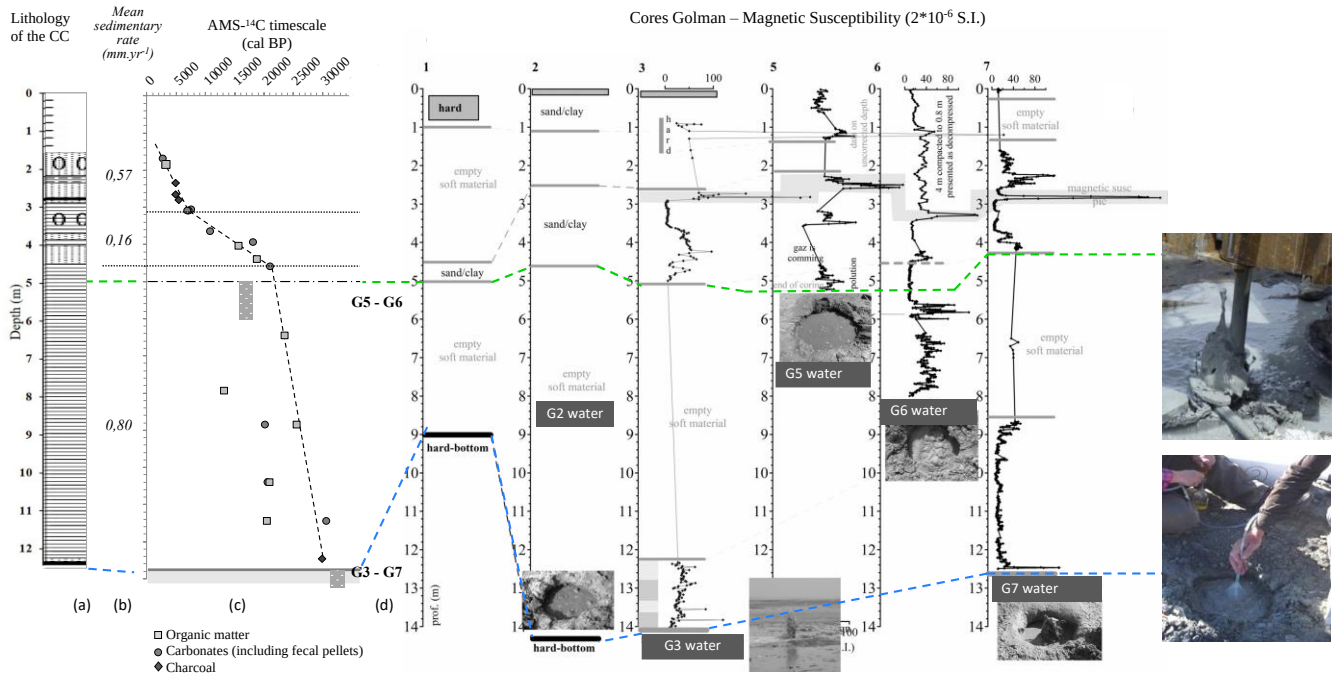

Figure 2: Lithology (a) and AMS-^{14}C chronology (b) of the Composite core (C-core) reconstructed based on the 7 boreholes drilled at the Sahar Chay River mouth during the 12016-2017 field works. The muddy waters from coring wells (c) are located with the corresponding empty sections.

Due to several empty sections, a single stratigraphic sequence (so-called “composite core”, i.e., C-core) of 10.9 m depth has been reconstructed based on available reliable data such as lithological changes, mineralogy and magnetic susceptibility, all these data allowing for the reconstruction of past environmental stages (Tudryn et al. 2021; Kong et al. 2022). Defined on AMS-^{14}C dating, two different phases have been defined (Fig. 2): (i) from 12,4 m to 4,5 m depth, phase A is characterized by a mean sedimentary rate (*msr*) of 0,16 mm.yr^{-1}, and (ii) phase B from 4,5 m to the core top present two sub-sections with *msr* of 0,80 mm.yr^{-1}.

Although many authors also highlight the exchanges between the lake and the waters of its catchment area,

they always emphasize (i) the fact that the lake is fed mainly by rivers, which are themselves supported by groundwater, and (ii) that direct flows between the lake and groundwater are low or non-existent (REFs). On the opposite, Javadzadeh et al (2020) have identified and mapped several "buffer" zones where lake water and groundwater exchange to and from the lake (Fig. 3). Our coring site is located at the mouth of the Shahr Chay River nearby of the only buffer zone west of Lake Urmia.

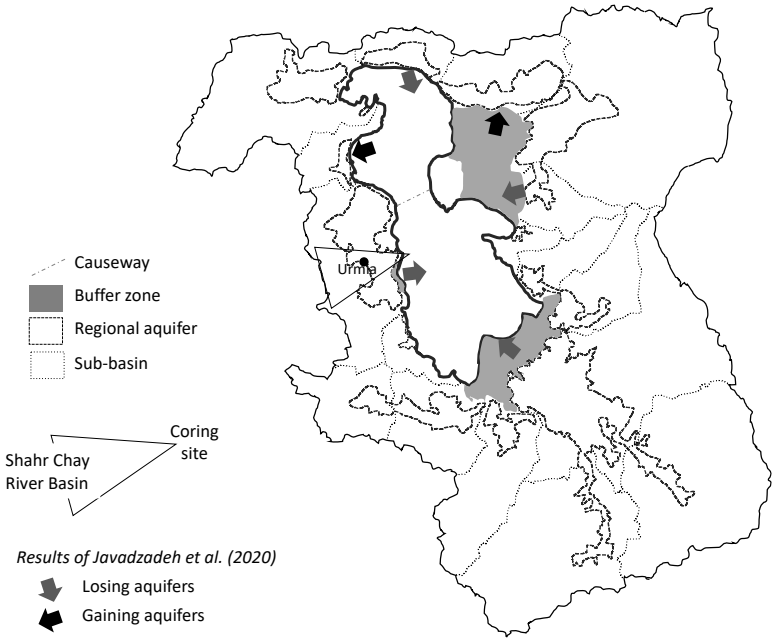

Figure 3: Location of the Golman 1 to 7 corings, in relation with the regional aquifers and buffer zones recognized by Javadzadeh et al (2020).

Stable isotopes of the modern reference system

Modern water of the Shahr Chay River basin displays values from -10,9 to +3,3 and between -71,0 and -3,3 for $\delta^{18}O$ and $\delta^{2}H$ respectively (Table 1 in Appendix 2).

In a $\delta^{18}O$ vs $\delta^{2}H$ diagram, all water samples, whether surface water or groundwater (Figure 4), show a classic pattern as they are plotted along a local precipitation line of equation interspersed between two stations located respectively at the West (Diyarbakir station, Turkey) and East (Tehran station) of the lake area (GNIP Database, IAEA/WMO, 2022). Based on the GNIP data, two different LWL can be defined for the Lake Urmia basin with deuterium excesses of +3 and +6, 5 for the two sub-groups considering only the surface water or both surface water and groundwater respectively, compared to those of Diyarbakir (+10. 6) and Tehran (+2.7). This

stable isotope distribution of modern Urmia water can likely be related to the seasonal distribution of precipitation during the year, producing a slightly different isotopic fingerprint between groundwater recharge through rainfall occurring at higher elevations in the Zagros Mountains and direct recharge on the catchment.

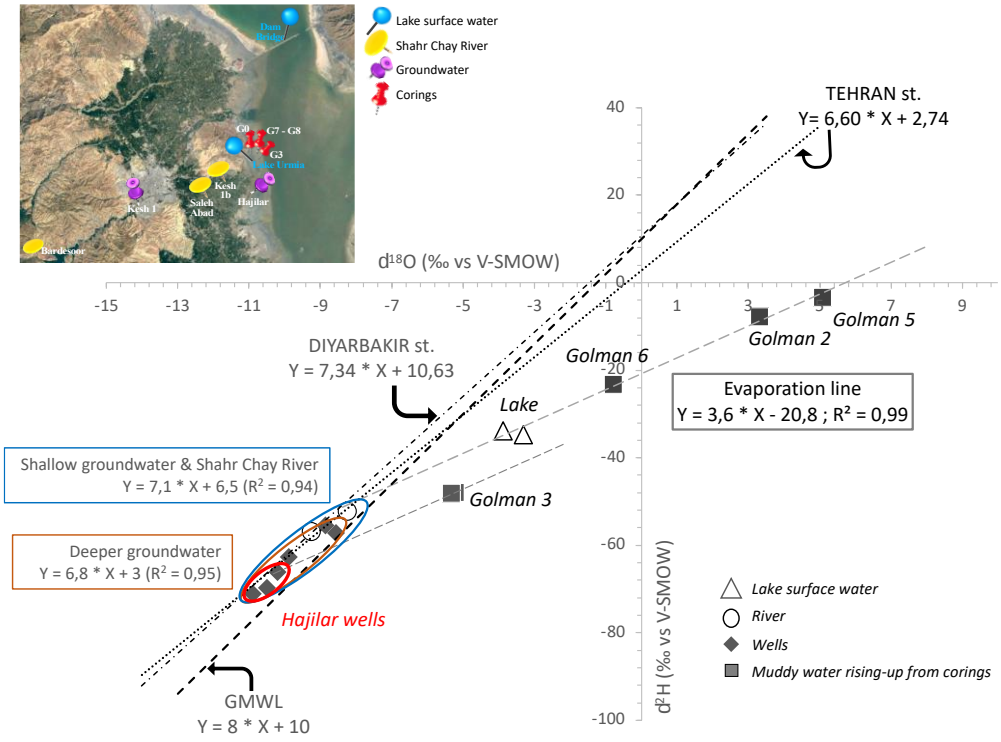

Figure 4: Stable isotope contents of surface and groundwater of Shahr Chay River basin and of muddy water retrieved form Lake Urmia corings. The MWL of Diyarbakir and Tehran stations are defined with the GNIP data (GNIP Database, IAEA/WMO, 2022).

Lake surface water samples collected in 2016 at the coring site and in the northern basin above the causeway show no difference in both conductivity values, i.e., 207 and 190 $mS.cm^{-1}$ respectively, and stable isotope compositions, i.e., -3,3/-34,6 ‰ vs V-SMOW and -3,9/-33,7 vs V-SMOW respectively. This does not confirm the fact that the causeway has been recognized as alterating both salinity (with increasing evaporation) and water fluxes between the two subbasins of Lake Urmia (Hemmati et al. 2021). Moreover, our isotopic values of the lake surface waters do not match with the data published by Mosaffa et al (2021; $\delta^{18}O$ = +1,7 and $\delta^{2}H$ = +5 ‰ vs V-SMOW) indicating a very high evaporation rate of the surface water probably due to sampling times at the beginning of September 2012 and in summer 2013.

Regarding the muddy samples recovered from the corings in relation with the modern lake, samples Golman 2, 5 6 as (Figure 2) well as that of the surface water (considering both core site and dam bridge samples; Table 1) are plotted on a clear evaporation line with a deuterium excess of -20,8 (R^2 = 0.99) intercepting the LMWL at the Shahr Chay River samples, clearly pointing out a single evaporation process from the Shahr Chay river water.

The two samples from Golman 3 (2016 and 2917) are distinct from this main isotopic relationship. Without additional geochemical elements and considering that Golman 3 and Golman 7 came up from equivalent depths during coring, we suggest the same evaporation process with a line slope of +3.6, implying that the isotopic compositions of the two G3 samples are in straight line with those of the Hajilar boreholes. This hypothesis is supported by the fact that wells in the Hajilar area showed significant outgassing associated with a strong sulfur odor during sampling, a fact that is very consistent with the outgassing of the muddy water from the Golman 3 core wells.

In a $\delta^{18}O$ vs Electric Conductivity diagram, surface and groundwater from the Shahr Chay catchment (except those from Hajilar wells) are plotted on very low $\delta^{18}O$ values and conductivities (0-20 $mS.cm^{-1}$) while the lake surface samples as well as the sludges seem to define a mixing line if we consider the reference processes described by Gat (1981) in his $\delta^{18}O$ *vs* Salinity relationship. This “mixing line” has to be considered as an artefact since it represents both evolution through depths and time and this likely confirm the unique geochemical process, i.e., evaporation, occurring in Lake Urmia sedimentation, as deduced from Figure 5.

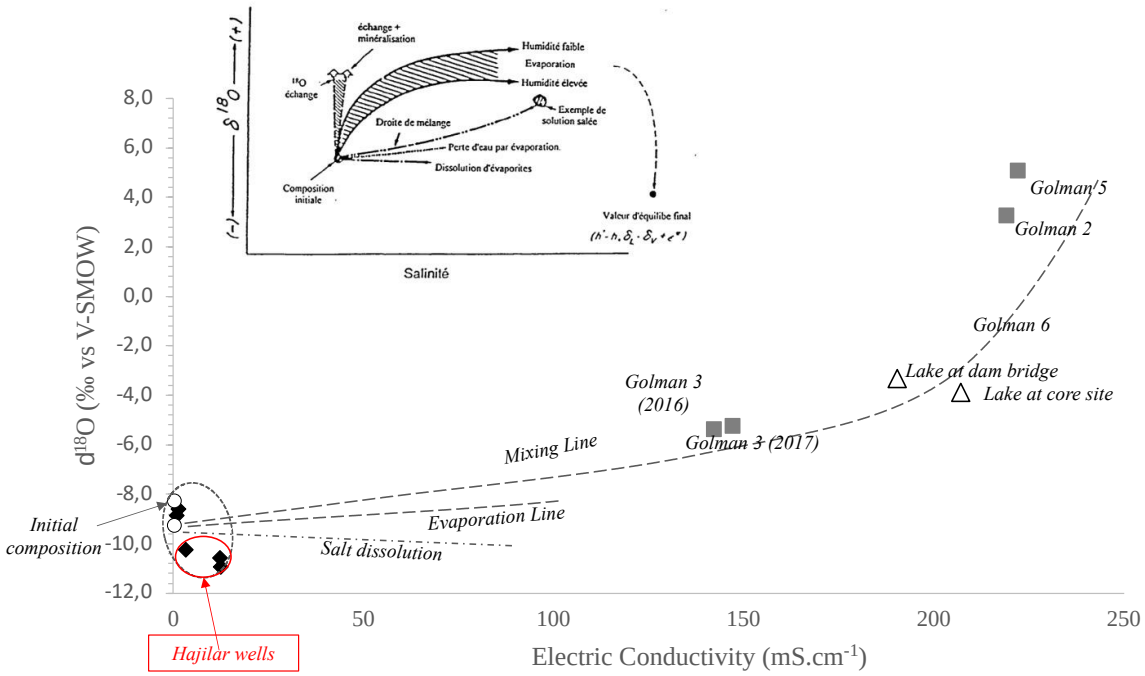

Figure 5: Diagram $\delta^{18}O$ vs Electric Conductivity – Evolution of modern water and muddy cored water with respect to the geochemical processes modified from those described by Gat (1981; in insert) for the $\delta^{18}O$ vs Salinity relationship.

Based on the stable isotope data, the muddy water in the cores can be interpreted as brines strongly evaporated from the surface water of the lake, which is in turn fed by the surface water of the Shahr River, and then trapped in the sediments. This trapping process could be observed during the 2016-2017 fieldwork when the already salty waters of the lake underwent an intense evaporation phase that produced in a few days covered with a layer of salt, itself covered a few days later with a layer of ochre-colored eolian dust.

Supported by the stable isotope contents, we can therefore consider that (i) these brines are remnants of these super-evaporated lake waters, probably formed during more arid climatic conditions associated with important aeolian inputs due to enhanced winds, and (ii) that this process of brine trapping and lens formation could have occurred very regularly over time since environmental reconstructions of Lake Urmia have shown that the lake has always been more or less salty (Tudryn et al, 2021; Kong et al., 2022a, 2022b).

Photos: Lake Urmia close to the coring site during the field works in 2016 and 2017. Note the fine film of ocher windmill dust which has settled on the salt crust and which could have acted as a waterproofing agent for the trapped brine lenses (credit: A; Tudryn).

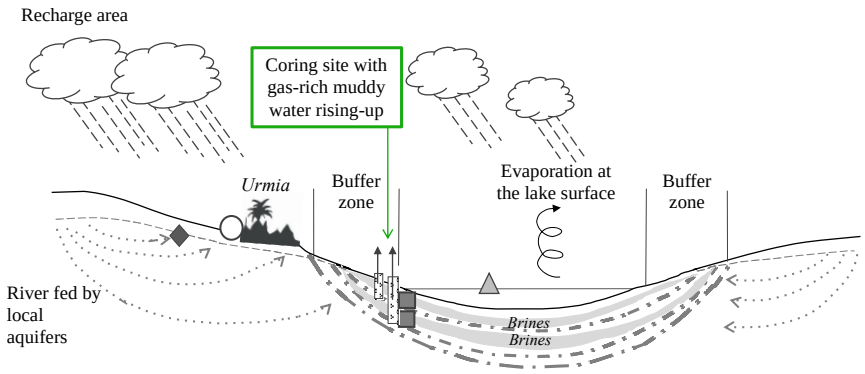

Figure 6: First schematic representation of Lake Urmia functioning with entrapped brines.

Carbon geochemistry and groundwater dating

Carbon geochemistry was studied extensively by determining ^{13}C contents and ^{14}C activities of all sampled waters as well as sludge when the amount of carbon in the samples allowed. Figure 7 highlights the different water groups by their isotopic fingerprints:

1- Surface and groundwater in the Shahr Chay River watershed (excluding wells in the Hajilar area) show homogeneous ^{18}O values between -8.3 and -9.9 ‰, associated with ^{13}C contents of -4.4 to 6.2 ‰ for surface water and -6.8 to -9.4‰ for groundwater, highlighting the impact of soil CO_2 here. Radiocarbon activities range from 68 to 92.4 pMC, showing the impact of carbonate formations in the watershed.

2- The waters collected from Hajilar wells have ^{18}O contents equivalent to those of the Shahr Chay River basin waters, but a considerable difference appears in the carbon geochemistry with ^{13}C contents from +14.2 to +19.1 ‰ and much lower ^{14}C activities.

3- The surface waters of the lake show a classical evolution, with ^{18}O levels around -3.6‰ indicating evaporation of water from the Shahr Chay River, an interpretation in agreement with ^{13}C levels that indicates a re-equilibration of the surface waters with the atmosphere. The ^{14}C activity of 93.3 pMC is lower than expected for total equilibrium due to a hard water effect that allowed us to correct the radiocarbon dating on the C-Core sediments (Kong et al., 2022).

4- Geochemistry is more delicate when dealing with the isotopic contents of the sludges coming up from the boreholes, as already shown in figures 4 and 5. While the ^{18}O contents can be interpreted in terms of evaporation rates and thus scraped brines, the highly enriched ^{13}C contents (-11,6 to +13,1 ‰) and the variable ^{14}C activity range from 1,6 to 16 pMC indicate that particular geochemical processes must be considered in relation to H_2S and probably CH_4 production. In all cases, isotopic contents indicate that these brines may represent semi-confined to fully confined environments, with no interaction with the lake surface water or with catchment groundwater.

This hydrogeochemical functioning of the Lake Urmia basin in its southwestern part is confirmed by the diagram of $^{13}C_{TDIC}$ content as a function of ^{14}C activity which makes it possible to define a logarithmic curve ($Y = -2.91 * \ln[X] + 13.95$; $R^2 = 0.99$) for the lake itself and its sludge and which is characterized by two poles: the first corresponds to the G3 mud brought up from a depth of 13 m and the second to the surface water of the lake. River waters and other wells (with the exception of wells in the Hajilar area) are clearly below this curve, currently seeming to point to a lack of relationship with brines. Only the waters of Hajilar are in agreement with the brines, which confirms the discussions in the field with the owners who indicate that these wells were deepened as the pumped waters became more saline.

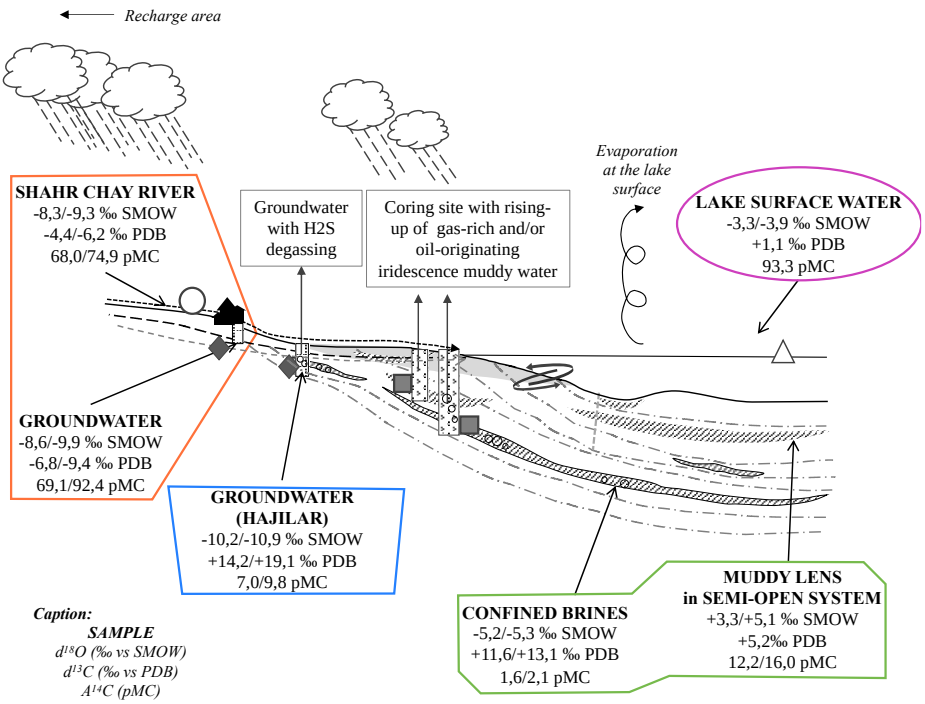

Figure 7: $\delta^{13}C_{TDIC}$ content versus ^{14}C activity diagram for surface and groundwater form the Shahr Chay River basin and for the lake surface waters

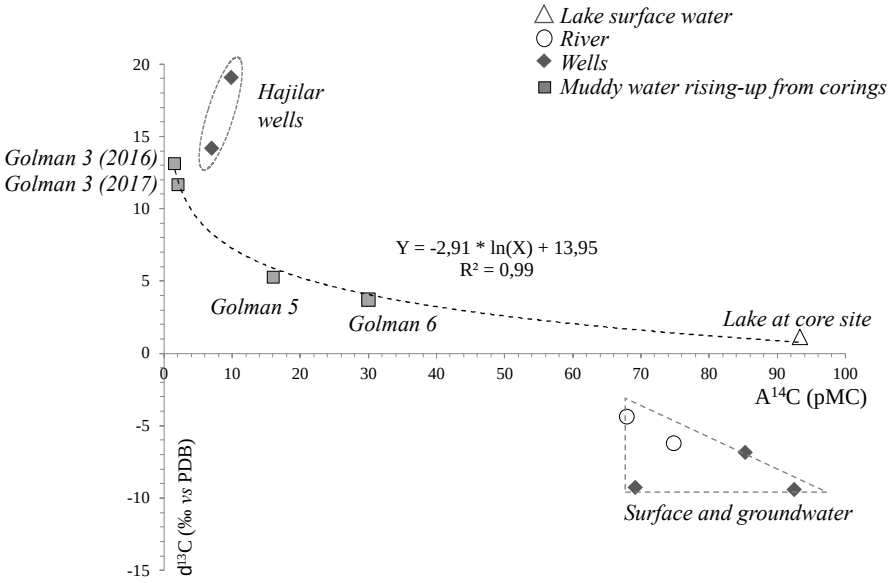

Figure 8: $\delta^{13}C_{TDIC}$ content versus ^{14}C activity diagram for surface and groundwater form the Shahr Chay River basin and for the lake surface waters

To avoid artifacts related to water pH (Tudryn et al., 2021), equilibrium partial pressures of CO_2 (P_{CO2}) in waters were calculated by taking into account the geochemical constants and corresponding fractionation factors of all dissolved carbon species involved (see Appendix). For this purpose, two end-members have to be defined by the $\delta^{13}C/A^{14}C$ couple, the first one related to the soil P_{CO2} in relation to the present vegetation and the second one representing the classical composition of ^{14}C-free geological limestone rocks without.

In a $\delta^{13}C_{equilibrating\ PCO2}$ (‰ vs PDB) versus $A^{14}C$ (pMC) diagram, several geochemical processes are highlighted given the poles defined for the watershed: (i) for the soil end-member, we took the average ^{13}C content of modern vegetation in the Shahr Chay River watershed equal to -16.8 ‰ vs PDB (Kong et al submitted) and rounded to -17‰ for ease of calculation program and $A^{14}C$ equal to 100 pMC, and (ii) for the geological end-member, the generally accepted compositions for carbonate rocks generally display $\delta^{13}C$ around 0 ‰ et a ^{14}C activity of 0 pMC.

1. the first process corresponds to the re-equilibration of the lake surface water (fed by surface water and shallow groundwater) with atmospheric CO_2 although the river inflow to the lake produces a ~35-pMC ageing at the coring time.
2. the second process is shown by the mixing between the two previously defined poles (soil and geological end-members) which introduces an evolution of the surface waters towards an enrichment in ^{13}C of the equilibrating CO_2 and a decrease of the ^{14}C activity of the waters.
3. the third process that is superimposed on this mixing indicates that the weight of the soil CO_2 pole in the system may be more important since some surface and ground waters evolve along a vertical line indicating a constant biogenic CO_2 and a decrease in ^{14}C activity.
4. the fourth process is the most particular since it highlights an isotopic fractionation of the waters of the deep wells (Hajilar) and of the muds brought up from the core drillings; this process implies a very important enrichment in ^{13}C as well as a slight increase in the ^{14}C activities of these waters. This pattern allows us to interpret the Hajilar well water as coming from an old brine lens of the lake reached during well digging, in agreement with Figure 8 and supported by the radiocarbon activity of the water, which is equivalent to the confined lens reached during coring.

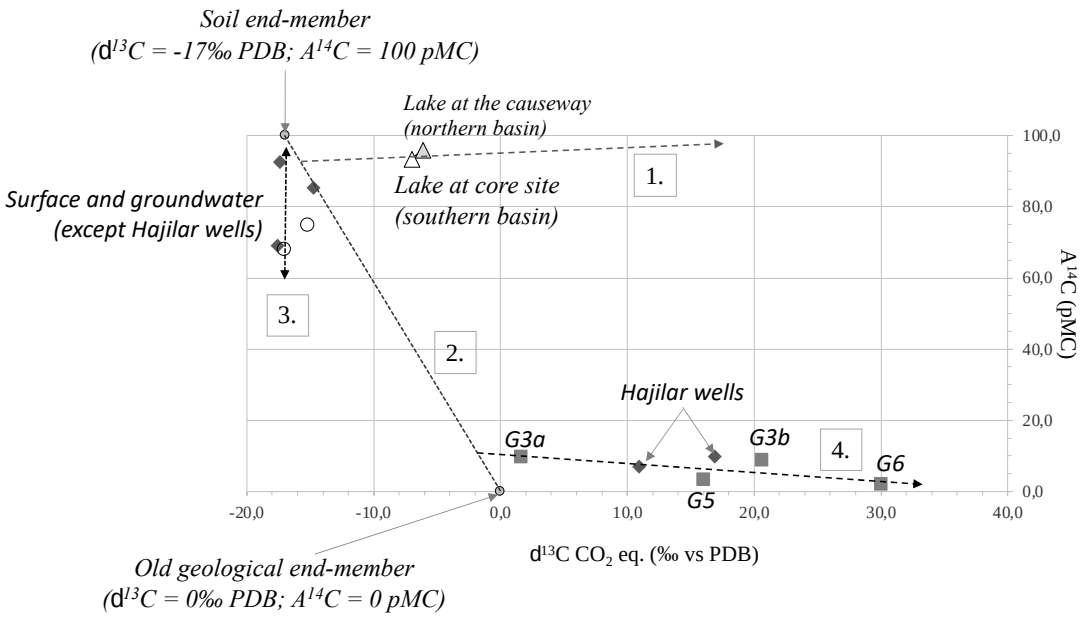

Figure 9: Diagram $\delta^{13}C_{PCO2}$ vs $A^{14}C$ and geochemical processes encountered in Lake Urmia basin.

As a first conclusion, we can deduce that at the regional level, groundwater does not seem to be connected directly to the lake, except for the upper levels of the shallow aquifer related to the base flow of the Shahr Chay River. However, most of the water entering the lake at the study site is directly from the river inflow.

Chronology of the paleoenvironmental stages

The establishment and validation of the radiocarbon time scale was done in close relation to the modern hydrogeochemical system of the lake, although it is very complex at first sight. Twenty ^{14}C-AMS dates performed on specific levels of the composite sequence allowed the definition of a precise and reliable chronology, but also highlighted discrepancies between the ages obtained on carbonate fraction and on organic matter when they could be performed on equivalent levels (Fig. 2; Table 2).

As shown in Figure 10, some of these levels show rejuvenation of the organic matter and carbonate dates relative to the certified chronology (dashed line). Taking the section between 12 and 9 m depth as an example, the quite visible rejuvenation occurs in opposite directions: organic matter is much younger than the expected age at depth and rebalances up the section, while carbonates are close to the certified chronology but rejuvenate as sedimentation progresses.

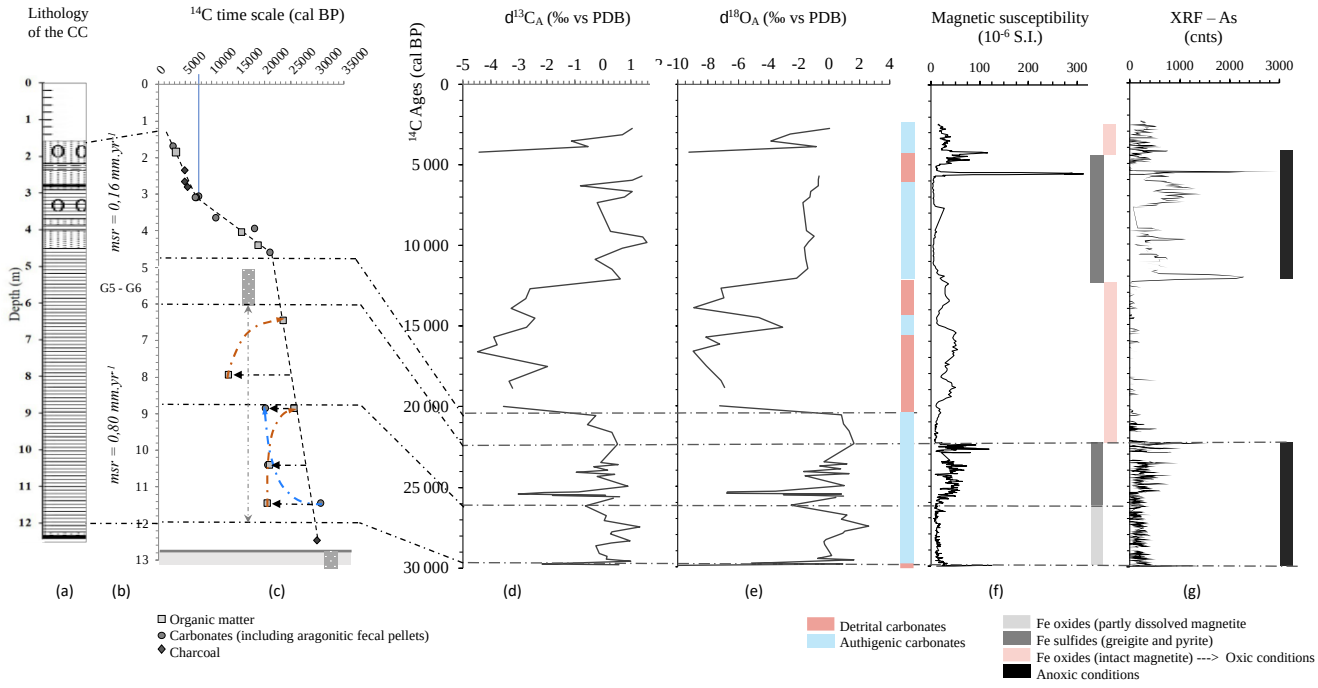

Fig. 10: Schematic representation of the overall exchange between Lake Urmia, surface water and groundwater in the Shahr Chay River sub-basin, including the behavior of lake sediments that form a near-tight barrier to direct groundwater recharge.

In order to understand the mechanisms of these reverse rejuvenations, we attempted to calculate the methane contribution that could explain these distortions.

Here we present the equations used for calculating the percentage of remaining CO_2 that would produce variable ^{13}C values and $A^{14}C$ activities measured on sediment samples and therefore an ageing/rejuvenation of the ^{14}C dating. These calculations are based on a Rayleigh process considering the ^{13}C content and ^{14}C activities of initial and final CO_2 and are valid when considering the hypotheses: (i) the initial CO_2 at -17‰ is largely over the $\delta^{13}C$ value of CH_4 considered at -86‰, and (ii) the initial CO_2 at a $A^{14}C$ activity of 100% is higher than that of CH_4 that is equal to 84 pMC.

T (°C)	T_K (K)	Fractionation factors # a	b	c	ε	^{14}C variation (%)
20	293,15	2,2800	15,176	-8,38	69,91981	16,08156

The equations of final conditions for the C system are as follows:

$$\delta^{13}C_{remaining\ CO2} = \delta^{13}C_{(CO2)0} - \varepsilon * \ln(f)$$

$$A^{14}C_{remaining\ CO2} = A^{14}C_{(CO2)0} - \varepsilon * 0{,}23 * \ln(f)$$

With: $\varepsilon = (a*10^6/T_K^2) + (b*10^3/T_K) + c = 10^3.\ln(\alpha_{CO2\text{-}CH4})$ and ^{14}C variation (%) = 0,23 * ε

Original conditions $A^{14}C_{(CO2)0}$	Original conditions $\delta^{13}C_{(CO2)0}$	f [##]	Final conditions $\delta^{13}C_{remaining\ CO2}$	Final conditions $A^{14}C_{remaining\ CO2}$
90	-17	1,00	-17,0	90,0
90	-17	0,95	-13,4	90,8
90	-17	0,90	-9,6	91,7
90	-17	0,85	-5,6	92,6
90	-17	0,80	-1,4	93,6
90	-17	0,75	3,1	94,6
90	-17	0,70	7,9	95,7
90	-17	0,65	13,1	96,9
90	-17	0,60	18,7	98,2
90	-17	0,55	24,8	99,6

[#], From Bottinga (1969) and T values ranging between 0 and 700°C;

[##], f = remaining CO_2 fraction after methanation.

We can observe that the ^{13}C content and ^{14}C activity of remaining CO_2 after methane production increases relatively to initial values. The production of a CH_4 fraction between 0.25% and 0.30% in brines trapped in lake sediments produces an enrichment of 4.6-pMC to 5.7-pMC in the ^{14}C activity of the remaining CO_2, these values of the order of magnitude of our data and confirms the presence of methane in agreement with the field data, and highlights its impact on the original geochemical parameter records in closed or semi-closed brine lenses.

Methane geochemistry

Methane impact on the carbon system may be seen through two pathways: oxidation of methane or early diagenesis of organic matter.

Hypothesis 1: Methane oxidation

Numerous studies have been conducted to understand the release of CH_4 into reservoirs as a source (or sink?) of greenhouse gases (e.g., Coleman et al. 1981; Gruca-Rokosz et al. 2020, 2021; Xueping Chen et al. 2022). In particular, Xueping Chen et al. (2022) studied the microbial factors involved in methane production and oxidation, and the regulation of anaerobic methane oxidation in freshwater reservoir sediments. They showed that (i) methanogenic bacteria were detected throughout the sediment depth profile and (ii) the coexistence of sulfate and iron oxidizing bacteria in the surface layer supports the possibility of sulfate and iron dependent methane oxidation.

During the drilling of the Lake Urmia sequences, the rising-up of the muddy waters was accompanied by H_2S odor but also by iridescence that could suggest the presence of polycyclic compounds of petroleum origin. Since Lake Urmia is located in a highly tectonic zone within which oil formations have been identified, methane could be a deep regional production which would rise through the geological formations via micro- and/or macro-porosities. Within the sludge in a closed system (anaerobic environment), the methane would be oxidized by the oxygen of the dissolved sulfate ions, which would therefore allow the formation of CO_2. Although this anaerobic methane oxidation coupled with sulfate reduction is a process described primarily in marine environments (Coleman et al. 2004), this reaction can occur in lake sediments being either of biological or chemical origin (REF).

$$CH_2O + SO_4 + CH_4 \text{ ---> } H_2S + 4O \quad (1)$$

$$CH_4 + 2O_2 \text{ ---> } CO_2 + 2H_2O \quad (2)$$

With the formation of CO_2, the recrystallization of a secondary carbonate phase could then occur.

However, our results do not confirm this hypothesis:

- the carbon involved in reaction (1) comes from deep, likely ^{14}C-free CH_4; in this case, the secondary carbonated phase produced will imply the ageing of the total carbonate fraction, which is not what we observe;
- the reaction (2) produces a drop in pH, leading to an acidification of the medium, even weak, that can lead to the dissolution, total or partial, of the newly-formed carbonates. This process cannot explain the rejuvenation of our samples.

Hypothesis 2: Early diagenesis of the organic matter fraction

The preliminary stage of early diagenesis corresponds to the degradation of the organic matter by bacteria that use the oxygen of the more easily released sulfates, in the sulfate reduction process.

$$2CH_2O + SO_4^{-2} \text{ ---> } 2HCO_3^- + H_2S \quad (3)$$

At the same time, there is a release of oxygen from the iron oxides, with the consequent production of iron sulfides like greigite (Fe_3S_4) and pyrite (FeS_2)

$$CH_2O + Fe_3O_4 + H_2S \text{ ---> } CO_2 + FeS_2 + 2H_2O \quad (4)$$

At an even more advanced stage of early diagenesis (depletion of the iron oxide stock), bacteria directly use the oxygen of the organic matter and produce methane:

$2CH_2O$ ---> $CH_4 + CO_2$ (5)

Our data seem to confirm this mode of methane production via reactions (3) to (5), especially in the section between 12 and 9 m depth:

- the carbon involved here comes from organic matter: the precipitation phase of the secondary carbonates is therefore of the same age as the surrounding sediments and may even be rejuvenated if we consider the biological fractionation factors involved in the early diagenesis reactions; this is in agreement with the rejuvenation of the samples which decreases towards the top of the section, thus highlighting the depletion of the oxygen supply stock and thus of the secondary carbonates.
- The presence of arsenic confirms this early diagenesis (with the appearance of arsenic sulfide) and even indicates that the process is already well underway at these depths;
- The smell of H_2S during coring also supports this hypothesis.

Throughout the C-Core, methane production is primarily related to incorporated brines and occurs during the Late Pleistocene period. Of course, our results are concentrated on the western part of Lake Urmia basin and should be confirmed by further investigations along the shores of the lake, especially in the southern part of the lake where most of the river water enter the lake.

Discussion and conclusion

Stable isotope levels clearly indicate that the waters in the catchment are aligned along an evaporation line originating in the Shahr Chay River. The groundwater ^{18}O and ^{2}H contents clearly show that they support the surface water (ref).

The interpretation of the stable isotope data and the radiocarbon activities of the waters of Lake Urmia collected in 2016-2017 was very delicate but the use of the stable isotopes of water together with those of carbon made it possible to understand at least the dynamics of the lake today and in the past, in relation to sedimentation and surface water-groundwater relationships. Altogether with previous multidisciplinary studies (Tudryn et al., 2021; Kong et al., 2022), they allow reconstructing, albeit still schematic, the functioning of Lake Urmia.

Figure 12, based on the geochemistry of the present-day hydrogeological system and on sludge data from the cored sequences, suggests the existence of a saline wedge in the lake bottom sediments, which provides a nearly impermeable barrier to exchange with surrounding aquifers and lake deposits. The trapped brine lenses collected during drilling must be much more numerous and probably form an impermeable barrier to exchanges with the water table directly on the banks or at the bottom of the lake. The hydraulic conductivity of the lake bed (ref) is probably overestimated. Only the shallow aquifer seems to have a relative importance for the lake water feeding through the basal support of inflowing rivers.

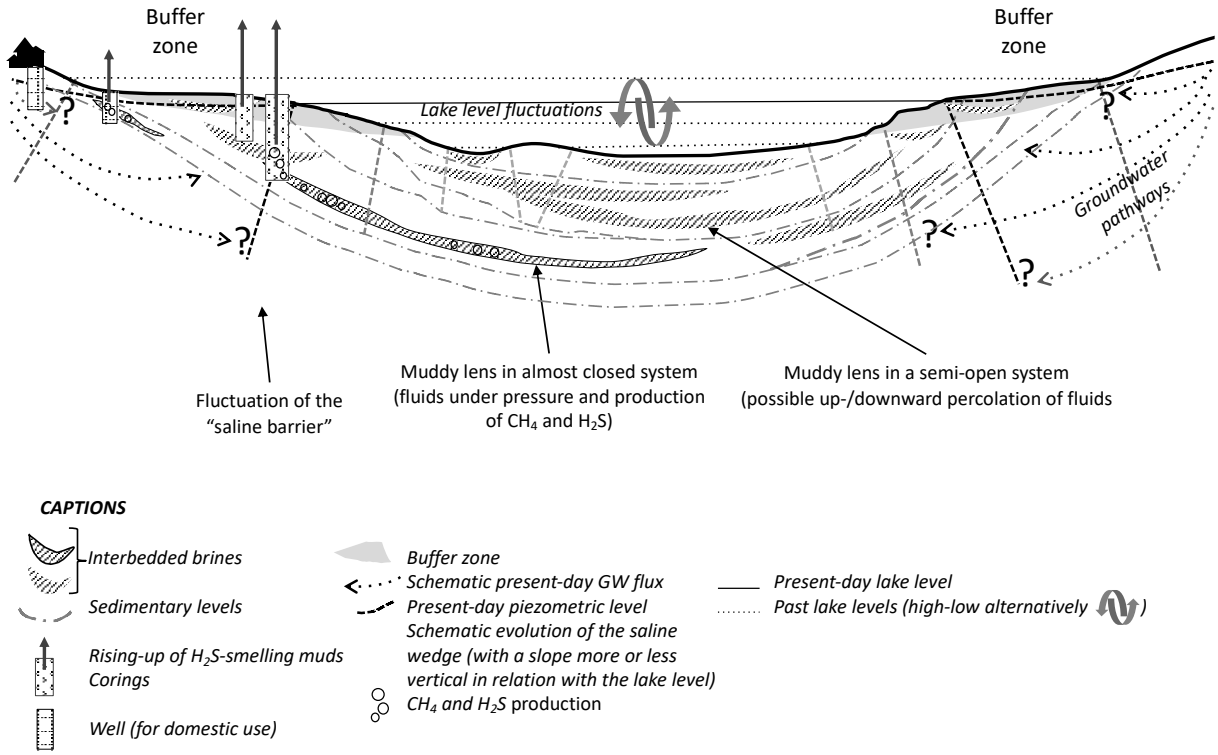

Fig. 10: Schematic representation of the overall exchange between Lake Urmia, surface water and groundwater in the Shahr Chay River sub-basin, including the behavior of lake sediments that form a near-tight barrier to direct groundwater recharge.

As emphasized by Marjani and Djamali (2014), Ataie-Ashtiani (2019), Javadzadeh et al. (2020) or Parizi et al. (2022), our results confirm that the survival of the lake is tightly linked to the surface water, themselves supported on the catchment areas by groundwater. In the vicinity of the lake, the groundwater is diverted by the saline crusted levels and flows in the direction of the main regional slope, i.e., towards the north of Lake Urmia.

Indeed, although there is no evidence of interactions between groundwater and the lake other than via base support from the rivers feeding the lake, our results may confirm the works of Javadzadeh et al. (2019) who model exchanges as a function of the hydraulic gradient between the lake and surrounding aquifers. The lake water including sediments and embedded brines appear to react like a coastal aquifer, with a saline wedge that prevents mixing with groundwater from the watershed at depth whose flows are related to the hydraulic gradient between the lake and the surrounding aquifers as well as to geological formations. Recent studies of surface water-groundwater relationships indicate that the horizontal continuity of geologic formations in the watershed plays an important role on the time required for the saltwater-freshwater interface to reach a new position after a change in recharge (McKnight et al., 2020). This is in relation with the differences in the flow properties of different geologic units on the response time and extent of saltwater intrusion, whether in deserts or any other area likely to have saltwater (Vaheddoost and Aksoy, 2017; McKnight et al., 2020; Parizi et al, 2022).

Thus, depending on the different stages of the lake evolution, i.e., high or low level, the salt wedge fluctuates but both in depth and laterally with a more or less significant time lag compared to the lake level. This could induce either the replenishment of the lake by river water during the lake level drop or the salinization of shallow groundwater along the shore during lake level rises. Unfortunately, the level of anthropogenic pressure due to the economic and societal development of the Lake Urmia region seems to prohibit the return of a sufficient supply of the lake by the rivers.

On a more global scale, if wetlands are by far the most methane-emitting natural ecosystems (about 70% of natural sources), lake ecosystems come second with 13% of methane emissions into the atmosphere (EPA - United State Environmental Protection Agency-, 2010 in Billard, 2015). This estimate is actually tending to increase, due to the better knowledge of the processes involved and of methane fluxes to the atmosphere, but also to the temperature increase (Bastviken et al, 2011). Moreover, contrary to what is widely accepted, regional to supra-regional differences in water storage decline in endoreic basins are emerging, either in areas under high anthropogenic pressure where water loss is exacerbated by increased evaporation from dams, pumping and overuse of water such as the Lake Urmia basin (Wang et al. 2017).

However, 30 and 99% of the methane produced by aquatic ecosystems, either in sedimentary anoxic zones, or in the hypolimnion when the water column is stratified, is consumed during transport to the atmosphere (Bastviken et al. 2008). As for Lake Urmia and others salt lakes, the interface between the sediments and lake bottom waters thus remains a key area for understanding the succession of paleoenvironmental phases but also for estimating the part that lakes, a fortiori salt lakes, constitute in GHG sources. Although anaerobic methane oxidation coupled with bacterial sulfate reduction can consume up to 80% methane at the water-sediment interface (Knittel et al., 2018), the oxidation process may not be always known or proven to be constant over time, and if it favors the precipitation of carbonates, the fluxes and isotopic composition of methane must be studied in order to be able to consider these carbonates as authigenic and then use them as environmental recorders.

References

Abbasian M.S. *et al.* Increasing risk of meteorological drought in the Lake Urmia basin under climate change: Introducing the precipitation–temperature deciles index. *Journal of hydrology* **592**, 125586 (2021).

Ahmady-Birgani H. *et al.,* Sediment Source Fingerprinting of the Lake Urmia Sand Dunes. *Nature/Scientific Reports* **8**, 1-14 (2018).

Alborzi A. *et al.* Climate-informed environmental inflows to revive a drying lake facing meteorological and anthropogenic droughts. *Environmental research Letters* **13**, 084010 (2018).

Alipour S. Hydrogeochemistry of seasonal variations of Urmia Salt Lake, Iran. Saline Systems **2**, 1-19 (2006).

Aravena R. *et al.* Carbon Isotope Composition of Lake Sediments in Relation to Lake Productivity and Radiocarbon. *Quaternary Research* **37**, 333-345 (1992).

Ashraf B. *et al.,* Quantifying Anthropogenic Stress on Groundwater Resources. *Nature Scientific Reports* **7**, 12910 (2017).

Bastviken D. *et al.*, Methane emissions from lakes: Dependence of lake characteristics, two regional assessments, and a global estimate. *Global Biogeochemical Cycles*, **18**, GB4009, doi:10.1029/2004GB002238 (2004).

Bastviken D. *et al.*, Freshwater Methane Emissions Offset the Continental Carbon Sink. *Science*, 331(6013): 50-50 (2011).

Bottinga Y. Calculated fractionation factors for carbon and hydrogen isotope exchange in the system calcite-carbon dioxide-graphite-methane-hydrogen-water vapor. Geochimica et Cosmochimica Acta 33(1), 49-64 (1969).

Çagatay M.N. *et al.* Lake level and climate records of the last 90 ka from the Northern Basin of Lake Van, eastern Turkey. *Quaternary Science Reviews* **104,** 97-116 (2014).

Coleman D.D. *et al.* Fractionation of carbon and hydrogen isotopes by methane-oxidising bacteria, *Geochimica et Cosmochimica Acta* **45**, 1033–1037 (1981).

Danesh-Yazadi M. & Ataie-Ashtiani B. Lake Urmia crisis and restoration plan: Planning without appropriate data and model is gambling. *Journal of Hydrology* **576**, 639-651 (2019).

Deutzmann J. & Schink B. Anaerobic oxidation of methane in sediments of Lake Constance, an oligotrophic freshwater lake. *Applied Environmental. Microbiology* **77**, 4429-4436 (2011).

Downing J.A. *et al.* The global abundance and size distribution of lakes, ponds, and impoundments, *Limnology and Oceanography* **51(5)**, 2388-2397 (2006).

Emami H. & Zarei A. Modelling Lake water's surface changes using environmental and remote sensing data: A case study of lake Urmia. *Remote Sensing Applications: Society and Environment* **23**, 100594 (2021).

Fontes, J-Ch. *et al.* Stable isotope and radiocarbon balances of two Tibetan lakes (Sumxi Co, Longmu Co) from 13,000 BP. *Quaternary Science Reviews* **12**, 875-887 (1993).

Fontes, J.Ch. *et al.* Holocene environmental changes in Lake Bangong basin (Western Tibet). Part 1: Chronology and stable isotopes of carbonates of a Holocene lacustrine core. *Palaeogeography, Palaeoclimatology, Palaeoecology* **120**, 25-47 (1996).

Gibert E. *et al.,* Comparing carbonate and organic AMS-^{14}C ages in Lake Abiyata sediments (Ethiopia): hydrogeochemistry and paleoenvironmental implications. *Radiocarbon* **41**(3), 271-286 (1999).

Gruca-Rokosz R. & Maksymilian C. Sediment methane production within eutrophic reservoirs: The importance of sedimenting organic matter, *The Science of the total environment* **799**, 149219-149219 (2021).

Gruca-Rokosz R. *et al.* Isotopic evidence for vertical diversification of methane production pathways in freshwater sediments of Nielisz reservoir (Poland), *CATENA* **195**, paper 104803 (2020).

Hemmati M. et al., Environmental effects of the causeway on water and salinity balance in Lake Urmia. *Regional Studies in marine Sciences* **44**, 101756 (2021).

Jalili, S. *et al.* The influence of large-scale atmospheric circulation weather types on variations in the water level of Lake Urmia, Iran. *Int. J. Climatol.* **X,** XX-XX (2011).

Javadzadeh H. *et al.,* Interaction of lake-groundwater levels using cross-correlation analysis: a case study of Lake Urmia, Iran. *Science of the Total Environment* **729**, 138822 (2020).

Jookadi G. *et al.,* Estimating the human contribution to groundwater depletion in the Middle East, from GRACE data, land surface models, and well observations. *Water Resources Research* **50**, 2679-2692 (2014).

Knittel K. *et al.,* Anaerobic Methane Oxidizers. In: T. J. McGenity (ed.), Handbook of Hydrocarbon and Lipid Microbiology, doi.org/10.1007/978-3-319-60063-5_7-1 (2018).

Kong T. *et al.,* Late 30,000 years of the southwestern Lake Urmia (Iran) evolution inferred from mineralogical indicators, *Quaternary Sciences Review* **JAESS-D-22-00365R1** (2022a).

Kong T. *et al.* 30,000 years of the southwestern Lake Urmia (Iran) paleoenvironmental evolution inferred from mineralogical indicators from lake and watershed sediments, *Under Review to Mineralogy* (2022b).

Leng M. *et al.,* Detrital carbonate influences on bulk oxygen and carbon isotopes composition of lacustrine

sediments from the Mediterranean. *Global and Planetary Change* **71**, 175-182 (2010).

Li, Y. *et al.* Provenance of inorganic carbon sinks in closed basins. *Water Resources Research* **58**, e2021WR030270 (2022).

Marjani A. & Djamali M. Role of exchange flow in salt water balance of Lake Urmia. *Dynamics of Atmospheres and Oceans* **65**, 1-16 (2014).

McKnight, S. V. *et al.* Impact of hydrostratigraphic continuity on brine-to-freshwater interface dynamics: Implications from a two-dimensional parametric study in an arid and endorheic basin. *Water Resources Research* **57**, e2020WR028302 (2021).

Mirgol B. *et al.*, Past and future drought trends, duration, and frequency in the semi-arid Urmia Lake Basin under a changing climate. *Meteorological Applications* **28**, DOI 10.1002 (2021).

Mosaffa M. *et al.* An investigation of the source of salinity in groundwater using stable isotope tracer and GIS: A case study of the Urmia Lake basin, Iran. *Groundwater for Sustainable Development* **12**, 100513 (2021).

Olsen, J. *et al.* Limnological controls on stable isotope records of Late-Holocene paleoenvironment change in SW Greenland: a paired lake study. *Quaternary Science Reviews* **66**, 85-95 (2013).

Oehlerich, M. *et al.* Effects of organic matter on carbonate stable isotope ratios (d13C, d18O values) – implications for analyses of bulk sediments. *Rapid Commun. Mass Spectrom.* **27**, 707–712 (2013).

Parizi E. *et al.*, Quantifying lake-aquifer water exchange: the case of Lake Urmia, Iran. *Hydrological Sciences Journal* **67**(5), 725-740 (2022).

Pashaeifar M. *et al.*, Spatial and temporal assessment of groundwater quality and hydrogeochemical processes in Urmia Lake basin, Iran. *Water Supply* **21**(8), 4328 (2021).

Raghoebarsing AA. *et al.* A microbial consortium couple's anaerobic methane oxidation to denitrification, *Nature: international weekly journal of science* **440**(7086), 918-921(2006).

Tudryn A. *et al.* Late Quaternary environmental changes of Lake Urmia basin (NW Iran) inferred from sedimentological and magnetic records, *Quaternary International* **589**, 83-94 (2021).

Vaheddoost, B. *et al.* Prediction of Water Level using Monthly Lagged Data in Lake Urmia, Iran. *Water Resources Management* **30**(13), 4951-4967 (2016).

Vaheddoost, B. & Aksoy, H. Interaction of groundwater with Lake Urmia in Iran. *Hydrological Processes* **32**, 3283–3295 (2018).

Wang, J. *et al.* Recent global decline in endorheic basin water storages. *Nature Geosciences* **11**, 926-932 (2018).

Wurtsbaugh, W. A. *et al.* Decline of the world's saline lakes. *Nature Geosciences* **10**, 816-821 (2017).

Xueping Chen *et al.* The anaerobic oxidation of methane driven by multiple electron acceptors suppresses the release of methane from the sediments of a reservoir, *Journal of Soils and Sediments* **22**, 682-691 (2022).

Zanchetta, G. *et al.* Late Quaternary palaeohydrology of Lake Pergusa (Sicily, southern Italy) as inferred by stable isotopes of lacustrine carbonates. *J Paleolimnology* **38**, 227–239 (2007).

Zarinmehr H. *et al.*, Prediction of groundwater level variations based on gravity recovery and climate experiment (GRACE) satellite data and a time-series analysis: a case study in the Lake Urmia basin, Iran. *Environmental Earth Sciences* **81**(6) (2022).

APPENDIX 1

Program. This paper falls into the Franco-Iranian project initiated and supported by the bilateral Gundishapur program, and follows the 2016 and 2017 field expeditions on the investigation of the Lake Urmia region and basin for paleoenvironmental reconstructions. Our research has also been supported by the Center for International Scientific Studies and Collaboration (CISSC, Iran), the TelluS Program of CNRS/INSU (France) and by the China Scholarship Council (CSC) for the PhD grant of Ms. T. Kong.

Methods

Study site. Core description and sampling. In 2016 and 2017, several sedimentary sequences have been cored in the SW part of Lake Urmia basin, from the very recently dried out, although muddy, part of the lake (Tudryn et al. 2021). Among the 8 cores collected with a mechanic corer, two were subjected of an in-depth multi-parameter sediment study, i.e. Golman 7 and Golman 6 of 12.5 m and 8 m long respectively (Tudryn et al. 2021; Kong et al. 2022a and 2022b). These two cores allow displaying a homogenous lacustrine composite core based mainly on magnetic susceptibility. Only 1,6-m depth is missing at the core top.

Stable isotopes. Stable oxygen and deuterium ($\delta^{18}O$, $\delta^{2}H$), expressed in % versus V-SMOW (Vienna Mean Ocean Water) were obtained on the TDIC (Total Dissolved Inorganic Carbon) for water samples from both surface and groundwater (lake, wells and river), as well as for mud samples rising-up from the coring tubing. The ^{18}O and ^{2}H

Contents were measured on a Laser Spectrometer at the GEOPS Laboratory (Orsay, France). Analytical uncertainties, including laboratory errors, are ± 0.1‰ and ± 2.0 ‰ for $\delta^{18}O$ and $\delta^{2}H$ respectively.

Stable carbon isotope contents ($\delta^{13}C$) of the Total Dissolved Inorganic Carbon (TDIC), expressed in ‰ versus V-PDB (Vienna Pee Dee Belemnite standard) were measured at the METIS laboratory (Paris, France) and calibrated with respect to the NBS19 calcite standard. Analytical uncertainties, including laboratory errors, are ± 0.1‰ for $\delta^{13}C$.

Isotopes in precipitation. In order to define the local Meteoric Water Line (LMWL) corresponding to rainwater on the Shahr Chay River basin, data from the GNIP database (IAEA/WMO) were used for three main stations surrounding Lake Urmia: Diyarbakir and Dalbahce (Turkey) and Tehran (Iran)- See Fig. 3 for station location.

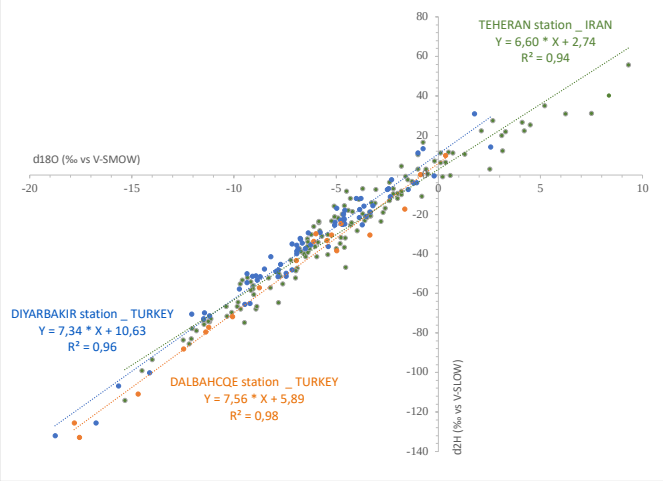

Figure 12: Isotope data in precipitation from 3 GNIP stations (WISER files, IAEA/WMO GNIP Network, 2022)

Radiocarbon dates. ^{14}C dating was performed at the ECHoMICADAS facility (CNRS-CEA Saclay, France). AMS ^{14}C measurements were performed on the inorganic carbonate fraction and diffused organic matter of bulk samples from the C-core, on handpicked plant remains and charcoals when present, as well as on water and muddy coring samples.

The organic fraction was submitted to the standard chemical protocol for AMS analyses: 3 successive hydrochloric acid/sodium hydroxide/hydrochloric acid baths, rinsing with deionized water up to neutral pH, and gently drying at 60 °C overnight.

The CO_2 gas was obtained (i) for organic samples by burning at 860 °C for 30 min, under vacuum, in presence of a mixing of copper (II)-oxide/copper (III)-oxide and silver thread, and (ii) for carbonates, by an H_3PO_4 acid attack under vacuum during one night in a thermostatic bath, and (iii) for water and muddy samples, by a direct H_3PO_4 acid attack on the TDIC of the samples.

Then, AMS-^{14}C targets were obtained by graphitization of the CO_2 gas on powdered iron with hydrogen at 650 °C for 100 min, and graphite compression under analytical plots. Aliquot of the CO_2 gas was then used for associated ^{13}C measurement. Graphite sources were prepared in GEOPS laboratory, and counted by accelerator mass spectrometry at LSCE laboratory (ECHoMICADAS facility, France).

For the A_o activity (initial activity), every dating of modern surface water or groundwater refer to the ^{14}C activity of the atmospheric CO_2 at the time of sampling, i.e., 2016-2017, and that can be determined with the data gathered by Hua and coauthors (2021). As deduced from Fig. X, the ^{14}C activity of CO_{2atm} is of 101,8 pMC.

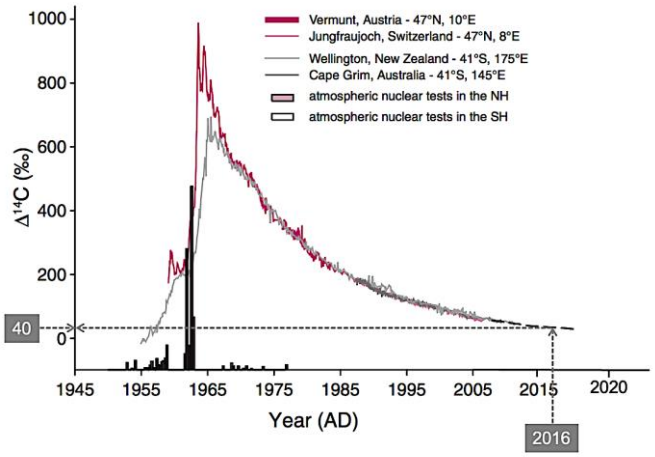

Year	$F^{14}C$ - Mean	1σ
2016	1,0188	0,0005
2017	1,0157	0,0005

Figure 13: Isotope data in precipitation from 3 GNIP stations (WISER files, IAEA/WMO GNIP Network, 2022)

Analytical uncertainties, including laboratory errors, are ± 0.1‰ for $\delta^{13}C$ and between 0.5 and 0.8 pMC for ^{14}C activity. All the dates established on sediments are converted to calendar ages according to the revised calibration program IntCal20 (Execute Version 1.10 html 2020; Table 2; Reimer et al., 2020).

APPENDIX 2: Data tables

Field mission	STATION	Type	Latitude	Longitude	Altitude	Total Alkalinity	Carbonate	Bicarbonate	Conductivity	Temperature	pH	$d^{18}O$	$d^{2}H$	$d^{13}C$	^{14}C analyse			Age ^{14}C	s
			N	E	(m)	(mg.L^{-1} $CaCO_3$)	(mg.L^{-1} CO_3^-)	(mg.L^{-1} HCO_3^-)	(mS.cm-1)	(°C)		(‰ vs V-SMOW)	(‰ vs V-SMOW)	(‰ vs PDB)	Nr	$F^{14}C$	1 s	(yr BP)	(yr)
2016	Golman 0	well	37°35'15.44"	45°15'19.70"	1278	184,0	0,0	224,5	1,178	14,8	7,35	-8,6	-57,1	-9,42	E2468	0,9241	0,00245	635	20
	Golman 2	coring				520,0	0,0	634,4	219	29,2	5,8	3,3	-7,7						
	Golman 3	coring	37°35'33,09"	45°16'31.20"	1268	1140,0	0,0	1390,8	147,1	20,2	6,35	-5,2	-47,9	13,10	E2477	0,0157	0,00096	33 370	490
	Golman 4	lake				564,0	148.8	385,5	207	21,3	8,02	-3,9	-33,7	1,14	E2476	0,9329	0,00245	560	20
	Shahrchay 1	river	37°31'35.24"	45°02'50.53"	1354	66,0	0,0	80,5	0,249	14	8,41	-8,3	-52,1	-6,22	E2475	0,7488	0,00212	2 325	25
	Shahrchay 2	river	37°33'16.93"	45°16'12.26"	1276	192,0	0,0	234,2	3,4	16,8	7,83								
	Dam Bridge 1	lake	37°46'31.62"	45°19'47.04"	1268	976,0	0,0	1190,7	190,2	27,9	7,53	-3,3	-34,6	9,00					
	Hajilar 1	well	37°33'22.00"	45°16'17.51"	1277	828,0	0,0	1010,2	3,12	15,4	6,29	-10,2	-66,1	14,20		0,0700			
	Hajilar 2a	well	37°33'09.07"	45°16'08.95"	1276	698,0	0,0	851,6	12,22	15,7	6,12	-10,5	-69,7	19,11		0,0981			
	Hajilar 2b	well	37°33'09.07"	45°16'08.95"	1276	414,0	0,0	505,1	12,39	16	6,63	-10,9	-71,0						
2017	Kesh1	well	37°32'28.788"	45°14'07.224"	1281		0,0	170,8	0,575	19,8	8,13	-9,9	-62,7	-9,26	E2473	0,6914	0,00210	2 965	25
														-8,69	E2474	0,6923	0,00203	2 955	25
	Bardesoor	river	37°26'14.592"	44°49'26.92"	1606		24,0	73,3	0,299	13,8	8,38	-9,3	-56,7	-4,38	E2470	0,6798	0,00201	3 100	25
	Saleh Abad	well	37°31'16.626"	45°10'52.812"	1294		0,0	95,3	0,884	14,1	7,28	-8,9	-55,4	-6,83	E2471	0,8525	0,00271	1 280	25
	Golman 3	coring	37°35'33,09"	45°16'31.20"	1268		0,0	3050,0	142	18,9	6,24	-5,3	-48,0	11,66	E2469	0,0206	0,00101	31 180	390
	Golman 5	coring					0,0	610,0	222	26,6	6,04	5,1	-3,3	5,25	E2471	0,1604	0,00122	14 700	60
	Golman 6	coring					0,0	610,0	206 (*)	-	-	-0,8	-23,2	3,70	E2570	0,3000	0,00116	9 670	30

Table 1: Geochemistry of surface and groundwater from Lake Urmia basin (Iran). and location of the cored sedimentary sequence at the Shahr Chay River mouth (north-western area). See Figures 2 and 4 for sample location.

(a)

Sample	Depth (cm)	Type (*)	Sample Nr	F^{14}C (pMC)	σ (b)	Measured ^{14}C ages (BP)	σ (b)	Mineralogy of the carbonate fraction Aragonite (%)	Calcite (%)	Dolomite (%)	Crystallinity of the carbonate fraction Aragonite	Calcite	Dolomite (‰ PDB)(c)	δ^{13}C
Lake surface water			E2476	93,46	0,250	540 (*) 1160 (**)	20							-1,10
Golman-5 core														
G5	2,34	Charcoal	B2087	0,5824	0,20	4 343	25							-14,50
G5	2,66	Charcoal	B2088	0,5787	0,20	4 394	22							-25,50
Composite core (Golman-6 and Golman-7 cores)														
G7-S1	1,70	$CaCO_3$	A17861	0,5580	0,32	4 266	26	95,9	3,1	1,0	0,095	***0,131***	0,370	
G7-S1	1,85	OM	B2295	0,5306	0,0017	5 091	25							
G7-S2	2.80	Charcoal	B2097	0,5547	0,40	4 734	22							-26,50
G7-S2	3,07	$CaCO_3$	A17862	0,3334	0,42	8 823	34	95,9	3,3	0,7	0,100	***0,130***	***0,150***	
G7-S2	3,09	$CaCO_3$	A17863	0,3579	0,41	8 253	33	96,7	2,3	<0,01	0,110	***0,130***	0,230	
G7-S2	3,09	Black FP (**)	A21543	0,3880	0,0036	7 600	80	100						
G7-S2	3,09	White FP (**)	A21542	0,3666	0,0035	8 060	80	(secondary carbonate precipitation suspected)						
G7 S3	3,65	$CaCO_3$	A17864	0,2377	0,53	11 540	42	93,9	4,2	1,8	0,143	***0,089***	0,380	
G7-S3	3,95	CaCO3	62002	0,1138	0,12	17 450	90	61,9	25,8	12,3	0,090	0,260	***0,190***	-3,77
G7-S3	4,05	OM	B2297	0,1529	0,10	15 088	66							
G7-S3	4,15	OM	B2100	0,0569	0,59	23 032	47							-25,3
G6-S2	4,40	OM	B2304	0,1124	0,001	17 561	76							
G6-S2	4,60	$CaCO_3$	62001	0,0662	0,12	21 810	140	58,4	30,2	11,4	0,080	***0,140***	0,200	
G6-S4	6,45	OM	B2300	0,0689	0,0005	21 488	63							
G6-S5	7,95	OM	B2299	0,1913	0,003	13 286	114							
G7-S6b	8,85	$CaCO_3$	62003	0,0554	0,12	19 800	170	53,2	21,1	25,7	0,080	***0,118***	***0,162***	
G7-S6b	8,85	OM	B2099	0,0830	0,12	23 240	82							
G7-S7	10.40	$CaCO_3$	62004	0,0551	0,11	23 280	170	41,0	44,8	14,2	0,085	***0,130***	0,260	
G7-S7	10.40	OM	B2104	0,0889	0,71	19 442	57							
G7-S8	11.45	OM	B2101	0,0942	0,68	18 976	45							
G7-S8	11.45	$CaCO_3$	62005	0,2139	0,10	30 890	390	67,2	24,5	8,3	0,098	***0,135***	***0,194***	
G7-S8	12.46	Charcoal	B2301	0,0005	0,001	25 591	96							-25,90

Detrital calcite: between 0.080 and 0.140
Detrital dolomite: below 0,200

(b)

Sample	Depth (cm)	Type (a)	Sample Nr	F^{14}C (pMC)	σ (b)	Measured ^{14}C ages	σ (b)	^{14}C Ages corrected from detrital fraction (yr BP)	^{14}C Ages corrected from a 2-kyr HWE (yr BP)	Calibrated ^{14}C Ages (cal BP)	2σ
Lake surface water		Water	E2476	93,46	0,250	540	20				
Golman-5 core											
G5	2,34	Charcoal	B2087	0,5824	0,20	4 343	25	4 340	4 340	**4 910**	-60/+60
G5	2,66	Charcoal	B2088	0,5787	0,20	4 394	22	4 390	4 390	**4 940**	-75/+100
Composite core (Golman-6 and Golman-7 cores)											
G7-S1	1,70	$CaCO_3$	A17861	0,5580	0,320	4 265	26	**4 560**	2 560	**2 720**	-205/+30
G7-S1	1,85	OM	B2295	0,5306	0,002	5 090	25	3 090	3 090	**3 295**	-75/+65
G7-S2	2.80	Charcoal	B2097	0,5547	0,400	4 735	22	4 730	4 730	**5 475**	-145/+105
G7-S2	3,07	$CaCO_3$	CaCO3	0,3334	0,420	8 825	34	**8 730**	6 730	7 595	-80/+70
G7-S2	3,09	Black FP (**)	A21543	0,3880	0,0036	7 600	80	*(secondary carbonate precipitation suspected)*			
G7-S2	3,09	White FP (**)	A21542	0,3666	0,0035	8 060	80	8 060	6 060	**6 920**	-180/+240
G7-S2	3,09	$CaCO_3$	CaCO3	0,3579	0,410	8 300	33	**8 300**	6 300	7 215	-55/+90
G7-S3	3,65	$CaCO_3$	CaCO3	0,2377	0,530	11 540	42	**11 520**	9 520	**10 850**	-245/+225
G7-S3	3,95	$CaCO_3$	62002	0,1138	0,12	17 450	90	16 870	14870		
G7-S3	4,05	OM	B2297	0,1529	0,100	15 090	66	15 090	13 090	**15 695**	-230/+235
G7-S3	4,15	OM	B2100	0,0569	0,59	23 032	47	23 030	21030		
G6-S2	4,40	OM	B2304	0,1124	0,0011	17 560	76	17 560	15 560	**18 845**	-135/+135
G6-S2	4,60	$CaCO_3$	62001	0,0662	0,120	21 810	140	**19 470**	17 470	**21 115**	-385/+575
G6-S4	6,45	OM	B2300	0,0689	0,0005	21 490	63	19 490	17 490	**23 510**	-260/+255
G6-S5	7,95	OM	B2299	0,1913	0,003	13 286	114	13 290	11290		
G7-S6b	8,85	$CaCO_3$	62003	0,0554	0,12	23 238	170	18 700	16700		
G7 S6b	8,85	OM	B2099	0,0830	0,123	23 240	82	23 240	21 240	**25 610**	-555/+375
G7-S7	10.40	$CaCO_3$	62004	0,0551	0,11	23 280	170	19 050	17050		
G7-S7	10.40	OM	B2104	0,0889	0,71	19 442	57	19 440	17440		
G7-S8	11.45	OM	B2101	0,0942	0,68	18 976	45	18 980	16980		
G7-S8	11.45	$CaCO_3$	62005	0,2139	0,10	30 890	390	28 500	26500		
G7-S8	12.46	Charcoal	B2301	0,0005	0,001	25 590	96	25 590	25 590	**29 950**	-290/+165

(*) Apparent Hard Water Effect (HWE)
(a) CaCO3: total carbonate fraction; OM: diffused organic matter; FP: fecal pellets (*Artemia*)
(b) Error bars represent one sigma deviation
(c) Accuracies on ^{13}C measurements are of ±0.05 and ±0.02% PDB for carbonates and organic matter, respectively
(d) *Stuiver, M., Reimer, P.J., and Reimer, R.W., 2021, CALIB 8.2 [WWW program] at http://calib.org*

Tables 2a and 2b: Radiocarbon dating on carbonated and organic samples form the Lake Urmia composite core, including correction steps considering the detrital fractions and the 2000-yrhard water effect. Timescale expressed in calendar ages. See Figures 2 and 4 for sample location.